University of Strathclyde

Department of Biomedical Engineering

Cystic Fibrosis Patient Monitor

Sean Donnelly MSci

2022

A thesis presented in the fulfilment of the requirements for the degree of Doctor of Engineering.

This thesis is the result of the author's original research. It has been composed by the author and has not been previously submitted for examination which has led to the award of a degree.

Signed:

Date:

ABSTRACT

Cystic Fibrosis (CF) is a genetic disease which affects the production of healthy cystic fibrosis transmembrane regulator (CFTR) proteins. These facilitate the transport of various salts across epithelial membranes throughout the body and their dysfunction leads to the development of life-limiting conditions across multiple organs. One consequence of CFTR dysfunction is that CF sufferers possess elevated levels of chloride (Cl^-) ions in their sweat. CF treatments which target the CFTR proteins to improve their functionality are increasingly being developed and becoming more widely available. Sweat Cl^- concentration is an important biomarker to gauge their efficacy. A wearable sensor capable of detecting Cl^- in aqueous media would allow sweat Cl^- levels to be monitored quickly and non-invasively and be a vital tool in the development of future CF therapies.

This work describes the development of a Cl^- ion selective electrode. It adapts existing wearable electrode technology through the addition of a UV-cured pHEMA hydrogel mixture to form a quasi-reference electrode. Laboratory tests found that conditioning the hydrogel in a 1 M KCl solution for 25 hours produced electrodes with consistent potentiometric responses to test solutions, enabling a calibration curve to be obtained with a sensitivity of 64.34 mV/dec over a Cl^- concentration range of 10 - 100 mM. This envelops both healthy and CF sweat Cl^- levels.

A study was conducted to examine the pHEMA electrodes' ability to operate whilst placed on the forearms of healthy volunteers. Whilst these tests highlighted some of the challenges faced by wearable devices, such as motion artefacts, five of the ten tests carried out demonstrated that the electrodes were capable of monitoring Cl^- concentration whilst placed on the body. They displayed a high degree of sensitivity which compared well to the lab bench tests conducted in parallel.

ACKNOWLEDGEMENTS

I would firstly like to thank my supervisor, Professor Patricia Connolly, for her valuable advice and guidance throughout my EngD project. I'm grateful for the input and unique insight provided by my clinical supervisor, Dr Gordon MacGregor, from the very beginning of this work. I would also like to thank those I worked alongside in the department, especially: Brian and Carol for their support and patience in dealing with my many queries over the years; and Aiden for his good company and willingness to discuss ideas. I would like to acknowledge the funding provided by the EPSRC that allowed me to conduct this research.

I will always be grateful for the support I have received from my family throughout my years of study. I wouldn't be where I am today without the work ethic (and maths tutelage) you gave me from a young age.

Finally, to Hannah. Your love and reassurance have kept me going through this write-up. Thank you.

LIST OF PUBLICATIONS

The following publications resulted from the work in this thesis:

1. Donnelly, S.; Ward, A.C.; MacGregor, G.; Connolly, P. Cystic Fibrosis Patient Monitor. In Proceedings of the BioMedEng19; London, 2019.

SYMBOLS

[X]	Concentration of Species X
A	Absorbance
A	Surface Area
a_x	Activity of Species x
C	Molar Concentration
C	Capacitance
c	y-intercept
D	Diffusion Coefficient
d	Optical Path
dl	Infinitesimal Length Vector
dS	Infinitesimal Vector Perpendicular to Surface S
E	Electric Potential
E	Electric Field Strength
E^0	Electric Standard Potential
F	Faraday Constant
F_D	Dilution Factor
G	Gibbs Free Energy
G^0	Gibbs Free Energy at Standard Conditions
I	Current
I	Intensity of Light
J	Flux
J_x	Conductance of solution x
K	Cell Constant
K	Equilibrium Constant

L_S	Sweat Conductivity
m	Linear Gradient
m	Mass
m_i	Mobility of Ionic Species i
$m_{target\ y}$	Pre-allocated Mass of Species y in Artificial Sweat Solution
MW	Molecular Weight
MW_{xy}	Molecular Weight of Compound xy
m_{xy}	Mass of Compound xy
$m_{y\ remaining}$	Mass Shortfall of Species y from Target Value
n	Number of Moles of Electrons
O	Oxidised Species O
P	Power
q	Electric Charge
R	Universal Gas Constant
R	Resistance
R	Reduced Species R
T	Temperature
V	Volume
$\bar{V}$	Mean Potential
V	Voltage
$V_{drift\_accounted}$	Measured Potentials Adjusted with Drift Potential
V_F	Forward Voltage
V_{LB2}	Potential from Lab Bench 2 Linear Equation
V_{meas}	Measured Potential of pHEMA Electrode
V_{OB}	On-Body Measured Potential

V_{OB}*	On-Body Measured Potential Adjusted with Mean Potential Offset
V_{Offset}	Potential Offset
V_S	Supply Voltage
W	Work Done
Z	Valency
γ	Activity Coefficient
δ	Accuracy of Measured Potential Against Calibration Potential
ΔV	Difference in Potential
ε	Absolute Permittivity
ε_0	Permittivity of Free Space
ξ	Accuracy of Measured Concentration Against Known Concentration
σ	Charge Density
φ	Electric Potential of Phase

ABBREVIATIONS

ACh	Acetylcholine
Ag/AgCl	Silver/Silver Chloride
ANS	Autonomic Nervous System
AQP5	Aquaporin 5 Channel
ASL	Airway Surface Liquid
ATPase	Adenosinetriphosphatase
$C_3H_5O_3^-$	Lactate
cDNA	Complementary Deoxyribonucleic Acid
CE	Counter Electrode
CF	Cystic Fibrosis
CFRD	Cystic Fibrosis Related Diabetes
CFTR	Cystic Fibrosis Transmembrane Regulator
CGMS	Continuous Glucose Monitoring System
Cl^-	Chloride
dec	Decade
DI	Deionised
DMPAP	2,2-Dimethoxy-2-Phenylacetophenone
ECG	Electrocardiogram
EDLC	Electric Double Layer Capacitor
EGDMA	Ethylene Glycol Dimethacrylate
EMA	European Medicines Agency
EMF	Electromotive Force
ENaC	Epithelial Sodium Channel

FDA	Food and Drug Administration
FEV1	Forced Expiratory Volume
HCO_3^-	Bicarbonate
HEMA	2-hydroxyethyl methacrylate
HEPES	4-(2-Hydroxyethyl)-1-Piperazineethanesulfonic Acid
Hg	Mercury
$Hg(SCN)_2$	Mercury(II) Thiocyanate
HVS	Healthy Volunteer Study
IHP	Inner Helmholz Plane
IRT	Immunoreactive Trypsinogen
ISE	Ion-Selective Electrode
K^+	Potassium
LED	Light Emitting Diode
MA	Motion Artefact
MC	Methylcellulose
mRNA	Messenger Ribonucleic Acid
MVCC	Mutation of Varying Clinical Consequence
Na^+	Sodium
NBS	Newborn Screening
NPD	Nasal Potential Difference
OCP	Open Circuit Potential
OHP	Outer Helmholz Plane
Op-amp	Operational amplifier
P.aeruginosa	Pseudomonas aeruginosa
PEA	Portable Electrochemical Analyser

pHEMA	Poly(2-hydroxyethyl methacrylate)
PVP	Polyvinylpyrolidone
QRE	Quasi-Reference Electrode
RE	Reference Electrode
SCE	Saturated Calomel Electrode
SHE	Standard Hydrogen Electrode
SSB	Sodium Sensor Belt
UV	Ultra Violet
WE	Working Electrode

TABLE OF CONTENTS

TABLES

FIGURES

1. Literature Review

1.1 Introduction

Cystic Fibrosis (CF) is a genetic disease which affects the body's ability to regulate chloride transport across various epithelial cells throughout the body. It affects 1 in 2500 Caucasian new-borns (1), making it the most prevalent life-limiting genetic disease within Caucasians (2). Comparable statistics are noted in those of Hispanic origin whilst those of African and Asian descent are less likely to inherit the disease. One consequence of the disease is an inability in the sweat glands to resorb chloride (Cl^-), leading to CF sufferers displaying a high concentration of Cl^- within their sweat. A new generation of CF treatments are emerging which target the proteins affected by the genetic mutations, aiming to re-instil their ordinary function, thus improve Cl^- transport throughout the body. The efficacy of these treatments can be gauged by monitoring the concentration of sweat Cl^- in a patient over the course of treatment. A change in sweat Cl^- concentration of 36% or more is considered clinically significant in such therapies. Current techniques of sweat Cl^- measurement are time-consuming or unsuitable for this task. Therefore, the development of a wearable device capable of serially monitoring sweat Cl^- levels of individual patients quickly and non-invasively could be used to investigate not only the treatment's efficacy in treating a wide range of CF patients but also aspects such as the drug's durability in maintaining these changes. Such a device would, therefore, be of great significance within this field.

This chapter reviews the literature which is relevant to the research reported in this thesis. Current techniques of CF diagnosis and monitoring are presented. The trends and technology involved with wearable sensors are then detailed before methods of Cl^- detection are addressed.

1.2 Cystic Fibrosis

Cystic Fibrosis (CF) is an autosomal recessive disorder which manifests due to a mutation within the gene responsible for the synthesis of the Cystic Fibrosis Transmembrane Regulator (CFTR) protein (3). There are six classes of mutation (I – VI) associated with the protein. At

least two of these must be carried by the parents, one from each, for a child to be born with the disease. CFTR is a protein which facilitates the passage of Cl^- through the cell membrane (4). As such, CF is a systemic condition, affecting the liver, pancreas and gastrointestinal organs as well as the lungs. The breakdown in ion transport means, amongst other manifestations, that NaCl is not sufficiently resorbed from sweat. This leads to larger-than-average salt concentrations in CF patient's sweat, a feature which has been anecdotally observed as early as the 17th century (5). The data shown in Table 1.1 is taken from a study conducted with 500 CF patients and 1000 control volunteers (6). It exemplifies the disparity in the levels of sweat Cl^- and Na^+. In particular, it found that the average sweat Cl^- concentration of CF patients was approximately six-times that of non-CF patients.

Table 1.1. Average concentrations of Cl^- and Na^+ ions in sweat samples of 500 CF patients and 1000 control patients (6).

	Sweat Ion Concentrations (mM)	
	Cl^-	**Na^+**
Control	16	23
CF patients	99	101

Until recently, treatment of CF had focussed on the management and relief of its symptoms. However, with the discovery of the gene which causes CF in 1989 (4), new treatments are emerging which target the CFTR protein itself. These are labelled CFTR modulators and several trials have been conducted, or are currently ongoing or scheduled, to investigate their efficacy in treating specific CFTR gene mutations. These trials often use the concentration of Cl^- in the participants' sweat as a marker of the drug's efficacy. Therefore, a method by which this concentration can be measured quickly and accurately would be an important tool in the development of these therapies.

1.2.1 Diagnosis and Monitoring

Since the effects of CF were observed there have been many iterations and models of diagnoses. Due to the early identification of a link between the saltiness of an infant's sweat with life-long health problems and a reduction in lifespan, the earliest attempts to diagnose CF focussed on the analysis of sweat. The first such clinical studies carried out involved wrapping test subjects in plastic in order to stimulate sweat. However, this proved to be very time consuming with adult subjects often required to spend two hours under the test conditions to obtain a suitable volume of sweat. Additionally, the procedure was noted to be uncomfortable, especially for infants. On occasions when an inadequate amount of sweat was being stimulated, hot water bottles were often added to the bag. Perhaps unsurprisingly, there were occasions were the subjects suffered from hyperpyrexia or even fatal heat stroke (7).

Due to these undesirable conditions, there was a requirement for new and less invasive modes of CF diagnosis. Described below are the techniques currently in practice.

1.2.1.1 Sweat Test

The sweat test is the gold standard for diagnosing CF and was an early alternative to the more hazardous techniques around at the time (8). It varies from the technique described above as it utilises the chemical pilocarpine in conjunction with a two-electrode arrangement placed on the skin. Pilocarpine is a positively charged substance which stimulates the sweat glands to secrete, its chemical structure is shown in figure 1.1.

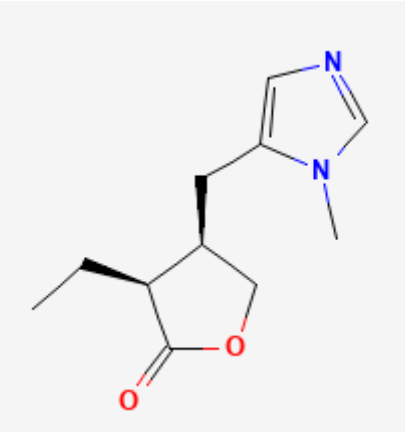

Figure 1.1. Chemical structure of pilocarpine. Retrieved from: https://pubchem.ncbi.nlm.nih.gov/compound/5910#section=2D-Structure

The electrodes allow a small electric potential to be applied across the patient's skin, meaning the positively charged pilocarpine is able to migrate across the skin and stimulate the target sweat glands (9). This process is known as pilocarpine iontophoresis and was first introduced in a study conducted by Gibson and Cook in 1959. The electrode configuration stays in place for around five minutes before the electrodes are removed, the skin cleaned and the sweat is collected. A strict protocol for sweat test diagnoses is set by the Cystic Fibrosis Trust (10) and the procedure should only be carried out in a CF Trust-accredited centre (8). However, the procedure has remained largely unchanged since its original use in 1959 (2). The remainder of this sub-section will describe the procedure followed to prepare the electrodes, apply and remove them, and subsequently collect the sweat sample.

The area of the patient's skin upon which the electrodes are in contact is initially cleaned with alcohol and distilled water respectively. After the skin has been cleaned, a Pilogel® Iontophoretic Disc (ELITech Group, Puteaux, France) is placed into the positive electrode contact, as shown in figure 1.2 (a). The Pilogel discs are standardised, 6 mm thick, 2.8 cm diameter agar gel cylinders which are comprised of 96% water, in which 0.5% pilocarpine nitrate has been dissolved. With the skin still damp from cleaning, to ensure an even contact between the gel and skin, both stainless steel electrodes are applied to the flexor surface of the lower arm, as shown in figure 1.2 (b) and secured with straps. The electrodes are subsequently connected to a power source which, when initiated, raises the current in seventeen 30s intervals.

Ultimately, this provides an iontophoresis current of 1.5 - 2 mA, depending upon the model of power supply utilised (7,9,11,12). This current is maintained for 5 minutes before reducing back to zero. The electrodes are then removed, and the area of skin covered by the Pilogel disc is swabbed with distilled water and dried.

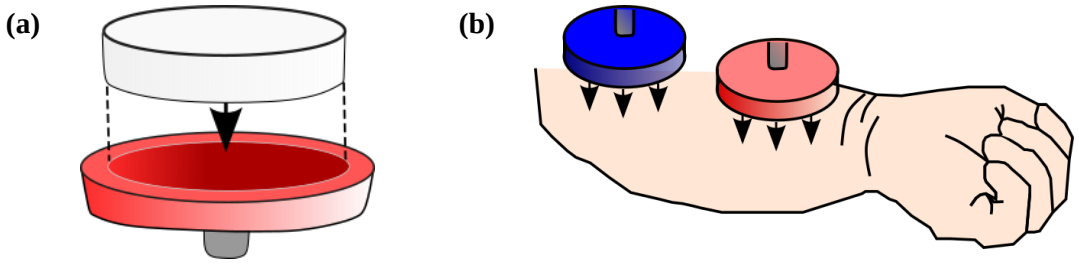

Figure 1.2. Schematic of pilocarpine iontophoresis sweat test. **(a)** A standardised Pilogel® Iontophoretic Disc is inserted into the recess of the positive electrode and, **(b)** placed upon the forearm of the patient alongside the negative electrode. Adapted from (9).

The collection of the sweat sample immediately follows. It is recommended that this is performed using a Macroduct® sweat collector (ELITech Group, Puteaux, France) – an instrument designed specifically for sweat collection and commonly used within a clinical setting. The small, disposable device, depicted in figure 1.3, consists of a hollow plastic tubing coiled into an outer casing. Within the tubing is a small amount of blue, water-soluble dye (≤10 nM) which is used as a visual indicator of sweat intake into the cavity. The casing is designed such that when it is applied tightly to the patient's forearm the skin will bulge into the cavity, expelling any excess air. It is kept in place via a strap around the patient's arm. At the central apex of the coiled tubing is a small entrance duct approximately 0.64mm in diameter (9). The force exerted by the Macroduct® on the skin is greatest around the plastic circular casing, hence the sweat is directed towards the centre of the coil, where the opening is located. Due to the absence of air within the cavity, the sweat is forced into the entrance duct via the hydraulic pressure created by the secretory glands covered by the collection device.

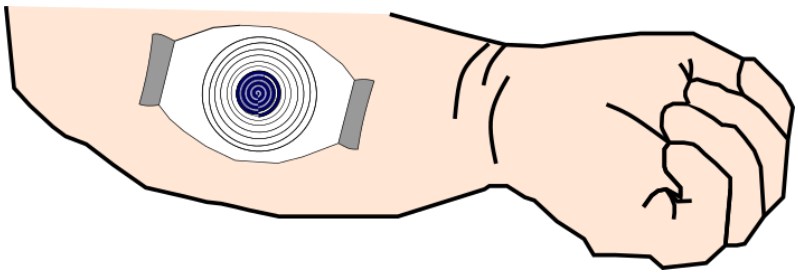

Figure 1.3. Depiction of Macroduct® sweat collection device applied to the forearm. Sweat is collected in plastic tubing, containing blue dye, coiled into the outer casing. Adapted from (9)

The collection time is set at 30 minutes, in which the tubing (with a volume of 85µl) is able to collect an average volume of sweat of between 50 and 60µl. The minimum acceptable sample size from this method is 15µl (10). This ensures that a minimum sweat rate and, consequently, electrolyte concentration has been obtained. In order to maintain a valid sample, the sweat rate must be no less than $1g/m^2$ per minute. If the rate is lower, then the electrolyte concentration is lower and there is a higher risk of evaporation of the sweat sample (8,10).

Immediately following the collection period, the tubing is severed from the casing and its contents taken away for analysis of its salt content. This process is covered later in this piece.

In addition to the Macroduct® collector method, another legitimate technique makes use of gauze or filter paper to collect the sweat. This was the method utilised by Gibson and Cooke in 1959. Sweat is induced in a procedure identical as that described above, but the Pilogel discs are replaced with a pilocarpine solution, applied to an unweighed disc of filter paper placed over the surface of the positive electrode. A piece of gauze or filter paper from a weighed sample is then placed over the area previously covered by the pilocarpine and used to collect the sweat for 30 minutes. It is subsequently removed, reweighed and analysed to determine its salt content (7).

Once sweat samples are analysed, physicians are able to gauge whether a patient is likely to have CF by noting the sample's Cl^- concentration and allocating it into one of three categories: negative; borderline/indeterminate; consistent with CF. The Cl^- levels set for these categories

are shown in Table 1.2. It should be noted, however, that these levels alone are not enough to arrive at a diagnosis. For example, it has been observed that neonatal patients possess an abnormally high concentration of Cl^- if they are measured to have >40 mM in their sweat (8,13). Likewise, concentrations of >60 mM have been seen to occur in patients by conditions other than CF. It is therefore required that any positive result acquired via a sweat test is followed by a repeat procedure at a later date along with one other diagnostic test (8,10,14).

Table 1.2. Reference values for sweat chloride for diagnosis of CF (10)

Diagnosis	**Chloride Concentration (mM)**
Negative	< 40
Borderline/Indeterminate	40-60
Consistent with CF	> 60

1.2.1.2 Genetic Testing

Should an initial sweat test return sweat Cl^- values which are consistent with CF, one of the follow-up diagnostic procedures would likely be a genetic test. Since it was discovered that a fault in the gene responsible for the synthesis of the CFTR protein was the cause of CF (4), there has been an effort to identify the mutations which may ultimately lead to the disease. To date around 2000 mutations have been isolated and reported in the CF Mutation Database (CFMD). There is a problem, however, in the fact the majority of these mutations have been observed in only one or a handful of patients and their clinical manifestations are wide-ranging (15). A consensus report by the Cystic Fibrosis Foundation (8) stated that in order to be classified as CF-causing, a mutation must fulfil at least one of the criteria outlined in Table 1.3.

Table 1.3. Criteria for a CFTR mutation to be classed as CF-causing (8,16)

Criterion	Physical Manifestation
1	Cause a change in the amino acid sequence that severely affects CFTR function and/or synthesis
2	Introduce a premature termination signal (insertion/deletion or nonsense mutations)
3	Alter the invariant nucleotides of intron splice sites (first two or last two nucleotides)
4	Cause a novel amino acid sequence that does not occur in normal CFTR genes from at least 100 carriers of CF mutations from the patient's ethnic group

Clearly, the criteria set out in Table 1.3 facilitates for a lot of potential permutations in terms of the pathogenicity and severity the mutations may cause. Due to this, projects such as the Clinical and Functional Translation of CFTR (CFTR2) project (15), were set up in an attempt to better understand the physical effects specific mutations have upon individuals. The study collected data for the 160 most-reported mutations from approximately 40,000 relevant patients to investigate the mutation's physiological effect (2,15). The CFTR2 team placed each mutation investigated into one of the four categories outlined in Table 1.4.

Due to the large number of possible mutations and mutation pairings, genetic testing is seen as a highly specific mode of diagnosis but with poor sensitivity (8). For this reason, it is rarely used in isolation as a diagnostic technique but instead used in conjunction with newborn screening.

Table 1.4. CFTR2 mutation categories. Adapted from (2,14)

Category	**Definition**
CF-causing	Individuals with two copies on separate alleles will likely have CF. This must be confirmed with a sweat test
Mutation of varying clinical consequence (MVCC)	A mutation that in combination with another CF-causing mutation or MVCC mutation may result in CF
Unknown/Unevaluated	Mutations that have not been evaluated by CFTR2 and may be disease-causing or benign
Non-CF-causing	Individuals with one or more of these mutations are unlikely to have CF (as a result of that allele)

1.2.1.3 Newborn Screening

Newborn screening (NBS) for CF refers to the testing of neonatal infants for levels of a pancreatic proenzyme named immunoreactive trypsinogen (IRT) (16). This is conducted via an IRT assay performed using a sample of the patient's blood (17). Elevated levels of IRT in infancy are consistent with the child having CF, however, much like genetic testing, NBS does not provide a high level of specificity due to the fact that IRT levels are often high in healthy infants.

1.2.1.4 Nasal Potential Difference

The flux of ions across epithelial membranes results in a potential difference across the membrane. As will be discussed in greater detail in Section 2.3.1, the loss of function of CFTR means that airway epithelial cells become impermeable to Cl^-. Combined with the loss in the ability to inhibit the epithelial sodium channel (ENaC), this leads to CF sufferers possessing a significantly higher negative potential difference across their airway epithelial cells than non-sufferers (8,18). Nasal potential difference (NPD) is quantified using potentiometric

measurements between a reference electrode on the patient's arm and a working electrode attached to a catheter in contact with the patient's nasal mucosa (19).

1.2.1.5 Diagnostic Algorithm

Often CF patients do not exhibit every physiological effect that the disease can cause. This has led to different classifications of CF which reflect the variability in phenotype experienced by the patient. These categories: classic CF and non-classic CF, are assigned to an individual by way of diagnostic algorithms which utilise a combination of the diagnostic techniques outlined above. Using this method, patients can be diagnosed with classic CF if they possess a sweat Cl concentration of > 60 mM and have one or more CF phenotype. Likewise, for individuals with a sweat Cl concentration of < 40 mM or of borderline level (40 – 60 mM) who also possess a CF phenotype in at least one organ system are assigned as having non-classic CF (14,16). An example diagnostic algorithm is provided in figure 1.4.

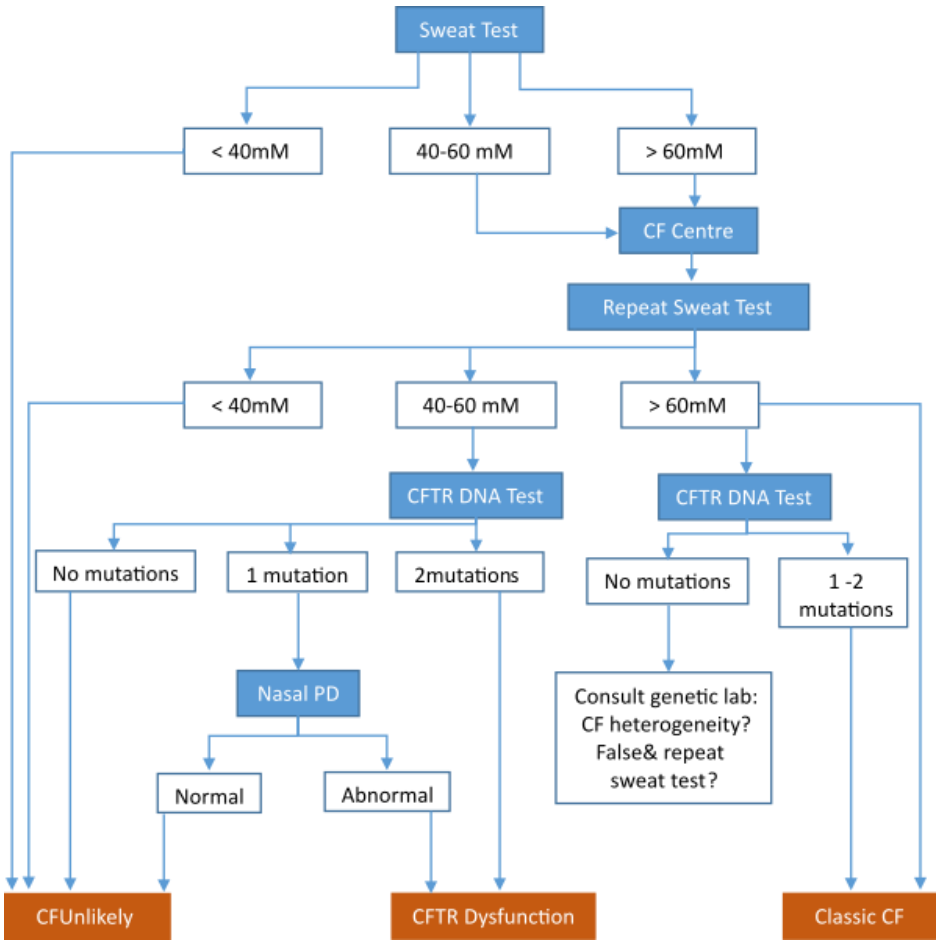

Figure 1.4. Example CF diagnostic algorithm. Adapted from (14,16).

1.2.2 Cystic Fibrosis Treatment

Until recently, the treatment of CF consisted mainly of techniques designed to alleviate its symptoms. These included airway clearance therapies, antibiotics and bronchodilators to treat the pulmonary obstructions and infections the patient would frequently encounter (2,20). These were often accompanied by enzyme replacement and caloric supplementation therapies in an attempt to counter the effects of pancreatic disease (21). However, ever since the CF-causing gene has been isolated, much of the focus in treating the disease has been on the development of therapies which address the underlying dysfunction of the CFTR protein or which directly address the underlying faulty gene.

1.2.2.1 CFTR Modulators

Much of the progress made in CF treatment over the past decade has been in the development of CFTR modulators. These come in the form of small molecules which are designed to restore partial or complete CFTR protein function (22). Just over 2000 CFTR mutations have been discovered, with only 10-15% categorised as CF-causing (23). Each of these mutations are separated into six classes according to their physical effects upon the CFTR protein itself (2,22). These mutation classes are depicted in figure 1.5 and should not to be confused with those defined in Table 1.2, which detail the criteria by which a mutation can be defined as being CF-causing. Due to the vast number of CFTR defects a patient may potentially possess, there is a wide diversity in functional defects of the protein. Therefore, any such treatment targeting the CFTR protein dysfunction would have to be mutation-specific (23). There are two categories of CFTR modulators: potentiators and correctors.

Mutation Class						
Healthy	I	II	III	IV	V	VI
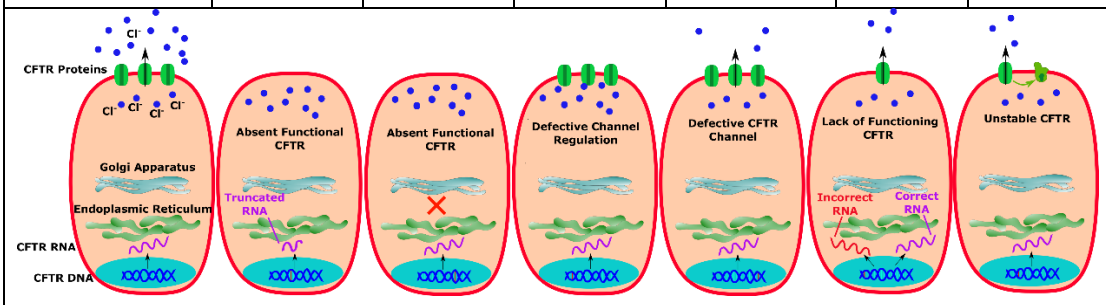						
Defect Type	No functional CFTR protein	CFTR trafficking defect	Defective channel regulation	Decreased channel conductance	Reduced synthesis of CFTR	Decreased stability of CFTR

Figure 1.5. CFTR mutation classes (I – VI) with schematic visualisation of their physical impact in comparison to healthy CFTR. Adapted from (2,24).

1.2.2.1.1 CFTR Potentiators

CFTR potentiators have been designed to bind to the CFTR proteins located at the cellular level and increase the time in which they are open (25). The purpose of this is to increase the Cl^- conductance across the membrane, restoring the natural flow of salts and, hence, the normal

hydrating mechanism for the epithelia. Such a treatment, therefore, is primarily aimed at patients who suffer from a Class III mutation, see figure 1.5, where their CFTR gating is defective. The most common of such mutations is G551D which affects approximately 4% of CFTR alleles worldwide. (22).

There is currently one CFTR potentiator available for treatment; Ivacaftor, figure 1.6.

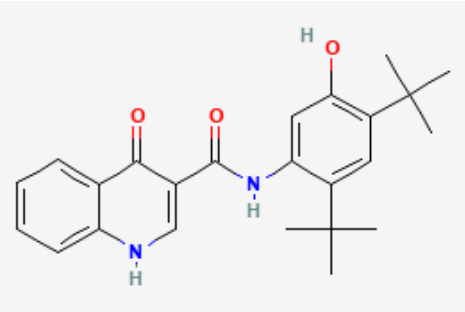

Figure 1.6. Chemical structure of pilocarpine. Retrieved from: https://pubchem.ncbi.nlm.nih.gov/compound/16220172#section=2D-Structure

This was produced by Vertex Pharmaceuticals (Boston, MA) and, in 2012, was approved by the United States Food and Drug Administration (FDA) and the European Medicines Agency (EMA) as a treatment for patients of 6 years and older with CF and who carry at least one copy of the G551D mutation (22,24). In the proceeding 3 years, the approval of use was extended to a further eight non-G551D gating mutations and to patients of 2 years and over. This was done following the findings in clinical trials such as KIWI, in which patients between 2 and 5 years of age, and possessed a CFTR gating mutation on at least one allele, were administered Ivacaftor over two separate periods of time (26). The results showed the patient's experienced significant decreases in sweat Cl^- concentration as well as increases in bodyweight and body mass index (BMI). CFTR function in patients receiving Ivacaftor is raised to only 35-40% compared to that of a normal non-CF sufferer. Despite this, observations made from trials have demonstrated clinical improvements in day-to-day life including rises in respiratory function and reductions in pulmonary exacerbations (22,23,26).

However, as noted above, the G551D mutation is found in around 4 % of CF sufferers, meaning it is only an effective treatment for a small proportion of patients (27). Due to most CF patients

being heterozygous for gating mutations – i.e. having two different effected alleles – combination therapies are seen as a way of treating a larger proportion of patients (22).

1.2.2.1.2 Combination Therapy

As the name suggests, combination therapy involves the combined use of one or more CFTR modulator therapies. This will likely take the form of a CFTR potentiator (such as Ivacaftor) as well as one or more CFTR correctors. The latter, in contrast to potentiators, are designed to bind to the mutant CFTR mRNA and correct their transcription or processing defects. In doing so, more stable CFTR proteins are created and more are available on the surface of cells to perform their normal function (23).

Combination therapies like this are necessary due to the amount of CF patients who possess complex CFTR mutations which can cause simultaneous CFTR gating, trafficking, and stability defects (22,27). The most common genetic mutation resulting in CF is Phe508del - a complex mutation with multiple defects which is found in ~80% of CF patients worldwide (24,27,28). The initial problem involving Phe508del-CFTR proteins is that of trafficking (Class II mutation, see figure 1.5), where very little of the misfolded proteins are able to reach the cellular membrane – leading to a depletion of CFTR (29). However, the proteins which are able to reach the apical membrane then exhibit a gating deficiency (Class III mutation), meaning that any treatment for patients with Phe508del-CFTR must be able to address both of these issues (30,31).

One combination treatment to have emerged in recent years is that of Lumacaftor, figure 1.7 (a), combined with Ivacaftor, named Orkambi (Vertex, Boston, MA). After exhibiting significant but modest results in trials (32), combination therapy containing Ivacaftor and Lumacaftor was approved by the FDA and EMA in 2015 for patients 12 years and over who

possess the Phe508del mutation. It has recently been made available in England for patients 12 and over and with two copies of the Phe508del mutation (33). Orkambi has only proved to be modestly effective, however, with patient's first forced expiratory volume (FEV1) only improving by 2 – 4% (27,34).

Symkevi (Vertex, Boston, MA) is another combination therapy approved for use and targeted at the Phe508del mutation. It combines Ivacaftor with the CFTR corrector, Tezacaftor, figure 1.7 (b) (Vertex, Boston, MA). The latter should, in theory, have an advantage over the use of Lumacaftor in that it does not induce CYP3A – an enzyme which is a substrate of Ivacaftor – and so does not interact with Ivacaftor (22,29). Consequently, smaller doses of Symkevi could be administered and provide similar outcomes to Orkambi combination therapy and therefore carry a greater benefit-to-risk profile for patients (29). Indeed, trials demonstrated an FEV1 increase of 3.75% in patients undergoing Symkevi therapy, as well as a 35% reduction in exacerbations and a sweat Cl^- reduction of 6 mM (34).

Perhaps the most promising combination therapy to date is Kaftrio (Vertex, Boston, MA), which is a triple combination therapy combining Symkevi with the CFTR corrector Elexacaftor, figure 1.7 (c) (Vertex, Boston, MA). Trials demonstrated that patients experienced an improvement in FEV1 of 11 – 14%, a 35% reduction in exacerbations, and a sweat Cl^- reduction of 6 mM (27,34–36). Kaftrio was approved for use in all parts of the UK in 2020, and became available in August 2021 (37).

(a)

(b)

(c)

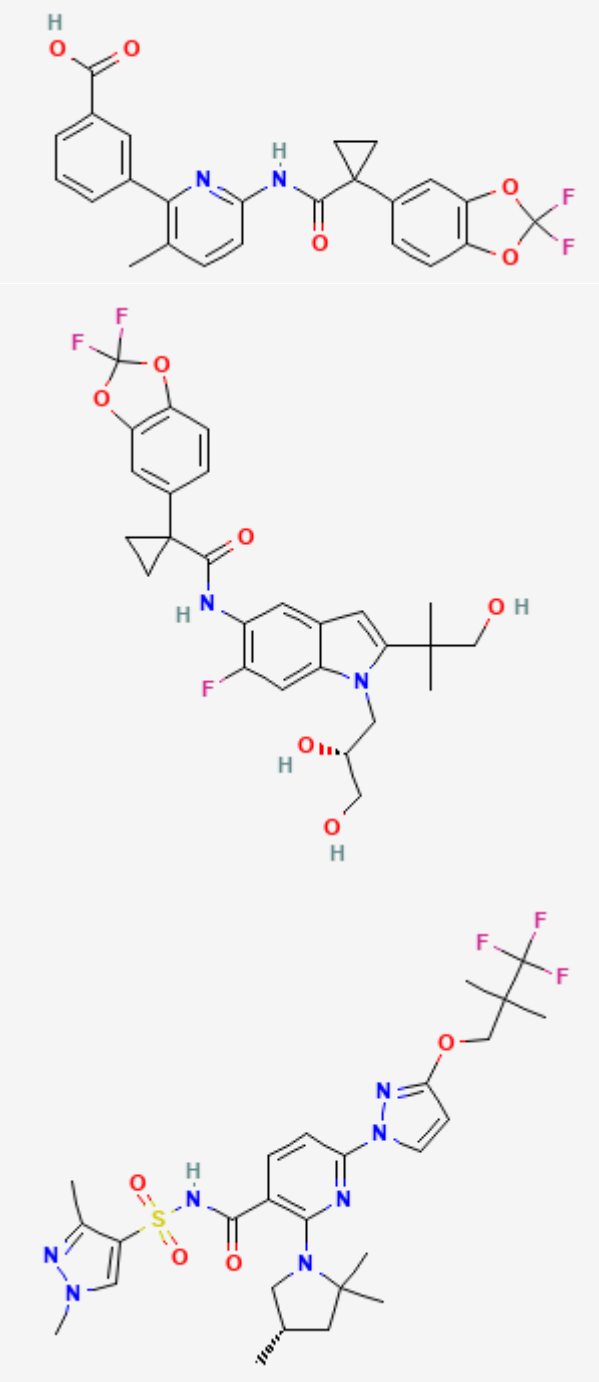

Figure 1.7 (a) Chemical structure of lumacaftor. Retrieved from: https://pubchem.ncbi.nlm.nih.gov/compound/16678941#section=2D-Structure
(b) Chemical structure of tezacaftor. Retrieved from: https://pubchem.ncbi.nlm.nih.gov/compound/46199646#section=2D-Structure
(c) Chemical structure of elaxacaftor. Retrieved from: https://pubchem.ncbi.nlm.nih.gov/compound/134587348#section=2D-Structure

Other companies such as AbbVie (Lake Blaff, IL) and Proteostasis Therapeutics (Boston, MA) are also involved in CFTR modulator combination therapies with trials currently ongoing (34,37).

1.2.2.2 Read-Through Agents

Class I mutations affect approximately 10% of CF patients (23). Nonsense or premature stop codon mutations result in truncated, unstable RNA which prematurely decays. Consequently, the individual is unable to produce the CFTR protein. Read-through agents are designed to 'overlook' the erroneous stop codon and proceed in creating the RNA (22). Alturen (PTC Therapeutics, South Plainfield, NJ) was a synthetic drug aimed at addressing this defect, however it did not prove to be effective in improving respiratory function or reducing the rate of pulmonary exacerbations and was discontinued in March 2017 (22,38). The development of read-through agents continues to be an active area of research, however, with several treatments currently under investigation (23).

1.2.2.3 Amplifiers and Stabilisers

Treatments such as amplifiers and stabilisers are being developed with the intention of combining them with new and existing CFTR modulators in order to enhance their effectiveness. Amplifiers, such as PTI – 428 (Proteostasis Therapeutics, Boston, MA) aim to increase the number of CFTR proteins within a cell, whereas stabilisers act to maximise the time in which the protein is able to survive on the cell membrane (23). A prominent example of a stabiliser is Cavosonstat (Nivalis Therapeutics, WA), which underwent two phase 2 trials in combination with Ivacaftor/Lumacaftor and Ivacaftor respectfully. However no marked improvement in lung function or sweat chloride concentration was observed in either study (22).

1.2.2.4 Future Therapies

As touched upon above, one of the major challenges in CF treatment is the vast diversity in functional defects from individual to individual. Additionally, many of the treatments which have emerged recently are targeted toward those with the common Phe508del mutation. To those patients who do not fall into this category one of the main hopes in CF treatment is that of gene therapy through the delivery of healthy CFTR complementary-DNA (cDNA). Such a treatment would not be mutation-dependent and so could be administered to all patients. However, the main challenge with this therapy has been in finding a suitable delivery vector for the cDNA (22,39).

Another avenue under investigation is that of gene editing via CRISPR/CAS9 technology (34,40,41). This technique directly targets the faulty section of DNA and edits its genetic code (42). By fixing the problem at source the faulty code is no longer passed to the RNA, hence the production of dysfunctional CFTR proteins would cease. However, gene therapies such as these often use viral vectors to reach their target, which can cause undesirable immune responses in host cells. Therefore, while promising, the use of such technology to treat CF is still at an early stage and the use of CFTR modulator therapies viewed as one of the most effective tools of treating the disease at present.

1.2.3 Summary

Section 1.2.2 aimed to give an overview of the CF drug therapies which have been introduced in recent years, in the form of CFTR modulators, as well as those which could emerge in the foreseeable future.

Table 1.5. Summary of approved and emerging CF treatments.

Treatment Modality	**Target Defect Type**	**Approved Drugs**
CFTR Potentiators	Type III gating mutations (eg. G551D)	Ivacaftor
CFTR Correctors	Types I, II, V. Commonly target Type II trafficking mutations (eg. Phe508del)	Lumacaftor Tezacaftor Elaxacaftor
Amplifiers	Types II, V	NA
Stabilisers	Type VI	NA
Gene Therapy	Independent of mutation type	NA

These therapies share a goal of restoring and enhancing the CFTR proteins' functionality and in doing so enhance the ability of the sweat duct to reabsorb Cl^- ions, reducing the Cl^- concentration within the individual's sweat. A change in sweat Cl^- exceeding 36% is considered clinically significant in CFTR modulator trials (43). Monitoring sweat Cl^- therefore provides a proxy for overall CFTR functionality which is vital for the homeostasis of organs such as the lungs and liver. This pathophysiology which is discussed in more detail in Section 2.3. Thus, the ability to monitor changes in sweat Cl^- over the course of CFTR modulator therapies provides a useful mechanism to characterise their efficacy in tackling the underlying CFTR dysfunction associated with CF. New technologies will be required to relieve the burden this monitoring would place on clinics performing time consuming sweat tests. As such, current sensor technologies which could be adapted for personal and wearable use are reviewed in the proceeding subsections.

1.3 Sensor Technology

A wide variety of biosensors are utilised in the healthcare sector to detect and monitor various targets within the human body using whole blood, urine, or sweat samples, for example. Blood glucose sensors have allowed diabetes sufferers the opportunity to manage their condition more effectively (44). Similarly, blood lactate biosensors have also demonstrated their clinically

value, with levels of lactate within the blood used as an indicator of organ failure as well as fatigue during exercise, with blood lactate levels rising from 0.5 – 1.5 mM during rest up to 25 mM during exertion (45,46).

Technological improvements over the last two decades have meant that sensor technologies are becoming increasingly scaled down and more sensitive. This has resulted in a rise in the number and variety of minimally invasive wearable sensors available both in personal and medical settings. Health services are seeing the potential of such devices as a way of monitoring aspects of patients suffering from non-life threatening or chronic illnesses without the need for them to leave their homes (47). Thus, the patients are less inconvenienced and hospital services are alleviated. Wearable sensors range from smart watches which monitor individuals' heart rates to devices intended to continuously monitor glucose and lactate levels transdermally (44–46).

The following section will describe the trends in wearable sensors and detail some of the high-profile examples that have emerged. It will investigate the demand for sensors which monitor electrolytes in sweat as well as those which are under development.

1.3.1 Trends in Wearable Sensors

1.3.1.1 Social

The number of wearable sensor devices designed for personal and social use has seen a dramatic increase in popularity in the past few years. Worldwide shipments of smart wearables were estimated at just under 223 million in 2019, and are expected to rise to 302 million by 2023 (48). Prominent examples of such devices include Google Fit, Fitbit and Apple Watch (48,49). At present, a large proportion of these are predominantly used as a pedometer or to monitor individuals' heart rate and energy usage. Devices intended to monitor physiological properties like electrolyte concentration are classed as medical devices, placing greater regulatory burdens on developers and resulting in a relative scarcity of such devices

commercially (47,50). One exception to this is the Gatorade Gx Sweat Patch (Gatorade, Chicago, IL) designed as a single-use patch, worn on the forearm, to monitor hydration levels during exercise. It measures both sweat rate and sweat Na^+ concentration via microfluidic collection and colorimetric sensing technology developed by Epicore Biosystems Inc (Cambridge, MA) (51,52). The rise in popularity of personal fitness monitoring means that it is likely devices such as this, with accompanying smart phone apps, will become more present in society.

1.3.1.2 Medical

Given the popularity of wearable devices and improvements made in wireless transmission and subsequent storage of data, health services are increasingly looking towards wearable devices as a way of minimising the frequency to which patients visit their facilities for care. One of the main reasons for this shift in strategy is the ever increasing elderly population and rise in the number of chronic disease sufferers in the developed world (49). High profile examples such as the near-patient testing devices: i-STAT (Abbott Inc, Chicago, Il) and Accu-Chek (Roche Diagnostics, Basel) provide platforms from which an individual's metabolites and electrolytes may be monitored via a hand-held device. They do so, however, through taking blood samples from the patient and therefore maintain a level of invasiveness which may not suit every patient; and a level of skill from the caregiver to obtain a good sample (53). Progress has also been made in wearable devices for the use of diabetic patients. Examples of such devices include the Guardian® Real Time Continuous Glucose Monitoring System (Guardian® RT CGMS) (Medtronic, Minneapolis, MN), and the FreeStyle Libre Flash Continuous Glucose Monitoring System (FSL-CGMS) (Abbott Laboratories, Chicago, IL). Both devices utilise small electrodes placed within the interstitial fluid, the thin layer of fluid surrounding subcutaneous tissue cells, to initiate an electrochemical reaction with the glucose in the fluid. The magnitude of the resultant signal from the electrode is then used to gauge the glucose concentration within the bloodstream (54). Measurements are taken at regular intervals: the

Guardian® RT CGMS takes up to 288 measurements per day (Medtronic), wirelessly transmitted and electronically stored to create a near-continuous picture of blood glucose levels and identify any subsequent trends. The Guardian® RT CGMS differs from the FSL-CGMS in that it requires a 2-hour initialisation period after initial application to the body, where it can remain operational for up to 3 days. Conversely, the FSL-CGMS, a recent iteration of a continuous glucose monitoring system, is factory-calibrated and can be worn by the patient for 14 days (56). Both devices require the glucose sensor to be inserted under the skin, hence maintain a degree of invasiveness. To date, a regulated medical device which is capable of measuring analytes in the blood, such as glucose and electrolytes, through the skin has yet to be developed.

Non-invasive sensors such as the GlucoWatch® by Cygnus Inc (now owned by Animas (West Chester, PA)) have been developed for commercial use. The GlucoWatch® used reverse iontophoresis to enhance the transport of glucose from the blood stream out across the skin barrier, allowing the device to continuously monitor an individual's glucose levels. However, users often claimed of skin irritation and a long warm-up time and the device has since been removed from circulation (53,57). Real life difficulties such as these mean that research into non-invasive sensors remains an area under development. Much of this research is focussed on ion selective electrodes (ISEs) as a way of monitoring patient's transdermal and sweat electrolyte and metabolite concentrations. The proceeding section will describe the types of ISE under development as well as how they are incorporated into devices.

1.3.2 Ion Selective Electrodes

The operating principle behind ISEs is rooted in the Nernst equation (detailed in Section 2.4.5), where the potential of the electrode immersed in an ionic solution is proportional to the ionic concentration of the solution (58). This often involves two electrodes, a reference electrode (RE) and a working electrode (WE), where the measured value is the relative potential between

the two electrodes in a process known as potentiometry. The RE has a fixed potential whereas an ISE is used as the WE, and its potential is dependent upon a specific ionic concentration of the solution under investigation, often by way of an ion-selective membrane. The Nernst equation and the theory of electrochemical cell potential measurement are explained in greater detail in Section 2.4. There are a number of ISE designs which have been developed with each having certain merits and drawbacks depending upon their intended function. The following will detail three such designs (inner-reference solution, solid contact, and hydrogel) and give examples of devices which incorporate the specific technologies.

1.3.2.1 Inner Filling Solution

Sensors which incorporated an inner solution were the first potentiometric sensors to be used to measure ion concentrations within a target solution. Such sensors employ a basic architecture of an inner filling solution separating an ion selective membrane from an internal reference electrode, as shown in figure 1.8. The filling solution is often comprised of an ionophore solution (the ion-selective element) within an organic solution (59). The potential which develops when the working electrode comes into contact with a test solution should, in theory, be the result of the activity of the ion under investigation within the test solution (60). The concentration of the target ion can then be estimated through the application of the Nernst equation, the theoretical framework which relates the activity of an ionic species within a solution to temperature and electric potential.

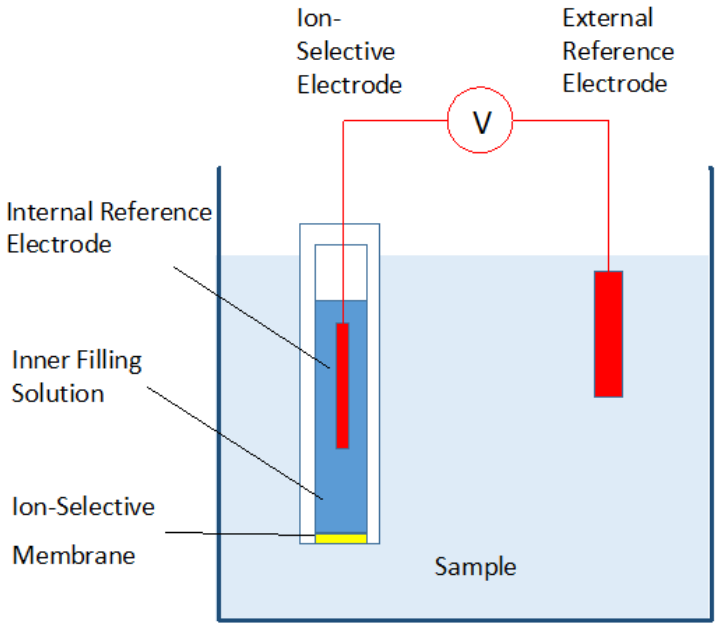

Figure 1.8. Simplified configuration of an ion-selective electrode which uses an inner filling solution

An example of a device which employs a reference electrode with an inner-reference solution is the Sodium Sensor Belt (SSB) (61). This makes use of an ISE setup with the intention of monitoring sodium levels within sweat in real time. The SSB is primarily aimed as a method by which hydration levels can be monitored however the diagnosis of CF is also a consideration of the authors (61). Inner solution electrodes were chosen for the device as previous attempts to use solid state electrodes, described later in this section, had resulted in non-Nernstian responses. The electrodes were fabricated in-house, with the reference electrode filled with a 0.1M potassium chloride solution on the day of use and capped using vycor glass. The working electrode surface was topped with a PVC membrane solution and a sodium ionophore layer. This ISE setup was connected to a potentiometer and the components held in place to a patient's lower back via a plastic platform attached to an elasticated belt (61). The sweat is absorbed from the surface of the skin via the capillary action of a collection patch and fed to the ISE setup.

The SSB was tested on study participants who were asked to undergo an hour's static cycle in order to stimulate sweat. However, this process of sweat stimulation is not suitable for participants with CF as they are at a higher risk of dehydration. Therefore, participants with CF exercised for a significantly shorter time. In order to assess the measurements obtained through the SSB, atomic absorption spectrometry (AAS) was used as a comparable method. The sodium concentrations measured through both methods maintain a similarity across the full testing procedure, despite noticeable scattering. The advantage of the SSB is that it offers real-time monitoring, therefore minimising the risk of the sample evaporating and giving inaccurately high concentration measurements (61).

1.3.2.2 Solid Contact Electrodes

Although ISEs which employ an inner filling solution have been developed to monitor concentrations of many ionic species, they possess a number of inherent disadvantages which include an insufficient resistance to a high pressure environment and a susceptibility to the evaporation of the inner solution (59). The latter limits the extent to which the electrodes can be miniaturised and therefore their ability to be incorporated into non-invasive, wearable sensors. Additionally, they require frequent re-calibration, affecting their ability to be reused (62). Instead, devices utilising solid, polymeric membranes on top of the electrode surface were developed. The membrane was intended to provide a homogenous medium for an ionophore layer. Although such ISEs do not possess an inner filling solution, they operate using the same principals of ion activity measurement through the potential between the sample and the membrane (59). The ionophore is comprised of neutral carrier molecules which act as a transport mechanism between these two layers for the ions of interest. These carrier molecules have a similar diameter to the target ions meaning that the ionophore implemented is specific upon the ion under investigation (60).

Many of the solid contact ISEs make use of a polymeric membrane consisting of poly(3,4-ethylenedioxythiophene):polystyrenesulfonate (PEDOT:PSS). This acts as an ion-to-electron transducer which enables the ionic activity of the sample to be converted to a measurable electric signal. The subsequent application of an ionophore then dictates the ion to which the electrode is sensitive to (59). The inherent flexibility of these materials has meant that there is a variety of ways in which they have been applied to a wearable device. These include electrodes printed onto a flexible plastic substrate (63), and those which are incorporated into skin-conforming materials and are able to measure multiple electrolytes and metabolites within the same wearable device (64).

1.3.2.3 Hydrogel Electrodes

Similar to the materials used in solid contact ISEs described in the previous section, hydrogels are polymeric materials. They are also, however, three-dimensionally cross-linked hydrophilic networks (65). The ability to alter the degree to which a hydrogel is cross-linked as well as its chemical composition means the internal structure of hydrogels can be tailored to suit a specific purpose. As such, hydrogels can be utilised in two different ways with regard to ISEs: to protect the surface of the sensor; and to modify the properties of the sensor (65).

Hydrogels were one of the first materials to be trialled as a mechanism to replace inner filling solutions within conventional ISEs (59,66). They had the advantage of drastically reducing the volume previously required by the liquid. They also provided a well-defined pathway for ion-to-electron transduction between the sample solution, and the electrode surface whilst forming a solid layer over the electrode surface (67). This, therefore, provided a more structurally stable surface upon which an ion-selective membrane, such as an ionophore, was able to be placed (66). For example, electrodes which incorporate a hydrogel layer have been manufactured which are sensitive to hydrogen and potassium ions (65,66).

Hydrogel-adapted electrodes are also commonly utilised as quasi reference electrodes (QREs). For example, a hydrogel layer may be applied over the surface of one electrode in a Ag/AgCl electrode pair and used as the basis of a Cl^- ISE. The hydrogel can then be immersed in a solution of high Cl^- concentration, allowing it to absorb the solution and act as a matrix to fix the Cl^- concentration at the electrode surface, in turn fixing the potential at that surface and provide a reference potential (65,68,69). The theory behind this application is discussed further in Sections 2.4.4 - 2.4.7.

This process has been used to manufacture several sensors for both healthcare and industry purposes with devices which measure the concentration of chloride ions in sweat (70–72) and in soils (68). The device described by Dam, Zevenbergen, and van Schaijk (70) utilises a UV-cured HEMA gel mixture, conditioned in 3M KCl for a prolonged period of time, to create the reference electrode. Alongside an array of Ag/AgCl working electrodes, these were incorporated into a wearable platform and tested on subjects, in which a sterile gauze was used to direct the sweat onto the collection area. The paper stated that the electrodes were stable for over a week in fluid and possessed a sensitivity toward chloride of 58 mV/dec (70). However, to date there does not seem to be any further development of a commercial device. Subsequent papers from the same authors have focussed on ISEs pertaining to potassium and sodium (71,73). Choi et al have also utilised chloride-saturated gel as a reference for a chloride ISE device (74–76). The first paper published by this group investigated the effect a salt bridge has on the potentiometric performance of a chloride sensor, namely in how its geometry affected the equilibration between the reference and test solutions. On-body tests were carried out by integrating the setup into a wristband. A reference chamber filled with 1M KCl saturated hydrogel (with internal Ag/AgCl electrode) and salt bridge was used in conjunction with a Ag/AgCl working electrode. A sensitivity of 50 mV/dec were reported by the team (74). The group's follow-up paper detailed the development of a wearable potentiometric sweat Cl^- sensor with an integrated salt bridge. This device utilised a 1M KCl-saturated agarose gel on

top of Ag/AgCl as a reference electrode. This was covered with a UV-curable resin. The salt bridge consisted of a small hole between the reference electrode setup and the test liquid (sweat) (75). The group claimed that the device displayed a sensitivity of 58.5 mV/dec. They have since used their device in direct comparison to the Sweat Test for the measurement of sweat Cl^- concentration, returning a correlation coefficient of 0.97 (76).

Although the design of such ISEs is relatively simple, there are a number of drawbacks which have seen developers opt for the technology described earlier in this section. Due to being in direct contact with any solution under investigation, the hydrogel's high capacity for absorbance means that over time it often takes on an excess of water causing the layer to expand. The added liquid means that Cl^- ions are able to slowly leach out, causing a drift in the measured potential and, hence, the device's sensitivity over time (67,71).

1.4 Measurement of Chloride

As the previous section has alluded, much of the effort in attaining a method of monitoring Cl^- concentration in sweat is being focussed on ISE technology. The ability to detect Cl^- levels in human sweat would be of importance in the diagnosis of Cystic Fibrosis and the monitoring of treatments of the disease. However, the loss of electrolytes such as Cl^- through sweat can also correlate to dehydration in individuals. Thus, a method of measuring such electrolytes in real-time would be of benefit to those involved in sport science.

Out with the area of medical care and fitness, monitoring of Cl^- levels can also be of significance in certain areas within engineering and agriculture. It is a substance which plays a major role in many corrosive processes, potentially compromising the structural integrity of a building, and its presence in soil can make an area of land unsuitable for farming (68).

The proceeding section will detail the techniques currently used to monitor Cl^- concentrations across a variety of disciplines.

1.4.1 Coulometric Titration

Titration is a well-established laboratory technique used to obtain the unknown concentration of a particular ion within a test solution. This is done by obtaining the point at which the correct amount of reagent has been added to represent chemical equivalence to a substance in the solution. In order to accurately measure this point, it has to be induced via a well-defined reaction and be characterised by a clear, observable change within the experiment (77). This change is known as the endpoint and the process by which it is achieved depends upon the area of research and the ion being analysed (77).

In the context of titration of biological samples, Cl^- concentration is ordinarily analysed using coulometric titration. Pure Ag^+ generating electrode(s) are immersed in the test solution and Ag^+ ions electrolytically released into the solution at a rate proportional to the applied current. These ions combine with the Cl^- within the test solution, they react to form an insoluble AgCl precipitate (78,79):

$$Ag^+ + Cl^- \rightarrow AgCl \quad (1.1)$$

The endpoint in this titration process is defined as the point at which all the Cl^- within the sample has precipitated and free Ag^+ ions become present within the solution. This is characterised by an increase in the potential measured between the indicator electrodes placed in the solution, triggering the cessation of the current generating the Ag^+ ion release. The current applied to the anode is of a known magnitude and is steady state, hence the quantity of Ag^+ ions released into the solution is directly proportional to the time in which the current is applied. The time taken to reach the endpoint, the titration time, is subsequently used to determine the concentration of Cl^- ions in the test solution by comparing it to the titration time of a solution of known Cl^- concentration (80,81).

One of the most common commercial devices which employ coulometric titration is the Chlorochek Chloridometer (ELITech Group, Puteaux, France) - an instrument which is used

to measure the chloride concentration within biological fluids. Coulometric titration is the industry-accepted method by which samples from Cystic Fibrosis sweat tests are analysed for chloride concentration. Therefore, the Chlorochek is often employed to analyse samples from Cystic Fibrosis sweat tests (14,82,83). For the device to operate effectively, the biological fluids being analysed must be incorporated into an assay solution consisting of nitric acid, acetic acid and gelatine. The latter acts to make the titration curve more linear whereas the acetic acid reduces the polarity of the solution, in turn, reducing the solubility of AgCl. The nitric acid provides the hydrogen atoms necessary for the cathodic reaction (78). Due to the work involved in the preparation of a test solution, a Chloridometer is mainly used as a benchtop apparatus within a laboratory setting (83).

1.4.2 Sweat Conductivity

The concept of gauging the concentration of a specific ion within sweat by measuring its electrical conductivity has been around for over half a century (84). It is based on the principle that the conductance of a solution consisting of electrolytes is dependent upon four properties: the species of ions present within the solution; the concentration of the ions; the temperature of the solution; and the geometry of the conductivity cell (84). Providing that a conductivity measurement device provides a durable conductivity cell and is able to maintain the test solution at a constant temperature, the electrical conductivity of the solution is, therefore, purely dependent upon the ion species contained within it and their respective concentrations (84) via the relationship:

$$L_s = (J_O - J_B)KF_D \tag{1.2}$$

Here: L_s represents the sweat conductivity ($\mu\Omega$ cm^{-1}); J_O and J_B the observed conductance of the sweat and blank solutions, respectively, at 25°C ($\mu\Omega$); K is the cell constant (cm^{-1}); and F_D

is the dilution factor. The latter accounts for the weight of the sweat sample and the volume of distilled water in which it is diluted. The cell constant is calculated using the equation:

$$K = {}^{L}/_{J} \tag{1.3}$$

where L and J are the specific and observed values of conductance for the sample solution for the specific test cell being used. This factor allows conductivity measurements obtained using different test cells to be compared to one another.

This method has been used in studies as a direct comparison to the traditional sweat test as a means of CF diagnosis. These studies reported that there was good correlation between the two methods (85,86). However, as there are many constituents present within sweat, including: sodium; potassium; chloride; and lactate, there are several contributors to the conductivity of the solution. As such, the value of conductivity retrieved represents a nonspecific measurement of the total anion activity within the solution (85). For example, the Cl^- concentration is estimated by way of the conductance value attributed to the NaCl molar concentration of the electrolyte (85,87). This means that the calculated Cl^- concentration is above that of the true value. Consequently, when sweat conductivity is used to diagnose CF, the indicatory concentrations used within sweat tests, as described in Section 1.2.1.1, must be elevated accordingly (86).

The Sweat-Chek (ELITech Group, Puteaux, France) is a common sweat conductivity analyser which is designed to be used in conjunction with the Macroduct® sweat induction apparatus as described in Section 1.3.1. The conductivity cell is situated below two stainless steel nozzles. These are covered by two tubes: one which allows the sweat sample to be transferred from the collection duct and into the conductivity cell; and one which stores the sample after it has traversed the cell. The conductivity cell gauges the electrical conductivity of the solution, after which the NaCl concentration is calculated and displayed on a digital display (87). Despite several studies reporting encouraging results when using the Sweat-Chek device to monitor

sweat chloride levels in comparison to the traditional sweat test method utilising coulometric titration (86,88,89), the latter technique remains the only approved method of diagnosing CF (14).

1.4.3 Colorimetric Absorbance

One method by which the chloride content of a sample may be measured is through the optical absorption properties of that sample. One such device which utilises this process is the HI 96753C Portable Chloride Photometer (Hanna Instruments, Woonsocket, RI). It is designed to measure chloride levels in water and waste water samples (90) by an adaptation of the mercury(II) thiocyanate ($Hg(SCN)_2$) method. This involves the addition of $Hg(SCN)_2$ to the solution under examination as well as iron(III) (Fe^{3+}) as a reagent. The Cl^- ions in the test solution cause the SCN ions to dissociate from the Hg^{2+}. The Fe^{3+} then binds with the SCN ions to form an orange-coloured complex which is a strong absorber of light of 450nm wavelength. The value of the complex's optical absorbance is proportional to the Cl^- concentration within the solution (80,90,91). If a light source of appropriate wavelength for absorption is directed at the solution, the fraction of incident light absorbed by the sample follows the Lambert-Beer law:

$$-log\frac{I}{I_0} = \varepsilon_\lambda C d, \tag{1.4}$$

$$A = \varepsilon_\lambda C d, \tag{1.5}$$

where A represents the absorbance, I_0 and I the intensity of light before and after absorption respectively, ε_λ the molar extinction coefficient at the wavelength λ, C the molar concentration of the sample and d the optical path the light undertakes (90). The HI 96753C is an all-in-one device which employs a light emitting diode (LED) light source to ensure a narrow wavelength spectrum. The arrangement which it employs is depicted in figure 1.9. The sample to be analysed is placed within a cuvette designed specifically for the instrument. This ensures that

the optical path for the light is fixed. Therefore, with both these variables fixed, the intensity of the light measured following the absorptive process is solely dependent upon the target ion concentration within the sample. After traversing the sample, the light is directed through a filter in order to obtain a narrow spectral bandwidth, as is shown in figure 1.9. It is then detected by a photoelectric cell which converts the incident light into an electric current. The magnitude of the resultant voltage is subsequently used by a microprocessor to calculate the chloride concentration of the sample, which is displayed on the screen of the instrument (90).

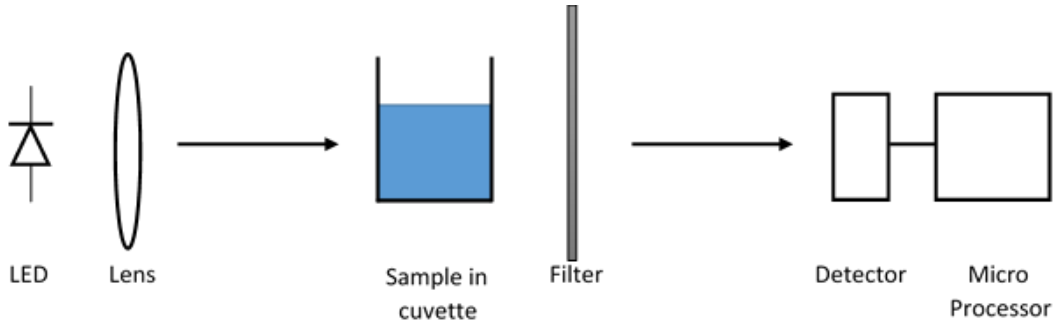

Figure 1.9. Schematic of setup employed by HI 96753C to measure Cl^- concentration within solutions via optical absorption.

More recently, this working principle has been used to develop wearable microfluidic patches to monitor sweat Cl^- concentration for sporting applications. The microfluidic channel contains a reagent which reacts with the Cl^- in the collected sweat to form a coloured solution whose intensity can subsequently be analysed using a smartphone camera for example (52,92).

1.5 Conclusion

In 1989, the gene responsible for the autosomal, recessive disease, Cystic Fibrosis, was isolated. It was discovered that mutations in the gene inhibited the production and/or function of the CFTR protein. This disrupts the regular transport of chloride across cells throughout many parts of the body, leading to life-limiting afflictions such as airway degradation and pancreatic disease. The malfunctioning Cl^- transport within sweat glands results in CF sufferers

displaying high sweat Cl^- concentrations. This symptom is the basis through which CF is diagnosed, by way of the CF Sweat Test. With the development of novel treatments which aim to restore CFTR function, the concentration of Cl^- within CF patients' sweat could potentially be used as a method of monitoring the treatments' efficacy. As described in Section 1.2, accounting for the preparation of the patient, iontophoresis, sweat collection, and subsequent analysis of the sample, the sweat test is a time-consuming procedure which requires highly trained medical staff to conduct it. This makes its use in monitoring the temporal changes in patients' sweat Cl^- over the course of their CFTR modulator therapy, for example, cumbersome for both the patients and the medical staff. Possessing a minimally invasive device capable of measuring sweat Cl^- levels quickly and accurately is, therefore, of clinical importance.

Given the significance attributed to detecting Cl^- ions in both a clinical and an engineering setting, there have been several techniques developed for the purpose of measuring chloride concentrations – such as ISE potentiometry.

The rise in popularity, and sophistication, of consumer wearable sensors has meant that this technology is increasingly being looked towards to carry out significant medical tasks, including the monitoring of sweat Cl^- concentrations. As a result, technologies like ISEs are being integrated into transdermal, wearable platforms with the intention of providing a non-invasive method of performing such tasks.

The motivation behind this doctoral project was to provide a method of measuring sweat Cl^- concentration which could allow the efficacy of emerging CF treatments to be monitored in a non-invasive and time effective manner. Therefore, the project aimed to develop a device:

- Capable of detecting the Cl^- concentration of an aqueous medium
- Sensitive to changes in the medium's Cl^- concentration over a range enveloping both healthy and CF sweat Cl^- levels (10 – 100 mM)
- Able to perform its function whilst placed on the skin

The remaining chapters will provide the theoretical background behind the project, detail the steps taken to develop a Cl^- sensitive device, and analyse its performance within the laboratory and on-body.

2. Theory

2.1 Introduction

This chapter aims to provide the technical framework and terminology through which the topics, ideas, and motivations concerning this thesis work may be introduced and discussed. The physiology of human skin and sweat ducts will be introduced to highlight the roles they play and how they function. From this the pathophysiology of CF is discussed, further highlighting the clinical need for a wearable Cl^- sensor. The chapter concludes by touching upon some topics in electrochemical theory which describe the concept behind the Cl^- sensor developed in this doctoral project.

2.2 Skin and Sweat Duct Physiology

The following subsections aim to provide the relevant background toward the physiology of the human skin in order to understand the environment in which wearable devices are expected to operate. Techniques used for drug delivery across the skin barrier, such as iontophoresis (used in the CF Sweat Test) will be described. Also discussed is the physiology of the sweat gland, its mechanism of secretion and the role it plays in ion reabsorption. From this we can better understand why this functionality breaks down in CF sufferers and why they exhibit elevated sweat Cl^- levels.

2.2.1 Skin Structure

The skin is the largest organ in the human body and plays a vital role in protecting against foreign bodies and maintaining homeostasis. It is composed of two different layers: the epidermis and the dermis (93).

The epidermis consists of several stratified layers. The outermost layer is the stratum corneum, which consists of 30 - 50 cell thick stratified squamous epithelium. These cells are avascular, keratinised and cornified and thus provides the body with protection against dehydration,

mechanical injury, and various pathogens which may lay on the skin surface (94,95). Below the stratum corneum is the epidermis, which can measure up to 180 μm in thickness. It is responsible for the generation of the stratum corneum and consists of three layers: the stratum granulosum; the stratum spinosum; and the stratum basale (94,96). The epidermis supports the production of new cells in order to replace the dead cells which are continuously sloughed away on the surface of the skin. As is depicted in figure 2.1, new cells are created at the stratum basale, nourished by the highly vascular dermis which lies beneath. These cells undergo continuous mitosis and migrate up through the epidermis, slowly dying as they progress further away from the blood supply. Keratinocytes, cells which produce keratin, are created within the epidermis. In a process called keratinisation, their composition begins to be dominated by keratin as they migrate toward the surface of the skin and degenerate. As the cells transition from the stratum granulosum into the stratum corneum they undergo cornification and transform into flattened, scale-like cells, corneocytes, which are surrounded by a highly crosslinked protein envelope. The processes of keratinisation and cornification ensure the cells are toughened and waterproof in order to provide an effective barrier to the external environment (94,96). Lying immediately below the stratum basale is the dermis, which in contrast to the epidermis, is highly vascular and is supported by collagenous, reticular and elastic fibres. Secretory glands, including sweat glands, are located in the dermis alongside hair follicles and numerous sensory receptors (94,97). This will be addressed in more detail in Section 2.2.2.

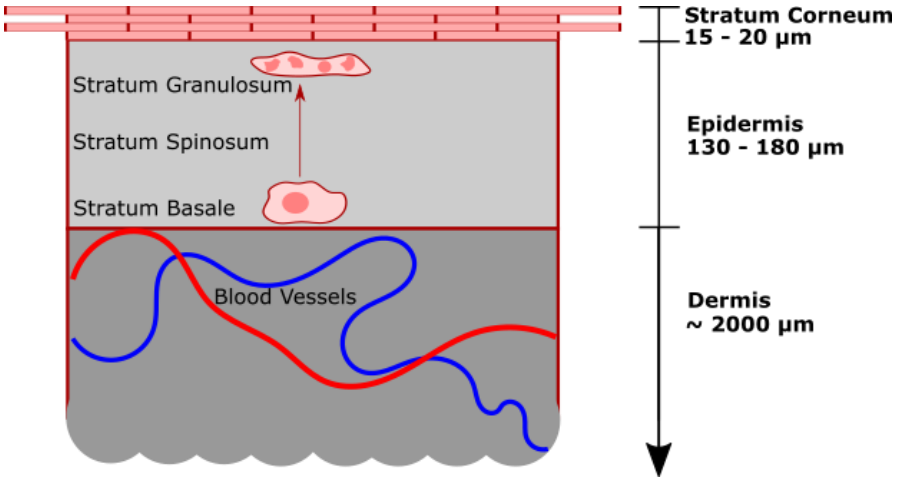

Figure 2.1. Schematic of composition of skin with approximate thicknesses. Depicted is the process of keratinisation of cells from the stratum basale through to the stratum granulosum. Cornification subsequently takes place and the cells form part of the highly lamellar stratum corneum (96).

2.2.1.1 Transdermal Drug Delivery

The accessibility of the skin makes it an appealing route for the delivery of drugs. Transdermal drug delivery can be split into two pathways: transepidermal, where the drugs must pass through the stratum corneum; or transappendegeal, which utilise sweat glands and hair follicles for the delivery of drug molecules (98). The earliest form of drugs which were designed for transdermal delivery were predominantly in the form of a wearable patch, for example a nicotine patch (99). The patch would contain a reservoir of the drug, creating a concentration gradient between the patch and the targeted dermis. The intention of this design is that the concentration gradient would encourage the drug to diffuse through the skin layers according to Fick's first law of diffusion:

$$J = -D\frac{dC}{dx} \tag{2.1}$$

where J is the molecular flux, D is the diffusion coefficient of the drug, and dC/dx is the concentration gradient (98). However, as was touched upon in the previous section, the stratum corneum consists of blocks of tough corneocytes surrounded by a lipid-rich environment, providing the body with an effective barrier to the outside environment (100). Therefore, only

certain drug molecules are able to permeate through this initial barrier. These tend to be small in size, allowing them to penetrate the stratified structure of the stratum corneum. As of 2014, each drug which had been given FDA approval for transdermal delivery had a molecular weight of < 500 Da (98,99,101,102). Such drugs also tend to be lipophilic but possess a sufficient aqueous and lipid solubility (log P (octanol/water) of between 1-3, where P is the partition coefficient of the molecule) to allow them to be resorbed into the body's systemic circulation (98,99). These echo Lipinski's rules which relate the physiochemical properties of compounds to the likelihood of their passive absorption. In addition to molecular size and lipophilicity, they state that molecules with five or more hydrogen bond donors and more than ten hydrogen bond acceptors will exhibit poor absorption or permeation (103).

The relative difficulty in molecules being able to penetrate the stratum corneum means that a very limited number of treatments are able to be delivered via a skin patch (98,99,101). Consequently, additional techniques have been developed to aid in the process of delivering these drugs through the skin and to their target. These can take many forms but can be split into two broad categories: passive and active methods. Passive methods involve the use of chemicals or emulsions to change the properties of the stratum corneum or the drug to maximise the drug's ability to permeate through the barrier. Penetration enhancers, such as alcohols, are commonly used for this purpose. They can have several mechanisms of action such as increasing the fluidity of the lipid-rich stratum corneum, or increaseing the drug's thermodynamic activity. Active methods, on the other hand, can act to mechanically bypass the stratum corneum barrier altogether, for example through the use of microneedles. Microneedles are minuscule projections of around 25 – 2000 μm in length and 1 – 25 μm in diameter and act to penetrate the stratum corneum to allow the direct application of drugs into the viable epidermis (98). Active methods of enhancing transdermal drug delivery can also utilise electricity, in the form of electroporation or iontophoresis. Electroporation involves the pulsated application of electric fields of strength 0.1 – 100 kV/cm upon the skin to form

aqueous pores in the lipid bilayers of the stratum corneum. This has shown to be effective in increasing the transport of a range of drugs, including those with high molecular weights, with drugs up to 40 kDa being effectively delivered via electroporation (98,100,104).

2.2.1.2 Iontophoresis

Iontophoresis, on the other hand, uses an application of a continuous or pulsed low voltage current to help drug molecules travel through the skin barrier (99). It is a technique which is extensively used in the diagnosis of CF, through the sweat test (Section 1.2.1.1). It involves the application of a small electric current, by electrodes placed on the skin surface, to enhance the movement of molecules across the skin. Iontophoresis induces three distinct mechanisms of transport: the drift current of charged molecules brought about by the applied electric field; an increase in the permeability of the skin due to the application of the electric field; and the convective, osmotic flow of polar or uncharged species (105,106). As such, the ionic flux caused by iontophoresis, J_{Ionto}, may be written:

$$J_{Ionto} = J_{drift} + J_{passive} + J_{conv}, \tag{2.2}$$

where J_{drift}, $J_{passive}$, and J_{conv} denote the ionic flux contributions of the drift current (caused by the electric field), passive diffusion (caused by the concentration gradient of the drug), and the convective flow, respectively (105). Mathematically, equation 2.2 can be described through a modified form of the Nernst Planck equation:

$$J_{Ionto} = -z_i m_i F C_i \frac{dE}{dx} - D_i \frac{dC_i}{dx} \pm C_i J_{conv}, \tag{2.3}$$

D represents the diffusivity (m^2s^{-1}) of the ionic species i, C is its concentration (mol l^{-1}), z its valency, m_i its mobility, F is Faraday's constant (C mol^{-1}), and E is the electrostatic potential (V) (106–108). Equation 2.3 comprises three additive terms which describe the contributions identified in equation 2.2, respectively, and highlight how the movement of molecules across the skin can be enhanced via iontophoresis. For example, the mobility of certain uncharged molecules, such as glucose, during iontophoresis is increased through the induced osmotic flow

(106). As such, enhanced levels of glucose are able to be extracted out across the skin barrier in a process known as reverse iontophoresis, and can therefore be used as a method of monitoring glucose levels (109–111). A notable example of this was the GlucoWatch®, mentioned in Section 1.3.2.3. Conversely, molecules possessing an electric charge will be affected by the applied electric field and can be transferred across the stratum corneum and toward their target through electrostatic repulsion. This process is depicted in figure 2.2, where a positively charged drug is delivered through the skin by the repulsion from the anode.

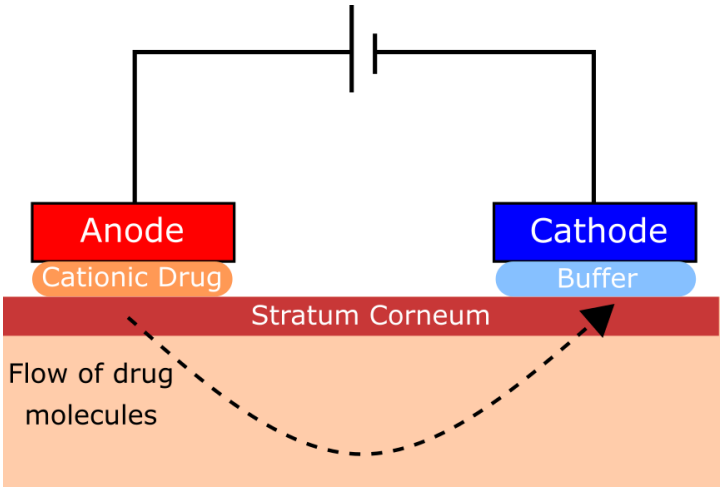

Figure 2.2. Schematic diagram showing the transdermal iontophoretic delivery of a cationic (positively charged) drug (98,112)**.**

This is the basis of iontophoretic delivery of the cationic drug, pilocarpine, in the CF sweat test, described in Section 1.2.2.1. There is still some uncertainty in the precise pathways of transport which the ions take through the stratum corneum. There is evidence which suggests that ions could use a paracellular route to traverse this barrier via a lipid layer surrounding the corneocytes (113). However, it is more widely acknowledged that the transappendageal route, via hair follicles and sweat glands, is one of the major pathways (107,113). Indeed, a study conducted in 1940 using iontophoretic delivery of methylene blue dye found that the patterns left by the dye were the sites of sweat gland pores, showing that the ions were readily accepted through these pathways (114). Both hair follicles and eccrine sweat glands contain a good

vascular network to allow their fat metabolising cells to receive nutrition. This then provides a pathway for drugs to be resorbed into the systemic circulation. This aspect becomes significant when the process of eccrine innervation sweat is discussed in Section 2.2.2.2.

It should be noted that this is a brief overview of transdermal iontophoresis. There are several factors which affect how well a drug can be transported through the skin via iontophoresis. These include the pH of the drug solution, the lipophilicity of the drug, and the impedance of the skin (98,100).

2.2.2 Sweat Glands

Sweat glands are a type of secretory gland within the body. They consist of tubular structures which secrete sweat onto the surface of the skin (94). There are two main types of sweat gland within the human body: eccrine and apocrine. Apocrine are the less numerous of the two. Their diameter is around ten times larger than eccrine sweat glands and they are restricted in their location to the axillary and pubic regions where they open into hair follicles rather than the surface of the skin as is the case with the eccrine variety. Although present from birth, apocrine sweat glands only begin their secretory function during puberty (94,115–117). It contrasts to the eccrine sweat gland in that it is controlled by the autonomic nervous system (ANS) and does not respond to parasympathetic stimulators such as acetylcholine (ACh), which will be explained further in this chapter with respect to the eccrine sweat gland. Apocrine sweat glands instead respond to strong emotional simuli (118). The exact function of apocrine sweat glands is not yet known, however their secretion does not play a major role in the thermoregulation of the body (115). The glands secrete a viscous, lipid-rich solution which can become odorous when exposed to bacteria when it reaches the surface of the skin (116,119).

Each person possesses around 2 – 4 million eccrine sweat glands in total, making them the most prevalent of the sweat glands within the body (115). They function as a thermoregulatory

tool for the body and are innervated through the sympathetic arm of the body's ANS. Figure 2.3 provides an illustration showing the difference in scale and location between eccrine and apocrine glands. Eccrine sweat glands are more pertinent to this study in terms of their ion reabsorption and how this effects the sweat Cl^- levels of CF sufferers, so these will be covered in more detail within this section.

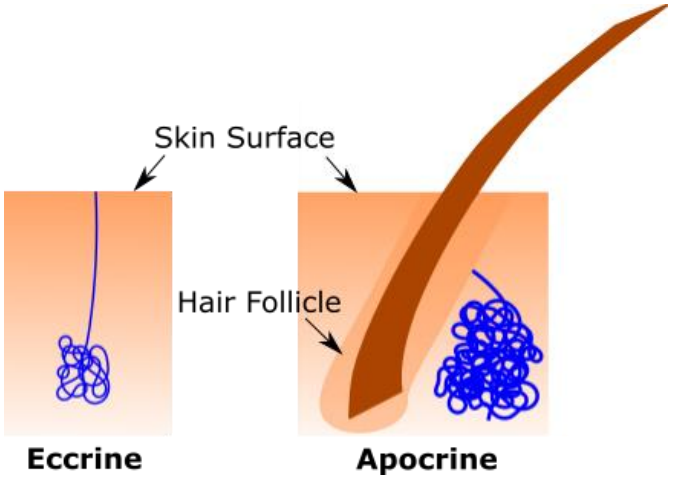

Figure 2.3. Illustration showing the differences in the scale and physical positioning of an eccrine and an apocrine sweat gland

2.2.2.1 Eccrine Physiology

Eccrine sweat glands are present across the near entirety of the body's surface area, with notable exceptions being the lips and the auditory canal (120). They are most densely populated in the glabrous areas, namely: the palms of the hand and soles of feet, where there are around 250 – 550 glands/cm^2. Density on non-glabrous skin is around 2 – 5 times less than this figure (94,115). The primary role of the eccrine sweat gland is to provide thermoregulation to the body by way of the evaporation of its secretion upon the surface of the skin. The glands also play a role in the retention of certain ions, including Cl^-. The remainder of this sub section will detail the physiological structure of the eccrine sweat gland and explore the mechanisms by which they perform their secretory and ion reabsorption functions (94,121).

2.2.2.1.1 Structure

Each eccrine sweat gland is in the form of an epithelial tubular structure measuring 3 – 5 mm in length, with the base, secretory coil lying deep in the dermis layer of the skin (93). They consist of two main functioning parts: the secretory coil and the duct, which are visualised in figure 2.4. In terms of its cellular makeup, the eccrine sweat gland is a bilayered gland. Basal and luminal cells comprise the inner and outer layers of the duct portion of the gland respectively. The secretory coil is made up of three cellular types: clear cells, dark cells, and myoepithelial cells. The latter form the inner layer of the coil while the clear and dark cells are the secretory (luminal) components (115,122).

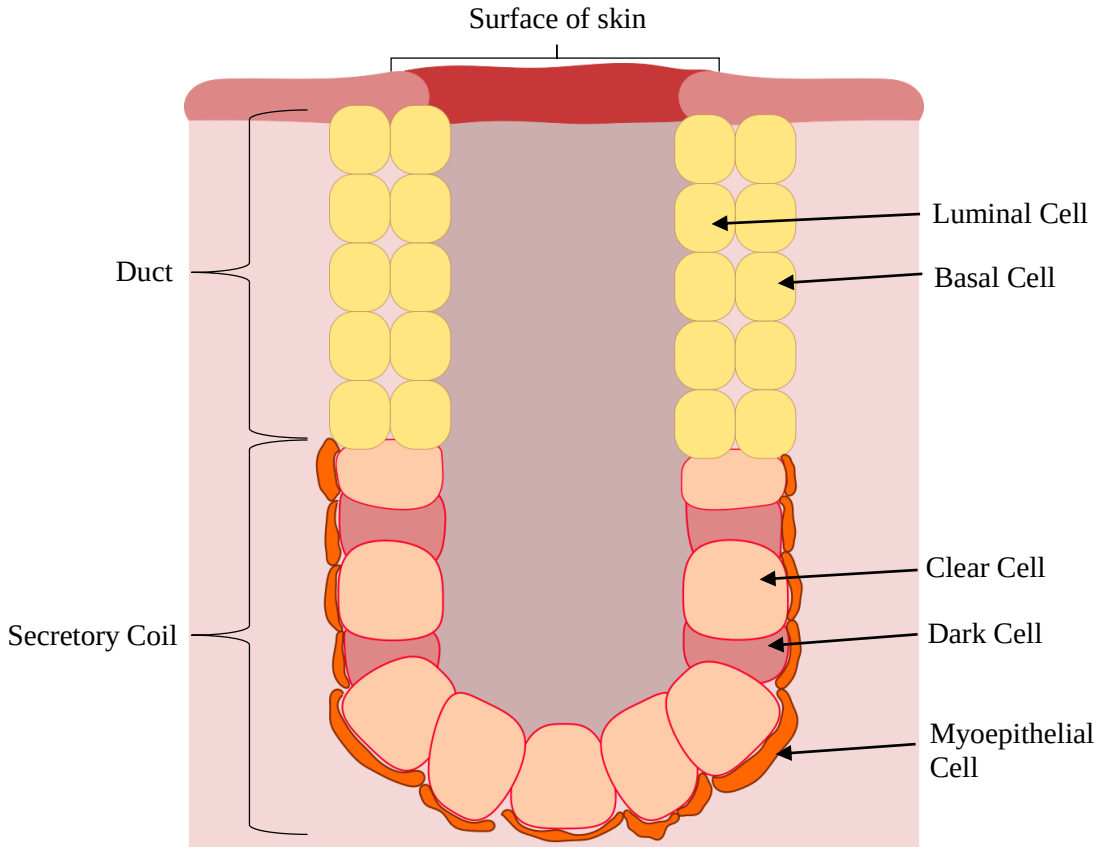

Figure 2.4. Cross-sectional view of an eccrine sweat gland showing a not-to-scale depiction of the duct and secretory coil components as well as the cells which comprise them. Adapted from (115)

Clear cells are responsible for the primary sweat secretion within the gland. The process through which this occurs will be covered in more detail in Section 2.2.2.1.2 below. Clear cells

contain a large amount of mitochondria, glycogen, and membrane villi, all of which point to the role the cell plays in the active secretion of water and electrolytes which make up the primary sweat (115,120–122).

Dark cells, by contrast, contain comparatively few mitochondria and membrane villi. Unlike clear cells, they can be stained using eosin, toluidine blue and methylene blue (123). This staining ability is what gives the cells their names. The exact function of dark cells is still unknown; however, they are known to secrete glycoproteins which react positively to periodic acid-Schiff (120,121).

Myoepithelial cells provide structural support for the secretory coil wall against the hydrostatic pressure it is subject to during sweat secretion (115,121). Their cytoplasm contains myofilaments with a small amount of mitochondria. In addition, myoepithelial cells are thought to provide a role in the regeneration of damaged sweat glands (120,122).

2.2.2.1.2 Mechanism of Secretion

Sympathetic nerve endings associated with the sweat glands release ACh which triggers a chain reaction of cellular contraction and ion flux through the cells of the secretory coil. Whilst some of the exact details are as yet unknown, it is generally accepted this flow of ions follows the Na-K-Cl cotransport model (124). This model is listed below and illustrated in figure 2.5.

1) Sympathetic stimulation leads to ACh release. This binds to the M_3 muscarinic receptor on the basolateral membrane of the clear cell (120).
2) This causes a sudden increase in the concentration of Ca^{2+} within the cytosol of the clear cell. The Ca^{2+} arrives via two sources: intercellular stores of the ion, likely from the endoplasmic reticulum; and through an influx from extracellular interstitial fluid (120,125,126).
3) K^+ and Cl^- ions are subsequently released from the cell through K^+ and Cl^- ion channels in the basolateral membrane and the apical membrane respectively (115).

4) This causes the clear cell to shrink (115,127).
5) Cell shrinkage signals the electroneutral influx of Na^+, K^+, and Cl^- by way of Na^+-K^+-$2Cl^-$ cotransporters (NKCC 1) (120,127,128).
6) The excess in intracellular Na^+ caused by step (5) leads to the activation of Na-K-ATPase pump on the basolateral membrane so that the cellular potential is prevented from becoming too large. This moves 3 Na^+ ions out of the cell in exchange for 2 K^+ ions. The pump action is combined with K^+ efflux from the cell via the K^+ channel on the basolateral membrane, ensuring that the cell potential remains negative (121).
7) This negative cell potential, in turn, provides the driving force which sees the cellular Cl^- transported across the apical membrane via Cl^- channels (115,121).
8) Increased Cl^- concentrations within the lumen depolarises the luminal membrane and provides an electrochemical gradient which attracts Na^+ to cross the tight cell junctions between the secretory cells. This pathway is termed the paracellular pathway and occurs because the basolateral membrane of the secretory cells are not readily permeable to the Na^+ ions (115,121).
9) Osmostic pressure between the cell and the lumen means that water can readily flow from the cell and into the lumen, via the aquaporin 5 (AQP5) channel. This creates a primary sweat secretion in the secretory coil lumen which is near-isotonic with respect to blood plasma (120,121,129).

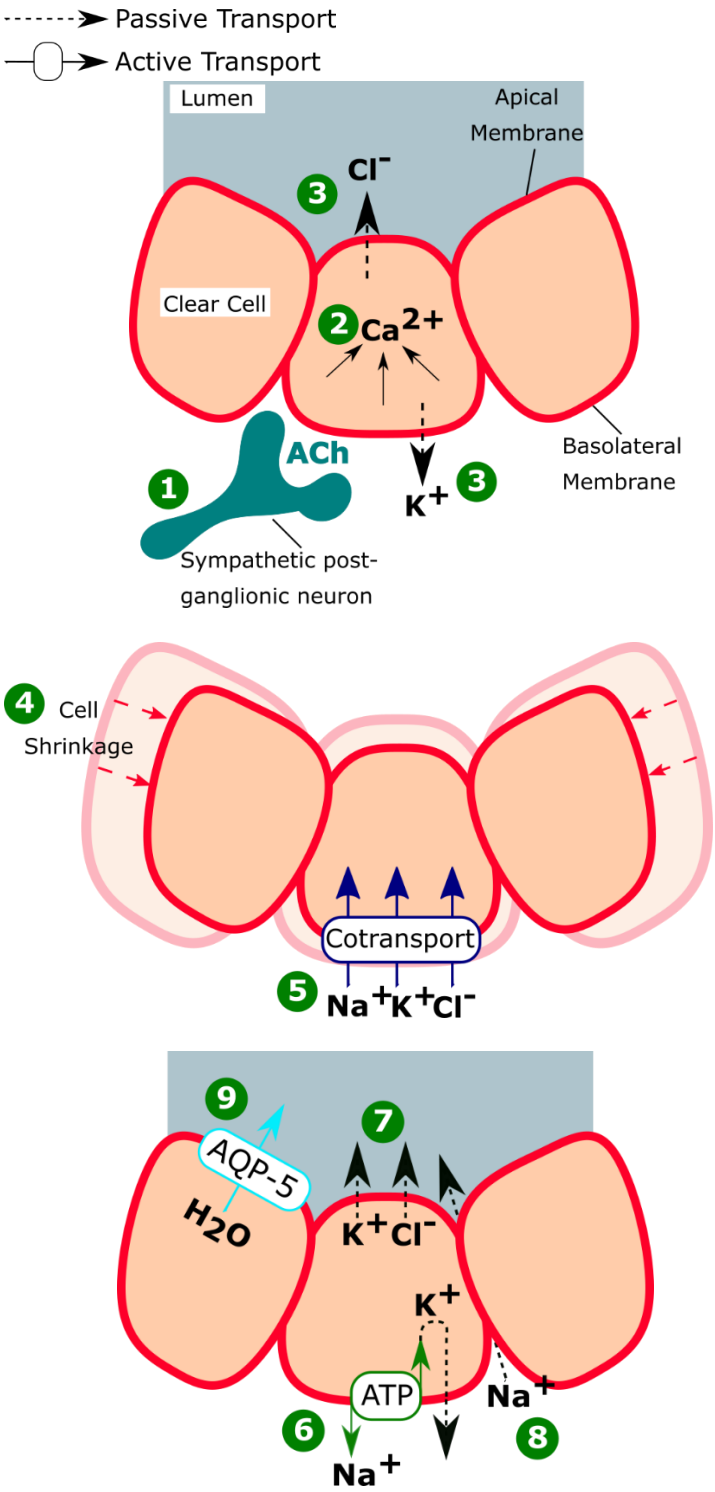

Figure 2.5. Illustration of the steps, described above, involved in the Na-K-Cl cotransport model of secretion of sweat from the secretory coil of an eccrine sweat gland. Adapted from (115).

2.2.2.1.3 Ion Reabsorption

The primary sweat which is secreted by the clear cells subsequently moves up, passing through the distal duct segment of the eccrine cell. As it does, its ionic composition is altered through the reabsorption of ions, primarily Na^+ and Cl^-, through the bi-cellular structure which comprises the proximal duct. Figure 2.6 provides an illustration of how these ions are reabsorbed. Na^+ ions are passively diffused across the apical membrane of the luminal cell from the primary sweat (126). On the basolateral membrane of the proximal duct's basal cells, Na^+ is actively transported across the membrane and into the interstitial fluid via Na – K – ATPase. This is accompanied with the passive efflux of K^+ ions through K^+ channels on the basolateral membrane (115,123). Cl^- ions diffuse passively through both the apical membrane of the luminal cell and the basolateral membrane of the basal cells via channels provided by CFTR proteins.

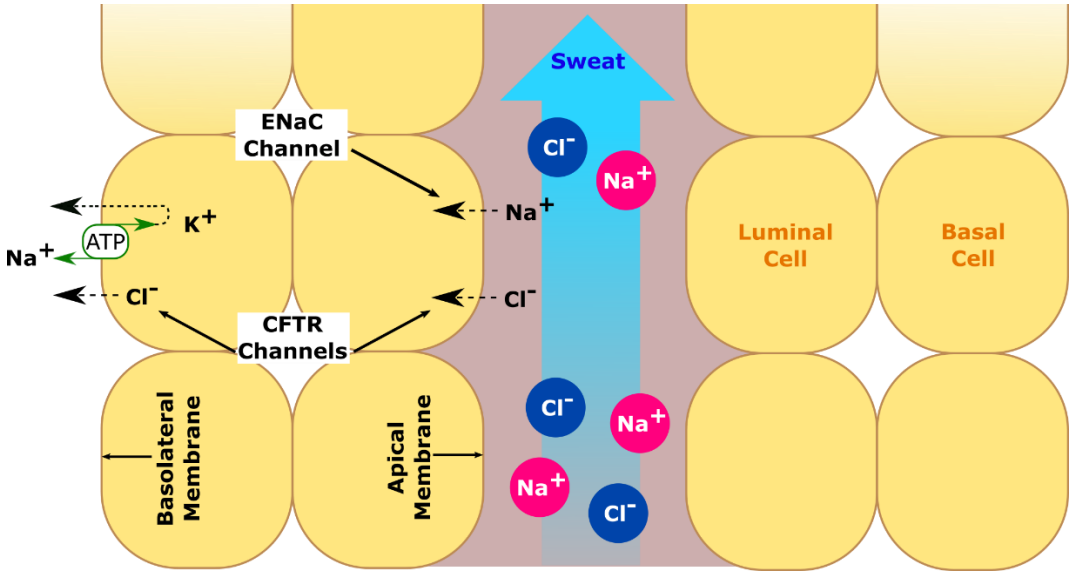

Figure 2.6. Ion reabsorption within the proximal duct of eccrine sweat gland (115).

The rate at which Na^+ and Cl^- ions are reabsorbed in the distal duct, and therefore the ionic composition of the final sweat solution, is predominantly determined by the number of CFTR

channels within the duct, and the rate at which sweat is secreted within the secretory coil (115,126). As CFTR channels are the gateway through which Cl^- ions are reabsorbed from the primary sweat, the abundance of CFTR channels within the duct has an obvious impact on the concentration of Cl^- in the sweat which reaches the surface of the skin. As has been touched upon, the defective nature of CFTR channels in CF patients is what gives rise to the characteristically high levels of Cl^- in their sweat (123,126). However, the activation of ENaC channels is dependent upon functioning CFTR channels, therefore the concentration of Na^+ ions is also affected by this factor (130). Additionally, it has been demonstrated that the rate of Na^+ reabsorption within the eccrine duct is inversely proportional to the rate of sweat production (131).

2.2.2.2 Eccrine Innervation

As the primary thermoregulatory mechanism in the human body, evaporation of sweat from eccrine sweat glands is integral to the homeostasis of the body. As such, innervation of the glands is controlled by the ANS (94). Studies have shown that sweating is in large part controlled by the core temperature of the body with a skin temperature being a contributing factor. It is considered that both these factors combine to give rise to the concept of mean body temperature, acting as a weighted sum of both the core body and skin temperatures, with the latter being more efficient in the induction of sweat (115,120,132). Thus, sweating is naturally induced through an increase in mean body temperature. This may occur in response to the temperature of the external environment or through physical exercise, though the latter also has several non-thermal factors which contribute to sweat output (133).

Eccrine sweat gland activity is controlled in large part by the hypothalamus. Signals are first triggered in the pre-optic hypothalamus and travel down the spinal cord, where neurons emerge from the ventral horn. The neurons synapse on the sympathetic ganglia where they interact with the sweat glands via the non-myelinated C fibres which entangle the periglandular tissue of the sweat glands (121,132,134). The majority of the sympathetic nerves which lead to the

eccrine glands are composed of cholinergic receptors whilst a smaller proportion are in the form of adrenergic receptors. As was mentioned briefly in previous sections, ACh is the neurotransmitter which stimulates the cholinergic receptors and initiates the sequence of events listed in Section 2.2.2.1.2 detailing the process of sweat secretion. This contrasts to the majority of sympathetic postganglionic neurons in the human body, which use norepinephrine as the neurotransmitter. Studies have shown that the effect of adrenergic agents, like norepinephrine, in stimulating the production of sweat is minimal in comparison to that of ACh. This demonstrates the predominantly cholinergic nature of eccrine sweat secretion (115,126,132). As such, ACh and similar analogues are regularly used to chemically induce the production of sweat for purposes such as CF diagnosis and CF therapy clinical trials.

The common most cholinergic agent used to stimulate the production of sweat is the ACh analogue, pilocarpine. This is the compound used to induce sweating within the CF sweat test, where it is applied to the skin in the form of a solid agar gel disc (containing 0.5% pilocarpine nitrate) (9). It is directed toward the target cholinergic receptors of the sweat gland via iontophoresis, see Section 2.2.1.2, where it stimulates a response and induces the production of sweat. The CF sweat test was detailed in Section 1.2.1.1. ACh can itself be used to induce sweat via iontophoresis (135,136) however, it only produces a small window of sweating due to the rapid time in which it is hydrolysed by the complementary enzyme acetylcholinesterase (AChE). In the body, such a response is preferable as rapid switching from sweating to non-sweating states is often needed. Pilocarpine and other cholinergic agents, such as carbachol, are preferred for sweat stimulation via iontophoresis as they are metabolised more slowly by the body and facilitate an extended period of localised sweating. Carbachol, for example hydrolyses 10^7 times slower than ACh. Using ACh alternatives, therefore, provides a better chance of obtaining a sample of sufficient volume which can be analysed (137).

2.3 Pathophysiology of Cystic Fibrosis

The role of the CFTR protein in regulating the transcellular movement of Cl^- as well as Na^+ ions (via indirect ENaC regulation) in eccrine sweat secretion was detailed in Section 2.2.2.1. However, CFTR proteins are present in the cellular makeup of organs throughout the body. Similar to sweat glands, they are located within the apical plasma membrane of the cells to facilitate the movement of Cl^- ions across the membrane (138). The absence or dysfunction of CFTR proteins which characterises CF, therefore, has a systemic effect on sufferers, impacting their body's ability in maintaining homeostasis in their airways, intestinal tract and other vital organs. The physical implications of this breakdown in functionality is dependent upon the cell's location within the body (22). The following section will describe some of the most frequent physiological complications associated with CF.

2.3.1 Airway

The exact mechanisms by which CFTR malfunction leads to the physical degradation of the airway is not yet fully understood. One aspect which seems to have a key role in how the CF airway develops, namely; is the lack of inhibition of the ENaC channel within the cells (2,139). CFTR acts to downregulate the ENaC channel activity within the airway epithelial cells of healthy individuals. Studies have shown, however, that CF airways do not appear to possess this function, leading to enhanced levels of Na^+ conduction through the cells (140,141). It is widely regarded that the hyper absorption of Na^+ within CF airways leads to the characteristic dehydration and thickening observed within CF patient's airway surface liquid (ASL), as is illustrated in figure 2.7 (129). A healthy ASL consists of a periciliary liquid layer beneath a mucus layer. The mucus is produced by submucosal glands and goblet cells and is inhabited by antimicrobial agents which act to kill bacteria. The periciliary liquid layer provides the cilia at the epithelium a medium in which to oscillate uninhibited and sweep away any mucous-covered bacteria. Consequently, when the ASL becomes thickened, the cilia are not able to function properly and cannot clear the airway effectively (22). This creates an ideal environment for bacteria to settle and grow, leading to chronic infections within the airway (2,142).

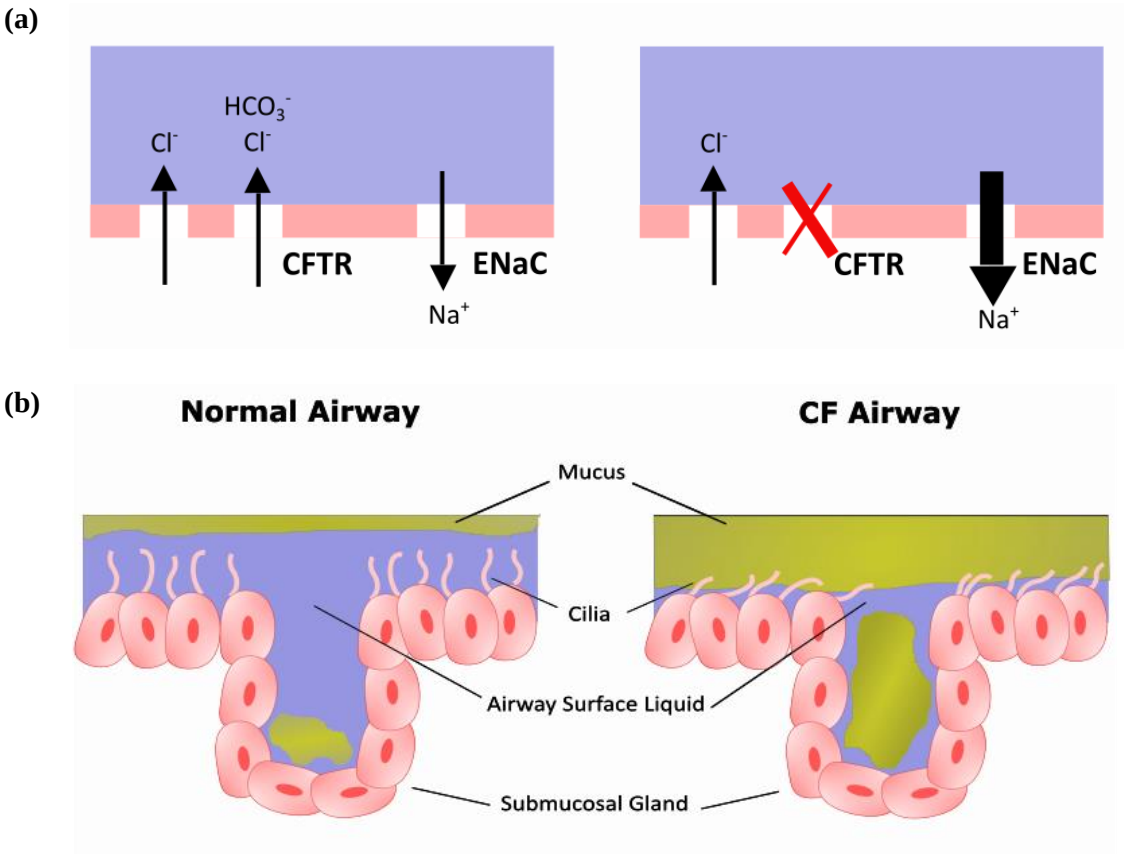

Figure 2.7. (a) schematic diagram showing the flux of ions across airway epithelia in normal and CF airways. The loss of CFTR function leads to enhanced Na^+ absorption via the ENaC channel. **(b)** illustration highlighting how, in comparison to a healthy airway, the CFTR dysfunction caused by CF leads to the ASL to become dehydrated and mucus-filled, inhibiting ciliary function.

It has been observed that *Haemophilus influenza* and *Staphylococcus aureus* are, on the whole, the two most prevalent airway microbial infections present in CF patients within the first few years of their life (143,144). Statistics obtained for the purpose of the UK Cystic Fibrosis Annual Data 2019 report (145) show, however, that the prevalence of certain pathogens changes with the age of the patient. Below the age of 16, only 5.2% of patients tested had a chronic presence of *Pseudomonas aeruginosa* in their airway. Over the age of 16, the percentage rose to 39.4% of patients, representing by far the most prevalent pathogen detected in the study (145). Once this species is established within the CF airway it is often impossible to fully rid (146). The near-constant presence of P.aeruginosa and other infections induces an inflammatory response in the airways which, over time, causes serious degradation in every day lung function and more acute pulmonary exacerbations (2).

2.3.2 Hepatobiliary

In a similar manifestation as that seen in the CF lung, the loss of CFTR function leads to a thickening of bile within the liver. Under normal circumstances, the protein functions on the apical surface of the cholangiocytes within the liver and is the main mechanism of hydration of the bile (147). The loss of this function results in thickened secretions and obstruction of the biliary network due to plugging. The subsequent accumulation of bile salts often results in hepatocyte injury as well as inflammation and fibrosis of portal tracts.

2.3.3 Pancreas

Pancreatic disease is observed in some form in almost every CF patient. It is thought to derive from ductal/glandular obstruction due to dehydrated macromolecules within the ductal lumen (147). The pancreas is an organ which carries out both endocrine and exocrine functions within the body (148). Consequently, pancreatic disease can manifest itself in a variety of ways within CF patients.

The common most type of pancreatic disease is exocrine pancreatic insufficiency. Here, the amount of enzymes secreted by the pancreas to aid in the digestion of the contents of the neighbouring intestine are not of great enough quantity (2,149). This results in an inability of nutrients to be adequately absorbed and leads to common clinical symptoms such as malnutrition, in addition to poor weight and growth gain (2).

However, the pancreas' endocrine function of maintaining the body's blood sugar levels, by use of the hormones insulin and glucagon, is also affected through the loss of CFTR function. The pancreas creates and releases these hormones via islet cells, which ordinarily contain the CFTR protein. Thus, as pancreatic disease progresses and the more islet cells are irrevocably damaged, there reaches a stage when the individual is not able to produce sufficient insulin and is said to have Cystic Fibrosis Related Diabetes (CFRD) (Haller et al., 2014; Ledder et al., 2014). A study conducted in 2008 involving 527 participants found that 19% of those aged between 11-17 suffered from CFRD compared with 45-50% of those over 40 years old (150).

2.3.4 Sweat Duct

The normal functionality of eccrine sweat secretion and ion reabsorption was detailed in Sections 2.2.2.1.2 – 3. It was explained that the fluid initially secreted from the secretory coil

is near-isotonic. Its ionic composition is altered through reabsorption to the surrounding cells via CFTR and ENaC channels as it moves up through the sweat duct (151). The reduced number of CFTR proteins and/or their dysfunction which is associated with CF, therefore, disrupts the normal process of ion reabsorption and effects the ionic composition of the sweat ultimately secreted on the skin surface. Unlike airway epithelial cells affected by the loss of CFTR function, CF skin sweat ducts do not exhibit an increase in Na^+ absorption. Conversely, Na^+ absorption has been shown to be greatly reduced within CF sweat duct cells (129). This is coupled with the characteristic loss of transmembrane Cl^- conductance, usually regulated by the CFTR protein. Consequently, CF patients exhibit significantly higher concentrations of Cl^- and Na^+ in their sweat in comparison to non-CF sufferers. Table 2.1 shows the measured concentrations of selected ions in the sweat of CF and non-CF patients. In this study, CF patients were found to have a sweat Cl^- concentration approximately six times that of non-CF individuals, and a sweat Na^+ concentration approximately four times higher (6,129).

Table 2.1. Average concentrations of selected ions in sweat samples of 500 CF patients and 1000 control patients (6).

	Sweat Ion Concentrations (mM)			
	Cl^-	**Na^+**	**K^+**	**Ca^{2+}**
Control	16	23	8	0.65
CF patients	99	101	15	0.83

The contrast in the sweat Cl^- levels shown in Table 2.1 is one of the reasons the sweat test (see Section 1.2.1.1) is the gold standard of CF diagnosis. However, the direct link between CFTR function and Cl^- levels within sweat means that sweat Cl^- concentration is now routinely used as a biomarker in examining the efficacy of emerging treatments (see Section 1.2.2) in drug trials (129,152). The time restraints brought about by the CF Sweat Test and its lab-based measurement process means it is difficult to routinely monitor this and reinforces the potential advantage of using a wearable sweat Cl^- sensor to monitor Cl^- levels over the duration of the treatment. Whether this is achieved by exploiting the (anecdotal) potential side effect of increased sweating from CFTR modulator treatments, or incorporating an iontophoresis setup, like the GlucoWatch® (Section 1.3.1.2), to stimulate secretion, there exists a clinical need for more accessible sweat Cl^- measurement.

2.4 Electrochemical Theory

This section provides an insight into the theoretical principles behind a potentiometric Cl^- ion sensor. It begins by introducing the electrostatic formation of a potential difference between two phases of matter. The makeup of an electrochemical cell will be explained as well as the act of measuring potential differences which develop within them. From this, the link between electrochemical potential and the activity of a chemical species is put forward through the introduction of the Nernst equation. Finally, the concept of a quasi-reference electrode (QRE) is introduced and its function within a potentiometric Cl^- ion sensor is explained.

2.4.1 Phase Potentials and their Interactions

When considering the potential of phases of matter, it is instructive to consider the electrostatic nature of their formation. In particular, the definition of potential within a phase is the work required to move one unit of charge from an infinite distance to a point of interest with spatial coordinates (x, y, z). In doing so, work is done against a coulombic field, and, assuming that there are no material interactions, the potential, ϕ, can then be described by (58,69):

$$\phi(x,y,z) = \int_{\infty}^{xyz} -\boldsymbol{E} \cdot d\boldsymbol{l}, \tag{2.4}$$

where **E** is the electric field strength and d**l** an infinitesimal tangent to the path in the direction of travel (58). If we then consider a single conducting phase of material, such as a metal or an electrolyte solution and move a hypothetical unit test charge from (x, y, z) to ($x^{'}$, $y^{'}$, $z^{'}$) within the conducting phase, then the potential difference between these points would be given by:

$$\phi'(x',y',z') - \phi(x,y,z) = \int_{xyz}^{x'y'z'} -\boldsymbol{E} \cdot d\boldsymbol{l}. \tag{2.5}$$

If there is no net current within the phase, then, by extension there is no net movement of charge carriers within the phase. Applying these conditions to equation 2.5 above, it is apparent that

the electric field strength within the conducting phase is zero, and the phase is in a state of equipotential (58).

With this in mind, we can look to Gauss' law, which relates the magnitude of charge, q, enclosed within a surface to the electric field strength of the surface:

$$q = \varepsilon_0 \oint \boldsymbol{E} \cdot d\boldsymbol{S}. \tag{2.6}$$

ε_0 is a constant of proportionality and is defined as the permittivity of free space (8.85×10^{-12} $C^2\,N^{-1}\,m^{-1}$), and d**S** is an infinitesimal vector perpendicular to the surface being considered (58). If we define the surface integral to be totally encapsulated within the conducting phase, then we have already seen that **E** = 0 in such a case. From Gauss' law, it then follows that there is zero net charge within the phase. Any excess charges which exist within a conducting phase must, therefore, be located on the surface of the conducting phase (58). This is depicted in figure 2.8:

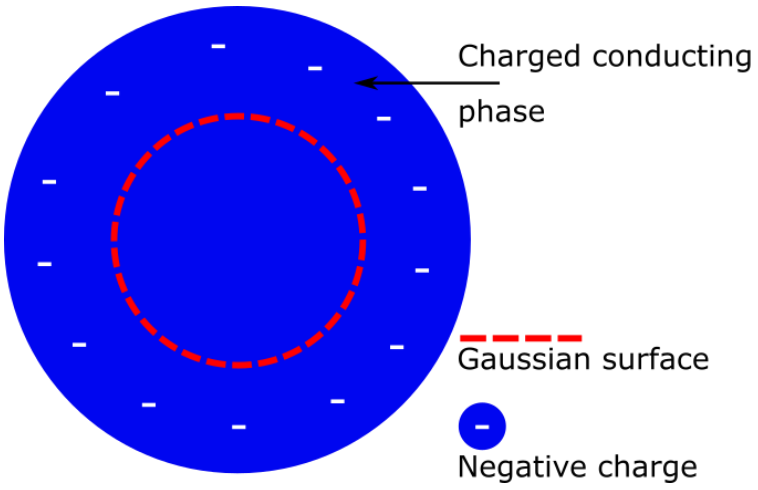

Figure 2.8. cross-sectional view of a conducting sphere. Excess charge gathers at the surface of the conducting phase. The internal Gaussian surface has not net charge enclosed. Adapted from (58)

In practical applications, we are more likely to encounter situations where two or more conducting phases are in contact with one another. It is informative to know what happens at such boundaries and how changes made to one of the phases can affect its neighbour. This may take the form of a charged metal sphere surrounded by an electrolyte solution such as that shown in figure 2.9 below. It is a simplified case showing a negatively charged metal sphere,

of net charge q_M, surrounded by an uncharged electrolyte solution, which in turn is surrounded by a vacuum.

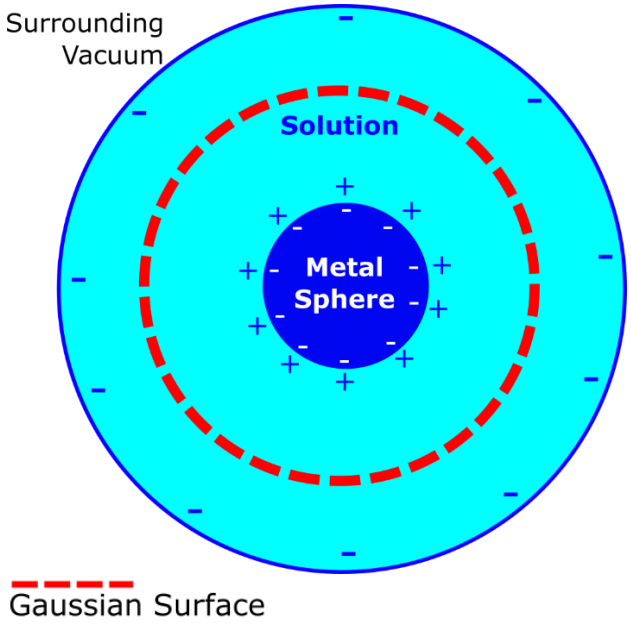

Figure 2.9. cross-sectional illustration showing the distribution of charge through an electrolyte solution when a charged metal sphere placed. Adapted from (58).

We know that the excess negative charges of the sphere will reside on its surface. In doing so, it creates a charge imbalance within the electrolyte with positive charges attracted to the solution – metal interface, as is shown in figure 2.9. We can apply Gauss' law by defining the surface to that shown in figure 2.9, completely inside the electrolyte solution phase. Since this is also a conducting phase in which there is no net current flowing, we again come to the conclusion that the electric field strength enclosed by the surface is zero and, hence, zero net charge exists. Therefore, at the metal – solution boundary there must be a distribution of positive charges, $q_{S,}$ such that it completely cancels that on the outer surface metal surface, q_M:

$$q_S = -q_{M.} \tag{2.7}$$

Likewise, if the Gaussian surface is shifted to the outer limit of the electrolyte, the enclosed charge must still be zero but the net charge of the metal, q_M, cannot have disappeared. We, therefore, conclude that outer limit of electrolyte has a distribution of negative charges with a

magnitude of q_M (58,69). This illustrates the interaction of charge carriers between phases of matter and how conditions imposed on a particular phase can affect the surrounding phases.

Taking the example of figure 2.9 further, we can plot the inner potential, ϕ, of each phase with respect to the distance from the centre of the metal sphere. This is depicted in figure 2.10.

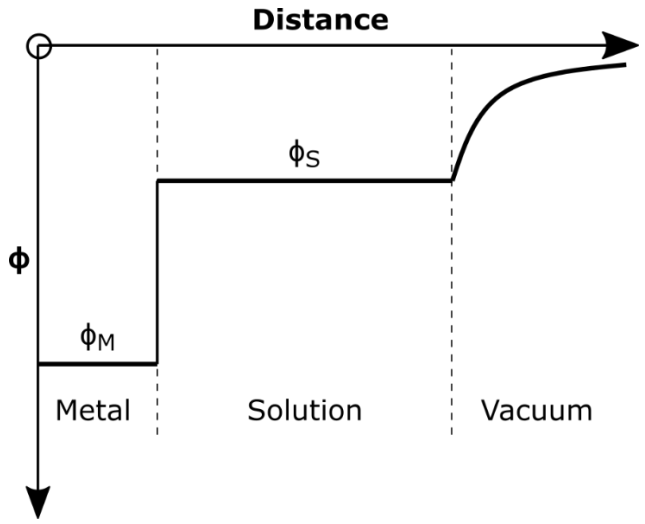

Figure 2.10. Example potential profile of a charged metallic sphere within an electrolyte solution. Potentials are plotted against radial distance from the centre of the sphere (58)**.**

The significant shift in potential between the solution and the metal shown in figure 2.10 is known as the interfacial potential difference and its magnitude is dependent upon the charge imbalance at the interface. As will be explained in the coming subsections the magnitude of the charge imbalance can be dictated by the types of materials which constitute the respective phases (58). The potential difference between material phases is, therefore, an indicator of the mechanics of interfacial boundaries and the composition of the materials involved.

2.4.2 Double Layer

The interfacial potential difference between a metal and a solution is less clear-cut than figure 2.10 would make it seem. This, in large part, is due to the existence of the electric double layer in which distributions of opposing charges gather at either side of the electrode – solution interface, analogous to a capacitor within an electrical circuit.

A capacitor is an electric component which stores energy in the form of an electric field. It consists of two metal plates separated by a non-conducting dielectric material (58). When placed in a circuit as shown in figure 2.11, the flow of electrons stemming from the battery is interrupted by the dielectric gap separating the two capacitor plates. The subsequent build-up of negative charge repels like-charges from the opposing capacitor plate before eventually the capacitor is said to be fully charged. At this point it acts like an open circuit and no current flows through the circuit. The magnitude of charge, q, accumulated by the capacitor at this point is given by the relation:

$$q = V \times C, \tag{2.8}$$

where V is the potential difference between the two plates measured, and C is the capacitance.

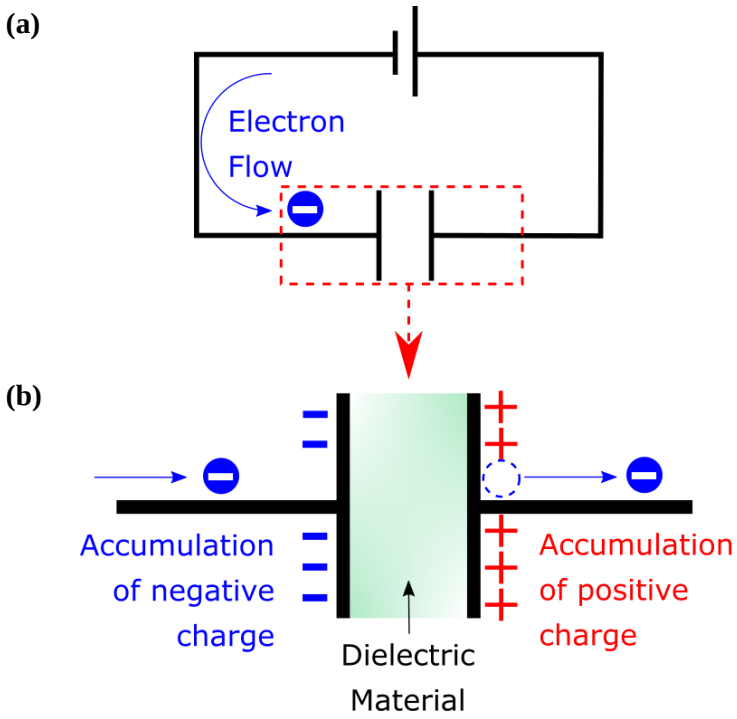

Figure 2.11. (a) Circuit diagram showing a capacitor connected to a battery power source. **(b)** Schematic representation of the charging capacitor. The accumulation of electrons on one plate causes the repulsion of electrons from the other. This leads to the build-up of positive charge on the opposing side and the formation of an electric field between the two plates.

In Section 2.4.1, equation 2.7, we have seen that at the interfacial boundary between a metal and a solution there, is a distribution of charge such that $q_S = -q_M$. This is analogous to the collection of opposing charges on the plates of a capacitor. In a situation involving a metal and a solution, however, the internal interactions between the solution's constituents means that

there is not a single, discrete separation of charges at the boundary. Rather, there are a number of layers between the metal and the solution. This structure is given the term: the electrical double layer. Its precise nature has been the subject of many models and revisions. We shall reference the Bockris, Devanathan, and Muller model to briefly discuss the nature of the double layer (153). In this model it is suggested that two layers exist between the metal and solution phases: the inner Helmholtz plane (IHP) with charge density ϕ_I C m^{-2}; and the outer Helmholtz plane (OHP). The IHP consists of solvent molecules (eg. water molecules) and ions which are said to be specifically adsorbed after either partially or completely losing the solvent molecules which surround them. The OHP consists of solvated ions (58,154), which, in combination with the bulk solution possesses a charge density of ϕ_D C m^{-2}. This model is illustrated in figure 2.12. The thickness of a double layer is dependent upon the concentration of the solution, with concentrations of 10^{-2} M usually possessing a double layer thickness in the order of 100 Å. As is shown in figure 2.12, the distance the IHP occurs from the metal is defined as the locus of the electrical centres of the specifically adsorbed ions. This layer possesses a charge density of σ_I. Due to the IHP, any solvated ions can approach the metal surface to a minimum distance defined by the locus of their electrical centres. Other such solvated ions can be diffused throughout the bulk of the solute phase, thus their contribution to the charge density, σ_D, comes from the entire diffuse layer, not just the OHP (58,153,154).

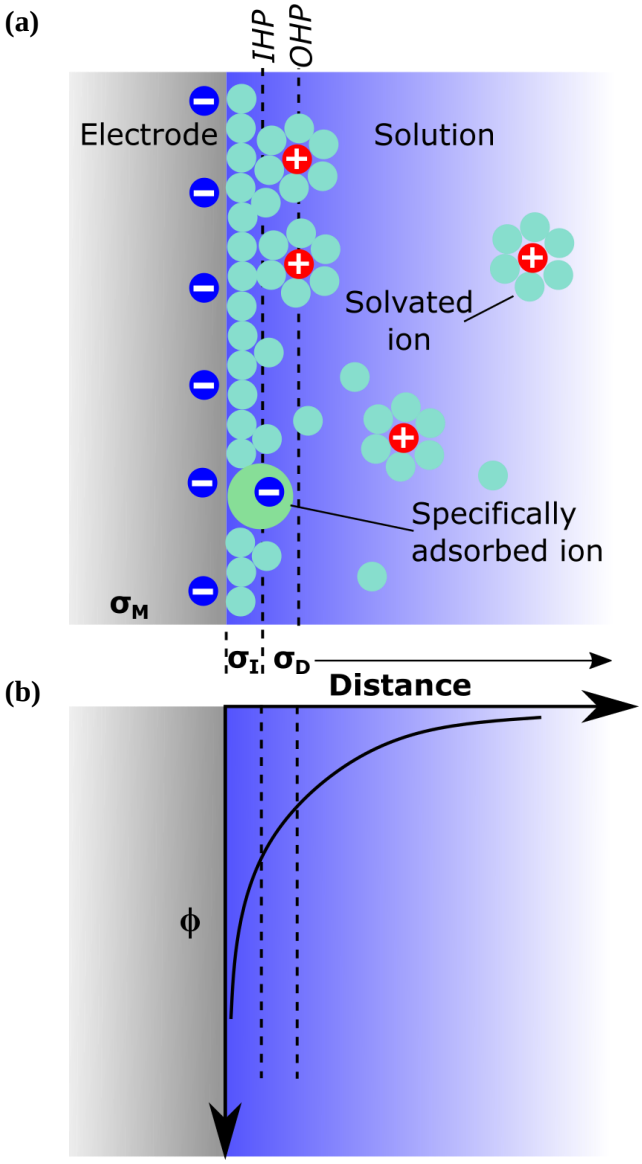

Figure 2.12. (a) Schematic representation of Bockris, Devanathan, and Muller model of the electric double layer caused by a metallic electrode in contact with an ionic solution. The contributions to each phases' charge density are shown alongside the positions of the IHP and OHP. The charge density attributed to the diffuse layer, $\sigma_{D,}$ extends into the solution bulk. **(b)** The resultant potential of the system, ϕ, plotted with respect to distance from the electrode surface (58,153)

We can therefore modify the relation given in equation 2.7 in Section 2.4.1 to represent the charge densities at the interfacial region, and to account for the contributions of the double layer:

$$\sigma_S = \sigma_I + \sigma_D = -\sigma_{M.} \tag{2.9}$$

The potential profile of a metal – solution interface with the effect of a double layer is shown in figure 2.12 (b). In comparison to the potential profile shown in figure 2.10, we can see that the interfacial potential difference between the metal and the solution is more diffuse due to the presence of the double layer.

2.4.3 Electrochemical Cells and EMF

In the study of electrochemistry, the material phases of interest are predominantly in the form of an electronic conductor (an electrode) and an ionic conductor (an electrolyte). The chemical reaction which occurs at such an interface is known as a half-cell reaction. For example, if a copper (Cu) electrode is immersed in a Cu^{2+} electrolytic solution, the electrode will oxidise and lose electrons to the surrounding liquid as characterised by the half-cell reaction:

$$Cu \rightarrow Cu^{2+} + 2e^{-}. \tag{2.10}$$

This can also be notated:

$$Cu|Cu^{2+}, \tag{2.11}$$

Where the vertical line represents the phase boundary between the solid Cu electrode and the Cu^{2+} electrolyte. As described in the preceding sub-sections, the subsequent collection of electric charges at both sides of the interface means there is a potential difference between the two phases. However, the potential difference across a single interface cannot be measured. This is because the physical act of observing the electrical properties of a phase boundary would inherently require the addition of at least one more interface (58). Instead, we must utilise an electrochemical cell where at least two electrodes are present. Doing so means that the difference between the interfacial potentials of each of the electrodes becomes the observable quantity. This is known as the cell's electromotive force (EMF), the maximum potential difference between the two electrodes. It is the summation of the individual interfacial potentials which make up the cell. For example, let us introduce another half-cell in the form of a Zinc (Zn) electrode immersed in a Zn^{2+} electrolyte solution such that its half-cell reaction is:

$$Zn \rightarrow Zn^{2+} + 2e^{-}. \tag{2.12}$$

or

$$Zn \mid Zn^{2+}. \tag{2.13}$$

By connecting the Zn electrode configuration of equation 2.13, to the Cu electrode configuration, equation 2.11, as is shown in figure 2.13, an electrochemical cell is created. It may be described by the two half-cell reactions at each electrode:

$$Zn \rightarrow Zn^{2+} + 2e^{-}, \tag{2.14}$$

$$Cu^{2+} + 2e^{-} \rightarrow Cu, \tag{2.15}$$

or:

$$Zn \mid Zn^{2+} \mid\mid Cu^{2+} \mid Cu, \tag{2.16}$$

where the double vertical lines represent the salt bridge shown in figure 2.13. Zn has a stronger tendency to lose electrons than does Cu, therefore when the two half cells are connected as in figure 2.13, electrons vacated from the Zn electrode migrate across the cell and combine with Cu^{2+} ions onto the surface of the Cu electrode. The salt bridge is necessary to provide a pathway for the ions in the solutions to move and complete the cell. Convention dictates that the electrode where reduction takes place is written on the right hand side.

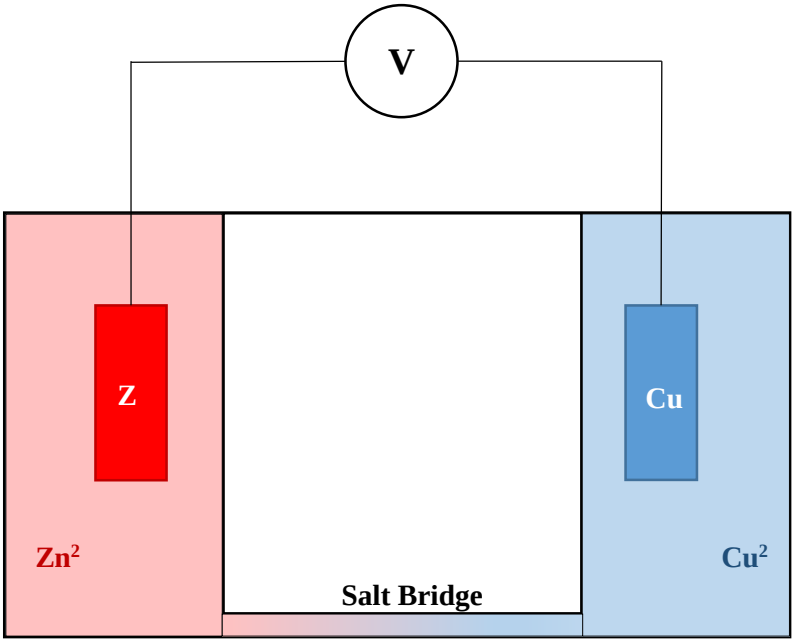

Figure 2.13. Schematic representation of $Zn|Zn^{2+}||Cu^{2+}|Cu$ electrochemical cell.

Cells like this are called Galvanic cells, where reactions occur spontaneously at the electrode contacts when they are connected via a salt bridge (58). We can define any such cell's EMF as the difference between the potentials developed at the two electrodes by the respective half reactions:

$$E = \phi_{right} - \phi_{left}. \quad (2.17)$$

Here, ϕ_{right} and ϕ_{left} denote the potential of the electrodes at the right and left of a cell notation (58,154,155). This concept is visualised in figure 2.14 by plotting the potential profile across our example $Zn|Zn^{2+}||Cu^{2+}|Cu$ electrochemical cell. A cell's EMF can also be described as its open circuit potential (OCP). This abbreviation will be used throughout this thesis to denote the measured potential between two electrode contacts value obtained using open circuit potentiometry (see Section 3.3).

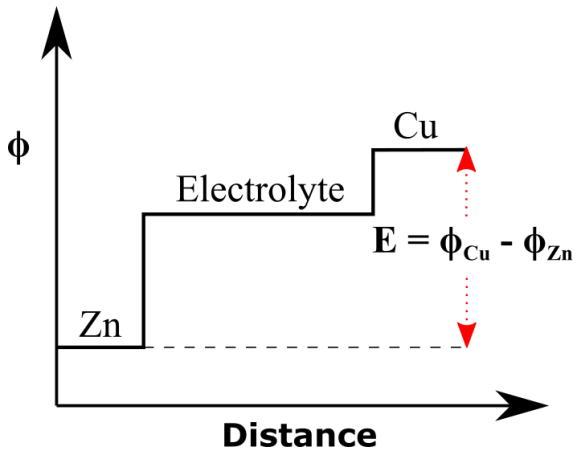

Figure 2.14. Simplified graphical representation of the potential profile across an electrochemical cell containing Zn and Cu electrodes. The cell's measurable potential is the difference between the potentials at the electrode contacts.

2.4.4 Reference Electrode

Given the myriad of half cells which could be combined to create an electrochemical cell, the measurement of any given cell's EMF is arbitrary. If, however, one of the electrodes used was such that its potential was known and fixed, then the measured potential would vary purely with the potential developed at the cell's other electrode. This is a way of standardising half of the electrochemical cell. The term given to the electrode of fixed potential is a reference electrode (RE), whereas the electrode whose potential is measured is the working electrode (WE). As such, when measuring the potential of an electrochemical cell, we are measuring the potential of the working electrode with respect to the known potential of the reference electrode. The internationally accepted standard RE is the Standard Hydrogen Electrode (SHE) which consists of a platinum, or another inert solid, electrode contained within a tube through which hydrogen gas can be fed through at a pressure of 1 atm (58,154,155). The tube is immersed in a hydrogen solution of unit activity (1 M). The half reaction which occurs is given by:

$$2H^+(aq) + 2e^- \leftrightarrow H_2(g), \tag{2.18}$$

where (aq) and (g) denote the aqueous and gaseous phases respectively. By convention, this half reaction has a value of 0 V. Furthermore, we can define a new parameter, the standard

potential, E_0, as the potential measured under standard conditions: atmospheric pressure (1 atm); a temperature of 25°C (275 K); and chemical species at unit activity (1 M). Thus, the standard potential for the half reaction shown in equation 2.18 is $E^0 = 0$ V. There are a number of other reference electrodes which are commonly used in experimentation including the Saturated Calomel Electrode (SCE) [$E^0 = +0.244$ V vs SHE] and a Ag/AgCl electrode [$E^0 = +0.197$ V vs SHE].

To summarise, the use of a reference electrode is necessary within electrochemical cell experiments as it provides a method by which we can measure and meaningfully define the potential which develops at the working electrode.

2.4.5 Nernst Equation

The Nernst equation provides a link between the measured potential of an electrochemical cell and the concentrations of the chemical species involved within the cell. If we consider the simple setup of a metallic electrode immersed in an aqueous solution of its own salt, such as the $Cu|Cu^{2+}$ half-cell in Section 2.4.3, then the particles at the interfacial boundary will be subject to a reduction-oxidation (redox) reaction. Such reactions involve the transfer of electrons from one species to the other. Taking a reduction reaction as an example, it may be written, generally, as:

$$O + ne^- \rightarrow R, \tag{2.19}$$

where O is the oxidised species, R the reduced species, and n the number of moles of electrons exchanged taken up by the reducing species. We can consider the change in the Gibbs free energy, ΔG (J), which would occur as a result of the electron exchange. ΔG is a measure of the spontaneity of a reaction. A negative value signifies a reaction is spontaneous: work is done by the cell, and its free energy decreases. Conversely, a positive value suggests that a reaction is not spontaneous: work has to be done on the system for a reaction to occur, increasing its free energy (58,156). The reduction reaction of equation 2.19 is spontaneous and will therefore have

a negative ΔG value. The Gibbs free energy is also the maximum amount of useful work that can be performed in a process (under constant pressure and temperature) (157). This can be combined with the expression for the work done, W, performed by an electrochemical cell as:

$$W = total\ charge\ \times\ potential, \tag{2.20}$$

$$W = nFE = -\Delta G, \tag{2.21}$$

$$\Delta G = -nFE. \tag{2.22}$$

Here, n is the number of moles of electrons, F represents the Faraday constant - the charge of a mole of electrons (96485.3 C mol^{-1}), and E is the potential of the cell (V) (58,157). Similarly, the change in free energy at standard conditions is given by:

$$\Delta G^0 = -nFE^0. \tag{2.23}$$

Furthermore, the thermodynamic identity relating the free energy of a reaction to the equilibrium constant of the reaction, K, is defined as:

$$\Delta G = \Delta G^0 + RT \ln K. \tag{2.24}$$

Here, R is the universal gas constant (8.3145 J mol^{-1} K^{-1}), and K represents the quotient of the activities of the individual chemical components within the reaction. In the case of the reduction reaction of equation 2.19, the equilibrium constant would take the form:

$$K = \frac{a_R}{a_O}, \tag{2.25}$$

Where $a_{R,O}$ represent the activities of the reduced and oxidised species respectively. Activity is a measure of the effective concentration of a species and is used to account for the non-ideal behaviour which stems from the interaction between molecules within the solutions. A species' activity is linked to its concentration through the relationship:

$$a_X = \gamma[X], \tag{2.26}$$

where a_X is the activity of species X (M), γ is its activity coefficient, and [X] is the concentration (M). In dilute solutions, the activity coefficient tends towards unity and the activity coefficient

approaches the value of the concentration. Unless otherwise stated, concentration terms will be used in this piece. Substituting equations 2.22 and 2.23 into equation 2.24:

$$E = \Delta E^0 - \frac{RT}{nF} \ln K. \tag{2.27}$$

This is the general form of the Nernst equation, which relates the measured potential of an electrochemical cell to the relative concentrations of the species involved in the cell reaction (58,154,156,157).

2.4.6 Concentration Cell

It has been demonstrated that a chemical potential develops at the interface between an electrode and the solution which surrounds it. The measurable potential of an electrochemical cell is subsequently defined as the difference between the potentials of the cell's constituent electrodes. However, if both of the electrodes were the same type then we create what is known as a concentration cell, consisting of two half cells which differ only in the concentration of their respective analytes. For example, take a concentration cell consisting of two Ag/AgCl electrodes: one placed in a Cl^- solution of 3 M concentration; the other placed in a Cl^- solution of concentration 1mM:

$$Ag(s)|\, AgCl\ (s)|\, Cl^-(aq, 0.001M)||Cl^-(aq, 3M)\ |AgCl\ (s)|Ag(s). \tag{2.28}$$

Where (s) and (aq) signify solid and aqueous phases respectively. The half reactions taking place at each electrode surface may be written:

$$AgCl\ (s) \leftrightarrow Ag^+ + Cl^-\ (aq), \tag{2.29}$$

$$Ag^+ + e^- \ \leftrightarrow Ag(s), \tag{2.30}$$

which can be combined to give the net reaction taking place at each electrode:

$$AgCl\ (s) + \ e^- \leftrightarrow Ag(s) + Cl^-\ (aq). \tag{2.31}$$

According to the Nernst equation then, at each electrode surface:

$$E_{right/left} = E^0 - \frac{RT}{nF}\ln\left(\frac{[AgCl(s)]}{[Ag(s)][Cl^-(aq)_{right/left}]}\right), \quad (2.32)$$

where "right/left" refers to the notation of the cell in equation 2.28 above, and [X] represents the concentration of species X in molar units. Adapting the relation of equation 2.17, from Section 2.4.3, the measured potential of an electrochemical cell may be written:

$$E = E_{right} - E_{left}. \quad (2.33)$$

Therefore, in this instance, we can write:

$$E = \frac{RT}{nF}\ln\left(\frac{[AgCl(s)]}{[Ag(s)][Cl^-(aq)_{left}]}\right) - \frac{RT}{nF}\ln\left(\frac{[AgCl(s)]}{[Ag(s)][Cl^-(aq)_{right}]}\right). \quad (2.34)$$

As the two electrodes are of the same material, both will have the same value of standard potential, E^0, and they cancel out. In other words, our points of reference are exactly the same for each of the half cells involved. Equation 2.34 can be simplified by noting that the concentrations of the solid Ag which comprise the electrodes will be equal and remain stable. Likewise, similar assumptions can be made for the stability of the AgCl salt which coat the electrodes as it is a sparingly soluble substance (68). Equation 2.34 then simplifies to:

$$E = \frac{RT}{nF}\ln\left(\frac{[Cl^-(aq)_{right}]}{[Cl^-(aq)_{left}]}\right), \quad (2.35)$$

where if a temperature of 25°C is assumed, recognise that n = 1 for this configuration, and convert to a logarithm of base 10 by multiplying by a factor of 2.303, can be written:

$$E = 0.059 \times \log_{10}\left(\frac{[Cl^-(aq)_{right}]}{[Cl^-(aq)_{left}]}\right). \quad (2.36)$$

It is important to note that equation 2.36 is in the form of a linear equation, with a gradient of value 59 mV/decade. The unit of $decade^{-1}$ simply relates to the fact that the x-axis in this linear equation is in base 10. This linearity provides an effective way of evaluating the performance of ion-selective electrodes and will be used in later sections. Substituting in the concentration values postulated earlier into equation 2.36 then gives:

$$E = 0.059 \times \log_{10}\left(\frac{3}{0.001}\right), \tag{2.37}$$

$$E = 0.205\,V. \tag{2.38}$$

What has been described, therefore, is an electrochemical cell where the OCP is dictated by the relative Cl^- concentrations within the respective half cells (58,154,155,158).

This is an important concept and forms the basis of the working principle of the Cl^- sensor this report is centred around. The following subsections will detail the further steps taken to develop this concept into a Cl^- sensor.

2.4.7 Quasi Reference Electrode

The concentration cell configuration can be further adapted if the Cl^- concentration in one of the half cells was fixed. Doing so would ensure, in theory, that the OCP would solely be proportional to the Cl^- concentration at the surface of the one remaining, working electrode:

$$E = 0.059\,log_{10}\left(\frac{[Cl^-(aq)_{FIXED}]}{[Cl^-(aq)_{left}]}\right). \tag{2.39}$$

This describes one potential configuration of a Cl^- sensor. The notation of which side of the cell is fixed is arbitrary. The process of fixing the Cl^- concentration in one of the half cells is another way of saying that the potential of one of the electrodes is fixed. This idea was covered in Section 2.4.4, where the necessity of having a reference electrode in order to measure the potential of an electrochemical cell was discussed. Common reference electrodes, however, have a number of drawbacks which can make their application within a concentration cell undesirable. This could take the form of the materials used for the electrode. A SCE, for instance, utilises mercury for its operation. In the context of wearable devices this is clearly undesirable. Other reference electrodes, like the SHE, tend to be bulky and impractical given their operational reliance on a flow of pure hydrogen gas.

Because of this, it is common to use configurations which fulfil the role of a reference electrode without possessing some of the rigorous attributes needed to be defined as such. These are

given the term quasi reference electrodes (QREs) (58,159,160). They often consist of a simple metallic electrode, such as a platinum wire, placed directly into the analyte solution. Their operation based on the assumption that if there is no appreciable change in the makeup of the bulk analyte solution then the potential of the QRE would stay relatively constant. However, the magnitude of this potential is unknown, therefore QREs like this must be regularly calibrated by measuring its potential against a bona fide reference electrode under a well-defined redox reaction (58,160).

In the context of a concentration cell, the application of a QRE is slightly different to the scenario of the platinum wire described above. As the electrodes which make up the cell are of an identical makeup, there would be no concentration-induced potential difference between them if exposed to the same analyte. Therefore, a method of fixing the concentration at the surface of the one of the electrodes must be attempted. This can be done by surrounding one of the electrodes with a matrix containing, and maintaining, a high concentration reference solution. To visualise this, take the Cl^- concentration cell described above in Section 2.4.6 but place the 3M Cl^- half-cell within a matrix which envelops the electrode contact. This is then placed, alongside the remaining electrode, in the 1mM Cl^- analyte, as shown in figure 2.15.

$$Ag(s)|\,AgCl\,(s)|\,Cl^-(aq, 0.001M)||Cl^-(matrix, 3M)\,|AgCl\,(s)|Ag(s). \qquad (2.40)$$

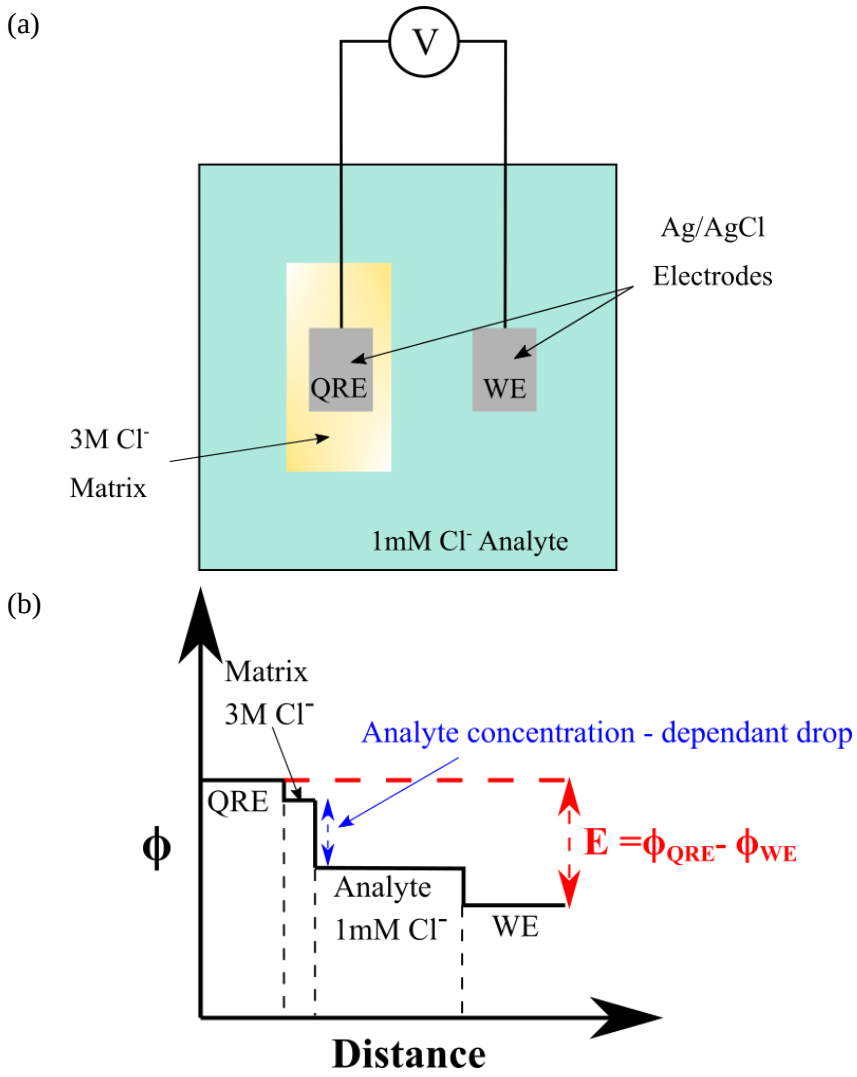

Figure 2.15. (a) schematic diagram showing the use of a QRE in a Cl^- concentration cell described by equation 2.40. **(b)** example potential profile of the cell highlighting the phases involved.

In this scenario, the electrode enveloped by the matrix is acting as the QRE with a stable concentration of 3M. It is not in direct contact with the 1mM analyte and should, to a large extent, be unaffected by changes in its concentration. Therefore, the OCP of the configuration of figure 2.15 is purely dependant on the potential developed at the WE by the concentration of the surrounding analyte.

$$E = 0.059 \log_{10}\left(\frac{3M_{\ FIXED}}{[Cl^-(aq)_{left}]}\right). \tag{2.41}$$

The concept of a concentration cell with an in-built QRE will be utilised within this thesis in the development of a wearable sweat Cl^- sensor. Further details are provided in Section 3.2.

2.4.8 Potential Drift by Diffusion

Due to the fact that the QRE matrix is in direct contact with the analyte solution, a concentration gradient exists between the high Cl^- concentration of the matrix and the comparatively low Cl^- concentration of the analyte. The presence of concentration gradients has been touched upon previously in Section 2.2.1.2. when discussing the process of transdermal drug delivery via iontophoresis. We can refer to Fick's first law of diffusion to describe the movement of molecules when in the presence of a concentration gradient:

$$J = -D\frac{\partial C}{\partial x}. \tag{2.42}$$

Relating equation 2.42 to our Cl^- concentration cell with QRE configuration, J is the flux of Cl^- ions ($m^{-2}s^{-1}$), D is the diffusion coefficient (m^2s^{-1}) and C is the concentration of Cl^- (M). Simply put, this means that the Cl^- ions will flow from the high concentration matrix into the lower concentration analyte (69,161).

Fick's first law is only applicable under steady state conditions, when the concentration profile $\partial C/\partial x$ is constant. However, in most real-world situations it is often the case that the concentration profile at a given point will change over time. Consider a cylinder in which a concentration gradient exists like that shown in figure 2.16 below. We can take two cross sections, each with area A, and separated by a distance Δx. The values of flux at the two cross sections, $J_{1,2}$, are different such that $J_1 > J_2$ (161).

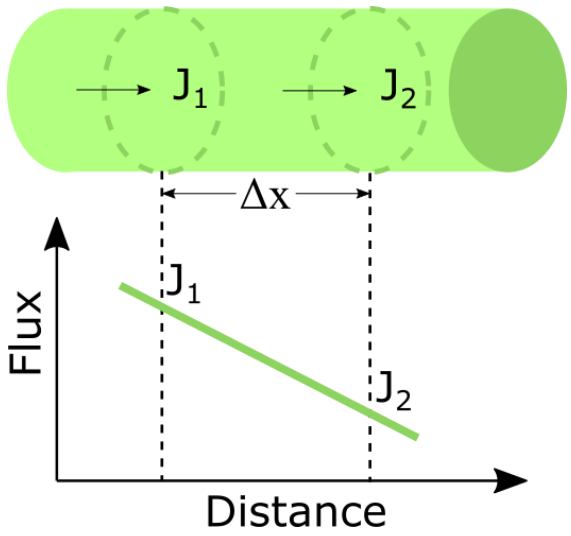

Figure 2.16. Change in flux between two cross sectional areas separated by a small distance Δx (161)

Acknowledging that the amount of material passing through cross sections 1 or 2 in a short time, δt, can be given by $J_{1,2}A\delta t$, then the difference in concentration between the two segments is:

$$\delta C = \frac{(J_1 - J_2)A\delta t}{A\Delta x}. \tag{2.43}$$

Given that δt and Δx are vanishingly small, this can be written:

$$\frac{\partial C}{\partial t} = -\frac{\partial J}{\partial x} \tag{2.44}$$

This is an expression of the conservation of mass in that particles within the system cannot be created or destroyed. Equation 2.44 can be combined with Fick's first law, equation 2.42, to give:

$$\frac{\partial C}{\partial t} = -\frac{\partial}{\partial x}\left(-D\frac{\partial C}{\partial x}\right), \tag{2.45}$$

$$\frac{\partial C}{\partial t} = \mathrm{D}\frac{\partial^2 C}{\partial x^2}, \tag{2.46}$$

assuming that D is a constant. Equation 2.46 is known as Fick's second law of diffusion (69,161).

In the context of the Cl^- concentration cell with QRE, Cl^- ions will migrate down the concentration gradient, from the high concentration reference matrix and into the surrounding low concentration analyte (74). Fick's laws of diffusion suggest that the relative Cl^- concentrations between the reference matrix and the analyte, and the length of time they are in contact will have an effect on the degree of the ion migration. Of course, a change in the Cl^- concentration of the reference matrix will cause a change in the potential at the barrier and, therefore, a change in the reference potential meaning the configuration would no longer be reliable in determining the Cl^- concentration of the analyte solution. Consequently, any such device should be tested to examine the length of time it is able to retain a steady reference potential.

2.5 Summary

Section 2 aimed to provide a foundation of knowledge for the range of topics which this thesis touches upon. This included a brief outline of the structure of human skin and the effective barrier it provides the body. Methods of overcoming this barrier for the purpose of drug delivery were touched upon, with attention given to iontophoresis. The physiology of the eccrine sweat gland was described and its function in ion reabsorption outlined. Cystic Fibrosis causes the breakdown of this functionality through faulty CFTR protein production, leading to CF sufferers exhibiting elevated levels of Cl^- in their sweat. This effect is used to diagnose CF through the sweat test, using pilocarpine iontophoresis, and also provides a way of monitoring the efficacy of emerging treatments which aim to restore CFTR function.

The electrostatic formation of potentials was described in Section 2.4. The emergence of potentials within electrochemical cells and their dependence on the concentration of the chemical species involved was evaluated through the introduction of the Nernst equation. From

this, the architecture of a concentration cell was described and how it may be used in combination with a quasi RE to create a Cl^- ion selective electrode configuration.

3. Materials and Methods

3.1 Introduction

This chapter will detail the materials and protocols used in the manufacture of the Cl^- sensitive electrodes developed throughout the project as well as the methods by which various aspects of their performance were tested. A healthy volunteer study was conducted to allow the sensor to be tested in a physiological environment. This chapter concludes by detailing the protocols used in the preparation and execution of the healthy volunteer study.

3.2 Chloride Sensor

Ag/AgCl electrodes were utilised for this project. A polymerised hydroxyethyl methacrylate (pHEMA) hydrogel mixture was used to provide a matrix structure around one of the electrode contacts due to its ability to absorb and retain liquid (162). This property enables it to be placed into a solution of high Cl^- concentration, and become saturated by it, therefore providing the roll of the quasi RE (QRE) described in Sections 2.4.6 and 2.4.7. The resultant electrochemical cell may be written:

$$Ag(s)|\, AgCl\ (s)|\, Cl^-(aq)||Cl^-{}_{pHEMA}\,|AgCl\ (s)|Ag(s). \tag{3.1}$$

As noted in Section 2.4.7, the measured potential for this cell is given by the Nernstian relation:

$$E = 0.059\, log_{10}\left(\frac{[Cl^-{}_{pHEMA}]}{[Cl^-(aq)]}\right), \tag{3.2}$$

where $[Cl^-_{pHEMA}]$ is the Cl^- concentration (M) of the pHEMA matrix which envelops one of the electrode contacts. The Cl^- concentration within the pHEMA is fixed by saturating the hydrogel in a 1M KCl DI water solution for 25 hours (see Section 3.2.5). This is then considered as the QRE of the configuration. The [Cl^- (aq)] term in equation (3.2) denotes the Cl^- concentration (M) of the aqueous test solution in direct contact with the remaining electrode contact, the WE. Therefore, the measured potential of the electrochemical cell shown in equation (3.2) is directly proportional to the Cl^- concentration of the test solution surrounding the WE.

The steps undertaken to make the hydrogel mixture and apply it to the electrodes utilised in the study are outlined in the remainder of this subsection.

3.2.1 HEMA Gel Mixture

The hydrogel mixture consisted of four ingredients: UV-sensitive 2-hydroxyethyl methacrylate (HEMA, Sigma Aldrich, Product No. 128635); polyvinylpyrolidone K-90 (PVP K-90, Sigma Aldrich, Product No. 81440) was used as an emulsifier; 2,2-dimethoxy-2-phenylacetophenone (DMPAP, Sigma Aldrich, Product No. 196118) as a photoinitiator; and ethylene glycol dimethacrylate (EGDMA, Sigma Aldrich, Product No. 335681) as a crosslinking agent. Fabrication of the solution is initiated by pipetting 18.6 ml of HEMA directly into a sealable glass container. The container was then affixed on an IKA KS 130 Basic orbital shaker (IKA, Staufen, Germany) and the speed slowly increased to 320 rpm. 2g of PVP and 0.8g of DMPAP were subsequently weighed into two separate weigh boats. The PVP was then incrementally tipped into the glass beaker on the orbital shaker. Incremental additions of the PVP into the HEMA avoids large clumping and ensured a quicker, more even emulsion of the solution. The DMPAP, whose chemical structure is shown in figure 3.1, was then added before 95 µl of EGDMA was pipetted into the mixture, completing its composition.

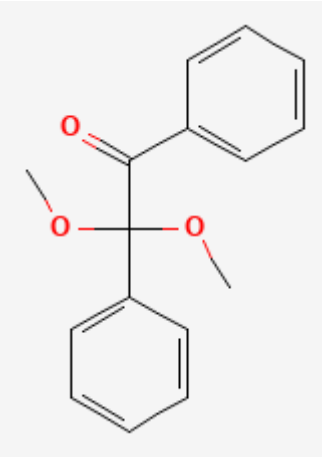

Figure 3.1. Chemical structure of DMPAP. Retrieved from: https://pubchem.ncbi.nlm.nih.gov/compound/90571#section=2D-Structure

The beaker was sealed and kept on the orbital shaker for a further 2-4 hours to aid the emulsion of the gel. The mixture was stored in the fridge.

3.2.2 Electrode

Woundsense ® Ag/AgCl electrodes (Ohmedics, Glasgow) were utilised throughout the project. These are primarily intended as a disposable sensor designed to monitor the moisture of a wound without disturbing the wound dressing (163). A porous film layer covers the electrodes, as shown in figure 3.2.

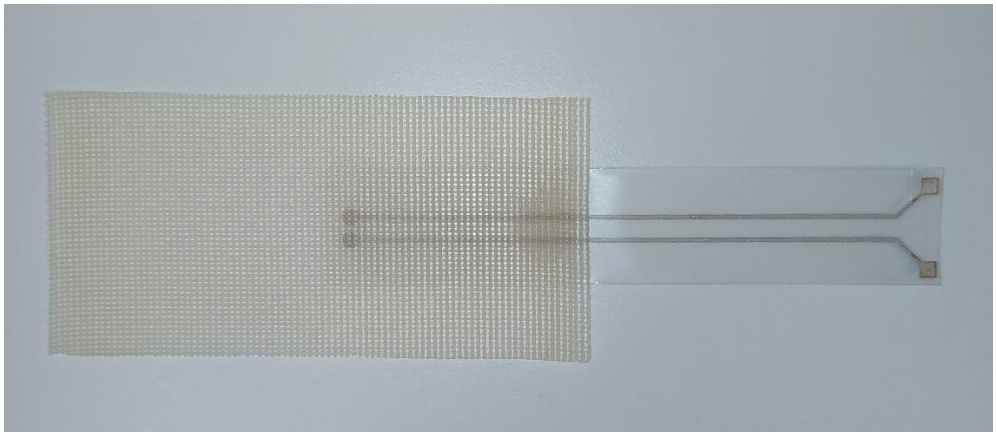

Figure 3.2. Woundsense electrode with porous film layer

The primary components of Woundsense consist of two parallel Ag/AgCl electrodes screen printed on a polyethylene substrate, the key dimensions of which are depicted in figure 3.3.

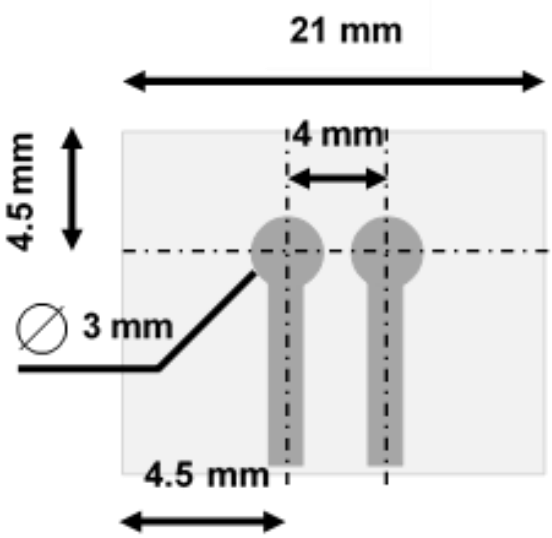

Figure 3.3. Illustration of Woundsense electrode with key dimensions

3.2.3 Electrode Adaption

A number of alterations were required to allow the Woundsense electrode to be used for the detection of Cl^- ion concentration. These consisted of preparing the electrode to enable a small volume of the HEMA hydrogel mixture to be contained over one of the electrode contacts. The first adaption was to remove the porous film layer to expose the electrode contacts. As described in Section 3.2.1, the HEMA mixture is stored as a viscous liquid and it therefore requires a well to hold it in place before it is able to be solidified via polymerisation. The well must have a diameter which is greater than or equal to that of the electrode contact in order for the HEMA mixture to envelope its surface. A disposable, plastic inoculation loop was chosen to provide the well structure. Its inner diameter of 4mm and its availability within the laboratory setting made it suitable to perform the role. The inoculation loop was secured to the electrode substrate using a segment of toupee tape adapted to allow the electrode contacts to remain exposed. To do this, an acetate sheet template was placed over the tape and a hole punch used to create two 4mm holes in positions corresponding to those of the Woundsense electrode

contacts. The tape was then placed over the electrode substrate, so the electrode contacts were still exposed and the outer layer of tape removed as shown in figure 3.4.

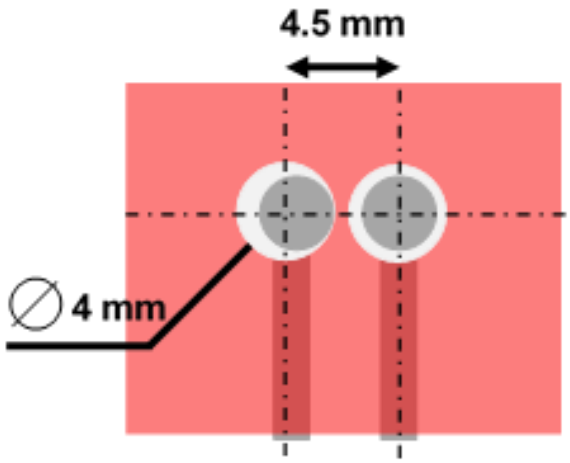

Figure 3.4. Illustration of toupee tape, cut using a template, placed over a Woundsense electrode. It should be noted that the left hole is not centred over the electrode contact. This is to ensure the punch holes do not overlap and affect the surface on which the well can be secured on to.

An inoculation loop (inner diameter: 4 mm; depth: 1 mm) was then removed from its stem and secured over the right hand electrode contact. Figure 3.5 depicts this stage of the electrode's development.

Figure 3.5. Woundsense electrode adapted with well for HEMA hydrogel mixture.

A Multipette Plus positive displacement pipette (Eppendorf, Hamburg, Germany) was then used to deposit 15µl of the HEMA hydrogel mixture into the well created by the inoculation loop.

3.2.4 HEMA Polymerisation

Following the deposition of the HEMA hydrogel mixture onto the electrode surface, it must immediately be polymerised to ensure it solidifies before it leaks from the well. The hydrogel's mechanism of polymerisation is via the absorption of UV radiation by the DMPAP photoinitiator component of the mixture.

Initially, polymerisation was carried out within a chamber containing a Mercury (Hg) bulb. The chamber, designed to dry ink on screen printed electrodes, was a convenient source of UV radiation to investigate the approximate time required to polymerise the hydrogel. It consisted of an inner, hollow space measuring 70cm × 70cm × 80 cm, where the electrodes could be placed to cure. This was accessed by a hatch on the front panel of the chamber. The Hg bulb was located at the top corner of the curing space as is shown in figure 3.6.

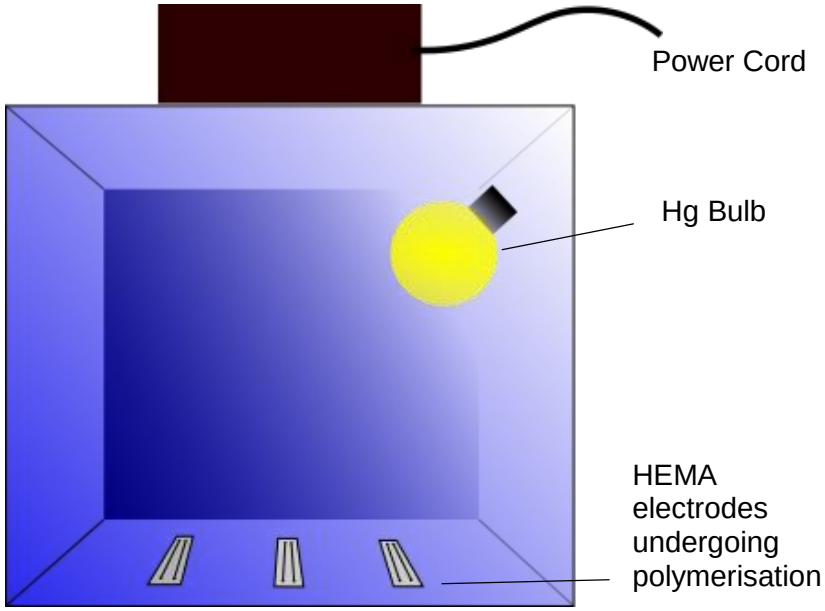

Figure 3.6. Perspective view of inside of Hg bulb chamber

Electrodes were placed in the chamber for an hour. By this point the HEMA had solidified to become pHEMA and was ready for the next stage of the manufacturing process. However, this method of polymerisation was deemed unsuitable given: 1) the hazardous nature of using a Hg bulb over a long period of time; and 2) the variance in UV intensity seen by each electrode as result of the chamber geometry, as shown in figure 3.6. An alternative method of polymerisation which allowed for a more consistent cure from electrode to electrode was, therefore, created.

3.2.4.1 UV LED Array

UV LEDs were seen as a cost effective and space saving alternative to the Hg bulb mechanism of polymerisation. Given that LEDs provide a monochromatic source of light, it was first necessary to find the exact wavelength of light which would be optimum for curing. The photoinitiator used in the gel mixture, DMPAP, absorbs UV radiation in the range of 310 – 390 nm (Sigma Aldrich; Glöckner, 2008; Mucci and Vallo, 2012). One of the main peaks in the emission spectrum of a Hg Arc bulb within this range is 365 nm. A number of 365nm LEDs were purchased (Osram, MA, USA) with the intention of creating an LED array within a light-tight, aluminium box with inner dimensions of 171 × 91 × 55 mm (Hammond Manufacturing, Ontario, Canada). Six LEDs could be fitted to the lid of the box in the configuration shown in figure 3.7.

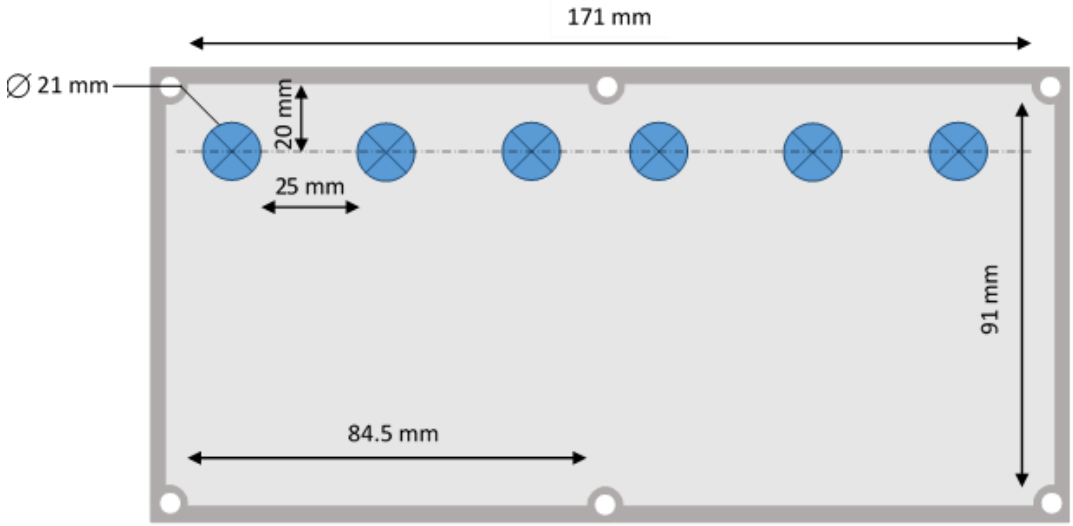

Figure 3.7. Dimensions of UV LED array within aluminium container. Not to scale.

The quoted minimum forward voltage, V_F, for each LED was 3.5 ± 0.04 V. The six LEDs were to be connected in series such that they would require a minimum forward voltage total:

$$V_{F\,Total} = 6 \times 3.5V, \tag{3.3}$$

$$V_{F\,Total} = 21 \pm 0.24\,V. \tag{3.4}$$

The power source used, Aim-TTi EL302T Triple (Aim-TTi, UK), allowed for the supply voltage and the current to be manually set. A supply voltage, V_S, of 30 V was decided upon, to ensure the minimum $V_{F\ Total}$ was met and to help the configuration be transferrable if the adjustable power supply was to breakdown. A ballast resistor was therefore implemented in series with the LEDs to ensure the voltage applied across the LEDs did not exceed their recommended forward voltage. The minimum value required for the resistor, R, was found by using Kirchoff's Circuit Laws and Ohm's Law:

$$R = \frac{V_S - V_{F\,Total}}{I}, \tag{3.5}$$

$$R = \frac{30 - 21}{0.7}, \tag{3.6}$$

$$R = 12.85\,\Omega, \tag{3.7}$$

where I is the current in the circuit. A value of I = 0.7 A was used to match the LED's quoted maximum operating current. The LEDs were fixed to the lid of the box using CW2400 epoxy resin (Chemtronics, USA) and linked to each other in series with a 15 Ω resistor (Arcol, Truro, UK), the closest value of resistor to that calculated through equations (3.5) – (3.7). The resistor had a power rating of 2.25 W in free air, and 20 W on heatsink. The power that the resistor would dissipate, P, within the circuit was approximated using the equation:

$$P = I^2R, \tag{3.8}$$

$$P = (0.7^2) \times 15, \tag{3.9}$$

$$P = 7.35\,W. \tag{3.10}$$

This value exceeded the resistor power rating in free air, therefore a heatsink (ABL Components, UK) was attached using the thermal tape accompanying the heatsink. A hole was drilled in the lid of the box and a cable tie fitted to allow the leads out of the box in order to connect to a power source. The configuration is shown in figure 3.8. The UV LED setup allowed the HEMA samples to be drop cast on up to 6 electrodes to be polymerised simultaneously. Using this apparatus to cure the gel samples involved placing the electrodes, with freshly deposited HEMA mixture, directly under the LEDs within the main segment of the box. This helped ensure that each HEMA gel sample received a consistent dose of UV radiation. The lid is then immediately secured on, and the power cables connected to the power source set to 30 V and 570 mA. These conditions are maintained for 15 minutes, an exposure time which was found to be optimum by experimentation (see Section 4.3.1), at which point the power source is turned off, the cables removed and the electrodes transferred out of the box before they go on to be conditioned.

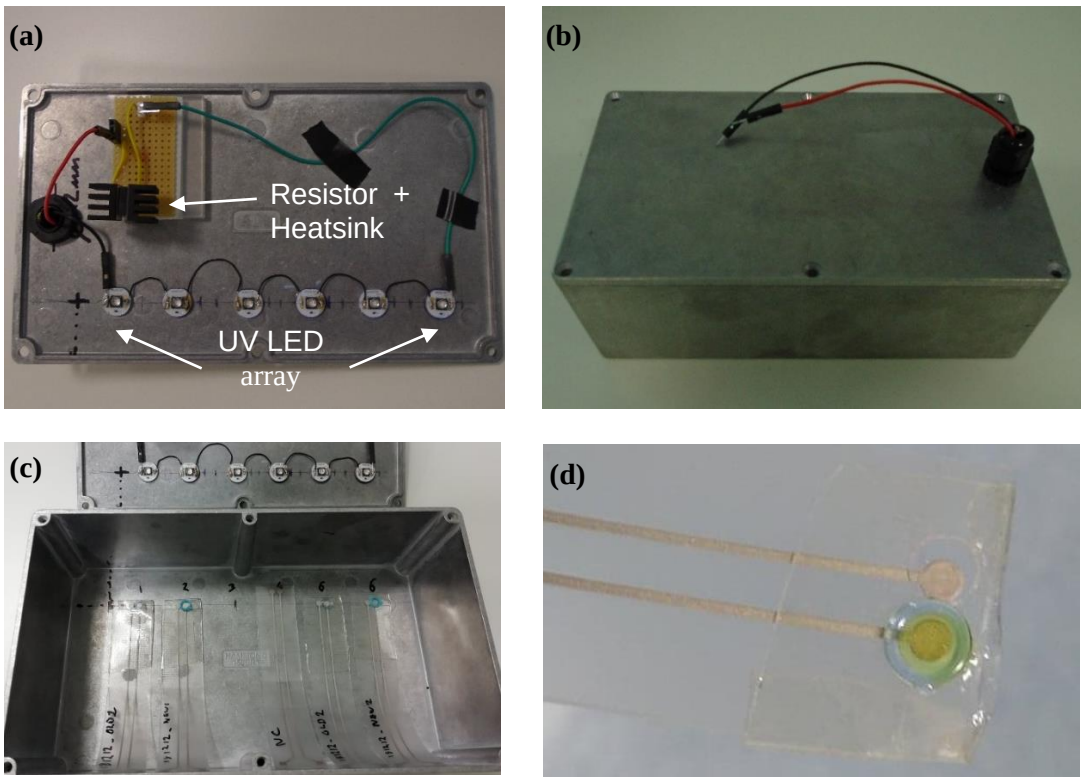

Figure 3.8. (a) UV LED circuit configuration, on base of aluminium box lid, used to polymerise HEMA mixture on electrodes. **(b)** view of setup with lid in place, and power leads unconnected. **(c)** view of setup with lid removed, showing how the electrodes are positioned within the box. **(d)** example of electrode with HEMA sample, contained within well, polymerised by the LEDs.

3.2.5 pHEMA Gel Conditioning

In Section 2.4.7, it was theorised that a matrix could be placed around an electrode contact and used to fix the Cl^- concentration at a stable level so that it may be used as a QRE. Here, the pHEMA gel is utilised as that matrix. The hydrogel's porosity following polymerisation means that it is able to absorb a solution throughout its volume (65). For the purposes of this study, therefore, the pHEMA electrode was submerged in a high concentration KCl DI water solution for a prolonged period of time, allowing the gel to absorb, and become saturated with the solution. The area around the electrode contact would then have a high, stable Cl^- concentration which would allow it to be used as a QRE. The methodology used to examine the nature of the gel's Cl^- uptake are outlined in Section 3.3.2.

The exact concentration of the KCl solution in which the electrodes were placed and the time they were left in the solution were variables which had to be studied. They, therefore, evolved as the project progressed and more data was collected. This evolution will be described in Section 4. The general process of conditioning the electrodes, however, was fixed and consistent throughout the investigations:

Following polymerisation, an amount of KCl was weighed directly into a sealable, plastic bijou container and 20 ml of DI water added to create a solution of known Cl^- concentration. Up to three electrodes can fit into the containers to be conditioned. Once the pHEMA samples on the electrodes are submerged within the solution, the containers are sealed, and the electrodes left to condition for a set period of time. Through experimentation, a conditioning period of 25 hours within a 1 M KCl solution was found to produce electrodes with consistent and sensitive potentiometric responses to incident Cl^- concentrations (see Section 4.3.2 and Section 4.4). When the conditioning time had elapsed, the electrodes were removed and rinsed with DI water to remove any residue from the conditioning solution. They were gently dabbed dry on a paper towel and placed in an oven set at 40°C for 2 hours. It was found that electrodes which are stored dry after being conditioned had a better potentiometric performance than those stored in KCl solutions – as you would find with many commercial reference electrodes. For this reason, an oven drying step at 40°C for 2 hours was incorporated to aid the drying process so that electrodes could be tested soon after being removed from the conditioning solution.

3.2.6 Summary

Section 2.4.7 introduced the concept of a Cl^- concentration cell which utilised a QRE in the form of a Cl^- saturated matrix enveloping one of the electrode contacts, shown again in figure 3.9. This section has detailed the steps undertaken to develop the same concentration cell QRE setup in the form of a wearable electrode. A Woundsense electrode was adapted by depositing a HEMA hydrogel composition onto one of its Ag/AgCl electrode contacts. This was

subsequently polymerised under a UV LED array, and conditioned in a KCl DI water solution in order to form the Cl^- saturated matrix of the QRE. This configuration is illustrated in figure 3.10.

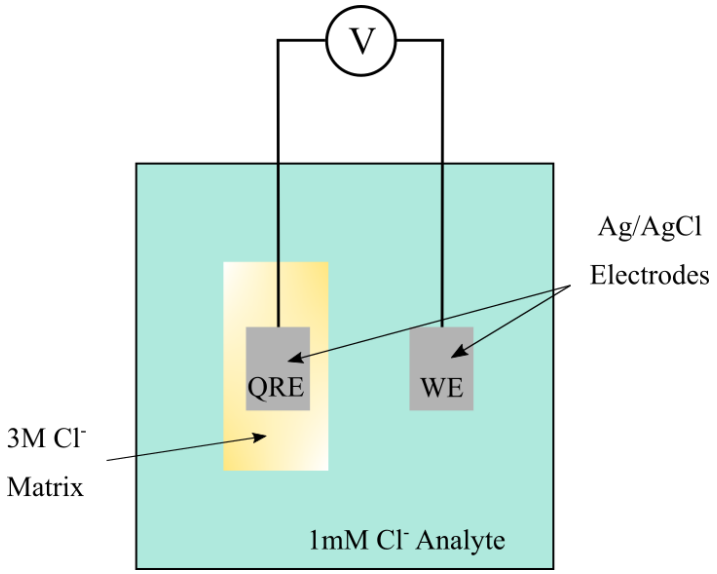

Figure 3.9. schematic diagram showing the use of a QRE in a Cl^- concentration cell

(a)

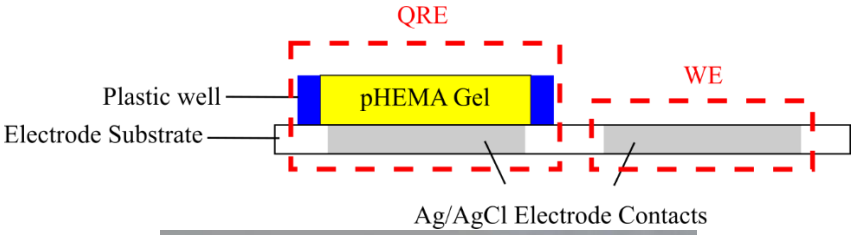

(b)

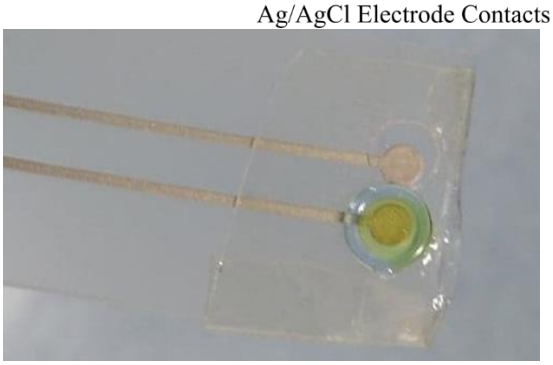

Figure 3.10. (a) schematic illustration showing cross section of Woundsense electrode adapted with pHEMA gel to form Cl^- concentration cell with QRE configuration shown in figure 3.9. **(b)** photograph of pHEMA adapted Woundsense electrode.

3.3 Open Circuit Potentiometry

As detailed in Section 2.4.7, within a concentration cell configuration containing a QRE, there is a direct link between the Cl^- concentration of the analyte solution and the measured potential between the two electrode contacts, the OCP. This relationship is characterised by the Nernst equation, as described in Section 2.4.5. Monitoring the OCP of the pHEMA electrode described in Section 3.2 can, therefore, be used as a way of investigating the conditioning of the pHEMA hydrogel QRE and evaluating the performance of the overall device as a Cl^- sensor.

Unless otherwise stated, a Palmsens Electrochemical Interface (Houten, Netherlands) was used to perform open circuit potentiometry to record the OCP of the pHEMA Woundsense electrode. It was configured in a two-lead mode by connecting the potentiostat's RE and CE clips together. Excel 2016 (Microsoft, Redmond, WA) was used to plot and analyse the data obtained via the methods described within this subsection. Several of the tests carried out within this subsection required the use of a commercial RE. When this was necessary, a 3M KCl commercial RE (InLab Reference Pro, Mettler Toledo, Columbus, OH) was used. This was regularly calibrated against a WE consisting of a Ag/AgCl wire. The Ag wire was initially sanded to smooth its surface and rinsed with DI water. It was then placed in a 200 mM $FeCl_2$ solution for 10 minutes to chloride its surface and rinsed in DI water again before use.

3.3.1 Chloride Sensitivity

To examine an electrode's sensitivity toward Cl^- concentration, test solutions of KCl were used. A 1 M solution was prepared by weighing out the required 1.49 g of KCl for a 20 ml volume into a bijou container before deionised water of said volume was added. Serial dilutions were then performed so that test solutions of varying decreasing Cl^- concentration were available. In the initial stages of the electrode's development, four test solutions were used. These consisted of KCl solution of concentrations: 1 M; 100 mM; 10 mM; and 1 mM. These provided a wide concentration range which enveloped both healthy and CF sweat Cl^- levels (~15 – 100 mM

(6)). They, therefore, provided a relatively quick way to gauge the electrode's sensitivity toward Cl^- concentration. As the treatment and conditioning of the pHEMA was refined throughout the project, the test solution concentration range became smaller and more in line with the physiologically relevant range quoted above. Consequently, plots showing the results of open circuit potentiometry tests analysing Cl^- sensitivity included in Chapter 4 illustrate the response to differing values of test solution concentrations. Additionally, as the pHEMA electrode are in a dry state following their conditioning process (Section 2.3.5), each electrode was placed in a 1mM KCl DI water solution for up to 10 minutes before it was used for a potentiometric test. This would rehydrate the gel prior to its initial use following conditioning and help minimise equilibration time of the electrode's OCP as it is placed in the initial test solution.

To record the OCP of the pHEMA Woundsense device, the Palmsens is first connected to the electrode by attaching the potentostat's RE/CE crocodile clip to the pHEMA-adapted electrode contact (the QRE) and the WE clip to the remaining electrode contact (the WE). The measurement procedure begins by lowering the electrode into the 1 mM test solution, ensuring that the electrode's QRE and WE are fully immersed, as is shown in figure 3.11 at an approximate depth of 12 mm.

Figure 3.11. pHEMA-adapted electrode submerged in KCl test solution during OCP measurement procedure

The Palmsens software was used to operate and record data from the device. A pre-programmed protocol was initiated when the electrode was lowered into the test solution. The protocol records the OCP between the pHEMA QRE and Ag/AgCl WE once every second for a period defined by the user. The complete experimental setup is shown in figure 3.12. The electrode was then removed from the 1 mM test solution, rinsed with DI water, gently dabbed dry, and placed in the 10 mM solution. OCP measurements were then taken for the remaining test solutions, ascending in concentration, following the same protocol.

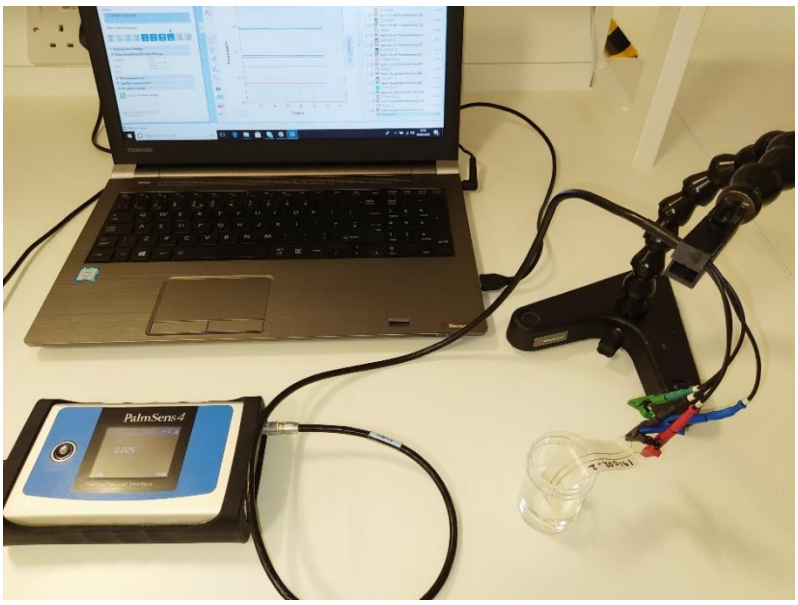

Figure 3.12. Experimental setup utilised for OCP measurement procedure.

On completion of the 1M KCl test solution measurement the electrode was again rinsed in DI water and dried, before it was again placed in the 1mM KCl solution and the process repeated. This was done until there had been enough iterations to gain the pHEMA Woundsense electrode's average potentiometric response toward each test concentration utilised and corresponding values of standard deviation. For each OCP test run undertaken, the data point occurring at a designated time point near the end of the 200 s run was taken as the potential for that test solution. The first few seconds in a new solution the potential often takes a period of time to settle at its equilibrium value, therefore the values occurring near the end of the measurement period are considered to be far enough along that this equilibrium value has been reached. Each data point was then imported into Excel where the mean potential value and standard deviation for each test concentration was calculated. The potential values were subsequently plotted against the corresponding test solution concentration and linear regression analysis performed. The subsequent sensitivity curve is in the form of the equation:

$$V = (m \times log_{10}C) + c, \tag{3.11}$$

where V is the measured electrode potential (mV), m is the gradient (mV/decade), C is the concentration of test solution (M), and c is the y-intercept. The value of m obtained from equation (3.11) was taken as the electrode's sensitivity toward the chloride concentration and was the value compared to the Nernstian limit of sensitivity of 59 mV/dec.

Following the Cl^- sensitivity testing procedure, each electrode was rinsed with DI water, dried, and stored in a sealed plastic pouch.

3.3.2 Conditioning Profile

From Section 2.4.6, we know that the measured potential in a Cl^- concentration cell configuration, like the pHEMA Woundsense device, is dependent upon the relative Cl^- concentrations at the electrode surfaces. However, this value will not be constant for the pHEMA electrode during its conditioning phase (see Section 3.2.5) as the Cl^- ions will take time to fully migrate through the gel's volume before reaching the electrode contact. As a result, the half-cell potential of the pHEMA electrode would also evolve throughout the conditioning period. If this potential was recorded, therefore, its profile may provide an insight into the rate of Cl^- uptake in the gel. To monitor this, the Palmsens WE and RE clips (the latter again shorted with the CE clip) were connected to the pHEMA-adapted electrode contact and a 3M KCl commercial RE (InLab Reference Pro, Mettler Toledo, Columbus, OH) respectively. Both were placed in the same KCl conditioning solution and the OCP between the two electrodes was measured for a minimum of 30 hours. The resultant plot of measured potential vs time was termed as a 'conditioning profile'. The measured potential, V_{meas}, is characterised by the Nernst equation. Here, we shall write it in terms of the potentiostat lead orientation:

$$V_{meas} = 0.059\, log_{10} \frac{[Cl^-_{RE}]}{[Cl^-_{WE}]}, \tag{3.12}$$

where [Cl^-_{WE}] and [Cl^-_{RE}] represent the Cl^- concentrations at the surfaces of the electrodes connected to the WE and RE leads of the potentiostat respectively. Equation (3.12) can be rearranged to give:

$$C_{WE} = C_{RE} \times 10^{\left(-\frac{V_{meas}}{0.059}\right)}. \quad (3.13)$$

Therefore, through substitution of the recorded values of V_{meas}, equation (3.13) may be used as a method of estimating the Cl^- concentration at the pHEMA electrode surface over the conditioning period.

On completion of the procedure, the pHEMA Woundsense electrode was removed from the solution, rinsed in DI water, gently dried and stored in a sealed plastic pouch.

As stated in Section 3.2.5, the process was performed using various concentrations of KCl conditioning solution. The characteristics of the resultant conditioning profiles could then be compared with each other.

3.3.3 Electrical Potential Drift

Potential drift studies were carried out to assess how well the pHEMA electrodes were able to maintain a consistent potential. In other words, a study of the rate at which the pHEMA gel samples lose Cl^- ions to the surrounding test solution.

The procedure used for these tests is similar to that described in Section 3.3.2 above for the conditioning profile tests. The RE Palmsens clip (shorted with the CE clip) was attached to the InLab Reference Pro electrode and the WE Palmsens clip attached to the pHEMA-adapted electrode, fully conditioned following the protocol in Section 3.2.5. Both electrodes were placed into a 20 ml KCl solution and the potential of the pHEMA electrode, with respect to the 3M KCl commercial reference electrode, recorded for 8 hours using the Palmsens potentiostat. This procedure was performed using KCl test solutions of concentration: 50, 75, and 125 mM respectively.

3.3.4 Calibration Curve

In the context of this thesis, a calibration curve describes a definitive linear relationship between Cl^- concentration and the measured potential from any pHEMA Woundsense electrode, as illustrated in figure 3.13. Obtaining this definitive relationship would be a measure of the reproducibility of the pHEMA Woundsense electrodes and provide a method of quantifying their accuracy (see Section 3.3.5).

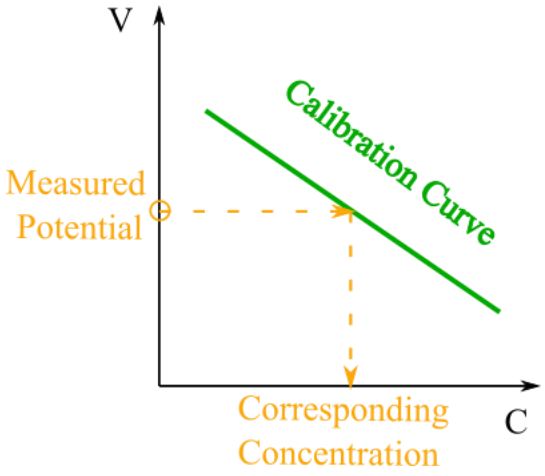

Figure 3.13. Principle of pHEMA calibration curve.

A calibration curve was obtained using 6 pHEMA electrodes. Each were made identically following the method outlined in Section 3.2, where 15µl of HEMA hydrogel mixture was deposited onto the electrode contact followed by a 15-minute cure under the UV LED array. Each electrode was then placed in a 1M KCl solution to condition for a period of 25 hours, after which they were rinsed with DI water and placed in a 40°C oven for 2 hours. Similar to the procedure outlined in Section 3.3.1 open circuit potentiometry tests were performed with each electrode using KCl DI water solutions of concentrations: 10; 50; and 100 mM, so that n=3 for the tests. The potentiometric response of an electrode to each of the test solution concentrations was averaged over its three iterations. These values were then averaged over the six electrodes for each test concentration. The averaged potentials, $\bar{V}$, were subsequently plotted against the corresponding concentrations, C, and linear regression analysis performed to obtain the calibration curve of the form:

$$\bar{V} = (m \times log_{10}C) + c, \quad (3.14)$$

as described in Section 3.3.1. Standard deviation was calculated for each test concentration with respect to the six averaged potentials (n = 6).

3.3.5 Accuracy

The calibration curve described in Section 3.3.4 provides a method of evaluating how accurate the pHEMA Woundsense device is in gauging the Cl^- concentration of a test solution. This investigation used a total of eight (n = 8) pHEMA Woundsense electrodes. Following conditioning, each electrode was placed in a 1mM KCl solution for 10 mins to allow the pHEMA hydrogel to rehydrate before being utilised for OCP measurements. The electrodes were rinsed in DI water, dabbed dry, and connected to the Palmsens potentiostat as described in Section 3.3.1. KCl DI water test solutions of concentration 10, 25, 50, 75, 100, 125 mM were utilised with each electrode and their potentiometric responses recorded for 120 s in each. These responses were averaged over the run time and the value taken as the electrode's response to the test solution. Each potential value obtained could then be substituted into a rearranged form of the general calibration curve (equation (3.15)):

$$C_{CC} = 10^{\frac{(\bar{V}-c)}{m}}, \quad (3.15)$$

to obtain an extrapolated value of concentration, C_{CC}, from the calibration curve. The deviation between the extrapolated and known test concentrations:

$$\xi = C_{TS} - C_{CC}, \quad (3.16)$$

is then calculated and used as a measure of the device's accuracy, ξ. In equation (3.16), C_{TS} represents the known concentration of the test solution.

3.3.6 Selectivity

Given that human sweat is composed of several ionic species, it was necessary to investigate whether any of these would be a significant source of interference within the potentiometric tests performed on the pHEMA Woundsense electrodes. As was described in Section 2.4.6, the concentration cell configuration utilised by the pHEMA electrode device detects Cl^- ion concentration via the change in equilibrium potential of the WE which results from the Ag^+ salt on the electrode surface associating with the Cl^- ions within the test solution. The same process is also possible if other negatively charged ions (anions) were present within the solution, thus changing the equilibrium potential and interfering with the desired signal.

In order to test to what extent the pHEMA electrodes are able to select the Cl^- signal over competing anions, OCP tests were carried out with test solutions containing the two other main anions found within sweat: bicarbonate (HCO_3^-); and lactate ($C_3H_5CO_3^-$) respectively (167). Both were examined separately. To investigate the device's sensitivity towards HCO_3^-, a 1M stock solution of $NaHCO_3^-$ (Sigma Aldrich, product no: S6014) was created using 20 ml of DI water and 1.68 g of $NaHCO_3^-$. Dilutions were then taken from this to create test solutions within the range 1 – 100 mM, each 18 ml in volume. 0.04 g of KCl was then added to each of the test solutions so that each would have a base Cl^- concentration of 30 mM. A sweat Cl^- concentration less than 40 mM is common and would return a negative result for a CF Sweat Test. OCP tests were carried out on the pHEMA electrodes using the Palmsens device in a method identical to that described in Section 3.3.1, where the electrode's potentiometric response to a solution was recorded, rinsed in DI water and dried. It was then placed in the next solution ascending in concentration and the OCP again recorded. This process was repeated in each test solution an additional three times so that n=4. The average potentials over the four iterations were calculated and the values plotted against their respective logarithmic concentrations. Linear regression analysis was then performed to obtain the electrode's sensitivity towards HCO_3^-.

The same method was used to test the electrodes' sensitivity toward lactate. Test solutions of the same concentration range were made using Sodium L-Lactate (Sigma Aldrich, Product No. L7022) within DI water starting with 2.24 g of in 20 ml to make a 1M stock solution. The dilutions were made and 0.04 g of KCl added to each of the 18 ml solutions to ensure a baseline Cl^- concentration of 30 mM.

3.3.7 Diffusion Cell

To examine the electrode's capability to detect Cl^- ion concentration in a more physiologically relevant scenario, a diffusion cell, shown in figure 3.14, was utilised to mimic the transdermal diffusion of ions. The cell was developed to provide a platform in which the reverse iontophoresis of ions and molecules could be studied (168). It uses a Biotech cellulose ester membrane because of its resemblance to invivo properties of human skin including its nano porosity and electric charge at pH 7. The membrane is placed taut between two chambers, with the lower chamber filled with a HEPES buffered saline solution to help support the pores of the membrane and maintain ion transfer through the pores.

3.3.7.1 HEPES Buffer

The HEPES buffer was made by adapting the protocol used in previous studies which utilised the diffusion cell (168). 2.98g of HEPES and 0.015g of NaCl are initially weighed and added to a beaker with 375ml of DI water. The beaker is placed onto a magnetic stirrer, a magnetic flea dropped into the solution and the stirrer switched on. Whilst the solution is mixing, an InLab Micro Pro pH probe ((Mettler Toledo, USA) is placed into the beaker and sodium hydroxide (NaOH) added until the Seven Compact pH meter (Mettler Toledo, USA) attached to the electrode showed that the solution had reached pH 7.4. The magnetic stirrer was then switched off and the flea removed from the solution. An additional 125ml of DI water was added to take the volume of the buffer up to 500ml, meaning the base NaCl concentration is 0.5mM. This low concentration was chosen so that a wide range of chloride concentrations could be explored within the test procedure described in the proceeding section.

(a)

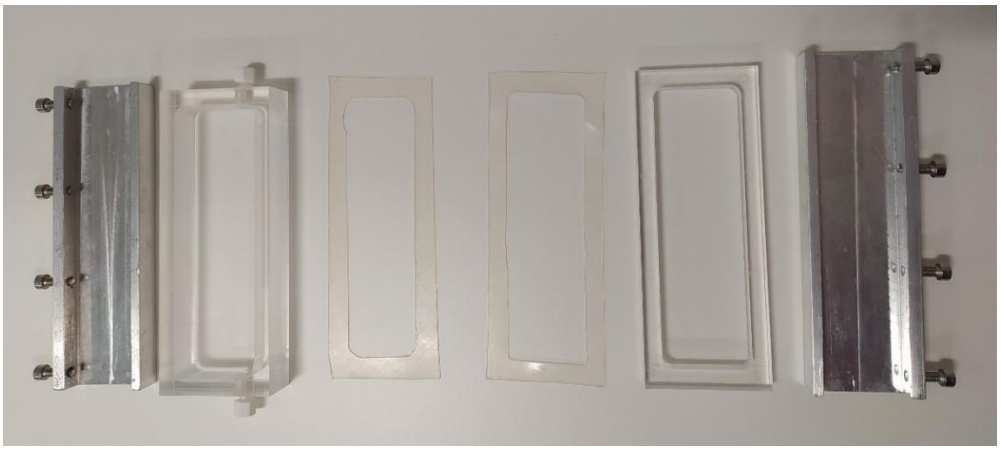

(b)

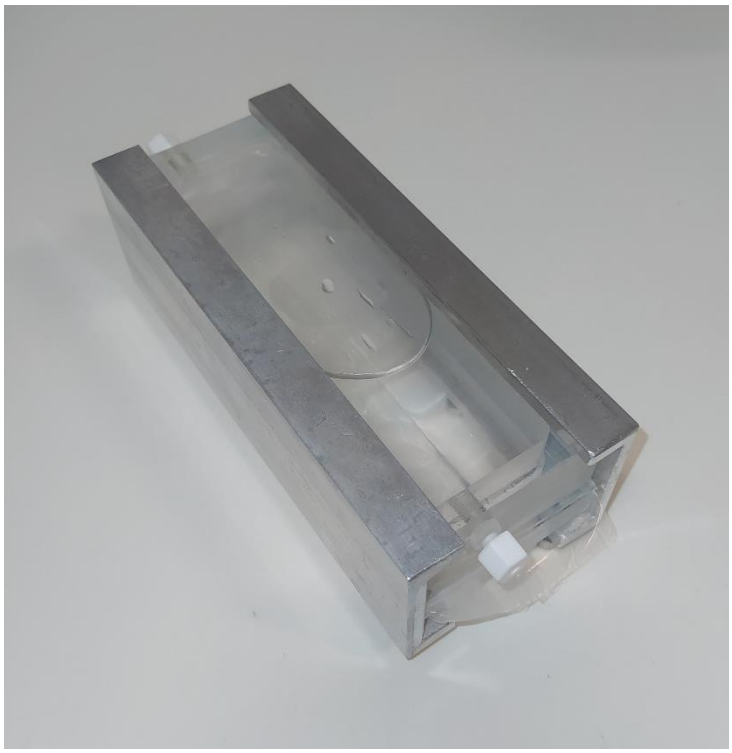

Figure 3.14. (a) Individual components of diffusion cell, including two rubber gaskets and two chambers which are held in place by the pair of metal brackets. Not shown here is the porous membrane. **(b)** Diffusion cell fully assembled, with porous membrane placed taut between the two gaskets and the chamber filled with a HEPES buffer.

3.3.7.2 Diffusion Cell Methodolgy

The experimental configuration, shown in figure 3.15, consists of two plastic blocks which sandwich a nano porous membrane between two rubber gaskets. The membrane was cut from

a roll of Biotech cellulose ester dialysis tubing (Spectra/Por®, Spectrum Labs, CA, USA) which is stored in a solution of sodium azide (0.05%). The dialysis tubing had a molecular weight cut-off of 100-500 Da and was chosen for its resemblance to human skin. The section of tubing was rinsed with DI water and cut along its side to create a flat membrane. This was then secured between the two plastic components comprising the diffusion cell, with the rubber gaskets ensuring there was a seal. Two metal brackets were then fastened in place with screws to secure the configuration.

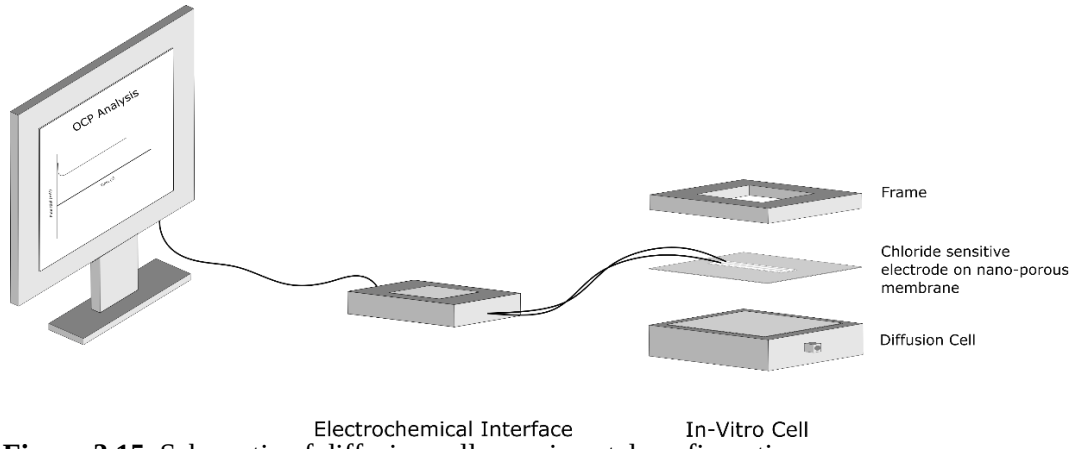

Figure 3.15. Schematic of diffusion cell experimental configuration.

The cell was filled with 120ml of the HEPES buffer described in the last subsection. The electrodes under test were adapted by the addition of a circular aperture with double side tape on both its sides, as shown in figure 3.16.

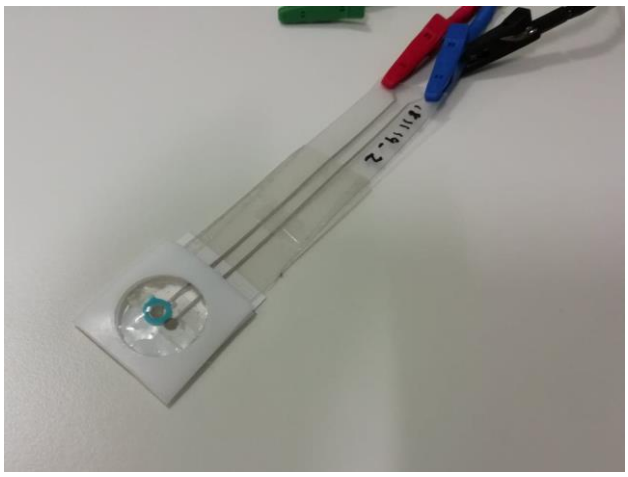

Figure 3.16. pHEMA Woundsense electrode adapted with circular aperture to act as a well for addition of MC gel mixture.

This provided a well for which 400µl of methylcellulose (MC) gel mixture could be deposited over the electrode contacts. The gel mixture consisted of a 0.1M phosphate buffer solution with 3% premium USP grade MC (Colorcon Ltd, Kent, UK) and 20% ethanol. MC gel was utilised as it had previously been used with the apparatus in tests of electrodes of similar on-body use. Additionally, it provided a useful medium between the electrode surface and the diffusion cell membrane for which the chloride ions could diffuse through.

A pHEMA electrode was fixed to the membrane using the adhesive surface it already possesses (see Section 3.2.3). Further tape can be placed between the electrode's back and the metal bracket of the cell to ensure the electrode stays in place for the duration of the test. The cell is positioned such that the membrane and electrode are on the cell's underside, ensuring there was no air bubble present at the membrane barrier. The Palmsens leads were attached to the electrode as described in previous sections (Palmsens RE clip to pHEMA QRE and Palmsens WE clip to Woundsense WE) and the Palmsens software set to continuously record the OCP. A photograph of the experimental setup is shown in figure 3.17.

The Cl^- concentration within the cell was kept at 0.5mM for a period of around 4000s. 2 ml additions of KCl solutions were periodically added to the cell via syringe to raise the Cl^-

concentration over the experimental period. The Cl^- concentration within the diffusion cell, C (M), was calculated using the equation:

$$C = \frac{m_{KCl}}{V \times MW_{KCl}}, \tag{3.17}$$

where m_{KCl} represents the total mass of Cl within the cell (g), V is the total volume of liquid within the cell (L), and MW_{KCl^-} is the molecular weight of KCl (g/mol). The mass and volume terms are iterative as they take into account the periodic 2 ml additions of KCl solutions.

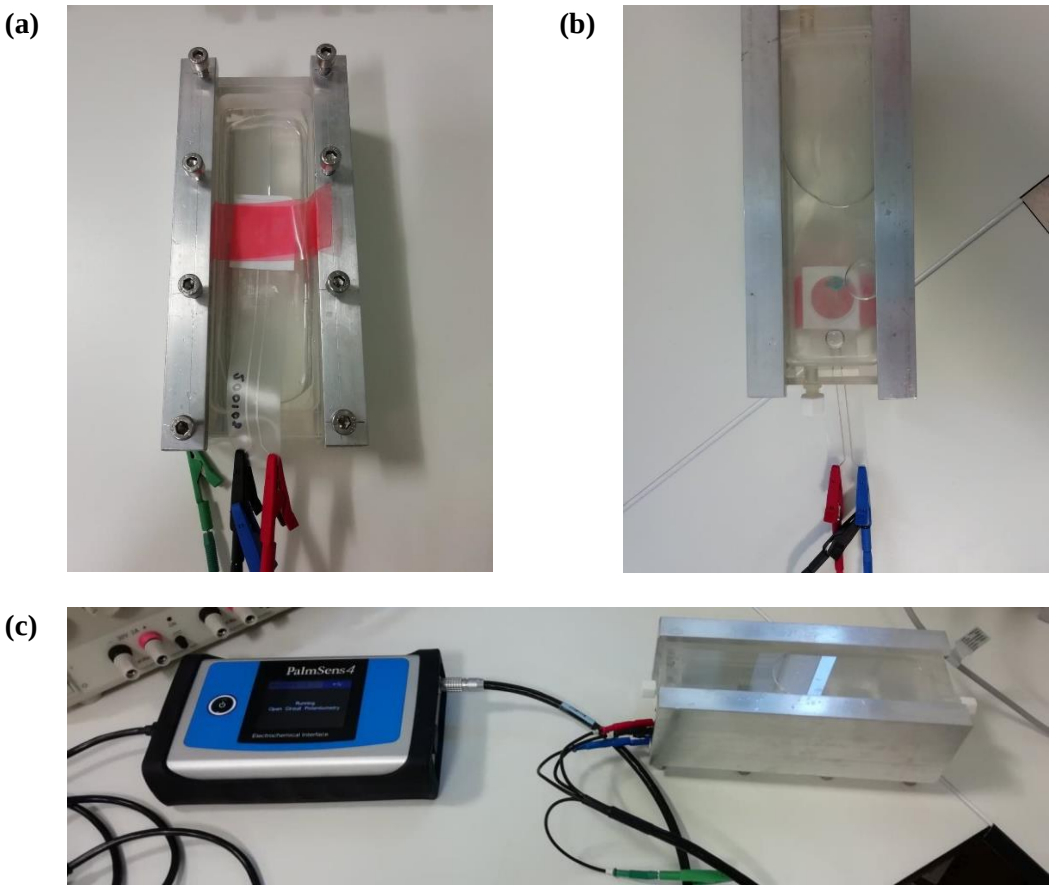

Figure 3.17. (a) pHEMA electrode secured to membrane on underside of diffusion cell using additional length of toupee tape. (b) Diffusion cell positioned upright, ensuring air bubbles are not present at the membrane surface. (c) Overall experimental setup showing Palmsens leads attached to electrode placed on underside of the diffusion cell.

3.4 Healthy Volunteer Study

To examine the electrode's performance within a physiological environment, it was decided to perform a healthy volunteer study(University of Strathclyde Ethics Permission DEC.BioMed.2020.288). The pHEMA electrodes would be placed directly onto a piece of foam located on the participant's skin. By using a fully programmable Portable Electrochemical Analyser (PEA) used by this research group in previous clinical studies (110), the OCP of the electrodes would be monitored and used to gauge the Cl^- concentration of an artificial sweat solution deposited onto the foam. The Cl^- concentration contained within the foam was altered during the procedure through the deposition of NaCl DI water solutions, or spikes, in order to examine the electrode's response to a physiologically relevant Cl^- concentration range. The following subsections will detail the protocols used to prepare for and execute the study.

3.4.1 Artificial Sweat Solution: Constituent Calculation

In the absence of a standard, accepted healthy sweat composition, the artificial sweat solution used in the study was made by initially setting out the desired components and their respective concentrations to roughly match the levels seen in healthy human sweat obtained in the literature (6,169). It should be noted that there does not Table 3.1 shows the chemical makeup of the solution along with their respective molecular weights and the initial intended concentrations within the sweat solution.

Table 3.1. Individual components of artificial sweat solution with molecular weights and intended concentrations.

Component	**Molecular Weight (g/mol)**	**Intended Concentration in Solution (mM)**
Sodium (Na^+)	22.990	23
Potassium (K^+)	39.100	10
Chloride (Cl^-)	35.453	16
Bicarbonate (HCO_3^-)	61.020	10
Lactate ($C_3H_5O_3^-$)	90.080	10
Calcium (Ca^+)	40.078	1
Urea	60.060	20

The components of artificial sweat were obtained through the dissolution of the following compounds: Sodium Chloride (Sigma Aldrich, Product No. S7653); Potassium Chloride (VWR, Product No. 26764.298); Sodium Bicarbonate (Sigma Aldrich, Product No. S6014); Sodium L-Lactate (Sigma Aldrich, Product No. L7022); Calcium Chloride (Sigma Aldrich, Product No. C1016); and Urea (Sigma Aldrich, Product No. U-1250), within deionised water.

The weights of the individual components needed to create the intended concentrations outlined in Table 3.1 were calculated using the equation:

$$m_x = V \times C_x \times MW_x, \tag{3.18}$$

where m_x is the mass of the component x (g), V is the volume of the artificial sweat solution (ml), C_x is the concentration of the component x within the solution (mol/ml), and MW_x is the molecular weight of the component x (g/mol). Table 3.2 shows the corresponding target masses of the constituents needed to fulfil the concentrations of Table 3.1 in a 250 ml solution.

Table 3.2. Target masses of individual component x within artificial sweat solution

Component	**m_{target} (g)**
Sodium (Na^+)	0.132
Potassium (K^+)	0.098
Chloride (Cl^-)	0.142
Bicarbonate (HCO_3^-)	0.153
Lactate ($C_3H_5O_3^-$)	0.225
Calcium (Ca^+)	0.010

Urea	0.300

The first component considered was bicarbonate as the $NaHCO_3^-$ was the only source with which the ion could come from. The following steps were adhered to:

1. The target value of m_{HCO3^-} from Table 3.2 is placed into the equation:

$$m_{xy} = m_{target\ x}\ \frac{MW_{xy}}{MW_x}, \tag{3.19}$$

   where m_{xy} and MW_{xy} are the mass and the molecular weight of the compound xy respectively. This gives the corresponding amount of $NaHCO_3^-$ to be weighed out.

2. The corresponding amount of sodium ions within the m_{NaHCO3^-} calculated in step 1 was obtained using the equation:

$$m_y = m_{xy}\ \frac{MW_y}{MW_{xy}}. \tag{3.20}$$

3. The value from equation (3.20) was then subtracted from the target sodium amount in Table 3.2 to gauge the remaining amount of sodium needed within the solution:

$$m_{y\ remaining} = m_{target\ y} - m_y. \tag{3.21}$$

The next constituent considered was lactate, where its entire allocation would be fulfilled with the $C_3H_5NaO_3$ compound. Steps 1-3 were repeated using the relevant masses and molecular weights, ensuring that the value calculated in equation (3.21) was used to give an up-to-date value of the remaining Na^+ needed. This outstanding amount of Na^+ was fulfilled using NaCl, utilising equation (3.19) to calculate the relevant quantity of the compound required. In doing so the amount of Cl^- ions required to meet the target value in Table 3.2 was updated. The solution's allocation of K^+ ions was then considered; with KCl the compound being used to satisfy it. Steps 1 -3 were followed to obtain the amount KCl which would have to be weighed out as well as the outstanding amount of Cl^- required. The one remaining compound which could be used to fulfil the Cl^- need was $CaCl_2$. Step 1 was therefore used to obtain the amount of $CaCl_2$ needed to meet the shortfall in Cl^-. The value obtained was then placed into equation

(3.20) to gauge the mass of Ca^+ this would give the solution. This value was greater than that set out in Table 3.2, but as it did not raise the concentration of Ca^+ in the solution to atypical physiological levels it was thought an acceptable compromise. The required mass for Urea matches the value given in Table 3.2.

The total mass of each compound calculated using the steps outlined above are shown in Table 3.3. Also provided are the corresponding ionic concentrations these amounts would give for a 250 ml stock solution.

Table 3.3. Masses of compounds in artificial sweat solution and the concentrations of individual ions

Compound	**Total Mass (g)**
Sodium Chloride (NaCl)	**0.044**
Potassium Chloride (KCl)	**0.180**
Sodium Bicarbonate ($NaHCO_3$)	**0.210**
Sodium L-Lactate ($C_3H_5NaO_3$)	**0.280**
Calcium Chloride ($CaCl_2$)	**0.083**
Urea	**0.300**
Component	**Concentration (mM)**
Sodium (Na^+)	**23**
Potassium (K^+)	**10**
Chloride (Cl^-)	**16**
Bicarbonate (HCO_3^-)	**10**
Lactate ($C_3H_5O_3^-$)	**10**
Calcium (Ca^+)	**3**
Urea	**20**

3.4.2 Artificial Sweat Solution: Manufacture

To make the artificial sweat solution, each of the compounds were weighed into individual weigh boats according to the masses listed in Table 3.3. 250 ml of DI water was placed into a glass beaker using the in-built measuring facility of the DI water dispenser (Milli-Q Integral, Merck, Germany). The beaker was placed onto the magnetic stirrer and a magnetic flea dropped into the water. The stirrer was switched on and set to 900 rpm. One by one the compounds were then mixed into the water, with time given to ensure their dissolution before the next compound

was added. Stirring was maintained for 10 minutes following the insertion of the final compound. The flea was subsequently removed from the solution and rinsed with DI water. The solution was poured into a sealable glass beaker, sealed and placed in refrigerated storage.

3.4.3 On-Body Tests

In preparation for their use in the Healthy Volunteer Study on-body testing, electrodes were prepared the day prior to a test. 15 µl of HEMA was deposited onto the electrodes and polymerised under the UV LED array following the protocol described Sections 3.2.3 – 3.2.4. The pHEMA was then conditioned in 1 M KCl for 25 hours before drying in a 40°C oven for two hours, see Section 3.2.5. The following subsections detail the protocols used to further prepare the pHEMA electrodes for on-body tests as well as the methodology involved in carrying out the tests.

3.4.3.1 Electrode Alterations

A number of alterations first had to be performed on the pHEMA electrodes to prepare them for on-body tests. The width of the Woundsense electrodes were reduced by removing two rectangular pieces of the polyethylene substrate either side of the electrode contacts using scissors. This process is shown in figure 3.18.

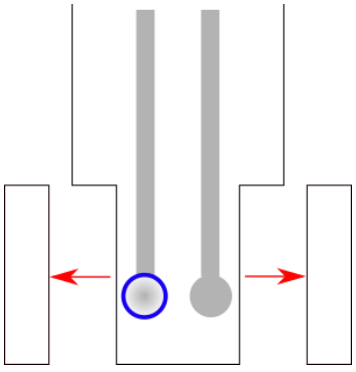

Figure 3.18. Width of Woundsense electrode is reduced by removing a section of substrate to either side of the electrode contacts.

Elements of Skintact ECG electrodes (DCC Vital, Dublin, ROI) were utilised to further adapt the pHEMA electrodes. The circular piece of foam from a Skintact electrode was removed and

a hole punch used to reduce its area to 78 mm^2. The foam was then stored in a bijou container. Immediately before the test procedure begins, a 10-100 µl micropipette (Eppendorf, Hamburg, Germany) was used to deposit 100 µl of the artificial sweat solution onto the surface of the foam and help it distribute evenly throughout the foam's volume so that the foam was saturated. The bijou container was then covered to store the foam until it was ready to be used. Sections 3.4.3.2 – 3.4.3.3 detail how the Healthy Volunteer Study test procedure is segmented into several parts, with multiple pieces of foam needed. The procedure outlined above was repeated for the required number of foam pieces.

The protective plastic covering was also removed from the Skintact ECG electrodes and a 3 mm opening made on its domed structure using a hole punch. This provides a portal through which additional depositions of solution can be made whilst the test is underway and the foam is in contact with the skin.

3.4.3.2 Artificial Sweat On-Body Protocol

The electrode was initially placed into a 10 ml KCl solution of concentration 1mM for 6.5 minutes. As touched upon in Section 3.3.1, this allows the pHEMA gel time to hydrate and the measured potential time to equilibrate. When the time had elapsed, the electrode was removed from the solution, rinsed with DI water and gently dabbed dry. It was then placed on the surface of the lab bench so that the electrode contacts were facing upward. From this point the procedure can be split into three segments: Lab Bench 1; On-Body; and Lab Bench 2. The PEA was programmed to measure the OCP of the electrode for a period of 89 minutes, via a removable SD card. The PEA adapter was attached to the electrode leads, and the device turned on.

The Lab Bench 1 segment of the procedure began by removing a foam segment from its bijou container using forceps and placing it over the electrode contacts, similar to the configuration shown in figure 3.19 below.

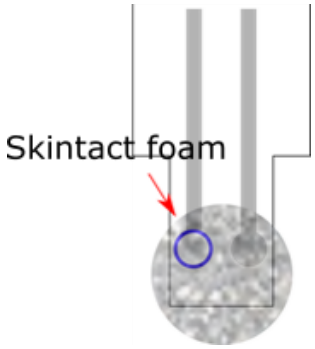

Figure 3.19. Schematic of configuration used for Lab Bench 1 segment of Healthy Volunteer Study test. The circular piece of foam from a Skintact electrode, pre-soaked with artificial sweat solution, was placed over the electrode contacts of the pHEMA-adapted Woundsense electrode.

A 0.1 – 2.5 µl micropipette (Eppendorf, Hamburg, Germany) was used to periodically increase the Cl^- concentration within the foam through the addition of 2.5 µl spikes of NaCl solution onto the surface of the foam. Given that the composition and volume of sweat solution within the foam was known, these additions of known volumes and concentrations of NaCl, elevated the Cl^- concentration in the foam to pre-calculated levels. The methodology used to calculate the spikes and their effect on the foam Cl^- concentration is explained in Section 3.4.3.5. Table 3.4 provides a breakdown of which spikes were administered with respect to the elapsed time on the PEA timer, the concentration of the spikes, and the subsequent Cl^- concentration within the foam.

Table 3.4. Breakdown of the administration time of 2.5µl NaCl spikes during Lab Bench 1 procedure. Also provided is the respective NaCl concentrations of the spikes and Cl^- concentration within the foam over the procedure.

	Spike No.	**NaCl Spike Concentration (M)**	**Calculated Cl^- Concentration in Foam (mM)**	**Time Administered (Minutes)**
Start			16.00	00:00
	1	1	40.00	13:00
	2	1.5	74.76	18:00
	3	3.5	154.42	23:00
End			154.42	28:00

Upon conclusion of the Lab Bench 1 segment, the foam was removed from the electrode using forceps, the electrode rinsed with DI water and gently dabbed dry.

The area of the participant's forearm where the electrode would be placed was swabbed clean using an isopropyl alcohol-based swab (e.g. Pre-Injection Swab). The on-body segment of the procedure then began by using forceps to remove an un-used foam from the bijou container being used to temporarily store it. The foam was placed on the forearm of the participant and the electrode placed over it such that the electrode contacts were touching the foam surface. Finally, the plastic dome (removed from the Skintact ECG electrode) was secured over the electrode and held in place with medium grade toupee tape located around its rim. A schematic of this configuration is shown in figure 3.20 to highlight how the dome's injection portal had to be located over the electrode/foam configuration. Figure 3.21 provides a view of the electrode placed on the forearm of the participant and secured by toupee tape. The body site was selected to match that of the CF Sweat Test (described in Chapter 1.2.1.1).

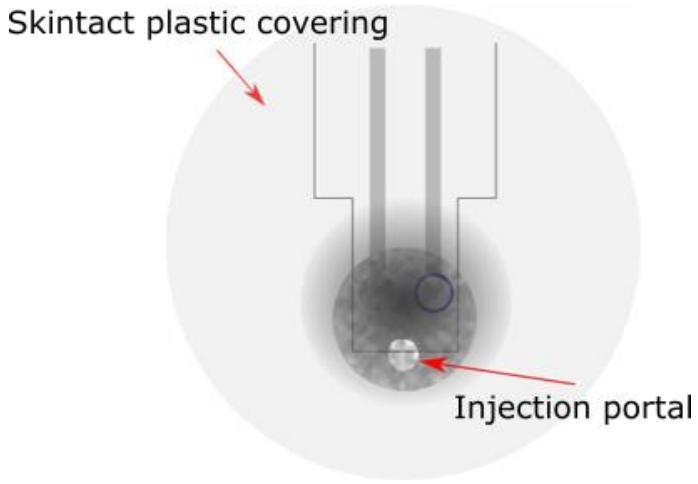

Figure 3.20. Schematic view of configuration used for on-body segment of Healthy Volunteer Study test showing the relative positioning of the foam, electrode, and plastic covering when viewed from directly above. The latter was positioned such that the injection portal provided access to a segment of the foam not covered by the electrode.

Figure 3.21 Example of how pHEMA electrode with foam is positioned and attached to forearm of participant. The plastic covering was secured over electrode using medium grade toupee tape around its rim. The PEA is shown connected to the electrode.

As in the Lab Bench 1 segment, 2.5 µl spikes of NaCl solution were periodically administered to increase the Cl^- concentration in the foam to pre-calculated levels, which envelops both healthy sweat Cl^- levels and values typical of CF sweat Cl^- levels. The Cl^- concentrations of the spikes, their administration time, and the resultant Cl^- concentrations within the foam are noted in Table 3.5.

Table 3.5. Breakdown of the administration time of 2.5µl NaCl spikes during On-Body procedure. Also provided is the respective NaCl concentrations of the spikes and Cl^- concentration within the foam over the procedure.

	Spike No.	NaCl Spike Concentration (M)	Calculated Cl^- Concentration in Foam (mM)	Time Administered (Minutes)
Start			16.00	30:00
	1	0.5	27.80	37:30
	2	1	50.95	45:00
	3	2	96.28	52:30
	4	2	139.55	60:00
End			139.55	67:30

On completion of the On-body segment detailed in Table 3.5, the plastic dome was carefully removed from the participant's forearm, followed by the electrode and foam. The area of skin was cleaned again using an isopropyl alcohol-based swab. The electrode was rinsed with DI water and gently dabbed dry.

The final segment of the procedure, Lab Bench 2, began by laying the electrode flat on the lab bench surface, identically to the configuration of Lab Bench 1. A piece of foam was removed from its bijou container and placed over the electrode contacts. The procedure followed for Lab Bench 1 was then repeated, with the timings of the NaCl spikes given in Table 3.6 below.

Table 3.6. Breakdown of the administration time of 2.5µl NaCl spikes during Lab Bench 2 procedure. Also provided is the respective NaCl concentrations of the spikes and Cl^- concentration within the foam over the procedure.

	Spike No.	NaCl Spike Concentration (M)	Calculated Cl^- Concentration in Foam (mM)	Time Administered (Minutes)
Start			16.00	69:00
	1	1	40.00	74:00
	2	1.5	74.76	79:00
	3	3.5	154.42	84:00
End			154.42	89:00

On completion of the test sequence, the PEA was switched off, its memory card removed, and the data moved to secure storage. The data was stored as an Excel spreadsheet, with the measured potentials and the elapsed time forming two columns of data. In noting the times at which the Cl^- concentration was spiked, the data can be separated into the segments of Lab Bench 1, On-Body, and Lab Bench 2. The measured potentials within each dataset were then allocated to a corresponding Cl^- concentration within the foam by noting the time in which they were recorded and matching it to the times shown Tables 3.4 – 3.6 above. The average potential over these periods was then calculated, and the values taken as the electrode's response to the Cl^- concentration at that time. The standard deviation over this time period was also calculated. The average potential values, and the standard deviation, were then plotted against their corresponding Cl^- concentration and linear regression analysis performed to obtain sensitivity curves for each part of the procedure.

The lab bench segments were performed to provide a method of comparison to the data recorded for the on-body segment. Extensive self-testing using the DEA with the pHEMA electrode to develop the protocol described in this chapter showed that the measured potential during LB1 segment was often still equilibrating. This meant it couldn't provide a reliable sensitivity curve to which the On-Body results could be compared. Consequently, the dataset acquired from the Lab Bench 2 procedure was used for this purpose.

Originally, 10 – 20 healthy volunteers had been anticipated to take part in the study. However, due to Coronavirus restrictions at the time of investigation, a smaller pool of participants had to be utilised. For this reason, a group of four volunteers was used to carry out a total ten artificial sweat solution on-body tests following the procedure outlined in this section.

3.4.3.3 Potential Offset Compensation

As will be discussed later in Section 5.3, in each HVS study carried out there was an apparent offset in measured potential between the On-Body and Lab Bench segments. The magnitude of the offset varies for each electrode; however, it appears relatively constant over the

experimental concentration range with On-Body measurements consistently more negative than the equivalent Lab Bench measurements. As such, an electrode-by-electrode method of compensating this offset was introduced to allow the two datasets to be compared more effectively. The steps undertaken were as follows.

1. The sensitivity of the curve was obtained for the Lab Bench 2 segment through linear regression analysis, as described in Section 3.4.3.2. This was of the form:

$$V_{LB2}(C) = m \times log_{10}C + c, \tag{3.22}$$

where V_{LB2} is the value of potential on the Lab Bench 2 linear relationship (V) corresponding to the foam Cl^- concentration, C (M); m is the gradient, or sensitivity (V/decade); and c is the y-intercept. The On-Body Cl^- foam concentrations, given in Table 3.5, were then substituted into equation (3.22) to obtain the corresponding values of potential on the LB2 linear relationship.

2. The average potential for each concentration in On Body test, V_{OB}, was calculated as described in Section 3.4.3.2.
3. The potential offset, V_{Offset}, between the values obtained in steps 1 and 2 for each concentration was calculated.

$$V_{Offset}(C) = V_{LB2}(C) - V_{OB}(C), \tag{3.23}$$

and a mean value obtained:

$$\bar{V}_{Offset} = \frac{\sum V_{Offset}}{n}, \tag{3.24}$$

Where n is the number of V_{Offset} values calculated using equation (3.23) above.

4. $\bar{V}_{Offset}$ was used to compensate for the average On Body potential value of each test concentration:

$$V_{OB}{}^*(C) = V_{OB}(C) + \bar{V}_{Offset}. \tag{3.25}$$

Equation (3.25) then provided the On-Body potential values, corresponding to each Cl^- test concentration, adapted to account for the offset between themselves and the Lab Bench 2 potential values.

3.4.3.4 Accuracy

The dataset obtained from equation (3.25) can subsequently be utilised to analyse the accuracy of the On-Body measurements. This is done in a similar manner to that described in Section 3.3.5 where comparisons were made between measured values and an established calibration curve. Firstly, the Lab Bench 2 linear equation (3.22) is rearranged so that the concentration becomes the subject. Secondly, the values of $V_{OB}{}^*$ obtained using equation (3.25) can be substituted in to obtain a corresponding value of concentration:

$$C_{OB}{}^* = 10^{\frac{(V_{OB}{}^*(C)-c)}{m}}. \tag{3.26}$$

These extrapolated values of Cl^- concentration can then be compared to the equivalent, 'known', Cl^- concentrations of the foam during the On-Body procedure, quoted in Table 3.5. The accuracy is then given by:

$$\xi = C_{OB} - C_{OB}{}^*. \tag{3.27}$$

3.4.3.5 Cl^- Spike Calculator

To approximate the Cl^- concentrations which would arise from the addition of small amounts of NaCl solution, a spreadsheet was created which accounted for the initial volume of sweat solution within the foam, and the concentration and volume of the additional spike. The purpose of the spreadsheet was to make the process as general as possible, so that volumes and concentrations could be changed if need be. The spreadsheet utilised the following steps to estimate the Cl^-concentration in the foam after an initial deposition of NaCl.

1. Calculate mass of Cl^- ions within initial deposition, $m_{Cl^- initial}$ (g)

The first step in approximating the final Cl^- concentration within the foam from the addition of a NaCl solution to the portal was to calculate the total mass of Cl^- within the foam from the

primary volume of sweat solution placed on the foam. In Section 3.4.1 the total mass of each individual ion needed to make a 250 ml artificial sweat solution with the intended concentration was calculated and is shown in Table 3.1. These were denoted M_x, the total mass of ion x within the 250 ml solution. From this the total mass of ion xwithin the initial volume deposited onto the foam, m_x, was estimated:

$$\mathrm{m}_{Cl^-\ initial} = M_{Cl^-}\left(\frac{V_{Initial}}{V_{Stock}}\right), \tag{3.28}$$

where V_{stock} and $V_{initial}$ are the volumes (ml) of the artificial sweat solution stock and the initial foam deposition respectively.

2. The concentration of NaCl spike solution, C_{spike} (mol/ml) was chosen
3. The volume of spike V_{spike} (ml) was chosen
4. The mass of Cl^- within spike volume was calculated

From the values chosen in steps 2 and 3 it was then possible to calculate the subsequent mass of Cl^- that would be present within the spike volume:

$$m_{Cl^-\ spike} = V_{spike} \times C_{spike} \times MW_{Cl^-}, \tag{3.29}$$

Where MW_{Cl^-} is the molar mass of Cl^- (g/mol).

5. New Cl^- concentration within foam calculated

The total concentration of Cl^- within the foam with the addition of the spike could then be estimated:

$$C_{Cl^-\ foam} = \frac{\sum m}{\sum V\ \times MW_{Cl^-}}. \tag{3.30}$$

In the instance of the addition of the first spike, the total mass was given by:

$$\sum m = \left(\mathrm{m}_{Cl^-\ initial} + m_{Cl^-\ spike}\right). \tag{3.31}$$

Likewise, the total volume of liquid within the foam was given by:

$$\sum V = (V_{initial} + V_{spike}). \quad (3.32)$$

Steps 2-5 could then be repeated to calculate the foam Cl^- concentration for any subsequent NaCl spike solutions, ensuring that the values for Σm and ΣV are iterated accordingly.

The same process could also be followed to estimate the concentration of Na^+ ions within the foam following the deposition of the NaCl spikes by using the corresponding values of M_{Na^+} and MW_{Na^+} in place of the Cl^- equivalent.

The Cl^- spike calculator used is shown in figure 3.22 with the sample values used for the Artificial Sweat On-Body procedure detailed in Section 3.4.3.2.

Spike No.	Volume on Foam (ml)	Weight of Cl (g)	Concentration of Spike (mM)	ENTER Volume of Spike (ml)	Weight of Cl in Spike (g)	Conc in Foam (mM)
1	0.1	5.67248E-05	500	0.0025	4.43163E-05	27.80487805
		Weight of Na (g)	Na Concentration of Spike (mM)		Na in Spike (g)	Conc in Foam (mM)
		0.000052877	500		2.87375E-05	34.63414634
	Volume in Foam	Weight of Cl (g)	Concentration of Spike (mM)	ENTER Volume of Spike (ml)	Weight of Cl in Spike (g)	Conc in Foam (mM)
2	0.1025	0.000101041	1000	0.0025	8.86325E-05	50.95238095
		Weight of Na (g)	Na Concentration of Spike (mM)		Na in Spike (g)	Conc in Foam (mM)
		8.16145E-05	1000		0.000057475	57.61904762
	Volume in Foam	Weight of Cl (g)	Concentration of Spike (mM)	ENTER Volume of spike (ml)	Weight of Cl in Spike (g)	Conc in Foam (mM)
3	0.105	0.000189674	2000	0.0025	0.000177265	96.27906977
		Weight of Na (g)	Na Concentration of Spike (mM)		Na in spike (g)	Conc in Foam (mM)
		0.00013909	2000		0.00011495	102.7906977
	Volume in Foam	Weight of Cl (g)	Concentration of Spike (mM)	ENTER Volume of spike (ml)	Weight of Cl in Spike (g)	Conc on Skin (mM)
4	0.1075	0.000366939	2000	0.0025	0.000177265	139.5454545
		Weight of Na (g)	Na Concentration of Spike (mM)		Na in spike (g)	Conc in Foam (mM)
		0.00025404	2000		0.00011495	145.9090909

Figure 3.22. Excel spreadsheet calculator used to estimate the Cl^- concentration within the foam in contact with the skin following the deposition of a NaCl solution of defined concentration and volume.

3.5 Summary

Sections 3.2 and 3.3 aimed to detail the materials and the experimental protocols used in the manufacture and development of the Cl^- sensitive pHEMA Woundsense electrode. The

procedures used to prepare for and execute a healthy volunteer study utilising the electrodes were also provided in Section 3.4.

4. pHEMA Electrode Preparation and Performance

4.1 Introduction

The concept of a Cl^- sensor in the form of a concentration cell was introduced in Sections 2.4.6 and 2.4.7. Key to this concept was the presence of a matrix of fixed Cl^- concentration enveloping one of the Ag/AgCl electrodes, shown in figure 4.1 (a). Forming a QRE, this would act to fix the half-cell potential at the electrode's surface. Therefore, the measured potential between the QRE and WE would be solely dependent upon the potential developed at the surface of the WE as a result of the Cl^- concentration of the surrounding electrolyte, as shown in figure 4.1 (b). In Section 3.2, it was noted that pHEMA hydrogel was utilised as the medium to provide the matrix around one of the electrodes due to its ability to intake and retain liquid following polymerisation. This configuration is presented in figure 4.1 (c).

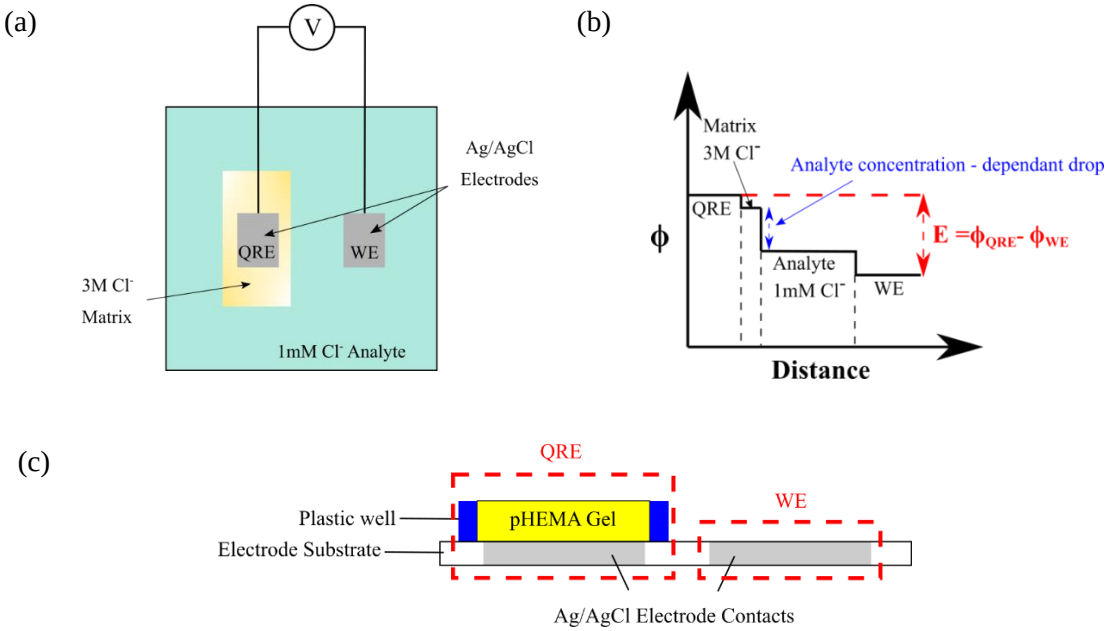

Figure 4.1. (a) schematic diagram showing the use of a QRE in a Cl^- concentration cell. **(b)** visualisation of the potential levels throughout the concentration cell configuration, highlighting the effect of the analyte Cl^- concentration on the measured potential. **(c)** schematic cross section of Woundsense electrode adapted with pHEMA gel to form Cl^- concentration cell QRE configuration.

Through the results of tests detailed in Section 3.3, this chapter reports and discusses the development of the pHEMA electrode as a Cl^- ion-selective electrode device. It will include investigations into the preparation of the gel such as its polymerisation time, its conditioning

time, and the concentration of its conditioning solution. The electrode's performance is analysed in terms of its sensitivity toward test Cl^- concentrations, its ability to maintain a consistent reference potential through potential drift tests, and its reproducibility. In addition, the potential of the electrode to be used in a physiological setting is investigated through the use of a diffusion cell.

4.2 UV Bulb Polymerisation

As was described in Section 3.2.4, a Mercury (Hg) arc bulb contained within an enclosed chamber was the initial method used to polymerise the HEMA gel samples deposited onto the Woundsense electrode surfaces. The chamber provided an opportunity to conduct a preliminary feasibility study to examine the approximate time needed to polymerise the HEMA sample, as well as the time needed for the pHEMA to exhibit a sensitivity toward the Cl^- concentration of test solutions. These results could then be used as a basis from which the gel preparation process may be adapted to optimise the electrode's potentiometric performance.

4.2.1 Curing Time

The process of polymerising the HEMA gel within the Hg bulb chamber was outlined in Section 3.2.4. Initial attempts at using the Hg bulb chamber focussed on identifying an adequate amount of time for the electrodes to be left in the chamber to ensure that the HEMA samples had polymerised. It was found that electrodes which had been exposed to the light from the Hg bulb for 30 minutes all exhibited a yellow, glassy gel sample when removed from the chamber as is shown in figure 4.2. This glassy appearance is characteristic of polymerised HEMA gels (170,171).

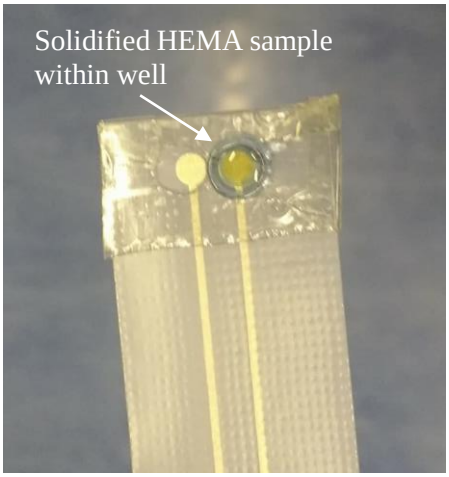

Figure 4.2. pHEMA electrode following 30-minute exposure to Hg arc bulb.

Given that a polymerisation time of 30 minutes appeared to produce a consistently solidified pHEMA sample in the electrodes tested, subsequent electrodes polymerised using the Hg bulb cabinet had a cure time of 1 hour to help ensure that polymerisation had been induced throughout the gel's volume. Fixing this variable meant that other aspects of the electrodes' preparation process could be investigated.

4.2.2 pHEMA Conditioning

As described in Section 3.2.5 the next stage in the electrodes' development was the conditioning phase, in which the electrode is placed into a KCl DI water solution to allow the pHEMA gel to become saturated with the solution. As such, this process was considered to consist of two variables: the concentration of the conditioning solution; and the length of time in which the electrode is conditioned within the solution. Investigations into the effect the concentration of the conditioning solution has on the conditioning process of the gel are presented in Section 4.3.2.2. For the purpose of this preliminary feasibility study, the concentration of the conditioning solution was set at 3 M KCl, in line with similar studies in the literature (70,170). Fixing the concentration of the conditioning solution allowed for investigations into the length of time required for the pHEMA to condition within the solution.

Four electrodes were used, with 15 µl of HEMA hydrogel deposited over one of their electrode contacts. Each electrode was cured within the Hg bulb chamber for 1 hour, as noted in the preceding section, before being placed in a 3 M KCl DI water solution to condition. Electrodes 1 and 2 were kept in the solution for 90 hours. Electrodes 3 and 4 were removed from the solution after 25 hours, a similar conditioning time to that reported in literature (70).

Following their respective conditioning periods, OCP tests were carried out on each electrode following the protocol described in Section 3.3.1. Measurements were made using a Solartron 1286 Electrochemical Interface (Hampshire, UK). The results of these tests are shown in figure 4.3.

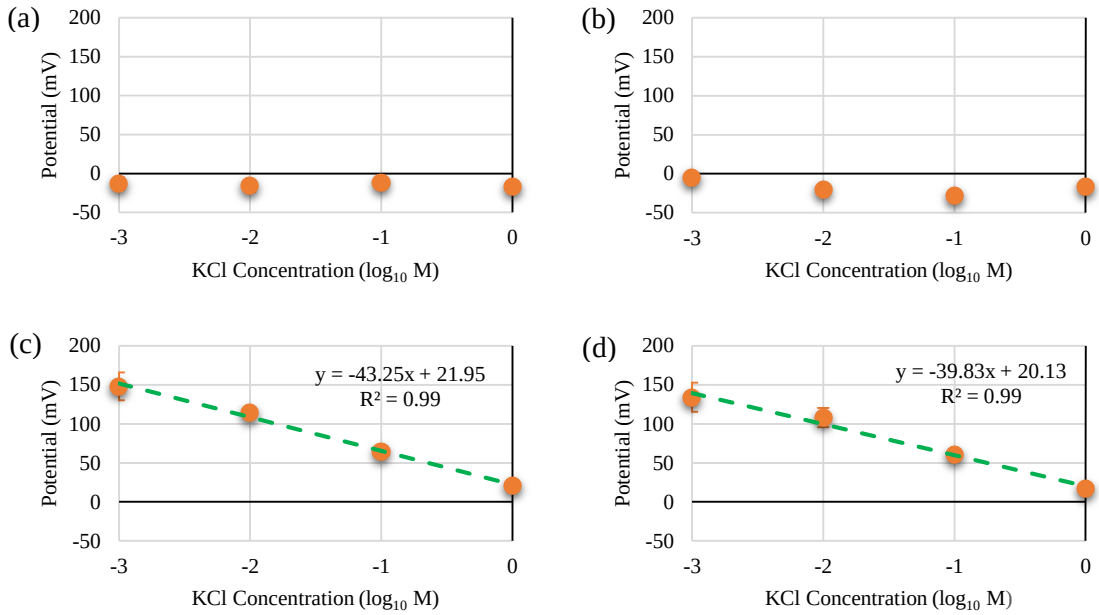

Figure 4.3. Potentiometric responses of four electrodes towards KCl test solutions. (a) and (b) show the responses of electrodes 1 and 2 respectively (n = 1). These were conditioned in 3M KCl for 4 days before being tested. (c) and (d) show the mean potential responses ± SD (n=3) of electrodes 3 and 4 respectively alongside the results of the linear regression analysis performed. These were conditioned in 3M KCl for 25 hours and stored dry for 3 days before testing.

There is a clear difference in the potentiometric responses of the electrodes in figure 4.3 (a) - (b) and those in figure 4.3 (c) - (d). Whereas the latter pair of electrodes display a clear

sensitivity toward the Cl^- concentration of the test solutions, electrodes 1 and 2 exhibit little to no sensitivity.

The results from figure 4.3 confirmed that the pHEMA electrodes had the capability to act as a Cl^- sensitive device, with two of the electrodes tested exhibiting very strong sensitivities toward the Cl^- concentration in the test solutions utilised. However, as touched upon in Section 3.2.4, the method of polymerisation was altered at an early point in the study. Therefore, the information gathered via Hg bulb gel polymerisation could not be directly built upon but instead could be used as a reference for further studies.

4.3 UV LED Polymerisation

The Hg bulb chamber was replaced by the UV LED array as the method of polymerisation, as detailed in Section 3.2.4.1. The differences in the architecture between the Hg bulb chamber and the LED array as well as the variation in emission spectra meant that the two curing techniques could not be considered equivalent. As such, any information that had already been gained about the gel's polymerisation time and its effect on the subsequent potentiometric performance of the device had to be re-examined.

4.3.1 Curing Time

To determine the appropriate time to cure the HEMA under the UV LED array, 15 µl of HEMA gel solution (detailed in Section 3.2.1) was deposited onto a single electrode, cured under the LED array for a set amount of time, before being removed and conditioned in 3 M KCl DI water solution for 25 hours (see Section 3.2.5). The electrode then underwent OCP testing, according to the protocol described in Section 3.3.1, using DI water test solutions of KCl concentration 1 mM, 10 mM, 100mM, and 1 M. The OCP test procedure was repeated a further two times for the electrode such that n = 3. The electrode's mean potentiometric responses could then be gauged and its sensitivity toward the test solution concentration calculated. This procedure was then repeated for 6 more electrodes, with the curing time for each new electrode

incrementally longer than the one examined before. Table 4.1 shows the time each was cured under the UV LED array.

Table 4.1. Duration of electrode's polymerisation under UV LED array.

Electrode No.	Polymerisation Time (Minutes)
1	2
2	5
3	10
4	15
5	20
6	25
7	30

4.3.1.1 Results

Figure 4.4 shows the measured potentials for each electrode's first OCP test, alongside their sensitivity curves obtained using the average potentiometric response to the KCl test solutions.

(a)

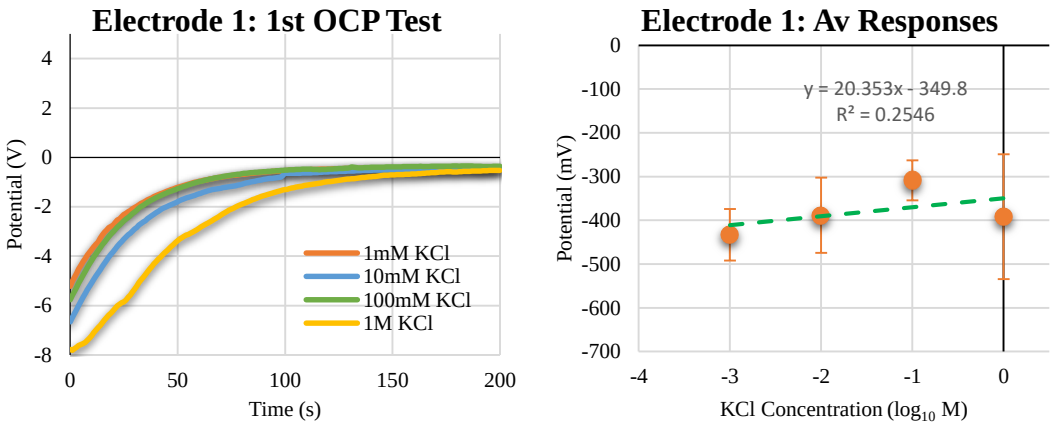

(b)

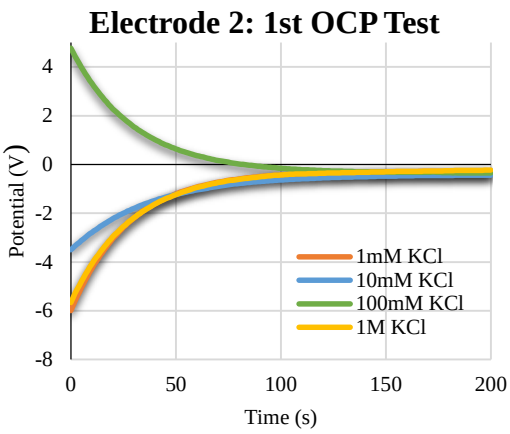
Electrode 2: 1st OCP Test
Potential (V)
Time (s)
1mM KCl
10mM KCl
100mM KCl
1M KCl

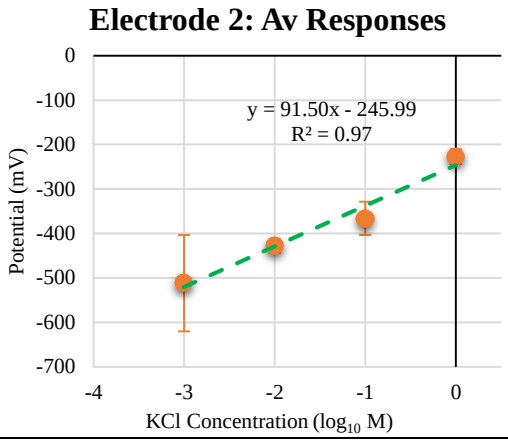
Electrode 2: Av Responses
y = 91.50x - 245.99
R² = 0.97
Potential (mV)
KCl Concentration (log10 M)

(c)

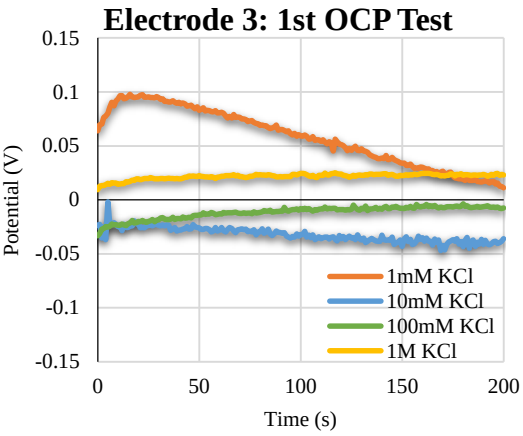
Electrode 3: 1st OCP Test
Potential (V)
Time (s)
1mM KCl
10mM KCl
100mM KCl
1M KCl

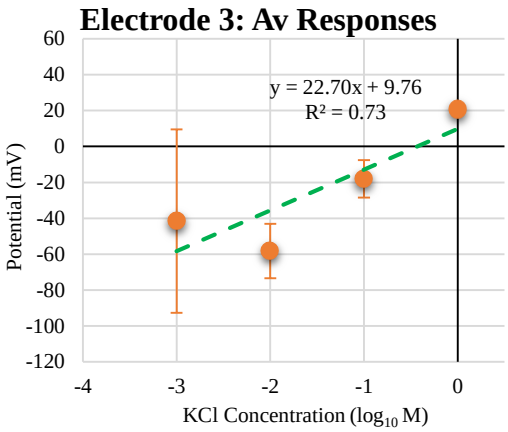
Electrode 3: Av Responses
y = 22.70x + 9.76
R² = 0.73
Potential (mV)
KCl Concentration (log10 M)

(d)

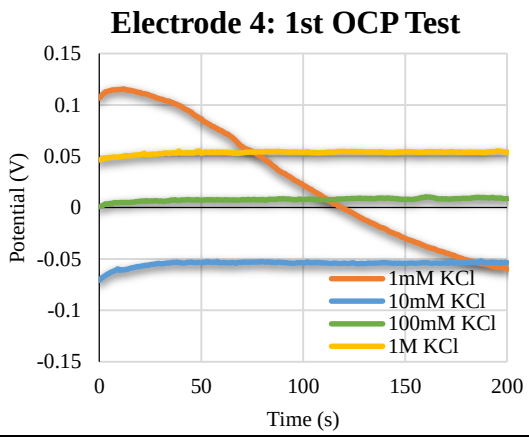
Electrode 4: 1st OCP Test
Potential (V)
Time (s)
1mM KCl
10mM KCl
100mM KCl
1M KCl

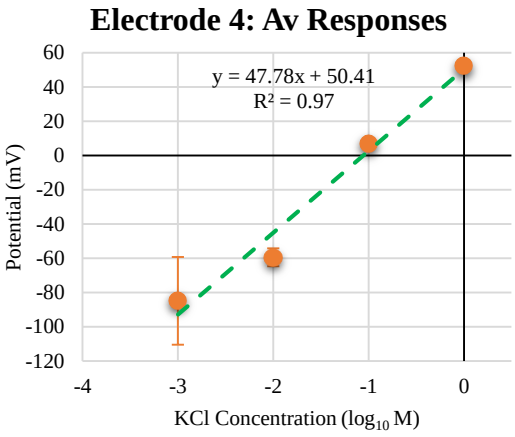
Electrode 4: Av Responses
y = 47.78x + 50.41
R² = 0.97
Potential (mV)
KCl Concentration (log10 M)

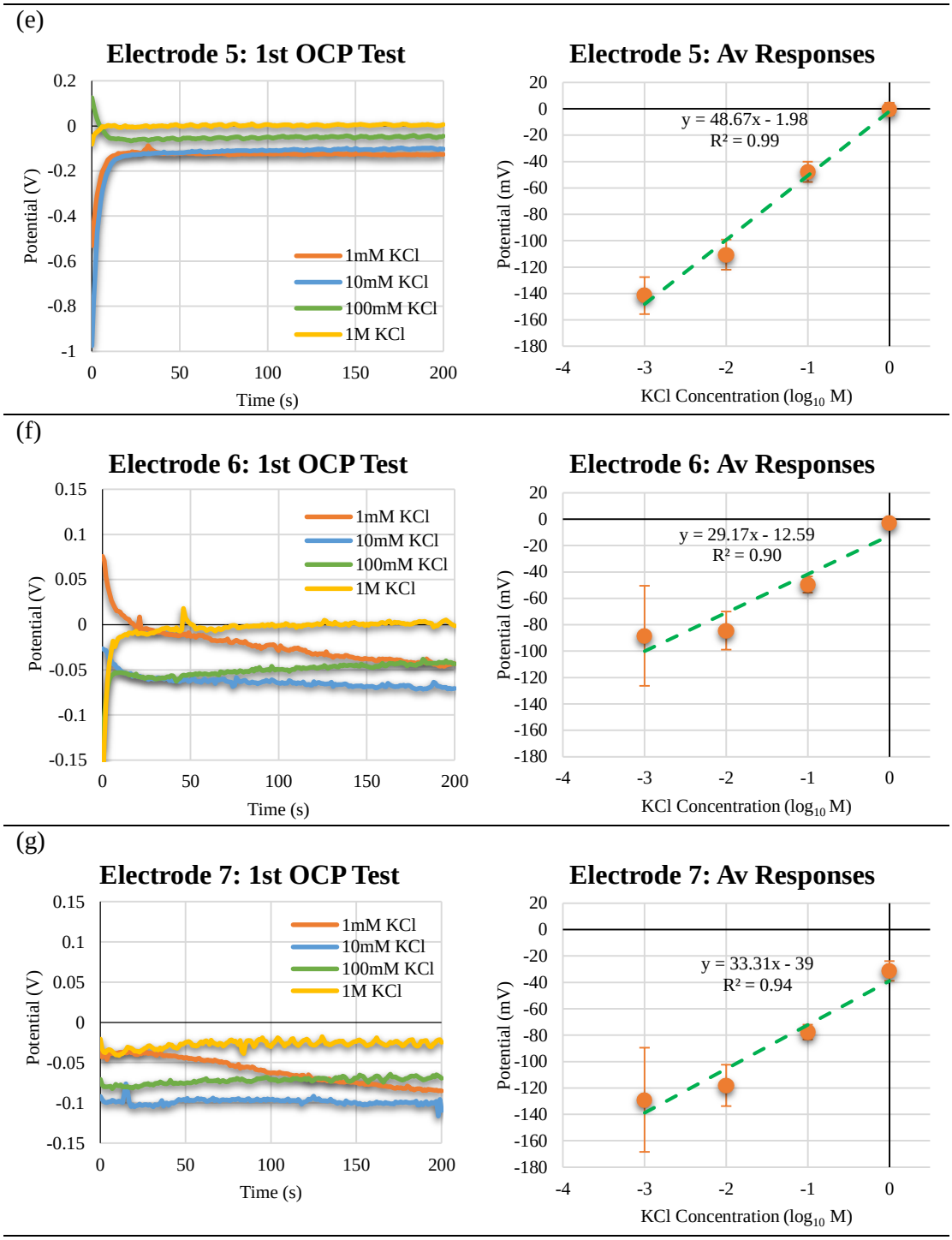

Figure 4.4. results obtained for investigation into HEMA gel UV LED polymerisation time. (a) - (g) pertain to Electrodes 1 - 7 respectively, whose polymerisation times are shown in Table 4.1. Shown for each electrode examined is: the temporal potentiometric responses of the electrode to the KCl test solutions for the initial OCP test performed upon it; and the mean potentiometric responses (n = 3) ± SD of the electrode plotted against the KCl concentration the test solution. Linear regression analysis is performed and shown where appropriate.

The measured potentials from the OCP tests of electrodes 1 and 2, figure 4.4 (a) and (b), exhibit extremely large initial potential values for each KCl test solution utilised. Electrode 1 returns values as large as -8 V when placed into the 1M KCl test solution. If we recall the discussion in Section 2.3.6, we know that the measured potential for a Cl^- concentration cell configuration like this is given by:

$$E = 0.059 \times \log_{10}\left(\frac{[Cl^-(aq)_{right}]}{[Cl^-(aq)_{left}]}\right). \quad (4.3)$$

If we assume that the Cl^- concentration at the QRE and WE electrode surfaces are 3 M and 1 M KCl respectively then we would expect to see a measured potential of magnitude approximately 28 mV. The large initial potentials of 4 - 8 V were continually observed in the remaining two OCP iterations for electrodes 1 and 2. In addition, the slow equilibration times exhibited mean that the measured potential had often not settled within the 200s measurement period. Consequently, the mean potentiometric responses of electrodes 1 and 2 show large values of standard deviation and, in the case of Electrode 1, no clear sensitivity toward the Cl^- concentration of the test solutions. Electrode 5, to a smaller extent, registers large initial voltages, however their lower magnitude and fast equilibration means it had little adverse effect on the electrode's performance. In contrast, the remaining electrodes exhibit potentiometric responses which are proportionate in magnitude to the relative Cl^- concentrations and are relatively stable for the test duration. These result in mean sensitivity curves which show a strong correlation toward the Cl^- concentration of the test solutions.

Electrodes 4 and 5, in particular, exhibit excellent sensitivity values approaching 50 mV/decade. This, alongside their steady and consistent potentiometric responses, were factors in choosing a cure time of 15 minutes for pHEMA electrodes polymerised using the UV LED array. Unless otherwise stated, results quoted in the remainder of this thesis were obtained using pHEMA electrodes polymerised under UV LED irradiation for 15 minutes.

4.3.1.2 Discussion

One possible explanation for the behaviour of Electrodes 1 and 2 noted above and shown in figure 4.5 (a) and (b), is the disturbance and re-formation of the electric double layer caused by the placement of the electrode into the test solution. If we recall from Section 2.4.2, an electric double layer forms when a collection of opposing charges gather at either side of the electrode - electrolyte boundary leading to the formation of a potential difference between the phases (58,154). This is illustrated again in figure 4.5.

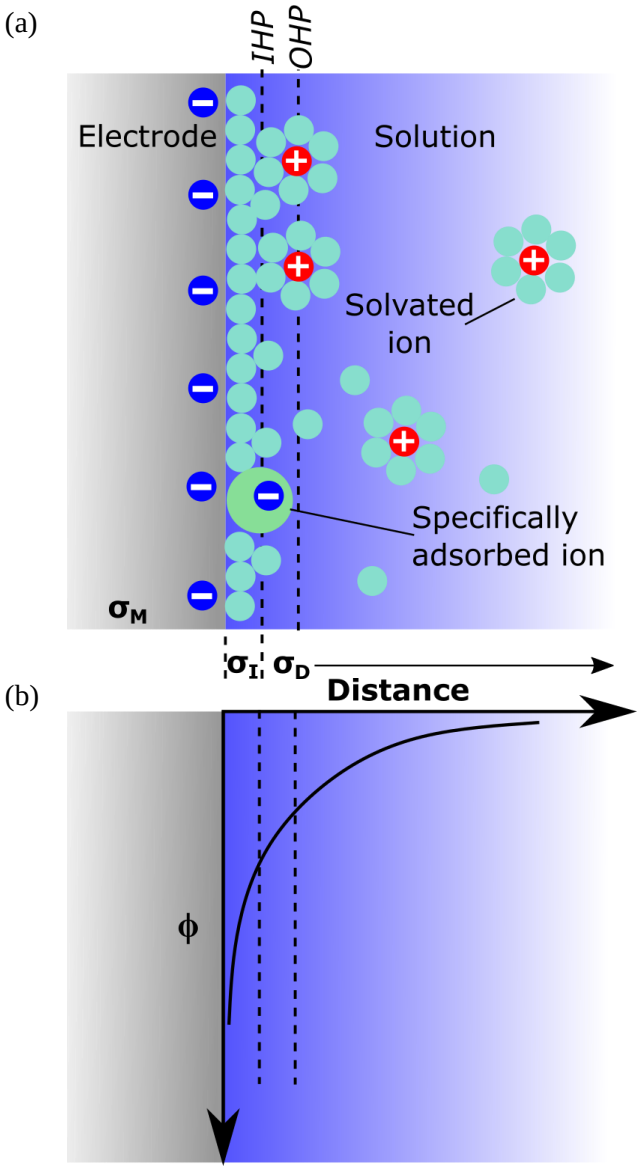

Figure 4.5. (a) Schematic representation of Bockris, Devanathan, and Muller model of the electric double layer caused by a metallic electrode in contact with an ionic solution, as described in Section 2.4.2 **(b)** The resultant potential of the system, ϕ, plotted with respect to distance from the electrode surface (58,153)

Rather than an electrode - electrolyte partition like that represented in figure 4.5 (a) above, when discussing the potentiometric responses of the pHEMA electrodes in the previous subsection, we must consider an electrode - hydrogel partition.

The potentiometric responses recorded for Electrodes 1 and 2 and shown in figure 4.4 (a) and (b), consistently show a large spike in potential at the onset of each test sequence. This coincides with the electrodes being placed into the test solution. Of the electrodes reported in Section 4.3.1.2, Electrodes 1 and 2, were polymerised for the shortest lengths of time: 2 and 5 minutes, respectively. This suggests that polymerisation time may affect the degree to which the measured potential is disturbed when submerged in a test solution. The hydrogel mixture utilised pHEMA to form the polymer network, DMPAP as a photoinitiator, and EGDMA to crosslink the network. The latter is required to prevent the hydrophilic polymer network from dissolving into an aqueous phase when hydrated (162,172). Studies have shown that the degree of polymerisation and the network structure of pHEMA hydrogels polymerised using UV irradiation are dependent upon the duration of irradiation (164,173,174). The study conducted in (164) reported on the effects of DMPAP photoinitiator concentration on the polymerisation rate of thick (up to 2 mm) UV curable hydrogels. The thickness of the pHEMA gels investigated in figure 4.4 is ~1 mm. The study found that while DMPAP is an efficient photoinitiator for such hydrogels, higher concentrations (> 0.25 wt %) of the substance can introduce a screening effect which slows the polymerisation rate of the entire hydrogel volume. This happens when the DMPAP closest to the UV source is initially consumed, producing light absorbing photoproducts in the process, which attenuates the light penetrating to deeper layers of the gel. This may lead to underlying layers of the gel being underpolymerised or completely unpolymerised (164). As noted in Section 3.2.1, 0.8g of DMPAP was used to make the stock HEMA hydrogel mixture, corresponding to 3.5 wt %. According to the study carried out by Glöckner (164), this would be considered a high concentration. Therefore, the HEMA gel mixture used in obtaining the results shown in figure 4.4 in the previous subsection may

experience a light screening effect when undergoing UV polymerisation. Consequently, it is possible that Electrodes 1 and 2 may not have had sufficient time in which to fully polymerise and thus contain a volume of unpolymerised gel, as illustrated in figure 4.6.

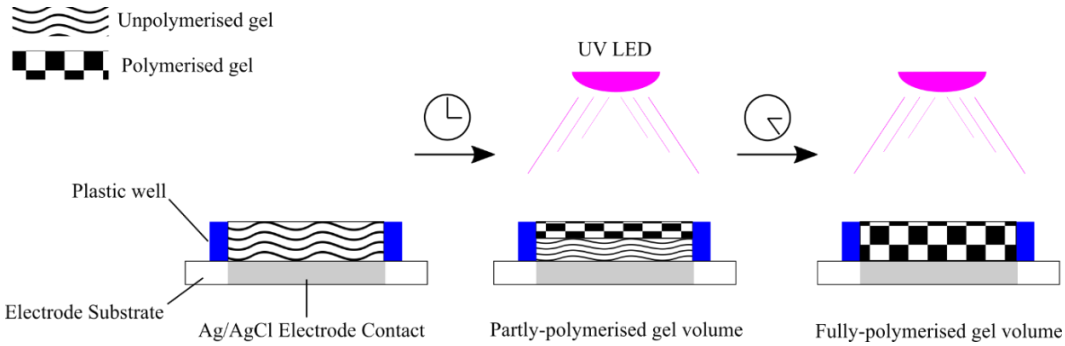

Figure 4.6. Cross-sectional view of HEMA gel deposited over Ag/AgCl electrode contact. Schematic shows the progression of HEMA polymerisation with exposure to UV radiation.

As described in Section 3.2.5, the electrodes are placed in a high concentration KCl DI water solution immediately after the UV LED polymerisation process. As such, the gel will be well wetted and ion-rich before it is placed into a test solution. An unpolymerised volume within the gel would provide a medium in which the ions are highly mobile (175). Consequently, the electric double layer which would form between the electrode contact and the unpolymerised gel volume would be highly susceptible to disturbance. Placing the electrode into a test solution, for example, could disturb the double layer, resulting in the large jumps in the measured potential observed in the OCP tests of Electrodes 1 and 2, figure 4.4.

The more settled and stable potentiometric responses observed in figure 4.4 are obtained from electrodes with a polymerisation time ≥ 10 minutes, more than twice as long as Electrodes 1 and 2's polymerisation times. These are similar to the times found for complete polymerisation for EGDMA-crosslinked HEMA gels in the study conducted in reference (174). They reported that complete polymerisation of the gels (whilst in solution) could take 10 - 30 minutes. The additional exposure that Electrodes 3 - 7 received in comparison to Electrodes 1 and 2 may

have given the gel samples sufficient time to fully polymerise, producing a polymer network volume more robust to physical disturbance.

The consistent and stable potentiometric responses of electrode 4 as well as the strong sensitivity it exhibited toward the Cl^- test concentration, meant its polymerisation time of 15 minutes (Table 4.1) was chosen as the polymerisation time for subsequent investigations.

4.3.2 pHEMA Cl^- Conditioning

Following the HEMA hydrogel's UV polymerisation, it is in a dry and glassy state. The hydrogel then undergoes a period of conditioning through immersion in a high concentration KCl DI water solution, as detailed in Section 3.2.5. When a crosslinked hydrogel like pHEMA is exposed to a solution, the molecular chains of the polymer undergo relaxation, allowing the solution to penetrate further into the hydrogel volume (176–178). This process is illustrated in figure 4.7, adapted from a study by Brazel & Peppas (176). It is through this mechanism we attempt to establish a stable Cl^- concentration within the gel barriers above the electrode contact, enabling it to be utilised as a QRE. Figure 4.8 shows a pHEMA hydrogel sample before and after the conditioning process, where it has gone from a dry, glassy state to a swollen, opaque one due to the absorption of the solution.

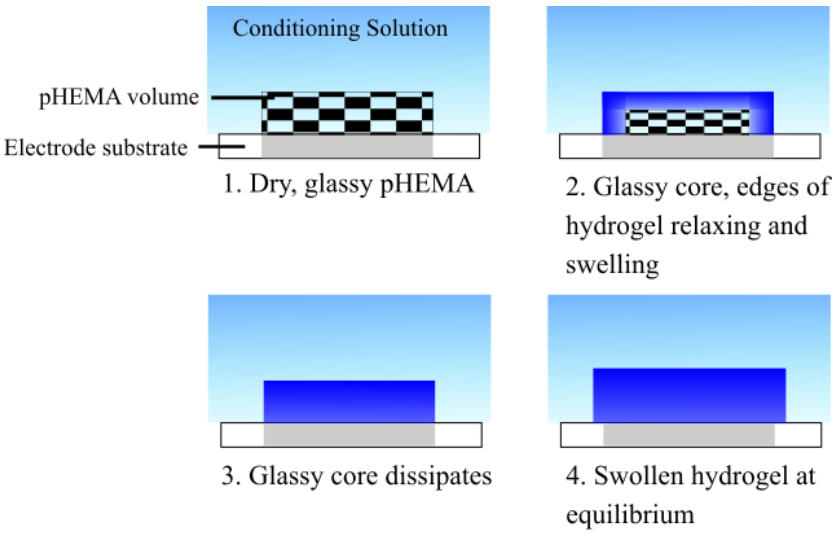

Figure 4.7. Schematic of water sorption progression in an initially dry, glassy pHEMA hydrogel. Adapted from (176).

(a) **(b)**

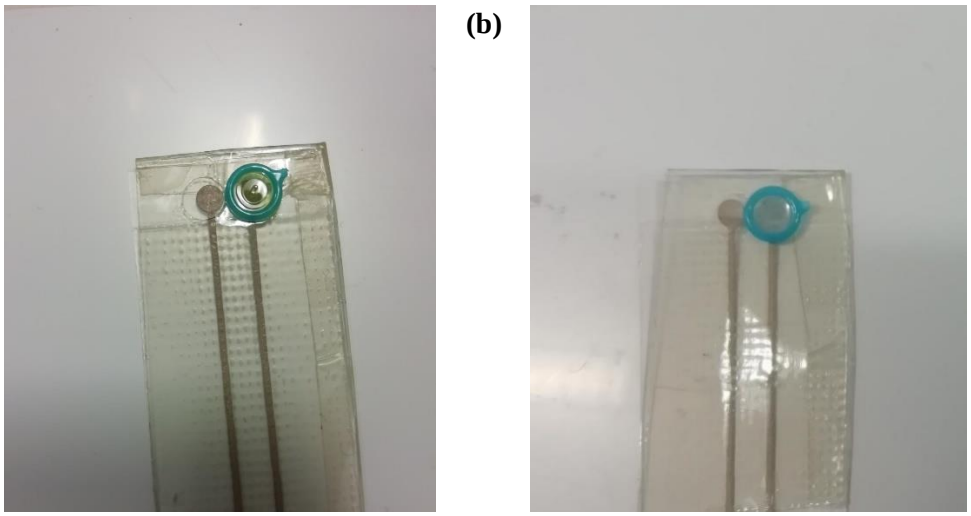

Figure 4.8. Woundsense electrode with: **(a)** dry, glassy pHEMA hydrogel before KCl DI water solution conditioning; **(b)** swollen, opaque pHEMA after conditioning.

As figure 4.7 suggests, the point at which the hydrogel has become fully saturated is dependent upon the length of time it is in contact with the solution. The methods used to investigate and quantify the conditioning process were detailed in Section 3.3.2. Whilst the pHEMA hydrogel electrode is conditioning in the KCl DI water solution, its OCP is measured with respect to a commercial 3M KCl Ag/AgCl RE. A plot of the pHEMA electrode's potential throughout the conditioning period is subsequently obtained. Equation 4.2 recalls the rearranged Nernst

equation introduced in Section 3.2.3, where C_{WE} and C_{RE} represent the Cl^- concentrations at the surfaces of the electrodes connected to the WE and RE leads of the potentiostat respectively.

$$C_{WE} = C_{RE} \times 10^{\left(-\frac{V_{meas}}{0.059}\right)}. \quad (4.2)$$

By substituting the measured potential values, V_{meas}, into equation 4.2, an estimate of the Cl^- concentration forming within the gel barrier layers can be made. We can, therefore, plot a profile of the Cl^- concentration with time, allowing us to gauge how it evolves over the conditioning period. It has been stipulated in previous chapters that the pHEMA electrode must possess a steady and consistent potential in order perform the role of a QRE. Within the plots obtained from the conditioning process this should be characterised by a sustained plateau in both measured potential and estimated Cl^- concentration within the effective barrier of the pHEMA hydrogel. The plots can therefore be used to gauge the appropriate length of the conditioning time.

4.3.2.1 3M KCl Conditioning: Results

Initial investigations into the preparation of the gel utilised a 3 M KCl DI water conditioning solution, as detailed earlier in Sections 4.2 and 4.3.1. Figure 4.9 shows the profiles obtained for a pHEMA electrode for this conditioning process. In figure 4.9 (a) the measured potential during the conditioning process can be split roughly into two segments: a phase which lasts approximately 20 hours displaying an equilibration from an initial large potential magnitude of ~8 V; and a more settled potential which maintains for the duration of the conditioning period. From figure 4.9 (b) we see that the large potentials registered in the initial phase result in such high estimated Cl^- concentrations that they far outweigh the 3 M KCl available from the conditioning solution. This suggests there is another process at play, possibly a double layer effect, which is causing such large values to be recorded.

(a)

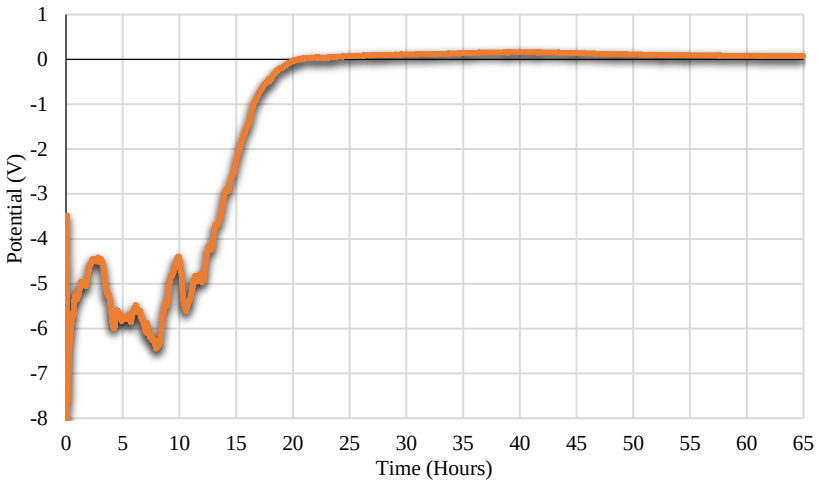

(b)

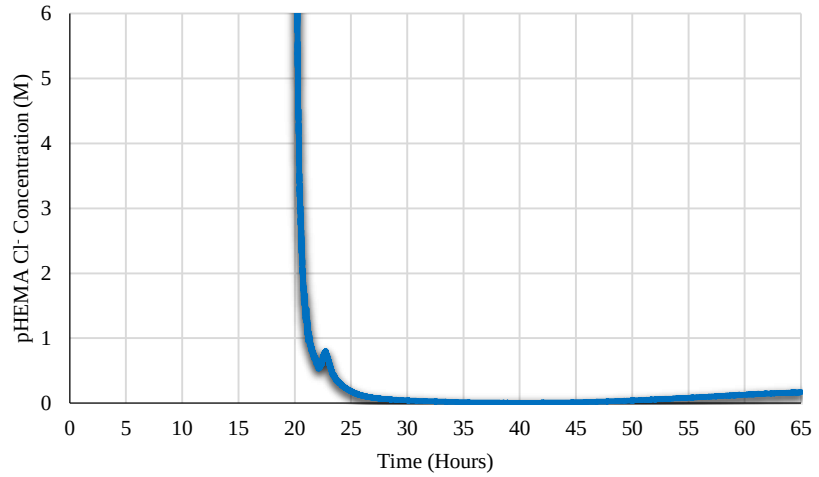

Figure 4.9. Conditioning profiles of electrode in 3 M KCl solution. (a) Measured potential of pHEMA electrode with respect to commercial RE. (b) Effective barrier Cl^- concentration estimated within pHEMA hydrogel.

Figure 4.10 provides a more scaled view of the profiles after the initial equilibration phase. Here it is evident that there is a distinct peak in measured potential, and a trough in estimated barrier Cl^- concentration after 40 hours of conditioning.

(a)

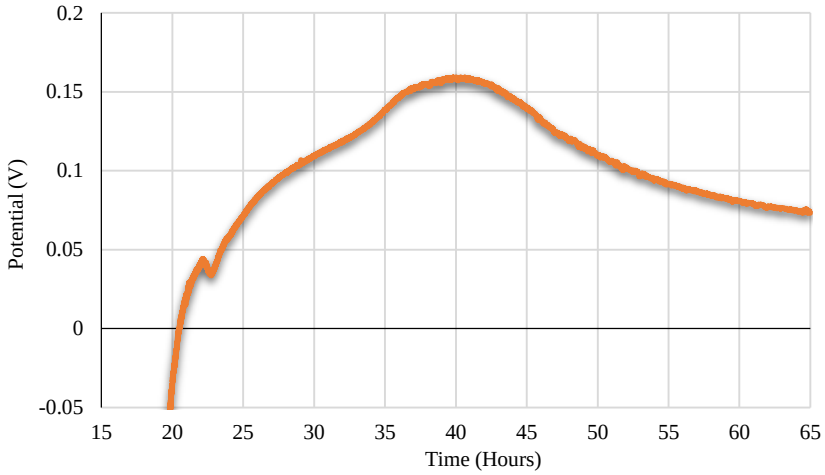

(b)

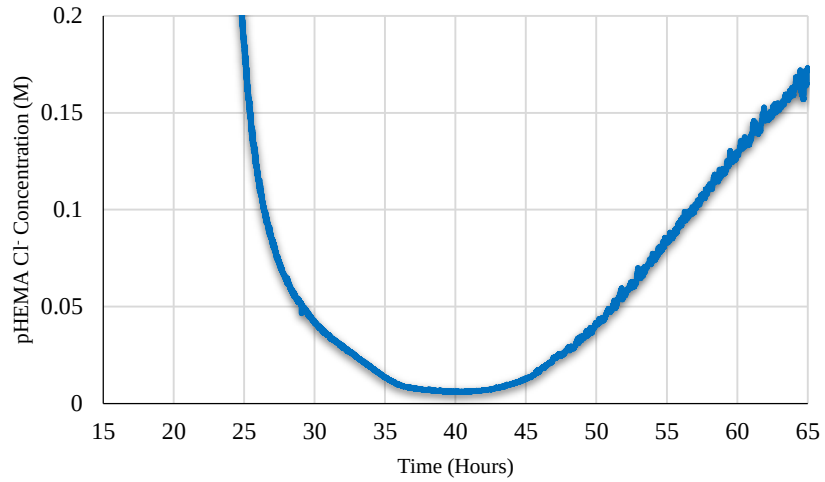

Figure 4.10. Enhanced views of 3 M KCl conditioning profiles showing (a) the peak in measured potential of pHEMA electrode and (b) the trough in the effective barrier Cl^- concentration of the hydrogel.

In the previous subsections of this chapter, the conditioning period was arbitrarily set at 25 hours. From figure 4.10 we can see that this point coincides with a period of flux both in measured potential and estimated barrier Cl^- concentration. The latter appears to be very rapid after 25 hours, suggesting that by this point, the effective barriers of the hydrogel had not yet reached a steady Cl^- concentration. After 65 hours of conditioning in the 3 M KCl solution, the measured potential appears to be plateauing, though this is less pronounced in the estimated barrier concentration. To further assess the effects of 3 M KCl conditioning time, the potentiometric performances of two electrodes were compared. Figures 4.11 and 4.12 display

the Cl^- sensitivity curves of electrodes with pHEMA QREs conditioned in 3M KCl DI water. The electrode shown in figure 4.11 was conditioned for 25 hours, while the electrode shown in figure 4.12 was conditioned for 90 hours, where the measured potential would be expected to have plateaued. It should be noted that different test concentrations are utilised in the tests shown in figures 4.11 and 4.12 as they were performed at different stages of the investigation into the pHEMA hydrogel. As explained in Section 3.3.1, the test concentration range narrowed as the project progressed to reflect typical sweat Cl^- levels. The data shown in figure 4.12 was collected at a later stage than that in figure 4.11.

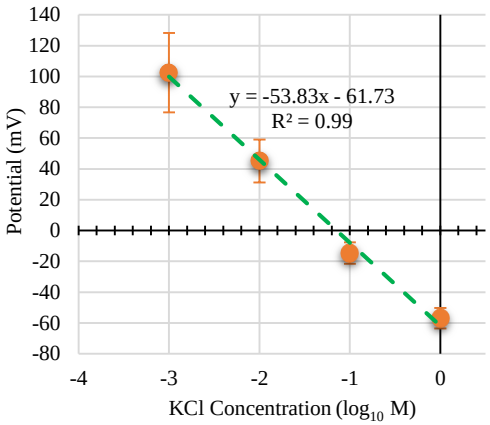

Figure 4.11. Sensitivity curve of electrode cured in 3M KCl for 25 hours. Data points represent the mean potentiometric responses ± SD (n = 4) to test solutions. Results of linear regression analysis performed are also shown.

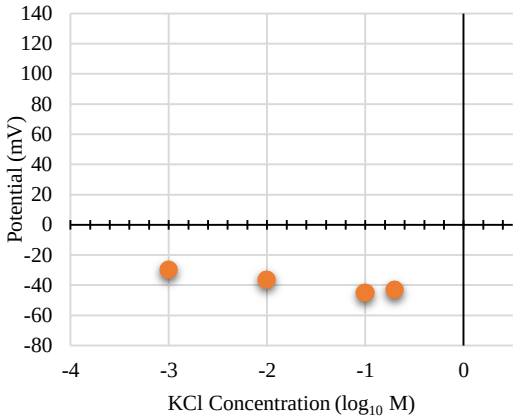

Figure 4.12. Sensitivity curve of electrode cured in 3M KCl for 90 hours. Data points represent the potentiometric responses (n = 1) to test solutions.

There is a marked difference in the potentiometric responses shown in the figures above. The electrode with pHEMA QRE conditioned for 25 hours, figure 4.11, shows a clear, near Nernstian sensitivity toward the Cl^- test concentration. This is similar to those shown in previous sub sections (figure 4.3 (c) and (d), Section 4.2.2; and figure 4.4 (d), Section 4.3.1.1) of electrodes also conditioned in 3 M KCl for 25 hours. Contrast this with the lack of sensitivity displayed by the electrode conditioned for 90 hours in figure 4.12. Recall from Section 4.2.2, figure 4.3 (a) and (b), that similar responses were measured from electrodes conditioned for 90

hours in 3 M KCl, following Hg bulb polymerisation. Perhaps counterintuitively, the electrode conditioned for a period of time which would allow for a steady reference potential to form shows little-to-no sensitivity toward Cl^- test solutions. This suggests that conditioning the pHEMA hydrogel for a prolonged period may have an adverse effect on the potentiometric performance of the electrode. The possible reasons for this are discussed in Section 4.3.2.3.

The lack of sensitivity exhibited by the electrode in figure 4.12 coupled with the large flux in effective barrier Cl^- concentration after 25 hours of conditioning, suggested that it may not be suitable to use a 3 M KCl solution to condition the pHEMA hydrogel. The proceeding subsection investigates how the conditioning profiles are affected by altering the concentration of the conditioning solution.

4.3.2.2 Altering Conditioning Solution Concentration: Results

Using the same protocol as that used to obtain the 3 M KCl conditioning profiles in Section 4.3.2 above, the potentials of two pHEMA electrodes were measured against a commercial 3 M KCl RE whilst they conditioned in 1 M and 2 M KCl DI water conditioning solutions, respectively. Figure 4.13 shows the conditioning profiles obtained from these observations, alongside the 3 M KCl profile from the previous subsection. The corresponding calculations of the pHEMA gel barrier Cl^- concentration are shown in figure 4.14.

(a)

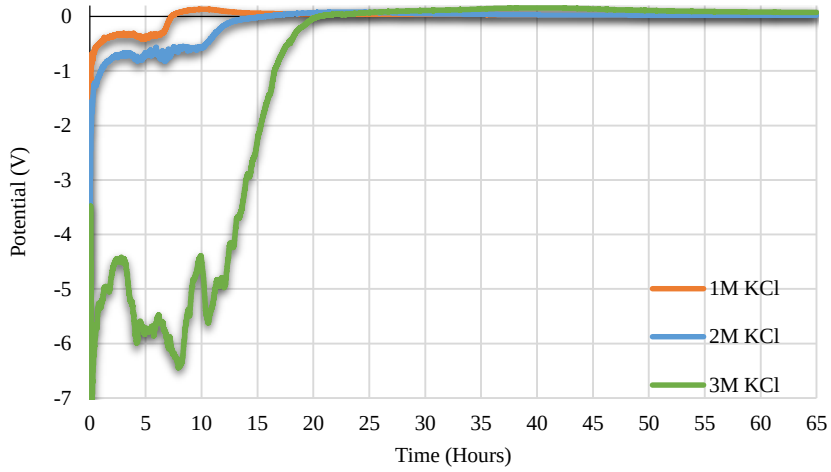

(b)

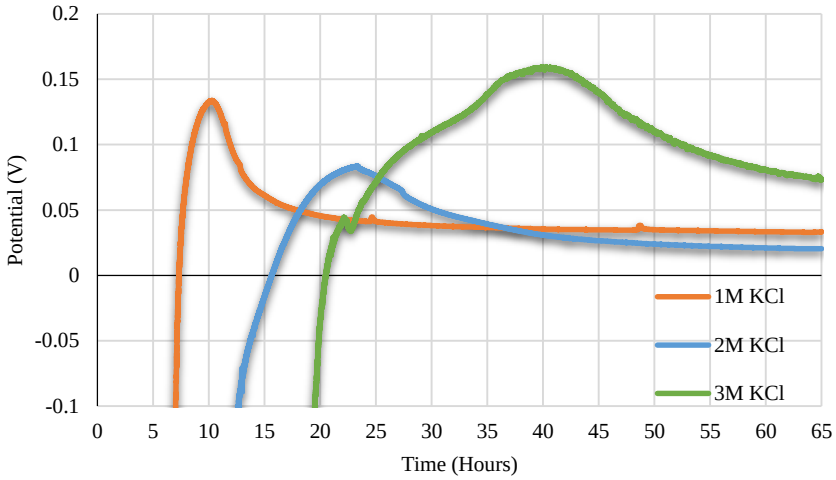

Figure 4.13. Potentials of three pHEMA electrodes, each measured against a commercial RE, whilst conditioning in KCl solutions of concentration 1 M, 2 M, and 3 M respectively, (a) Potentials recorded over full measurement period. (b) Focus on the time periods in which there are peaks in the measured potentials.

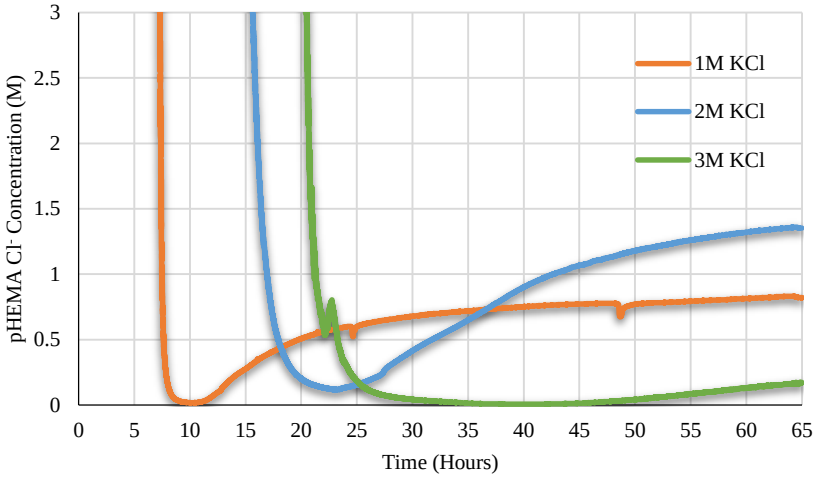

Figure 4.14. Effective barrier Cl^- concentrations estimated within pHEMA gel electrodes throughout their respective conditioning processes.

The key findings from figures 4.13 and 4.14 are summarised in Table 4.2. From figure 4.13 (a) it is apparent that each of the profiles follow roughly the same pattern: an equilibration from an initially large potential, before reaching a peak, and gradually plateauing in potential. However, attributes such as the location of the potential peak and the rate of change of potential change are different for each profile. Examining the initial equilibration phase, we see from figure 4.13 (a) that the 1 M and 2 M KCl profiles undergo a much more rapid equilibration compared to the 3 M KCl profile. The peak in measured potential for the 1 M KCl concentration occurs quickest after around 10 hours, followed by the 2 M KCl profile at around 23 hours, and the 3 M KCl at 40 hours. Additionally, the peaks of the latter two concentrations are drawn out and elongated. This makes the plateauing in potential a more gradual process. In contrast, the peak of the 1 M KCl profile is pronounced, exhibiting a sharp decline followed by a consistent plateau for the remainder of the observation period. When viewed in the context of the effective barrier concentration in figure 4.14, a similar pattern emerges. The potential peak corresponds to a trough in estimated effective barrier concentration, as was previously seen with the 3 M KCl profiles in the previous subsection. Unlike the 3 M profile, where the effective barrier concentration is slow to recover following the trough, the 1 and 2 M KCl profiles in figure 4.14

exhibit a marked increase in the estimated Cl^- barrier concentrations. The 1 M KCl profile reaches a steady concentration of magnitude similar to that of the conditioning solution after around 25 – 30 hours of conditioning. This suggests that the pHEMA hydrogel has become saturated with Cl^- ions and the electrode possesses a stable potential. Recalling figure 4.1 (b) and (c), Section 4.1, this is a key criterion for the electrodes use as a QRE within a Cl sensor. Contrast this to the estimated effective barrier concentration of the 3 M KCl profile where after 65 hours of conditioning the concentration has reached a magnitude of around 0.2 M, a fraction of the 3 M conditioning solution concentration. In addition, the estimated concentration has not plateaued by this point, suggesting that a steady effective barrier Cl concentration has not yet been reached. These factors may help explain the poor potentiometric performances of electrodes with pHEMA QREs conditioned in 3 M KCl in excess of 65 hours, such as figures 4.3 (c,d) in Section 4.2.2, and figure 4.4 in Section 4.3.2.1. Possible reasons as to why the 3 M KCl conditioning profiles behave this way are explored in the proceeding discussion.

Table 4.2. Summary of conditioning profile characteristics with respect to conditioning solution concentration.

Conditioning Solution Concentration (M)	Approximate time of measured potential peak / estimated barrier Cl^- concentration trough (Hours)	Notes
3	40	• Prolonged period to reach potential peak/concentration trough • No indication of steady Cl^- concentration within gel barrier after 65 hours of conditioning • Estimated barrier Cl^- concentration at very low levels • Poor potentiometric performance of electrodes conditioned in 3M KCl for prolonged period
2	23	• Indications of stable Cl^- concentration being reached after 65 hours of conditioning • Magnitude of estimated barrier Cl^- concentration approaching that of the conditioning solution

Conditioning Solution Concentration (M)	Approximate time of measured potential peak / estimated barrier Cl^- concentration trough (Hours)	Notes
1	10	• Stable measured potential / estimated Cl^- concentration observed after ~25 hours of conditioning • Magnitude of estimated barrier Cl^- concentration approaching that of the conditioning solution • Consistent potentiometric responses with good sensitivity obtained from electrodes conditioned in 1 M KCl for 25 hours (See Section 4.4).

4.3.2.3 Discussion

It is possible that the large initial potentials measured in the initial stages of the conditioning process, figure 4.13, is the result of a double layer effect. Notably, there is interest in the use of certain polymers to form electric double layer capacitors (EDLC), or supercapacitors. Conventional capacitors store energy within a dielectric material via an electric field, where the capacitance is given by:

$$C = \frac{\varepsilon A}{d}, \tag{4.3}$$

where ε is the absolute permittivity of the dielectric (F m^{-1}), A is the surface area of the capacitor (m^2) plates, and d is the separation between them (m). EDLCs utilise electrode materials with large surface areas, like porous hydrogels, to store energy through the enhanced double layer effect which occur when they come in contact with an electrolyte solution (175,179–181). This is illustrated in Figure 4.15.

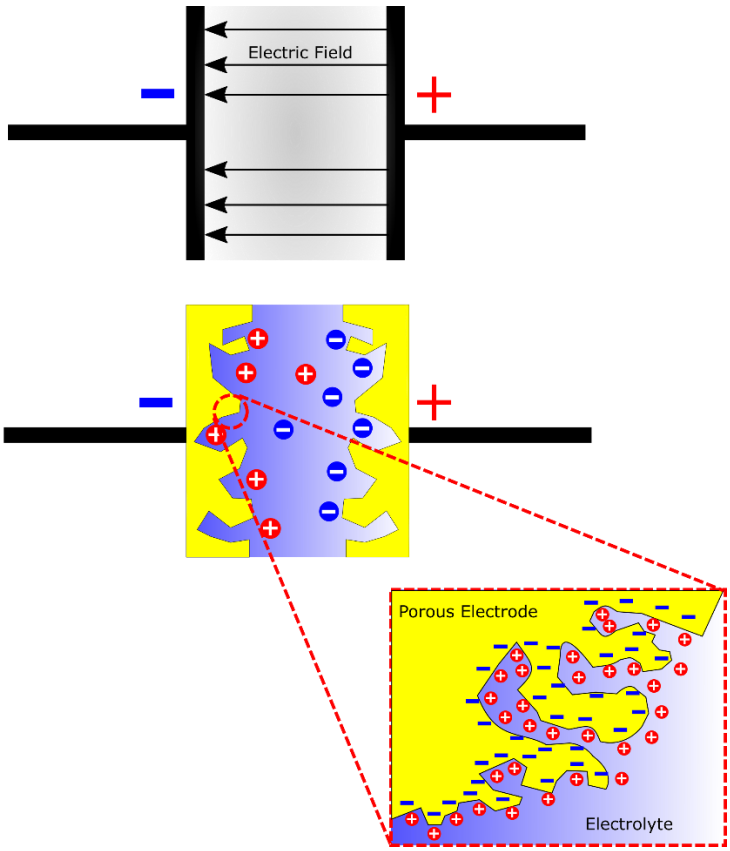

Figure 4.15. schematic representations of electric charge storage in: **(a)** a conventional capacitor, through the generation of an electric field within a dielectric material; and **(b)** an electric double layer capacitor (EDLC) utilising the large surface area of a porous material to enhance the electric double layer effect detailed in Section 2.4.2. Adapted from (175).

It should be noted that normal metallic electrode contacts will not be perfectly smooth, as is illustrated in figure 4.15 (a) above and will contain imperfections which increase their surface area. The extent of this in comparison to the materials used to create EDLCs, however, is insignificant. Such a device was developed using UV polymerised pHEMA hydrogel in study conducted by Kim, Kannan, and Chung (182). Whilst conventional dielectric capacitors typically have capacitances in the nF to µF range, capacitors exploiting materials with large surface areas and electrolytes can have capacitances ranging from 10 µF - 100 mF (183,184). Typically these have operating potentials of around 1 - 100 V (183). Capacitance is defined as the ratio of charge, Q, to the voltage, V, across the capacitor, meaning capacitors utilising materials of large surface area can store ~10 C of charge (183).

Using the Palmsens potentiostat to perform an impedance spectroscopy reading on the pHEMA electrode when it is first placed into the conditioning solution, it was estimated that the capacitance of the configuration during this period could be as high as 0.7 mF, comparable to the magnitudes of the capacitors utilising materials of large surface areas quoted above. Although this was not investigated in depth in the current work programme, such tests suggested that the capacitive properties of the sensor are high and initial currents could subsequently have large spikes from C×dV/dt capacitive current effects. It is plausible, therefore, that the large potentials recorded in the initial stages of the pHEMA hydrogel's conditioning could be the result of the formation of electric double layers enhanced by the large surface area of the pHEMA.

Another point of interest is that of the variation between the conditioning profiles shown in figures 4.13 and 4.14 which hint that the concentration of the conditioning solution affects the dynamics of the solution's uptake within the hydrogel. It is worth considering first the relationship between the concentration of the conditioning solution and the time taken to record a steady effective barrier concentration. Assuming that the penetrant transport through the hydrogel is purely dictated through Fick's 1st law, equation 4.4, then one would expect a steady state to occur, and a steady concentration to be measured, more rapidly with increasing concentration of conditioning solution.

$$J = -D\frac{\partial C}{\partial x}. \tag{4.4}$$

Here, J is the flux of penetrant ($m^{-2}s^{-1}$), D is the diffusion coefficient (m^2s^{-1}), and C is the concentration of the penetrant (M). Conversely, in figure 4.14, there is an apparent delay in the time taken to reach a steady effective barrier concentration with increasing conditioning solution concentration. Studies have found that the transport of solutes through swellable hydrogels such as pHEMA may be non-Fickian in nature and dictated by the relaxation of the polymer as it transitions from a glassy to a swelled state, termed Case II transport (185,186).

Often, however, it is the case that the penetrant transport through a hydrogel is a combination of Fickian and Case II (178,187), mathematically described by the relationship (176,188):

$$\frac{\partial C}{\partial t} = \frac{\partial}{\partial x}\left(D_{1,2}\frac{\partial C}{\partial x} - vC_1\right), \tag{4.5}$$

where C_1 is the concentration of penetrant, $D_{1,2}$ is the diffusion coefficient, and v is the velocity (ms^{-1}) of the penetrant front. The "$-vC_1$" term characterises the constant velocity Case II transport of the system. Hopfenberg and Frisch (188) studied the transport of hydrocarbons through glassy polystyrene. They found that Case II transport occurred when penetrant activity was relatively high (activity: 0.5 – 1), and was accompanied by time dependent anomalies in diffusion (188). Studies have demonstrated that Case II transport can occur in pHEMA hydrogels including those containing PVP (176,178), similar to the composition used in our investigations. This may explain the apparent increase in the time taken to reach a steady concentration with the increase in conditioning solution concentration observed in figure 4.14. Further study would be needed to investigate this.

Another point of interest during the conditioning studies, and previously in Section 4.2.2, is the poor potentiometric performance of the electrode conditioned in 3 M KCl for 90 hours, figure 4.12. A study conducted by Lee and Bucknall (173) examined the swelling behaviour and network structure of UV polymerised hydrogels. It found that immersion in high concentration saline solutions for prolonged periods led to the partial disintegration of the polymer networks of n-vinyl-2-pyrrolidone (VP) and HEMA hydrogels (similar composition to the hydrogel used in our studies). In addition, they noted that cracking may occur when the hydrogel is exposed to the saline solution. This is known as crazing, and was also noted by Hopfenberg and Frisch (188), among others (176,178), to occur when penetrants of high activity (defined by the authors as 0.85 – 1) (188) apply stress to the dry polymer network as they are absorbed. In these scenarios, therefore, the hydrogel's ability to act as a matrix to retain a steady Cl concentration and perform as a QRE, could be compromised. This may explain the poor

potentiometric performances of electrodes conditioned in 3 M KCl solutions for prolonged periods of time.

These points suggest that there is a balance to be struck when conditioning the pHEMA hydrogel, between ensuring that the barrier gel layers possess a steady Cl concentration and limiting the time in which it is exposed to the potentially destructive saline solution. Consequently, a 3 M KCl conditioning solution was deemed unsuitable for this application. Examining again the effective barrier Cl^- concentrations estimated, shown in figure 4.16 after 20 hours, we can see that although the barrier gel layers exposed to the 2 M KCl solution exhibit an equilibrium Cl concentration, this is only after 65 hours of conditioning. This could be considered a prolonged period time and therefore potentially damaging to the gel.

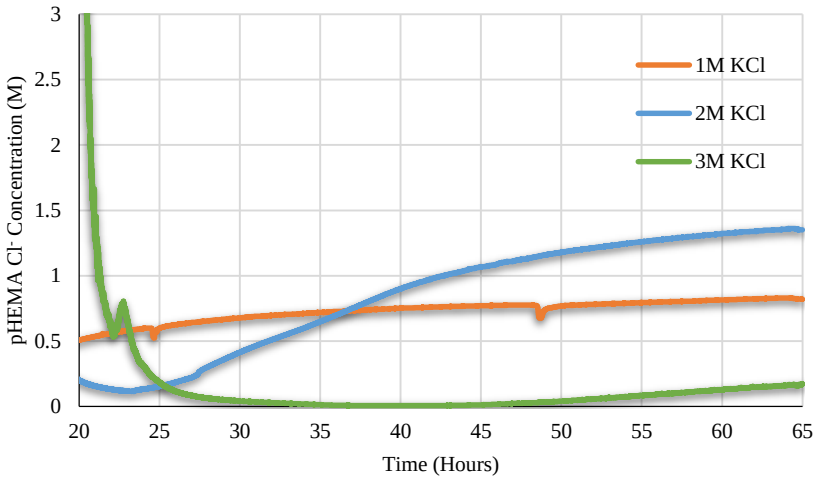

Figure 4.16. Effective barrier Cl^- concentrations estimated within pHEMA gel electrodes during the latter stages of the conditioning processes.

In addition, the need to wait for a minimum of 65 hours for hydrogel electrodes to condition is impractical in terms of their manufacture and subsequent testing. In figure 4.16, it is clear that the only suitable candidate for conditioning solution concentration is the 1 M KCl solution, which takes around 25 hours to reach a steady estimated Cl^- concentration. As such, pHEMA electrodes for subsequent tests and analyses, unless otherwise stated, were conditioned in a 1 M KCl solution for 25 hours.

4.4 Calibration Curve

With the hydrogel's conditioning process established, the next stage of the sensor's development involved obtaining a calibration curve for the pHEMA Cl^- sensor. The protocol described in Section 3.3.6 was used to examine pHEMA electrodes conditioned in 1 M KCl for 25 hours. The purpose of this was to provide a mechanism through which a Cl^- concentration could be obtained from a measurement of potential, as illustrated in figure 4.17. Consequently, the sensor could be used to determine the Cl^- levels in 'unknown' samples such as human sweat.

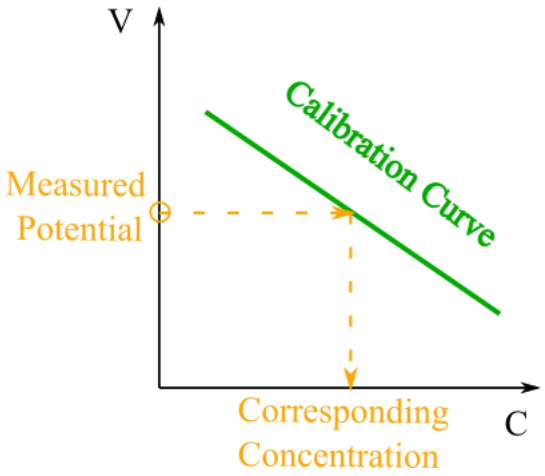

Figure 4.17. principle of calibration curve.

4.4.1 Results

The calibration curve shown in figure 4.18 was obtained using the average potentiometric responses of six pHEMA Cl^- sensors toward KCl DI water test solutions of concentration 10, 50 and 100 mM respectively.

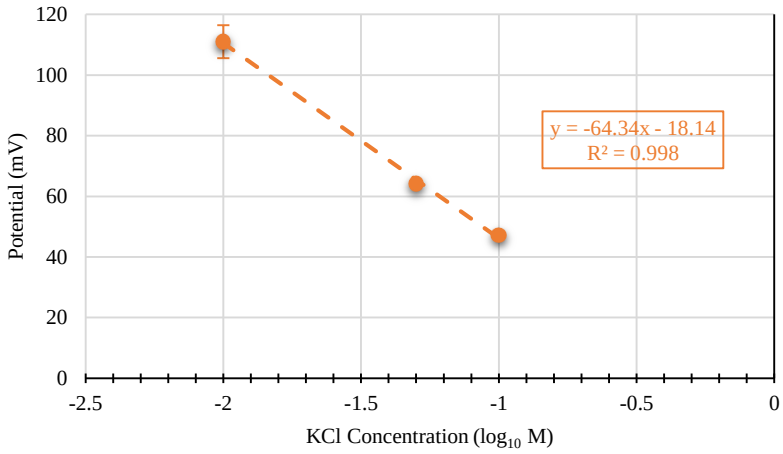

Figure 4.18. Calibration curve obtained from six pHEMA electrodes. Data points represent mean potential ± SD (n = 6). KCl test solutions of concentrations 10, 50, and 100 mM were utilised. Results from linear regression analysis performed on each dataset are also given.

Table 4.3. Mean potentiometric responses (n = 6) recorded for each test solution concentration. Data was used to obtain calibration curve.

Test Solution Concentration (mM)	Mean Potential (mV)	SD (± mV)
10	110.98	5.44
50	64.03	0.97
100	47.23	0.72

The electrodes used to obtain the calibration curve in figure 4.18 each exhibited a high degree of sensitivity toward the Cl^- concentration of the test solutions. This is illustrated in the near Nernstian sensitivity of 64.34 mV/decade obtained from the linear regression analysis performed on the mean potentiometric responses of the electrodes. This compares well to the reported sensitivities of 58 mV/dec and 58.5 mV/dec of Cl^- sensitive hydrogel electrodes from the literature (70,75) (Section 1.3.2.3). The study by Dam et al (70) uses a similar pHEMA hydrogel mixture to create a pseudo RE. This however was conditioned in a 3M KCl solution for 24 hours, a conditioning concentration which did not produce electrodes with good potentiometric performance when examined with the pHEMAWoundsense electrode, as described the previous sub-section. Choi et al (75), on the other hand, utilised a UV-curable

resin to provide the matrix structure over their pseudo RE. Their device was reported to have a sensitivity of 58.5 mV/dec toward the Cl^- concentration of test solutions. Additionally, the consistency of the potentiometric responses of the electrodes toward the test solutions results in small levels of deviation across the six electrodes utilised, as is shown in Table 4.3. This provides a degree of confidence that the electrodes are reproducible, and that the linear equation obtained may be used as the method of measuring the Cl^- concentrations of test samples. As such, the calibration curve can be obtained by rearranging the equation shown in figure 4.18:

$$C = \frac{(V + 18.14)}{-64.34}. \tag{4.6}$$

Bearing in mind the x-axis in figure 4.18 accounts for the logarithmic concentrations of the test solutions, the calibration curve becomes:

$$C = 10^{\frac{(V+18.14)}{-64.34}}. \tag{4.7}$$

Here, C is the Cl^- ion concentration of the test solution (M) and V is the measured potential (mV). Equation 4.7 will be used in proceeding chapters as a method of analysing the accuracy of the electrodes' sensitivity toward Cl^-.

4.5 Accuracy

The calibration curve given by equation 4.7 was used to gauge the accuracy of newly conditioned electrodes in returning a Cl^- concentration. This was performed according to the protocol described in Section 3.3.5 where, following their conditioning process, electrodes were first placed in a KCl DI water solution of 1 mM concentration to allow their potential to equilibrate. The sensors' average potentiometric response toward KCl test solutions of concentrations of 10, 25, 50, 75, 100 and 125 mM was calculated and placed into an adapted version of equation 4.7 to obtain the corresponding concentration:

$$C_{CC} = \left(10^{\frac{(V+18.14)}{-64.34}}\right) \times 1000, \tag{4.8}$$

where C_{CC} denotes the concentration extrapolated from the calibration curve in mM and V the average potentiometric response to the test solution in mV. The value obtained was then compared to the known concentration of the test solution, C_{TS}:

$$\xi = C_{TS} - C_{CC}. \tag{4.9}$$

The value of ξ, therefore, is a measure of the accuracy of the sensors. In total, eight electrodes were used to collate values of ξ for each test concentration.

A similar method was employed to assess the deviation of the measured voltage from the calibration value. To do so, equation 4.8 was rearranged and adapted such that the subject, V_{CC}, provided the voltage values on the calibration curve corresponding to the test solutions concentrations utilised:

$$V_{CC} = \left(-64.34 \times log_{10}\left(\frac{C_{TS}}{1000}\right)\right) - 18.14, \tag{4.10}$$

This process is illustrated in figure 4.19. Table 4.4 provides the values of V_{CC} obtained by placing the test concentrations into equation 4.10.

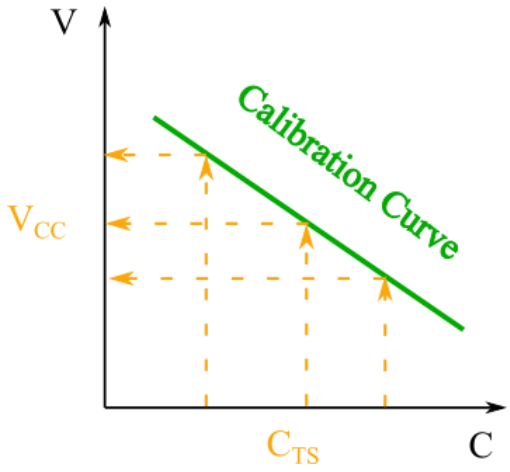

Figure 4.19. Illustration of process to obtain calibration curve potentials (V_{CC}) corresponding to the test solution concentrations (C_{TS}) used in accuracy study.

Table 4.4. Calibration curve potentials, $V_{CC,}$ corresponding to KCl test concentrations, C_{TS}, calculated via equation 4.10.

C_{TS} (mM)	V_{CC} (mV)
10	110.54
25	84.93
50	65.50
75	54.24
100	46.20
125	39.96

The V_{CC} values shown in Table 4.4 were used in conjunction with the calculated mean potentiometric response of the electrode toward a test solution, V, as a further method of examining the measurement accuracy of electrodes in comparison to the calibration curve.

$$\delta = V_{CC} - V \tag{4.11}$$

Figure 4.20 shows a series of box plots examining the spread of values of ξ and δ obtained for each test solution concentration.

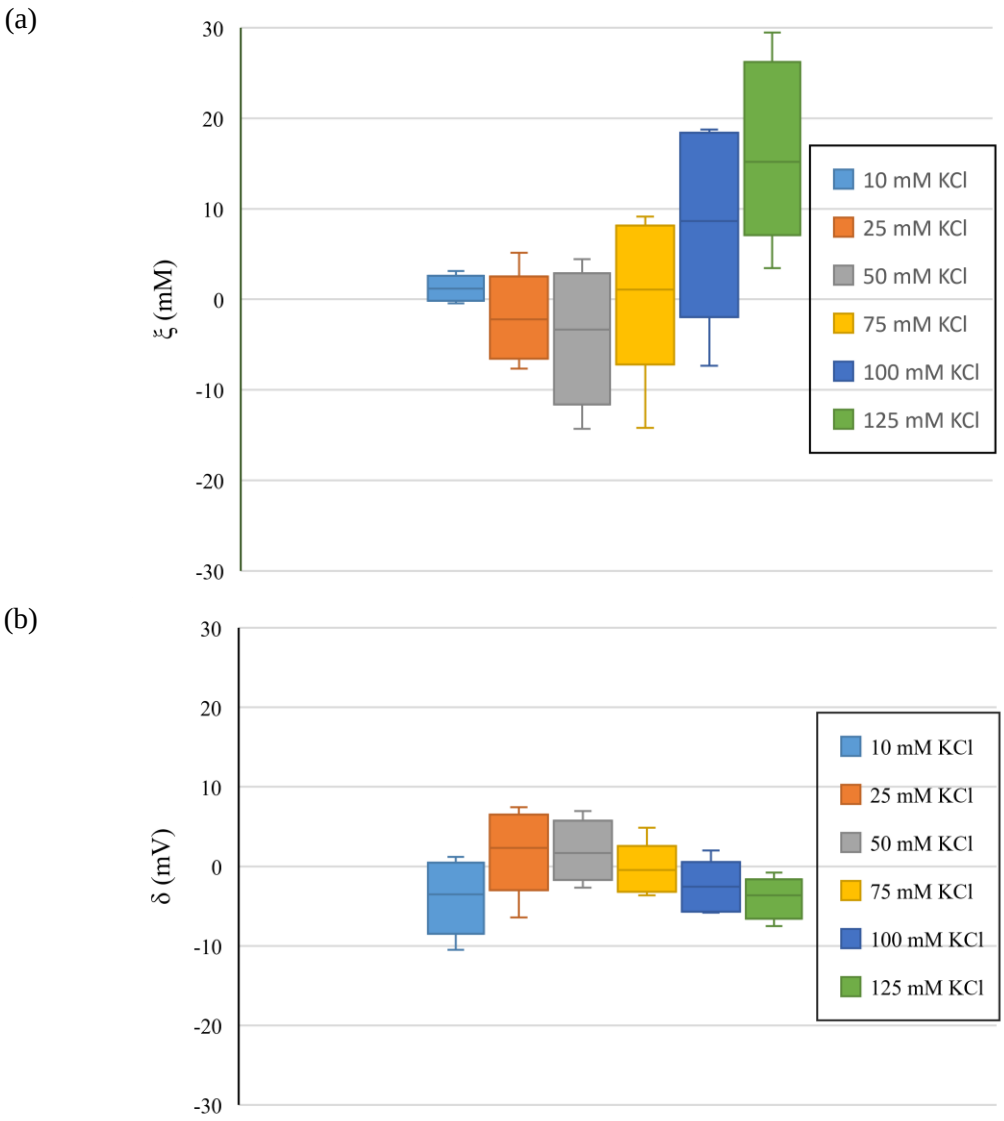

Figure 4.20 Boxplots displaying the array of values obtained to gauge the measurement accuracy toward KCl test solutions (concentrations provided in the legend). Each boxplot represents data acquired using n = 8 pHEMA Cl^- sensors. (a) The spread of ξ values obtained, representing the difference between the known concentration of the test solution, C_{TS}, and that extracted from the calibration equation, C_{CC}. (b) The spread of δ values obtained, representing the difference between the known calibration curve value of potential, V_{CC} (see figure 4.19) and the measured potential, V.

4.5.1 Discussion

Figure 4.20 (a) shows that as the KCl test concentration increases, then the spread of concentration values returned by the sensor via equation 4.10 becomes wider. However, figure 4.20 (b) shows that over the same range the disparity in measured potential from calibration

potential becomes smaller. The logarithmic nature of the Nernst equation means that for larger concentrations, small variations in measured potential are magnified when they are placed into equation 4.10 to obtain a concentration. To demonstrate this, Table 4.5 shows the effect that changing the measured potential by just 1 mV has on the resultant concentration extrapolated for the 10, 50, and 100 mM KCl test solutions.

Table 4.5. Demonstration of how the magnitude of the test concentration can lead to a larger ξ values.

KCl Test Solution Concentration (mM)	**V_{CC} (mV)**	**δ (mV)**	**C_{CC} (mM)**	**ξ (mM)**
10	110.54	-1	10.36	-0.36
		1	9.65	0.35
50	65.50	-1	51.95	-1.95
		1	48.36	1.64
100	46.20	-1	103.64	-3.64
		1	96.48	3.52

Table 4.5 shows that a deviation of 1 mV from the value of V_{CC} for 100 mM KCl test solution will result in a measurement error ten times that an identical deviation in voltage would cause for the 10 mM KCl solution. This explains why the largest spread of ξ values displayed in figure 4.20 (a) originate from the 100 and 125 mM KCl solutions. It should also be noted that both these distributions are shifted into the positive half of the graph, meaning that the extrapolated concentrations values gained tended to be slightly undervalued. The calibration curve was obtained using test solutions of 10, 50, and 100mM, therefore it cannot be certain that the linearity extends to 125mM and the consistent undervalued concentrations may be the result of this. However, the measured potentiometric response toward any of the concentrations utilised was never more than 10 mV away from the value on the calibration curve. Although larger deviations will unavoidably occur from higher concentrations, the consistency in the potentiometric responses from electrode to electrode is encouraging. Figures 4.20 (a) and (b) demonstrate that conditioning the pHEMA electrode in 1 M KCl for 25 hours produces a device

which has very consistent potentiometric responses to a Cl^- concentration range of 10 – 125 mM which envelopes both healthy and elevated CF sweat Cl^- – related values. The reference values used for sweat test CF diagnoses, noted in Section 2.2.3.1, are provided again in Table 4.6. This shows that the Cl^- sensors are reproducible and provide a consistency enabling them to be used in a healthy volunteer study and potentially form the basis of a commercial device.

Table 4.6. Reference values for sweat chloride for diagnosis of CF (10)

Diagnosis	Chloride Concentration (mmol/L)
Negative	< 40
Borderline/Indeterminate	40-60
Consistent with CF	> 60

4.6 Potential Drift Studies

Potential drift observations were carried out to investigate the extent to which Cl^- ions were able to diffuse out from the pHEMA matrix over time. As explained in Section 2.4.8, when the gel is exposed to a test solution a concentration gradient will form between the high Cl^- concentration within the effective barriers of the hydrogel and the comparatively low Cl^- concentration of the surrounding solution. This gradient acts to draw the ions out of the gel, according to Fick's laws of diffusion, potentially altering the barrier Cl^- concentration and causing the reference potential to drift. As such, this section investigates the pHEMA gel's susceptibility to this occurrence. Using pHEMA electrodes conditioned in 1 M KCl for 25 hours, tests were performed according to the protocol outlined in Section 3.3.3. The OCP of the pHEMA electrode was measured against the 3 M KCl commercial reference electrode whilst it was placed in a KCl DI water test solution over an 8 hour period.

4.6.1 Results

Figure 4.21 (a) shows the measured potential of three pHEMA electrodes placed within test solutions of concentration: 50, 75, and 125 mM KCl respectively. Figure 4.21 (b) provides the effective Cl^- barrier concentrations over the same period estimated using the measured potentials. Figure 4.21 (a) shows that the measured potential of the electrode increases at a steady rate after around 1 hour of observation. When viewed in the context of the estimated effective barrier Cl^- concentration within the hydrogel, figure 4.21 (b), this period translates as a sustained decline in estimated Cl^- concentration. Focussing on the measured values over the first 2 hours of observation, as illustrated in figure 4.22, there is a period of stability for approximately 1 hour after the electrode is immersed in the test solution.

(a)

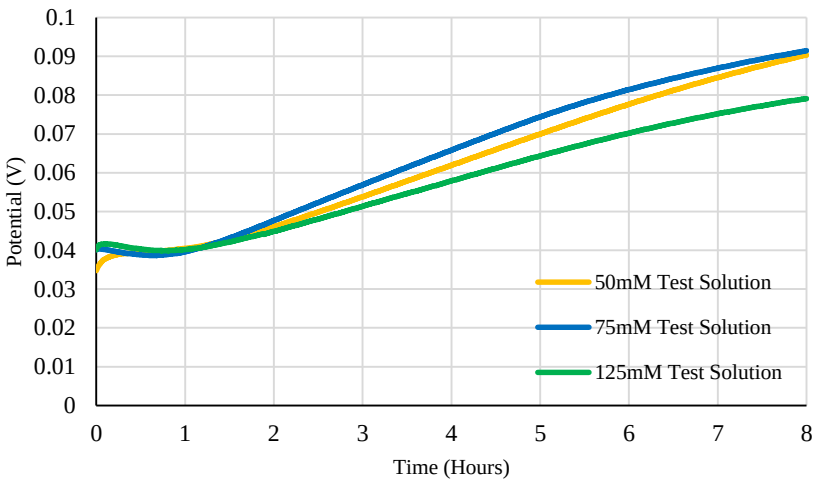

(b)

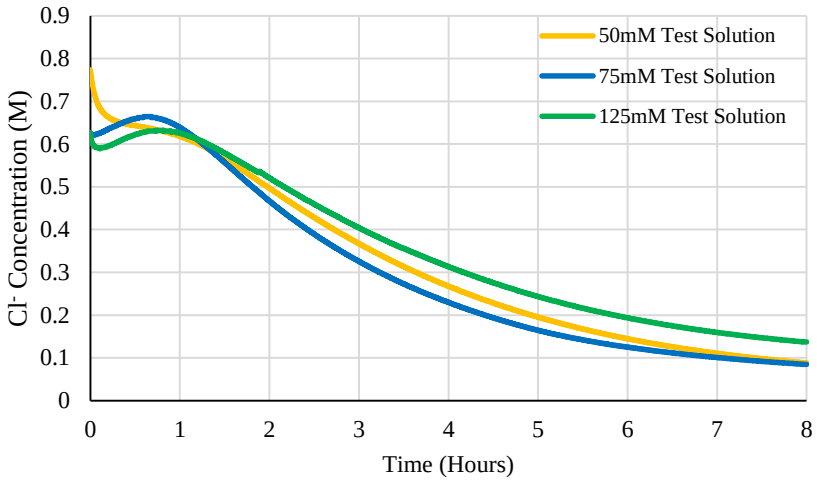

Figure 4.21. (a) Measured potential of pHEMA electrodes (vs 3 M KCl commercial reference) whilst placed in KCl DI water test solutions. **(b)** corresponding effective barrier Cl^- concentration estimated over the observation period.

(a)

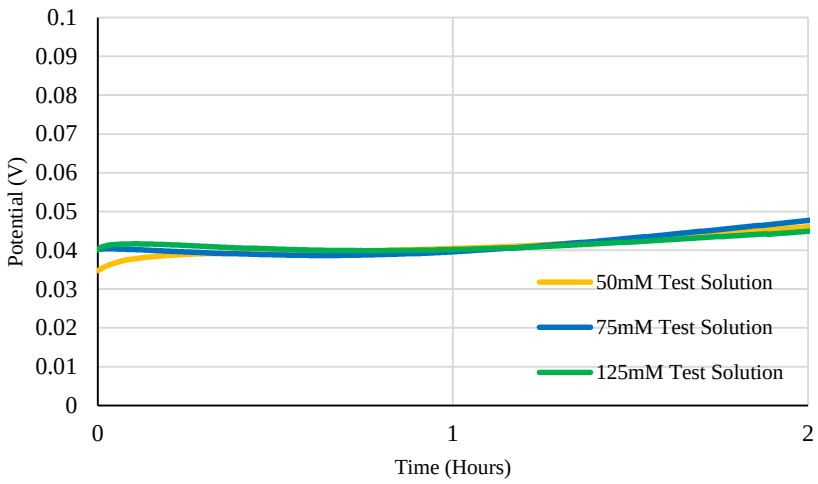

(b)

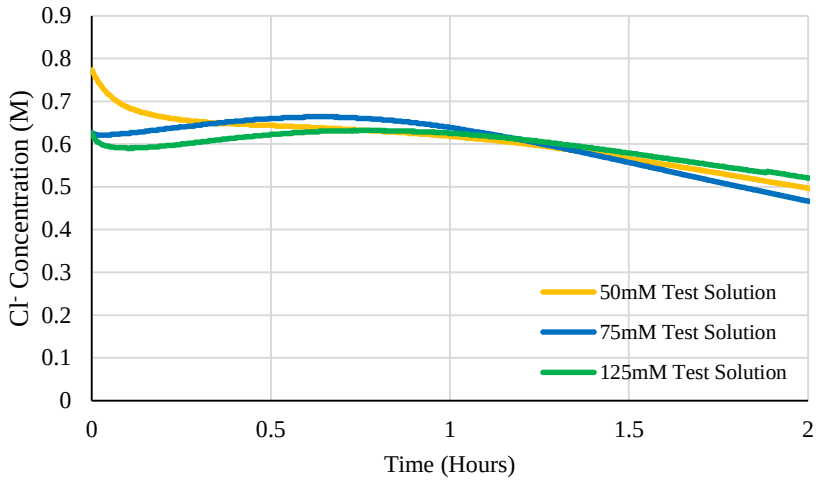

Figure 4.22. (a) Initial 2 hours of measured potential of pHEMA electrodes (vs 3 M KCl commercial reference) whilst placed in KCl DI water test solutions. **(b)** corresponding effective barrier Cl^- concentration estimated over same observation period.

4.6.2 Discussion

The device reported by Choi et al (75) was able to maintain a constant reference potential for a longer period than the pHEMA electrode, exhibiting a constant potential for 2 hours. Although the potential drift exhibited in figure 4.21 (a) after approximately 1 hour of immersion markedly affects the reference potential for the remaining observation period, the rate of drift appears fairly constant. As such, it is conceivable that the drift could be accounted for by subtracting the drift voltage from the measured voltage. If the onset of the drift, for

convenience, is taken at the 1-hour mark then we can calculate the difference in potential, ΔV, between here and the final reading after 8 hours:

$$\Delta V = V_{t=8} - V_{t=1} \tag{4.12}$$

Between t =1 hour and t = 8 hours, 2520 data points are registered. The measured potentials which lie within this range, V_n, can then be altered to account for the potential drift:

$$V_{drift\_accounted} = V_n - \frac{n \times \Delta V}{2520}, \tag{4.13}$$

where n is an integer between 1 and 2520. Figure 4.23 shows the results of using this technique to alter the measured potentials shown in figure 4.21 (a).

(a)

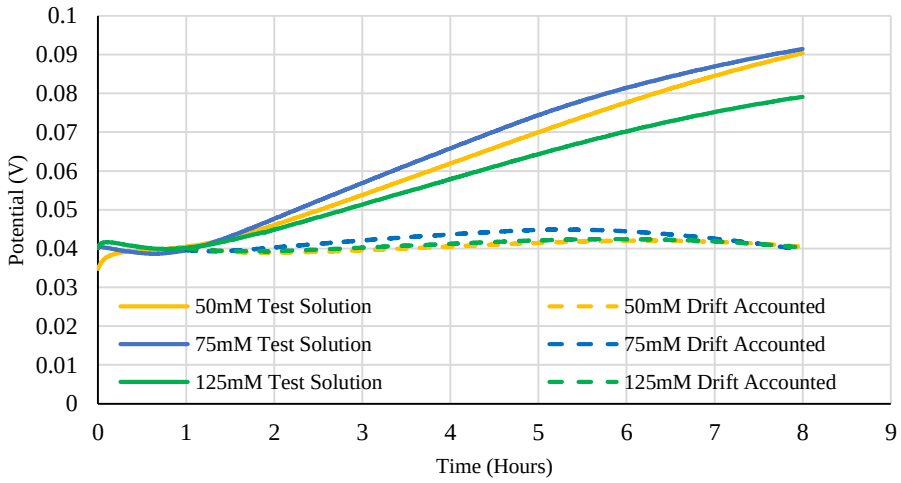

Figure 4.23. Measured potential of pHEMA electrode (vs 3 M KCl commercial reference) whilst placed in KCl DI water test solutions. Potential drift subtracted from measured potential values after 1 hour.

Figure 4.23 shows that by accounting for the potential drift through the use of equation 4.13, the potential value remains relatively constant for the remaining 7 hours of observation. This demonstrates that the rate of potential drift is consistent over this prolonged period of time. Therefore, if the device was required to operate continuously for over an hour, the drift in its

reference potential could be accounted for relatively simply by employing a technique similar to that suggested in equation 4.13.

The results presented in this chapter highlight that the pHEMA hydrogel electrode is not comparable to a commercial reference electrode in terms of the stability of its reference potential over a prolonged period of time. The pHEMA electrode is able to provide a stable potential for approximately 1 hour before noticeable drift begins. The rate of this drift, however, was shown to be relatively constant, meaning that its effects could be offset by subtracting the drift from the measured potential. The pHEMA hydrogel electrode, therefore, shows promise that it can perform the role of a QRE and be used to provide a stable reference potential within a sweat Cl^- sensor configuration.

4.7 Selectivity

As explained in Section 2.3.4, human sweat is made up of several ionic components. These may act to interfere with the potentiometric signal of the pHEMA Cl^- sensor when monitoring a sweat sample, possibly introducing errors to the subsequent measurement. To examine the device's ability to distinguish between the concentration of Cl^- and other ions, OCP tests were carried out in accordance with the protocol detailed in Section 3.3.5. Lactate ($C_3H_5O_3^-$) and Bicarbonate (HCO_3^-) are the common most anions found in sweat after Cl^- (167). As such, these selectivity studies utilised DI water test solutions of $NaC_3H_5O_3$ and $NaHCO_3$ to register the device's potentiometric response over a concentration range of 1 – 100 mM. Each of the test solutions possessed a base Cl^- concentration of 30 mM in line with the average concentration of Cl^- in healthy human sweat.

4.7.1 Results

The potentiometric responses recorded from these studies are shown in figures 4.24 and 4.25 below.

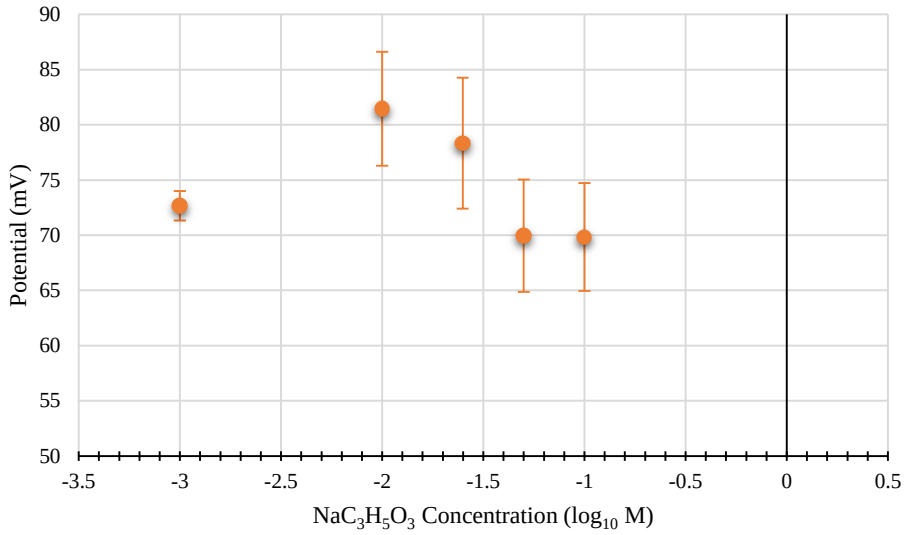

Figure 4.24. Sensitivity curve of pHEMA electrode toward Sodium L-Lactate ($NaC_3H_5O_3^-$) solutions of concentration 1, 10, 25, 50, 100 mM. Data points represent mean potential ± SD (n = 3).

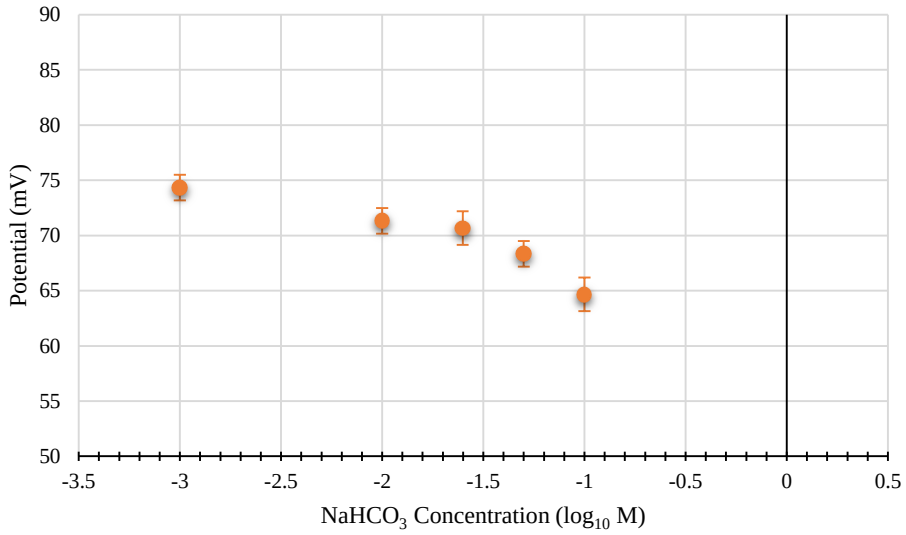

Figure 4.25. Sensitivity curve of pHEMA electrode toward Sodium Bicarbonate ($NaHCO_3^-$) solutions of concentration 1, 10, 25, 50, 100 mM. Data points represent mean potential ± SD (n = 3).

4.7.2 Discussion

Both figures 4.24 and 4.25 show that the pHEMA electrodes exhibit very little sensitivity to both the $NaC_3H_5O_3$ and $NaHCO_3$ solutions over the concentration ranges utilised (1.84 mV/dec and 4.32 mV/dec respectively). It has been observed that the average concentration of lactate and bicarbonate in healthy human sweat extracted from the forearm, where it is anticipated our device will be deployed, is 10.52 (± 1.89) mM and 2.38 (± 3.29) mM respectively (169). Additionally, a study conducted in 1986 demonstrated that, unlike Cl^- concentration, there were no apparent variations in the levels of $NaC_3H_5O_3$ and $NaHCO_3$ between CF patients and healthy individuals (167). The concentration ranges explored in figures 4.24 and 4.25 demonstrate that the pHEMA Cl^- sensor should be able to operate and investigate the Cl^- concentration of human sweat samples without experiencing interference from $NaC_3H_5O_3$ or $NaHCO_3$.

Bearing in mind that each test solution has a base Cl^- concentration of 30 mM, we can utilise the rearranged form of the calibration curve, given by equation 4.7, to obtain the potentiometric response expected from the pHEMA device toward a Cl^- concentration of 30 mM by assigning this value to the variable C_{TS}.

$$V_{CC} = \left(-64.34 \times log_{10}\left(\frac{C_{TS}}{1000}\right)\right) - 18.14, \tag{4.14}$$

$$V_{CC} = \left(-64.34 \times log_{10}\left(\frac{30}{1000}\right)\right) - 18.14, \tag{4.15}$$

$$V_{CC} = 79.84\, mV. \tag{4.16}$$

This matches up well with the measured potentials shown in figures 4.24 and 4.25. Therefore, given that the device is intended to be used on CF patients with Cl^- sweat concentrations which far outweigh that of $C_3H_5CO_3^-$ and HCO_3^-, it is thought that any interference in measured potential brought about by the presence of these anions will be minimal.

4.8 Diffusion Cell

During the pHEMA electrode's development, it was tested upon a diffusion cell which utilised a nano porous membrane. The cell was initially developed as a mechanism to study the reverse iontophoresis of ions and molecules (168). It therefore provided a platform on which to test the device's ability to detect Cl^- ion concentration whilst placed on a skin-like membrane. For the reader's convenience, the experimental configuration is shown again in figure 4.26.

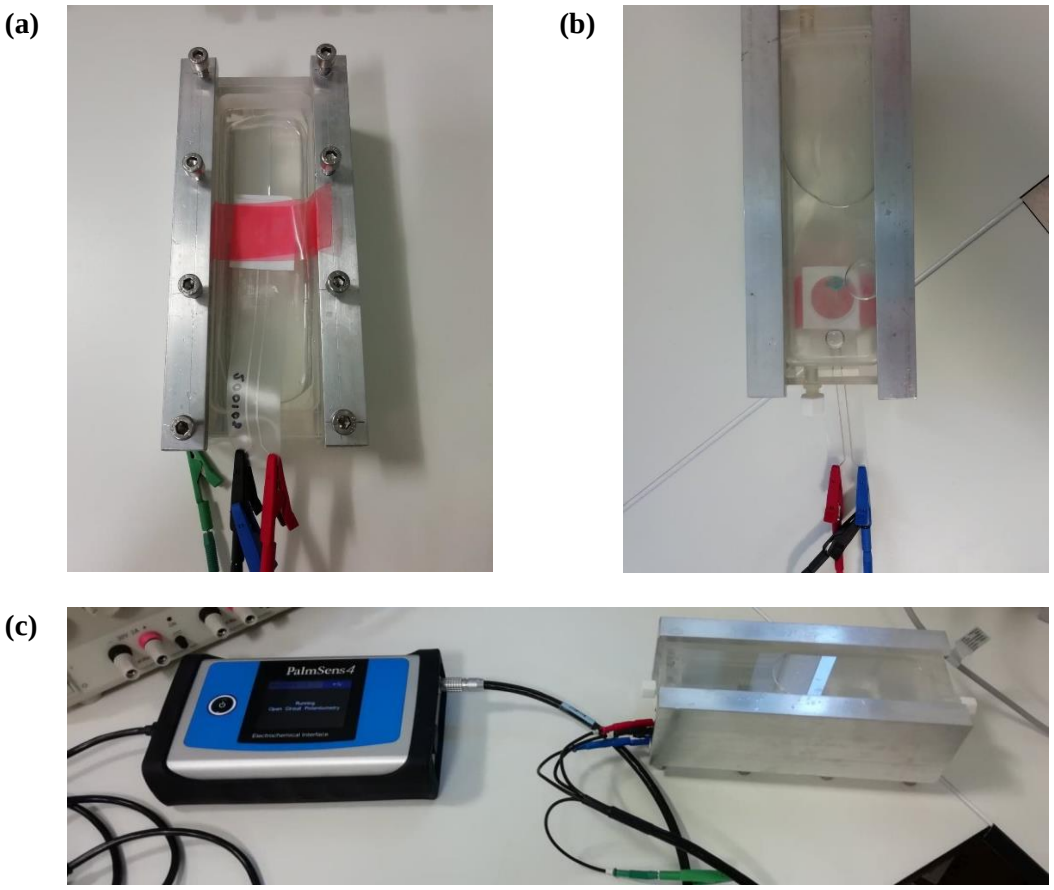

Figure 4.26. (a) pHEMA electrode secured to membrane on underside of diffusion cell using additional length of toupee tape. (b) Diffusion cell positioned upright, ensuring air bubbles are not present at the membrane surface. (c) Overall experimental setup showing Palmsens leads attached to electrode placed on underside of the diffusion cell.

This test was performed at an earlier stage in the electrode's development, at which point the electrode's conditioning process had not been fully established. The pHEMA hydrogel utilised in this examination was conditioned in a 2 M KCl DI water solution for 23 hours. As described

in Section 3.3.7 the cell consisted of two plastic blocks which sandwiched a nano porous membrane between two rubber gaskets. This cell contained 120 ml HEPES buffer solution with a Cl^- concentration 0.5 mM. Periodic supplements of KCl were added to increase the Cl^- concentration of the HEPES solution contained within the cell over the measurement period, according to the protocol described in Section 3.3.7.2.

4.8.1 Results

Figure 4.27 shows the potentiometric response of an electrode placed on the diffusion cell.

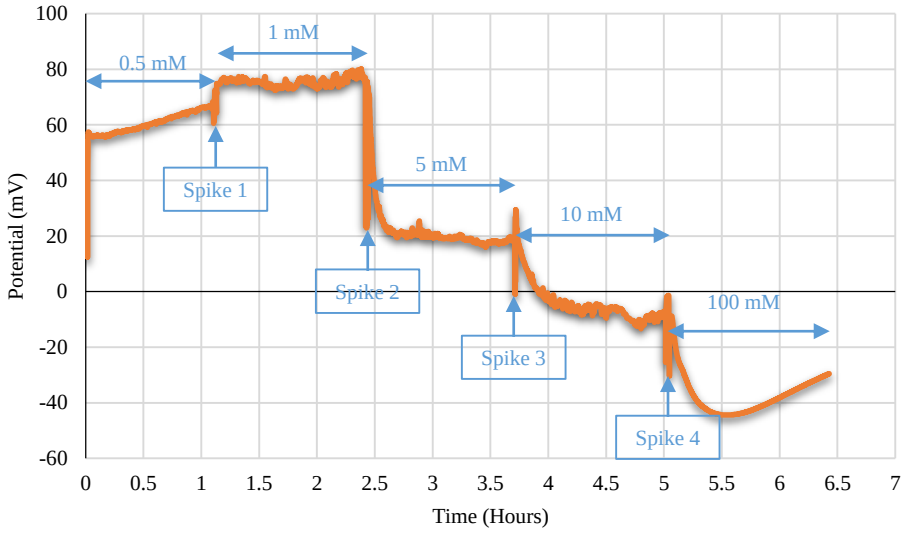

Figure 4.27. Potentiometric response of electrode placed on diffusion cell. Electrode conditioned in 2 M KCl solution for 23 hours. Noted on the graph are the times at which Cl^- spikes were administered and the subsequent Cl^- concentration which these made the cell's filling solution.

What is immediately clear from figure 4.27 is that there are definitive changes in measured potential which coincide with the administration of the Cl^- spikes. The measured response toward the initial concentration of 0.5 mM KCl does not quite reach an equilibrium, however after the application of each of the spikes the potential is seen to respond quickly and equilibrate after approximately 10 minutes. The exception is the last Cl^- spike which took the cell Cl^- to 100 mM, where the measured potential is initially seen to decrease before gradually rising until

the examination's conclusion. After over 6 hours of measurement this is likely due to the potential drift of the reference potential.

As noted earlier, the diffusion cell study shown in figure 4.27 was conducted before the pHEMA conditioning process had been fully established and the electrode used to obtain the results shown in figure 4.27 did not undergo the same conditioning as that used for the calibration curve described in Section 4.4. The test was conducted using electrodes conditioned in 1M KCl for 25 hours such as those used to obtain the calibration curve, however the onset of potential drift (see Section 4.6) proved problematic, as is shown in figure 4.28.

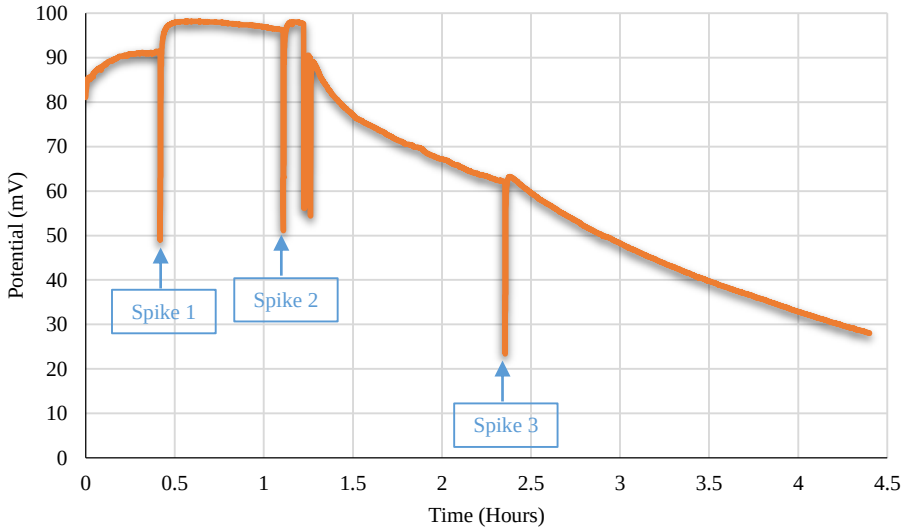

Figure 4.28. Potentiometric response of electrode placed on diffusion cell. Electrode conditioned in 1 M KCl solution for 25 hours, as per calibration curve.

Figure 4.28 shows that after approximately 1 hour of measurement there is a continual loss in the magnitude of measured potential, aligning well with the point at which the drift in reference potential of the pHEMA electrode became apparent in the potential drift studies, Section 4.6. Compensating for the potential drift in this scenario is more difficult though due to changes in the cell's Cl^- concentration over this time. Despite the addition of a Cl^- Spike 3, there is little change in the trajectory of the measurements. Therefore, compensating for the drift after 1 hour of observation, similar to Section 4.6.2, would only provide a steady potential for the remaining

duration when we would expect to see two distinct potentiometric responses in accordance with the change in Cl^- concentration. Focussing on the first hour of measurements in figure 4.28, however, the pHEMA electrode device exhibits a relatively quick equilibration to the initial cell concentration, and a clear response to the first spike at around 0.4 hours before maintaining a steady potential.

Therefore, although it is difficult to draw any definitive conclusions from either figure 4.27 or figure 4.28 given the reasons outlined above, taken together we can say that the pHEMA electrode demonstrates an ability to detect changes in the Cl^- concentration of a fluid across a skin-like, nano porous membrane. These investigations, therefore, provided a preliminary proof-of-concept experiment indicating that the device is capable of forming the basis of a wearable Cl^- sensor. Following the establishment of the pHEMA conditioning process of a 25-hour condition in 1 M KCl DI water solution, efforts focussed on developing a protocol for a healthy volunteer study (HVS), to examine the sensor's ability to perform in a real-world environment. This protocol is described in Section 3.4 and the results of the HVS are presented and discussed in Section 5.

4.9 Conclusion

The results and comments presented in this chapter chart the development of the pHEMA gel preparation process and the effects this had on the performance of the Cl^- ion selective electrode device.

The initial method of polymerisation utilising a Hg bulb chamber allowed a rough gauge of the necessary time needed for the HEMA to take on the glass-like appearance which accompanies its polymerisation. When the polymerisation method was subsequently switched to the UV LED array, it was found that a time of 15 minutes under the array produced electrodes with the most stable and consistent potentiometric responses of the polymerisation periods investigated.

Monitoring the potential of the pHEMA electrodes whilst they underwent conditioning helped to determine the appropriate Cl^- concentration for the conditioning solution as well as the time in which the pHEMA should be immersed within it. Measurements taken using a 3 M KCl conditioning solution demonstrated that a stable potential could not be obtained even after 65 hours of immersion. However, pHEMA Cl^- sensors conditioned for this amount of time continually exhibited little-to-no sensitivity toward Cl^- concentration, possibly due to damage the prolonged exposure to the concentrated saline solution had upon the polymer network. Conversely, conditioning profiles obtained using a 1 M KCl conditioning solution exhibited a stable potential after 25 hours of conditioning. Electrodes conditioned for this length of time in a 1 M KCl solution for 25 hours displayed a high degree of sensitivity toward Cl^- concentration through the calibration curve obtained from the potentiometric responses of six pHEMA electrodes conditioned in this way. The response exhibited a sensitivity of 64.34 mV/dec, just above that of the Nernstian value 59 mV/dec and similar to sensitivities of Cl^- sensors reported in literature (58 mV/dec (70) and 58.5 mV/dec (75). The potential drift tests highlighted some of the sensor's shortcomings in that the reference potential was seen to undergo a sustained period of drifting after 1 hour immersed in the test solutions. However, the electrodes exhibited a consistent and stable reference potential for the initial hour of continuous measurement. Furthermore, the rate of drift exhibited by the electrodes over the observation period was stable and, therefore, could be compensated for if required. In addition, electrodes examined using the calibration curve showed very low variation in their potentiometric responses toward the test solutions, indicating a good level of reproducibility. Studies conducted utilising a diffusion cell designed to mimic the transdermal diffusion of ions showed that the pHEMA device was able to distinguish changes made to the Cl^- concentration of the solution within the cell. Additionally, the electrodes displayed low sensitivity toward the main competing anions found in human sweat at their physical concentrations.

Combined, these findings suggest that the pHEMA electrode device has the potential to be further developed to monitor the Cl^- concentration within CF patients' sweat and, therefore, help gauge the efficacy of emerging treatments.

5. Healthy Volunteer Study

5.1 Introduction

This section will provide the results of the HVS tests carried out in accordance with the protocols detailed in Section 3.4. A Portable Electrochemical Analyser (PEA) device, used by this research group in previous clinical studies (110), was utilised to monitor the pHEMA Woundsense electrode's potential throughout the procedure. Preliminary lab-bench tests conducted with the PEA and pHEMA electrode showed that the potentiometric responses recorded were comparable to those measured using the Palmsens potentiostat in terms of sensitivity toward the test solution Cl^- concentrations. Despite there being a difference in the magnitudes of the potentials recorded by the PEA and the Palmsens, the difference is fairly consistent for each of the test solutions and was therefore considered as a constant potential offset. The measured outputs of the respective devices from these tests are shown in Appendix: A.

Four healthy volunteers were used to conduct a total of ten HVS tests, University of Strathclyde Ethics Permission (DEC.BioMed.2020.288). Table 5.2 provides a profile of the volunteers.

Table 5.1. Profile of volunteers used in HVS.

Volunteer Number	Gender	Age
1	Male	20 - 29
2	Male	20 - 29
3	Male	50 - 59
4	Female	40 - 49

As described in Section 3.4.3.2, each HVS test procedure lasted 89 minutes and was split into three parts: Lab Bench 1, On-Body, and Lab Bench 2. The On-Body portion of the tests were carried out using foam saturated with artificial sweat solution placed onto the forearm of participants, similar to that shown in figure 5.1 and detailed in Section 3.4.3.2.

Figure 5.1. Example of how pHEMA electrode with foam is positioned and attached to forearm of participant. The plastic covering was secured over electrode using medium grade toupee tape around its rim. The PEA is shown connected to the electrode.

The potential developed by the pHEMA Woundsense electrode placed over the foam was recorded by the PEA device. Additional solutions of NaCl were administered to alter the Cl^- concentration within the foam over the test period. Lab Bench tests were carried out for each individual test to provide a means of evaluating the on-body results. Table 5.2 provides a breakdown of the relative durations of these segments.

Table 5.2. Summary of HVS test procedure.

Segment	Duration (Minutes)	Summary of Procedure (See Section 3.4.3.2)
	PEA switched on:	Measurement initiated.
Lab Bench 1	00:00 – 28:00	• pHEMA electrode laid flat on lab bench surface. • Foam segment (pre-soaked with 100 µl of artificial sweat solution) placed over electrode contacts. • Micropipette used to add 2.5 µl spikes of NaCl DI water solution to periodically increase Cl^- concentration within foam. Notes: preliminary tests examining the use of PEA alongside the pHEMA electrode showed that the measured potential of the electrode underwent a prolonged period of equilibration. This segment is used to allow the measured potential to settle before the electrode is placed on the volunteer's skin.
	28:00 – 30:00	• Foam removed and discarded. • Electrode rinsed with DI water and gently dabbed dry. • Volunteer's skin cleaned with alcohol swab.
On-Body	30:00 – 67:30	• Fresh foam (pre-soaked with 100 µl of artificial sweat solution) placed onto forearm of volunteer. • pHEMA electrode placed over foam and held in place using circular plastic covering and toupee tape (figure 5.1). • Micropipette used to add 2.5 µl spikes of NaCl DI water solution to periodically increase Cl^- concentration within foam.
	67:30 – 69:00	• Plastic covering, and electrode removed from skin. • Foam removed and discarded. • Electrode rinsed with DI water and gently dabbed dry. • Volunteer's skin cleaned with alcohol swab.
Lab Bench 2	69:00 – 89:00	• pHEMA electrode laid flat on lab bench surface. • Foam segment (pre-soaked with 100 µl of artificial sweat solution) placed over electrode contacts. • Micropipette used to add 2.5 µl spikes of NaCl DI water solution to periodically increase Cl^- concentration within foam. Notes: Lab Bench 2 potentiometric response used as the marker against which On-Body segment is compared.
		PEA switched off: Measurements saved to SD card.

The method summarised in Table 5.2 was conducted for each of the ten HVS tests carried out. Table 5.3 provides a further breakdown of the On-Body and Lab Bench 2 segments highlighted in Table 5.2. The time in which the NaCl spikes are administered as well as the estimated foam Cl^- concentration (see Section 3.4.3.5) throughout the test are also detailed.

Table 5.3. Breakdown of the administration time of 2.5µl NaCl spikes during On-Body and Lab Bench 2 segments of HVS. Also provided is the respective NaCl concentrations of the spikes and Cl^- concentration within the foam over the procedure.

		Spike No.	NaCl Spike Concentration (M)	Calculated Cl^- Concentration in Foam (mM)	Time Administered (Minutes)
On-Body	**Start**			16.00	30:00
		1	0.5	27.80	37:30
		2	1	50.95	45:00
		3	2	96.28	52:30
		4	2	139.55	60:00
	End			139.55	67:30
Lab Bench 2	**Start**			16.00	69:00
		1	1	40.00	74:00
		2	1.5	74.76	79:00
		3	3.5	154.42	84:00
	End			154.42	89:00

The potentiometric responses for the On-Body and Lab Bench 2 segments were then obtained by calculating the average potential recorded over each inter-spike period and plotting it against the corresponding foam Cl^- concentration. In doing so, the response recorded during the On-Body segment could be compared to that recorded during the Lab Bench 2 segment. This is presented in Section 5.3. The results of the HVS will be discussed in terms of the device's success in monitoring the Cl^- concentration, the complexity of the operating environment, and any possible improvements which could be made.

5.2 On-Body Tests

This subsection will provide the results from the On-Body portions of each HVS test carried out. Some of these results did not exhibit the sensitivity toward the Cl^- concentration within the foam as was expected. The possible reasons for this will be discussed in this Section 5.2.2.

5.2.1 Results

Figure 5.2 shows the potential recorded by the PEA device over the On-Body segment of each of the ten HVS tests carried out. These comprise the measured potential plotted with respect to time from 30:00 minutes to 67:30 minutes of the test protocol as detailed in Table 5.3, with the pHEMA electrodes placed on the volunteers' forearms similar to that shown in figure 5.1 above. For reference, figure 5.3 provides the measured potential from one of the Lab Bench 2 segments carried out, where the electrode is laid flat on the lab bench surface. Direct comparisons between the average potentiometric responses measured during the On-Body segment and the Lab Bench 2 segment are provided and discussed in Section 5.3.

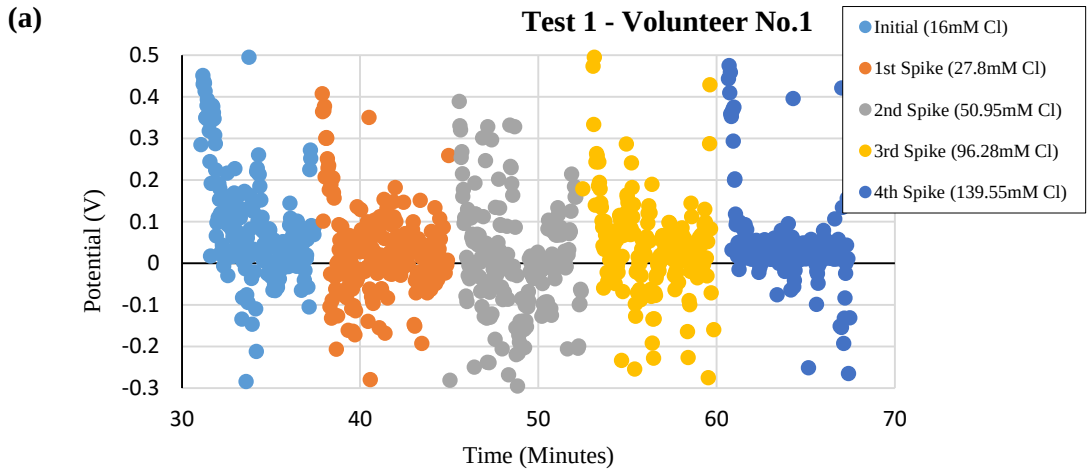

(b)

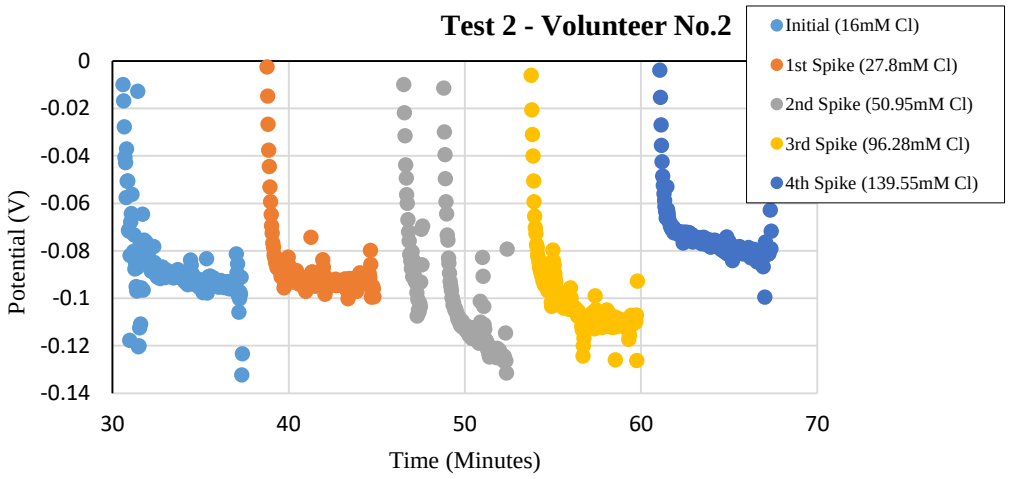
Test 2 - Volunteer No.2
Initial (16mM Cl)
1st Spike (27.8mM Cl)
2nd Spike (50.95mM Cl)
3rd Spike (96.28mM Cl)
4th Spike (139.55mM Cl)
Potential (V)
0
-0.02
-0.04
-0.06
-0.08
-0.1
-0.12
-0.14
30
40
50
60
70
Time (Minutes)

(c)

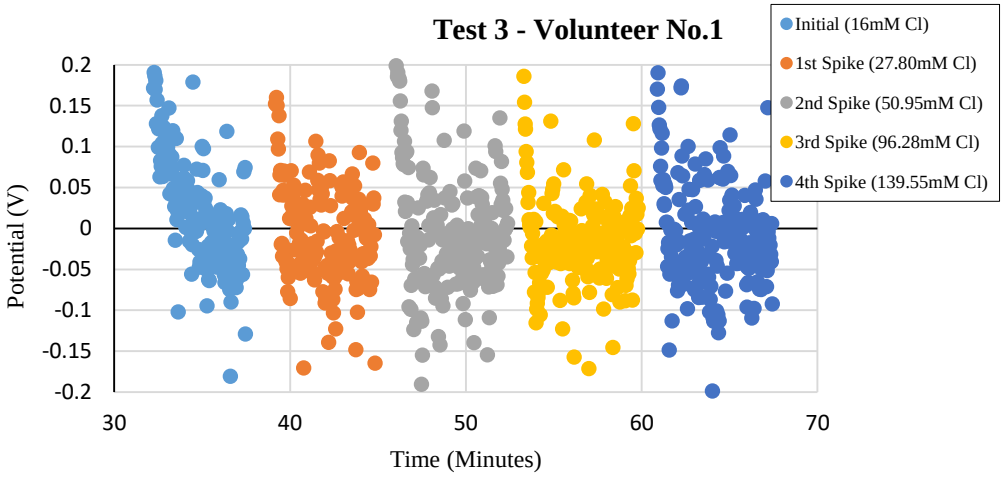
Test 3 - Volunteer No.1
Initial (16mM Cl)
1st Spike (27.80mM Cl)
2nd Spike (50.95mM Cl)
3rd Spike (96.28mM Cl)
4th Spike (139.55mM Cl)
Potential (V)
0.2
0.15
0.1
0.05
0
-0.05
-0.1
-0.15
-0.2
30
40
50
60
70
Time (Minutes)

(d)

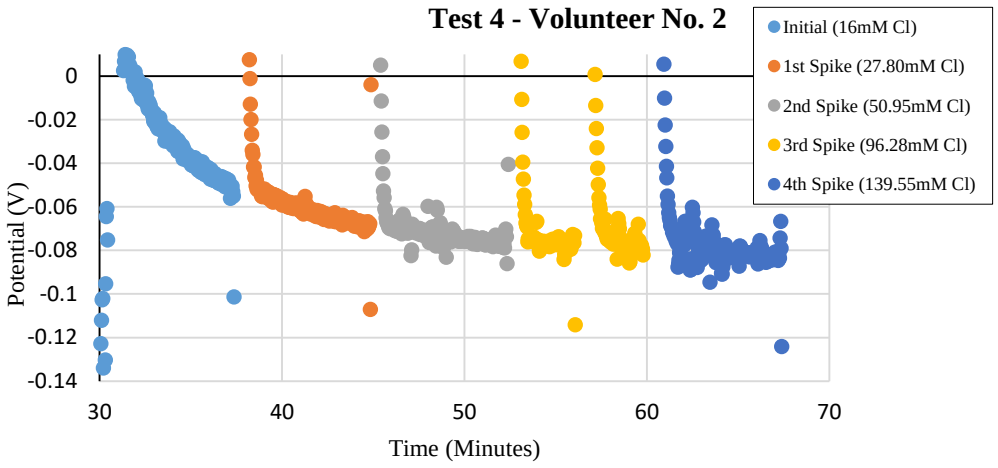
Test 4 - Volunteer No. 2
Initial (16mM Cl)
1st Spike (27.80mM Cl)
2nd Spike (50.95mM Cl)
3rd Spike (96.28mM Cl)
4th Spike (139.55mM Cl)
Potential (V)
0
-0.02
-0.04
-0.06
-0.08
-0.1
-0.12
-0.14
30
40
50
60
70
Time (Minutes)

(e)

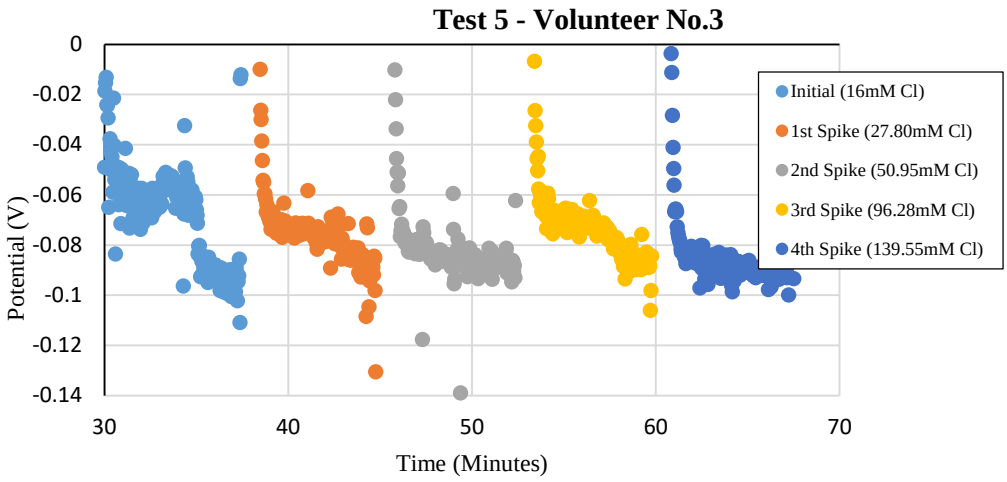
Test 5 - Volunteer No.3
0
-0.02
-0.04
-0.06
-0.08
-0.1
-0.12
-0.14
Potential (V)
30
40
50
60
70
Time (Minutes)
Initial (16mM Cl)
1st Spike (27.80mM Cl)
2nd Spike (50.95mM Cl)
3rd Spike (96.28mM Cl)
4th Spike (139.55mM Cl)

(f)

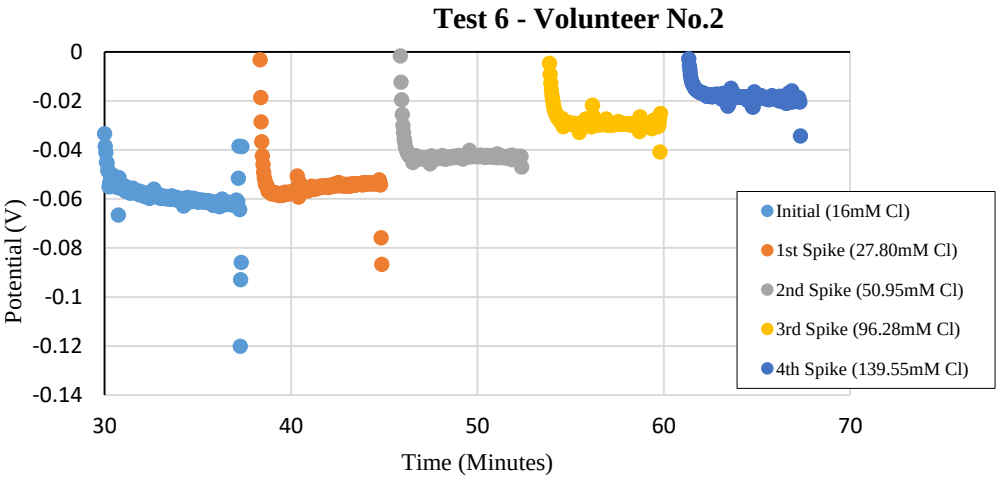
Test 6 - Volunteer No.2
0
-0.02
-0.04
-0.06
-0.08
-0.1
-0.12
-0.14
Potential (V)
30
40
50
60
70
Time (Minutes)
Initial (16mM Cl)
1st Spike (27.80mM Cl)
2nd Spike (50.95mM Cl)
3rd Spike (96.28mM Cl)
4th Spike (139.55mM Cl)

(g)

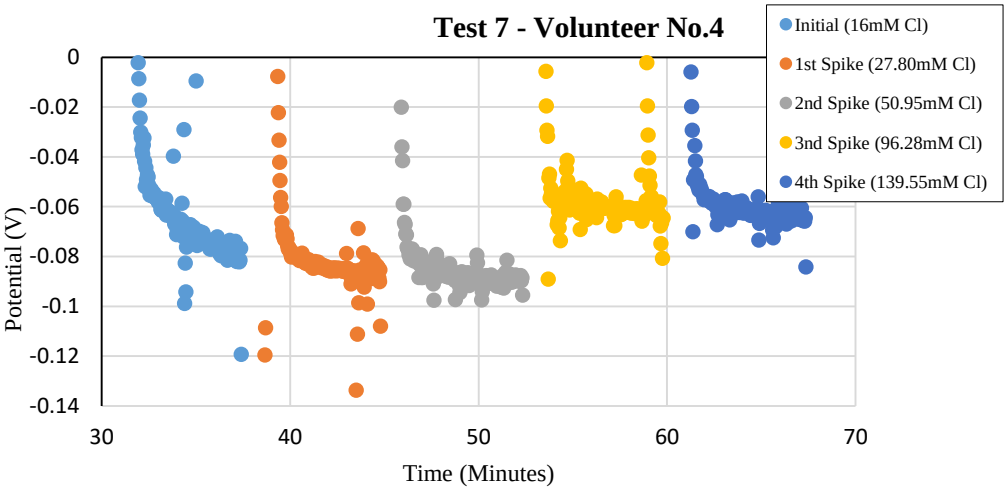
Test 7 - Volunteer No.4
0
-0.02
-0.04
-0.06
-0.08
-0.1
-0.12
-0.14
Potential (V)
30
40
50
60
70
Time (Minutes)
Initial (16mM Cl)
1st Spike (27.80mM Cl)
2nd Spike (50.95mM Cl)
3nd Spike (96.28mM Cl)
4th Spike (139.55mM Cl)

(h)

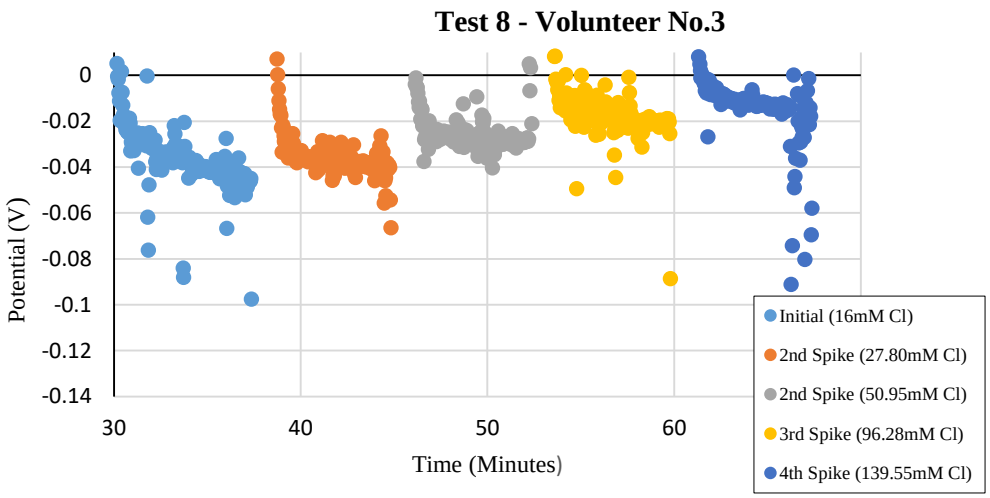

(i)

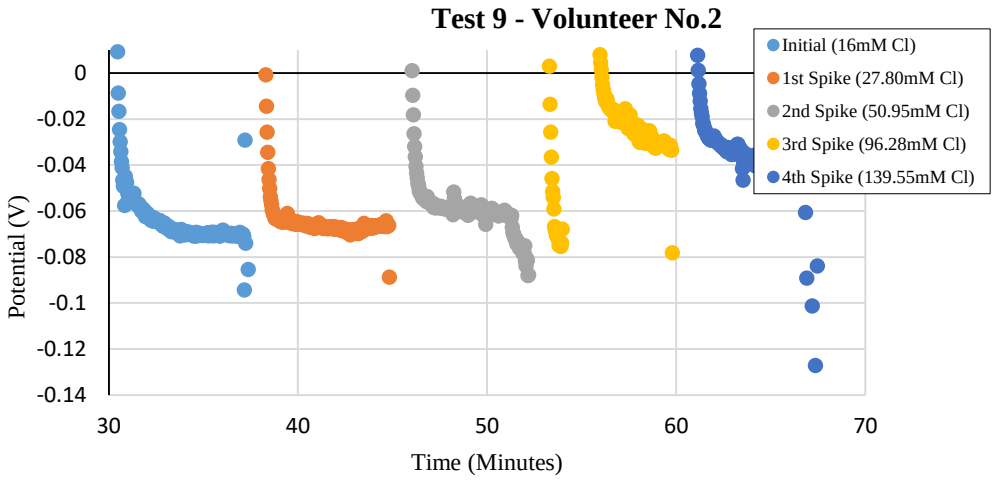

(j)

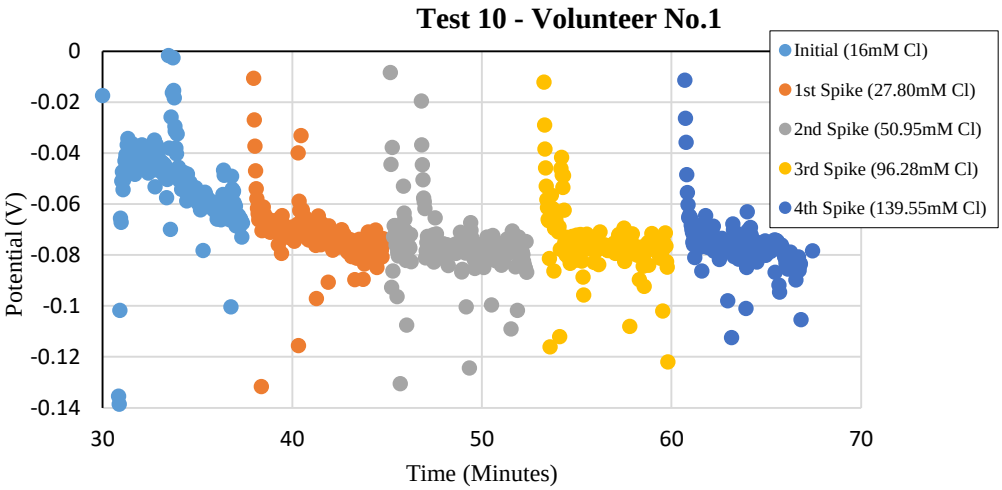

Figure 5.2. (a) – (j) measured potentials for the on-body segment of HVS tests 1 – 10 respectively, where pHEMA electrodes placed on skin of volunteers as shown in figure 5.1. Volunteer which took part in each of the tests is noted. The legend provides the calculated Cl^- concentration within the foam over the test period.

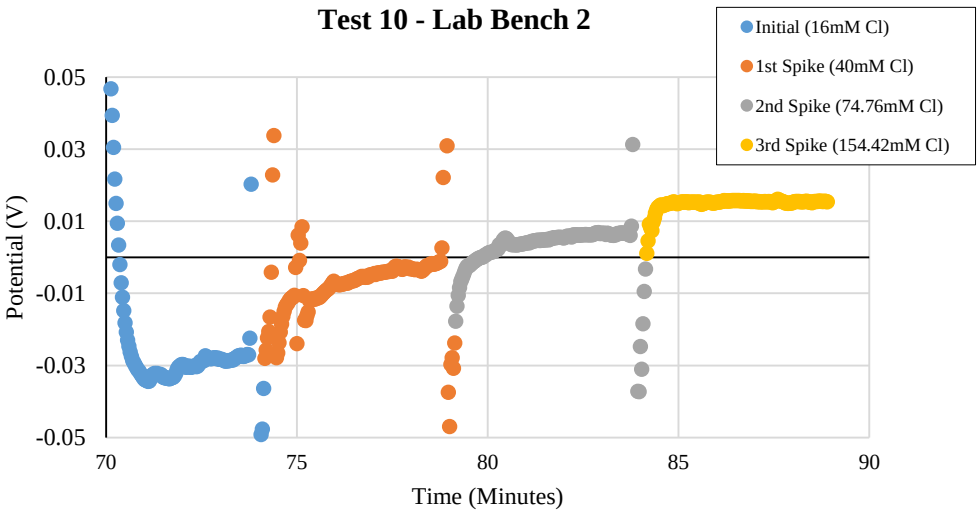

Figure 5.3. Measured potential from Lab Bench 2 segment of HVS Test 10. The legend provides the calculated Cl^- concentration within the foam over the test period.

The results shown in figure 5.2 (b, f, g, h, i) provide a glimpse that the pHEMA electrode can exhibit a degree of sensitivity toward the Cl^- within the foam when placed on the volunteer's forearm, similar to that shown when the electrode is placed flat on the lab bench, figure 5.3. The accuracy of these responses, relative to the electrode's Lab Bench 2 potentiometric response, will be analysed in Section 5.3.

5.2.2 Discussion

The remainder of the responses shown, figure 5.2 (a, c, d, e, j), do not exhibit the desired sensitivity toward the changing Cl^- concentration. In comparison to the Lab Bench tests (e.g. figure 5.3) where the measured potential is relatively stable and exhibit a change in potential when a NaCl spike is administered, some tests are hampered with high levels of interference and others exhibit a continual decline in their measured potential, despite the application of the NaCl spikes.

5.2.2.1 Motion Artefacts

From observation in carrying out the HVS, motion artefacts (MA's) were identified as a significant contributor to the noise observed in the on-body measurements. Their occurrence

can be explained by recalling the discussion of Sections 2.4.1 and 2.4.2 where it was found that electrostatic interactions between charged species at interface boundaries can introduce defined separation of charges, known as the electric double layer. When a conducting material is placed above the skin, in this case the artificial sweat-soaked foam, the stratum corneum creates a boundary between it and the underlying conducting layers of skin. This gives rise to a capacitive effect analogous to the electric double layer at the electrode – electrolyte boundary (189–191). The stability of these layers can be disturbed through the participant's movement or through vibrations in the immediate environment, altering the settled potential of the half-cell. The overall measured potential is therefore also observed to fluctuate and undergo equilibration whilst the system settles again (192). Examples of the MA's incurred during the on-body tests can be seen below in figure 5.4. The act of depositing the NaCl spikes throughout the procedure results in periodic MA's characterised by large jumps in potential proceeded by quick equilibration. This is not exclusive to the On-Body segment, the measured potential was also seen to jump with the NaCl deposition during the Lab Bench segments, as is shown in figure 5.3.

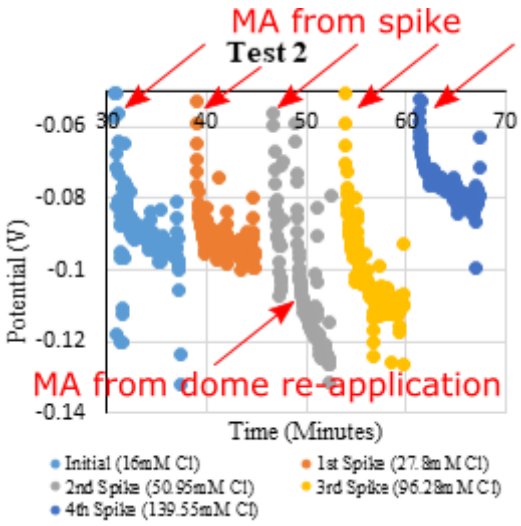

Figure 5.4. Example of motion artefacts, and resultant potential equilibration, in HVS Test 2. Periodic MA's are caused by the application of NaCl spikes. Plastic dome became unstuck from participant's skin during procedure. Its reapplication caused a further MA.

Figure 5.4 also shows an example of a MA caused by the re-application of the plastic dome covering the electrode and foam after it became unstuck from the participant's forearm. This leads to the next point of discussion.

5.2.2.2 Electrode Placement

The placement of electrodes was also thought to play a role in the erroneous results seen in figure 5.2. In a number of tests, the electrodes were placed on the participant's forearm such that its length was perpendicular to the length of the forearm, as shown below in figure 5.5 (a).

(a)

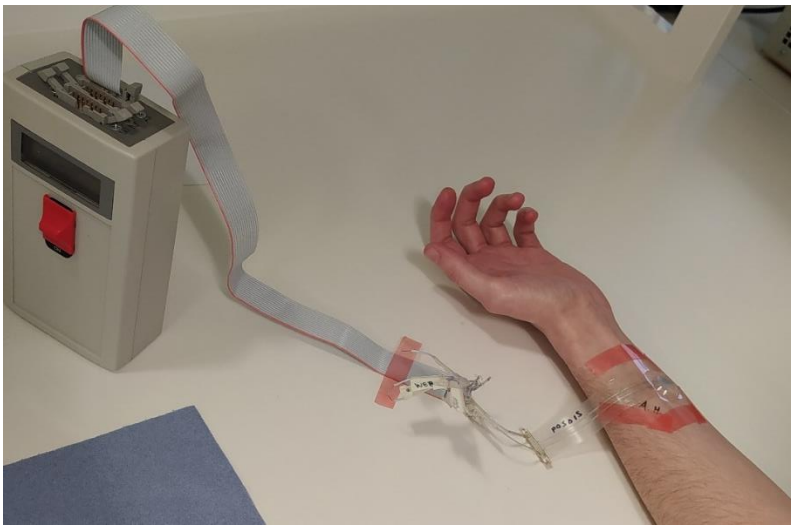

(b)

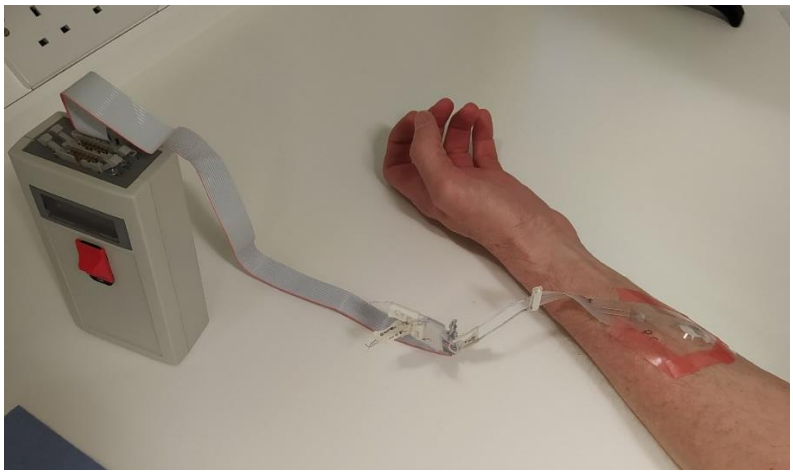

Figure 5.5. (a) On-body test 4 configuration showing electrode positioned perpendicular to the length of the participant's forearm. **(b)** On-body test 8 configuration showing electrode positioned more centrally on the ventral forearm and more parallel to its length.

This was to limit the amount of hair on the participant's arm which would be exposed to the tape used to secure the plastic dome, therefore minimising the discomfort when the electrode was removed. However, this positioning meant that both the electrode/foam configuration and the plastic dome were more susceptible to the curvature of the arm. This made the likelihood of electrode displacement away from the foam surface more probable, especially when the plastic covering came unstuck from the skin. It may also help to explain the responses recorded in tests 4, 5, and 10, shown again in figure 5.6, where there appears to be no sensitivity toward the changes in Cl^- concentration. Instead, there is a gradual equilibration of the potential to a level of ~ -80mV which is roughly maintained for the duration of the procedure.

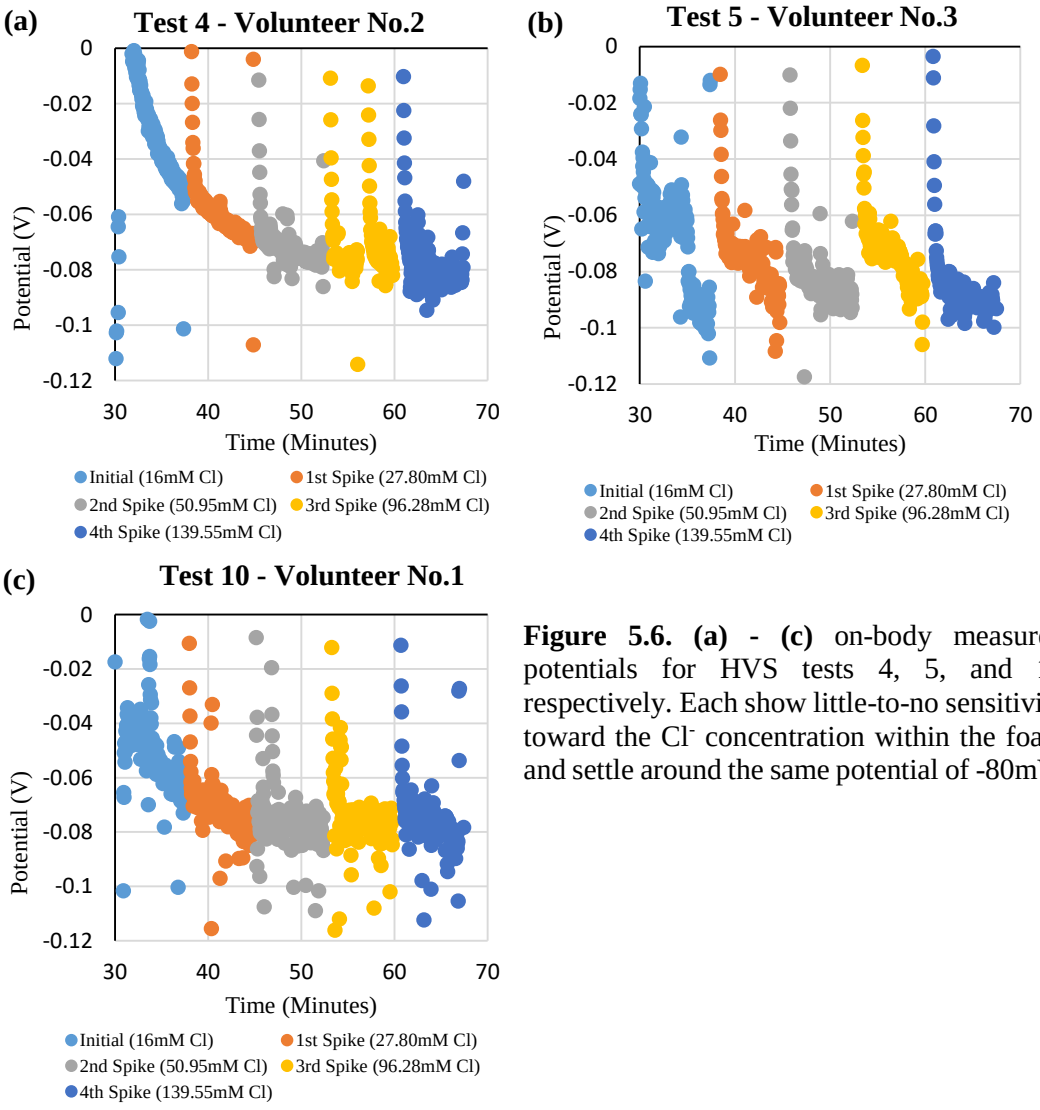

Figure 5.6. (a) - (c) on-body measured potentials for HVS tests 4, 5, and 10 respectively. Each show little-to-no sensitivity toward the Cl^- concentration within the foam and settle around the same potential of -80mV.

Had the electrode and foam become separated, even partially, then it is possible that the electrode would not detect the changes in Cl^- concentration. This may also explain the response seen in Test 2, figure 5.4. The measured potential was relatively constant during the initial two test concentrations before the plastic dome was re-secured to the participant's skin. After this point there is a visible shift in electrode response and a sensitivity toward the Cl^- concentration is exhibited. It is thought that in securing the dome, contact between the electrode and foam was re-established, thus providing a better potentiometric response to the test concentration. From Test 6 onward, in order to mitigate the occurrence of electrode / foam displacement, the electrode was placed nearer the proximal end of the ventral forearm with its length more parallel to that of the arm's, as shown in figure 5.5 (b). This provided the foam and electrode a larger, flatter surface to rest upon, helping ensure a more consistent contact between the two. The number tests which exhibited good potentiometric responses to the Cl^- concentrations (Tests 6, 7, 8 and 9) occurred after these changes were implemented.

5.2.2.3 Skin

Another factor which could have affected the measurements is the surface of the skin itself. As mentioned in Section 5.2.2.1, the stratum corneum will exert an influence on the distribution of ions in the foam and, therefore, influence the measured potential. The structure and state of the participant's skin, such as its thickness and hydration, could affect the extent of this. The potential responses measured for Tests 1 and 3, shown below in figure 5.7 (a) and (b) respectively, exhibit large and sustained levels of interference with both showing a continual oscillation in potential over a range of nearly 200 mV. Both tests were performed on the same participant.

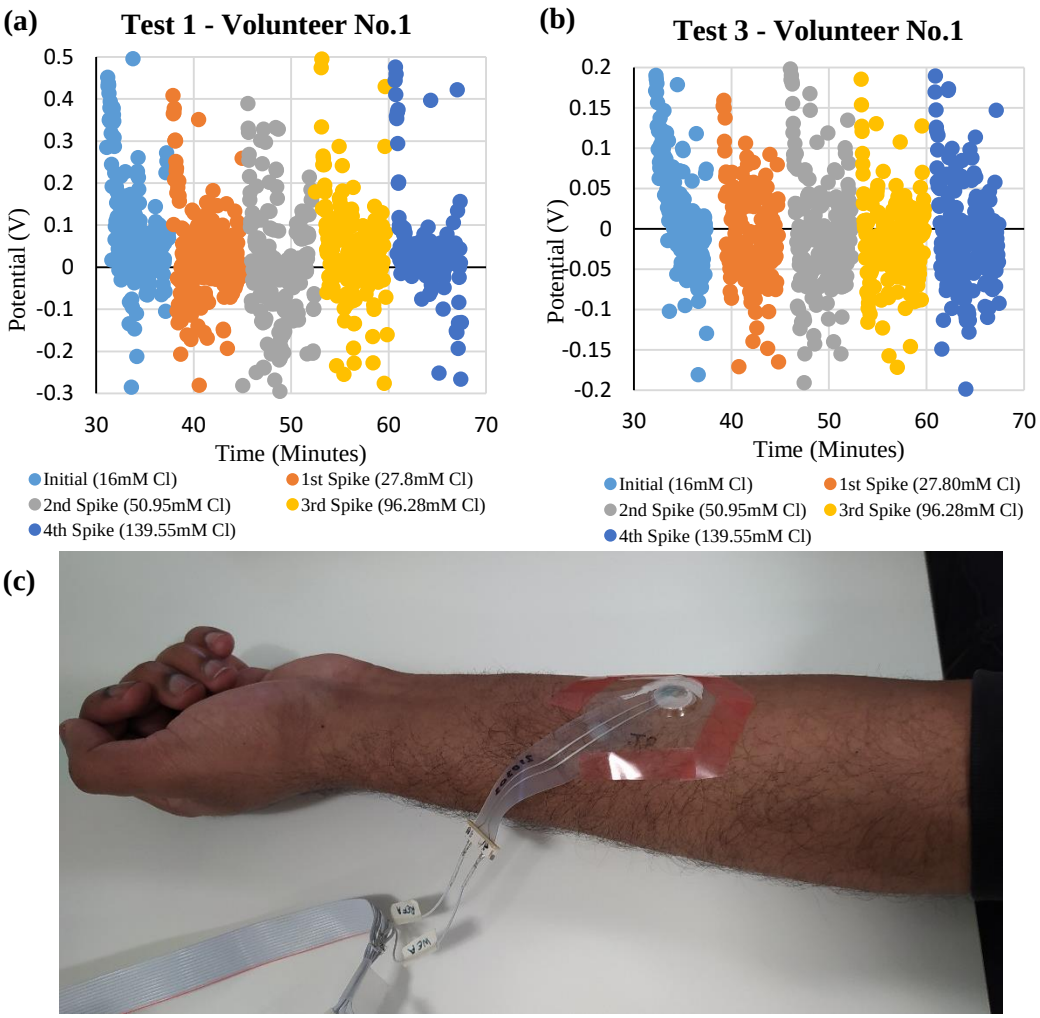

Figure 5.7. (a)-(b) On-Body measurements for HVS Tests 1 and 3. Both tests were performed on the same participant (Volunteer No.1), shown in **(c)**, and exhibit similar levels of noise not seen in other tests.

The magnitude and sustained nature of the noise means it is unlikely to be wholly attributed to motion or electrode / foam uncoupling, as the participant remained relatively still for the duration of the procedures. Unlike the other volunteers, the participant for Tests 1 and 3 possessed a relatively high density of hair on their forearm. This may have contributed to the levels of noise seen in figure 5.7 (a - b) through introducing a source of interference to the foam and the distribution of ions within it.

5.2.2.4 Shielding

Finally, it was evident during the HVS tests, that the configuration was susceptible to interference from conductive bodies in its vicinity, possibly acting to alter the capacitance of the configuration (193). This was clear from the jumps in potential observed when a hand, for example, would approach the configuration. With both the Woundsense electrode and the leads connecting to the PEA device exposed to the environment, they could act as antenna for electrostatic interference and exacerbate any interference due to motion (193). To minimise this effect in the future, a bespoke adapter with sufficient shielding should be made for the electrode to connect to the PEA. Minimising the length of the electrical leads throughout the setup would also be beneficial.

5.3 Accuracy

This subsection aims to evaluate the On-Body performance of individual pHEMA electrodes by comparing their On-Body potentiometric response toward the foam Cl^- concentration to that of their respective Lab Bench 2 potentiometric response. This process was detailed in Section 3.4.3.2 where, for each electrode, the average measured potential over each On-Body time period defined in Table 5.3, is plotted against the corresponding Cl^- concentration within the foam over the same period. The same process can be performed for each electrode's Lab Bench 2 segment. This produces two Cl^- concentration sensitivity curves for each HVS test conducted: one obtained through On-Body measurements; and the other obtained from the Lab Bench 2 procedure. The latter is, therefore, used as a marker against which the On-Body response can be compared. As discussed in the preceding subsections, the On-Body segments conducted in Tests 1, 3, 4, 5, and 10 exhibited little-to-no sensitivity toward the foam Cl^- concentration. As such, they are not considered in this chapter. Figure 5.8 shows the On-Body and Lab Bench 2 potentiometric responses obtained from Tests 2, 6, 7, 8, and 9.

The results of each HVS test shown in figure 5.8 display an apparent offset between the On-Body and the Lab Bench measurements. The precise origin of this offset is unclear. As discussed in Section 5.2.2.1, the act of placing the electrode and foam onto the skin will create an additional capacitive effect at the skin / foam boundary, which could give rise to a potential offset. Such effects are commonly observed in on-skin electrode measurements (189,194,195). A common technique to mitigate them is to strip away the layers of the stratum corneum through cleaning agents or abrasion (189,191). Microneedles may also be employed to bypass the effects of the stratum corneum. Due to contact restrictions during the time of the study, and for the general comfort of the participant, it was decided not to employ such measures. Chloride ions residing on the skin surface and dispersing into the foam would also act to skew the on-body measurements. However, the On-Body potentials measured are consistently lower in magnitude in comparison to the Lab Bench potentials, which would correlate with lower concentrations upon the Lab Bench linear regression. If skin Cl^- levels were a source of interference then we would expect to measure larger potentials than those of the Lab Bench tests, which would correspond to higher-than-expected Cl^- concentrations. This, in combination with the cleaning of skin before the electrode is placed on the arm, suggests that skin Cl^- is not the source of the offsets observed in figure 5.8. Another possible explanation for the offset is a difference in the grounding configuration between the Lab Bench and On-Body segments. Whereas the Lab Bench segment involved measurement whilst the electrode was placed directly on the lab bench surface, On-Body measurements were taken whilst placed on the arm (resting upon the lab bench surface) of the participant seated on a laboratory stool. This change in configuration may alter the grounding of the circuit, which has an additional grounding path through the HV's body when it is in place as opposed to a lab bench patch which has a fixed ground and relative positions to the instrument. This situation is acting to shift the measured potential from the electrode and introduce the offset in potential we observe between the Lab Bench and On-Body results.

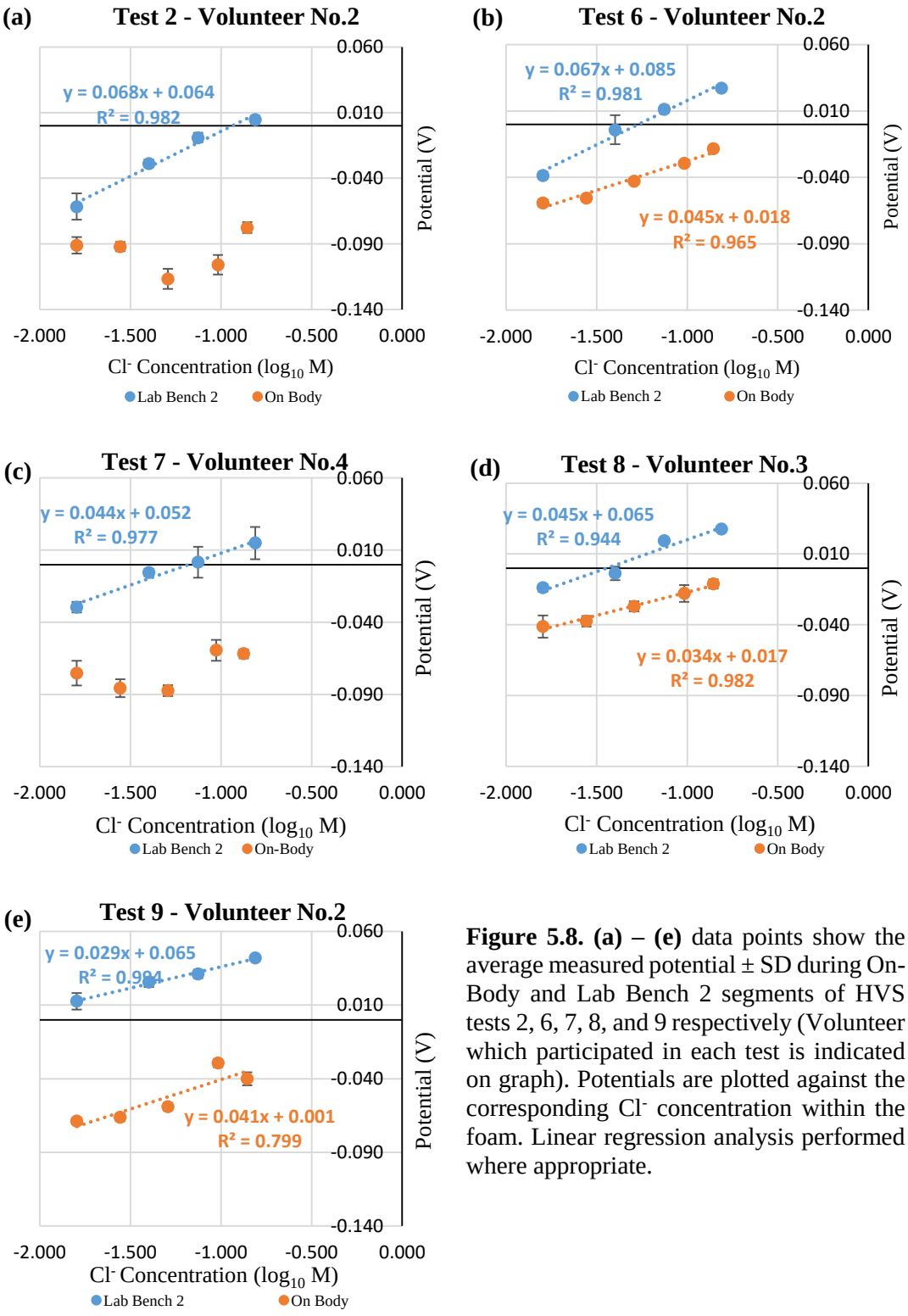

Figure 5.8. (a) – (e) data points show the average measured potential ± SD during On-Body and Lab Bench 2 segments of HVS tests 2, 6, 7, 8, and 9 respectively (Volunteer which participated in each test is indicated on graph). Potentials are plotted against the corresponding Cl^- concentration within the foam. Linear regression analysis performed where appropriate.

Instead, the On-Body potentials were retroactively adjusted to account for this offset, following the procedure detailed in Section 3.4.3.3. The compensated results are shown below in Figure 5.9.

(a)

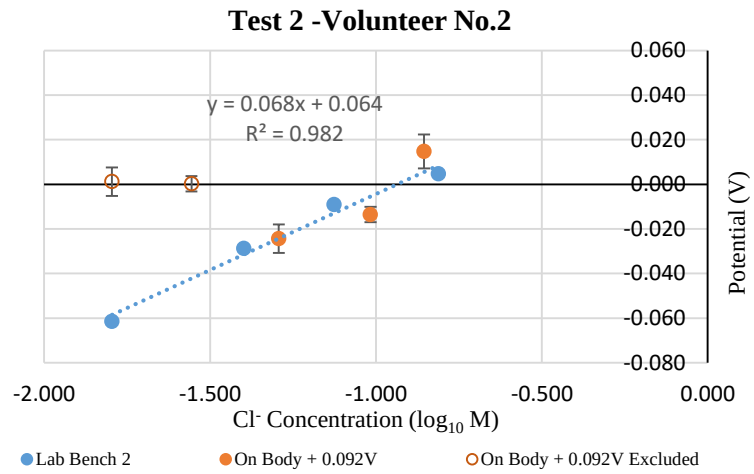

(b)

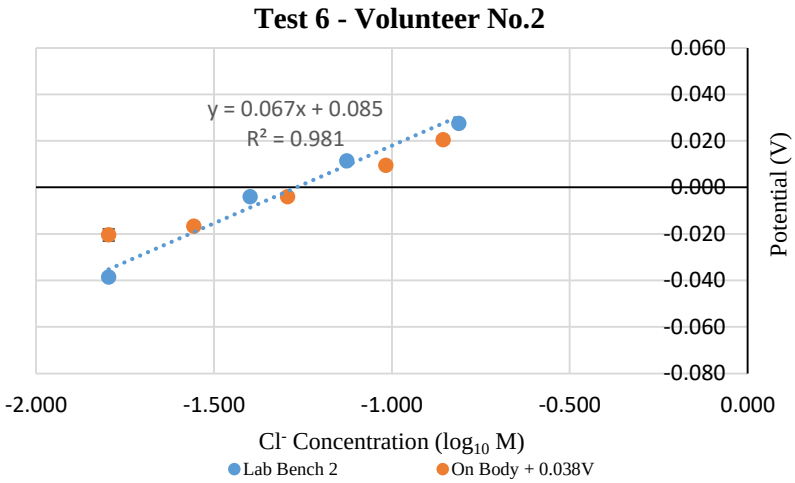

(c)

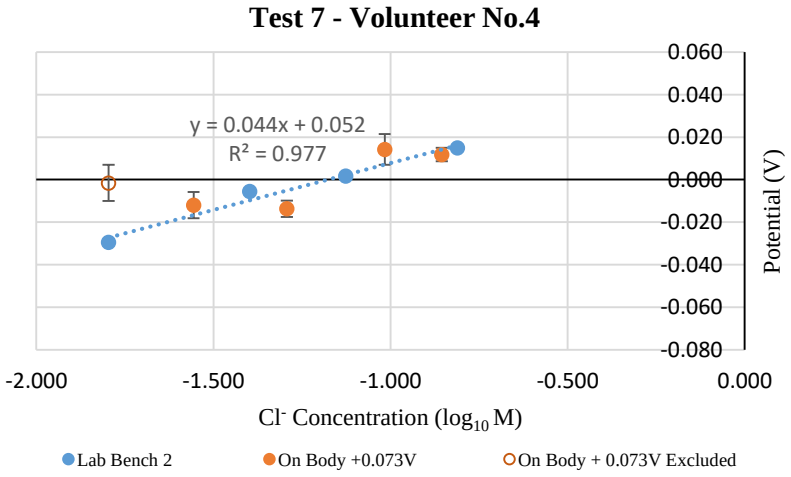

(d)

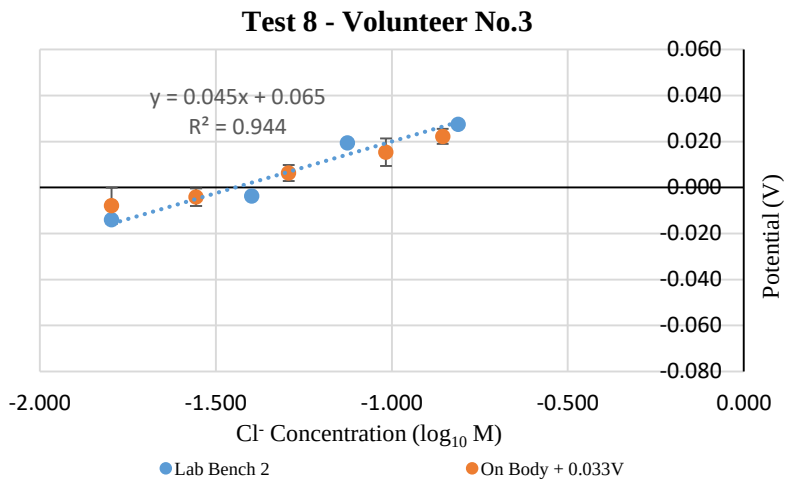

(e)

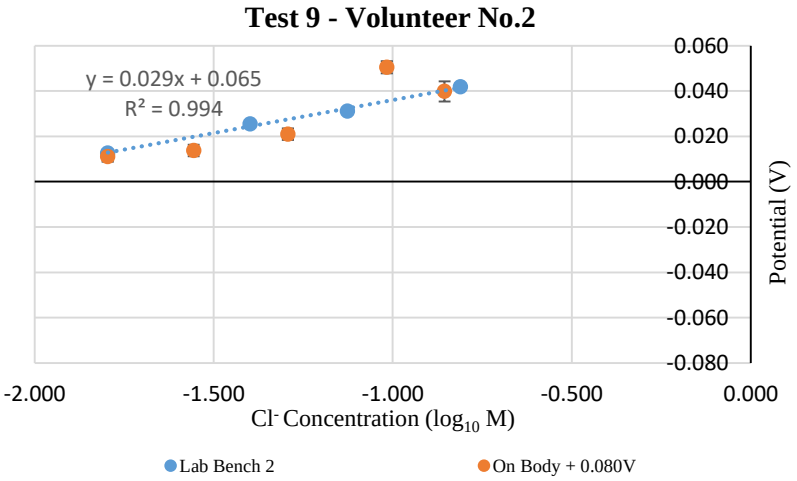

Figure 5.9. (a) – (e) data points show the average measured potential ± SD during On-Body and Lab Bench 2 segments of HVS tests 2, 6, 7, 8, and 9 respectively (Volunteer which participated in each test is indicated on graph). Potentials are plotted against the corresponding Cl^- concentration within the foam. Linear regression analysis performed where appropriate.

It should be noted that data points in Tests 2 and 7 were omitted when calculating the average value of offset. As can be seen in figure 5.2 in Section 5.2.1, these points do not appear to follow the sensitivity shown in the measurements which proceed it. As such, they skew the value of the offset, limiting our ability to compare the two datasets. The possible reason for these outliers in the context of Test 2, namely electrode / foam uncoupling, was discussed in Section 5.2.2.2.

When the measured On-Body potentials are compensated with the average offset, it is clear that both they and the Lab Bench 2 measurements match up well in terms of their respective magnitudes and sensitivity. This provides an opportunity to use the linear relationship obtained for the Lab Bench 2 data to extrapolate concentration values from the On-Body potentials. As detailed in Section 3.4.3.4, the linear relationships shown for each of the tests in figure 5.9 were rearranged to the form of equation 6.1 below. The adjusted On-Body potentials, $V_{OB}{}^{*}$, could then be substituted in to extrapolate a corresponding value of concentration, $C_{OB}{}^{*}$:

$$C_{OB}{}^{*} = 10^{\frac{(V_{OB}{}^{*}(C) - c)}{m}}. \tag{6.1}$$

The accuracy of these extrapolated values, ξ, was then determined by subtracting it from the known Cl^- concentration of the foam:

$$\xi = C_{OB} - C_{OB}{}^{*}. \tag{6.2}$$

These values of accuracy, with units adjusted to mM, are listed in Table 5.4. Figure 5.10 shows the spread of these accuracy values with respect to each individual test, while figure 5.11 shows the distribution of the accuracy values when collated with respect to Cl^- test concentration.

Table 5.4. Accuracy, ξ, of HVS On-Body concentration measurements. * denotes where data points were omitted from offset value calculation. The percentage error is given in brackets, denoting ξ as a percentage of the true foam Cl^- concentration.

	ξ (mM)				
Foam Cl^- Concentration (mM)	**Test 2** Volunteer No.2	**Test 6** Volunteer No.2	**Test 7** Volunteer No.4	**Test 8** Volunteer No.3	**Test 9** Volunteer No.2
16.00	-103.24* (645%)	-10.65 (67%)	-30.45* (190%)	-7.96 (50%)	2.19 (14%)
27.80	-87.75* (315%)	-2.53 (9%)	-7.24 (26%)	-1.19 (4%)	10.76 (39%)
50.95	0.74 (1%)	4.21 (8%)	18.82 (37%)	1.32 (3%)	20.76 (41%)
96.28	24.02 (25%)	21.97 (23%)	-42.30 (44%)	17.34 (18%)	-21.97 (228%)
139.55	-49.11 (35%)	31.07 (22%)	17.54 (13%)	27.64 (20%)	3.97 (3%)

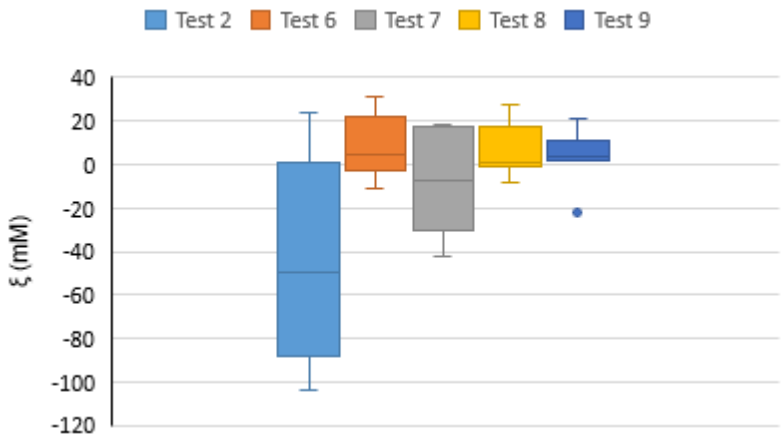

Figure 5.10. Box plots displaying the distribution of accuracy of extrapolated concentration values, ξ, grouped in terms of the test conducted. Dots denote outliers.

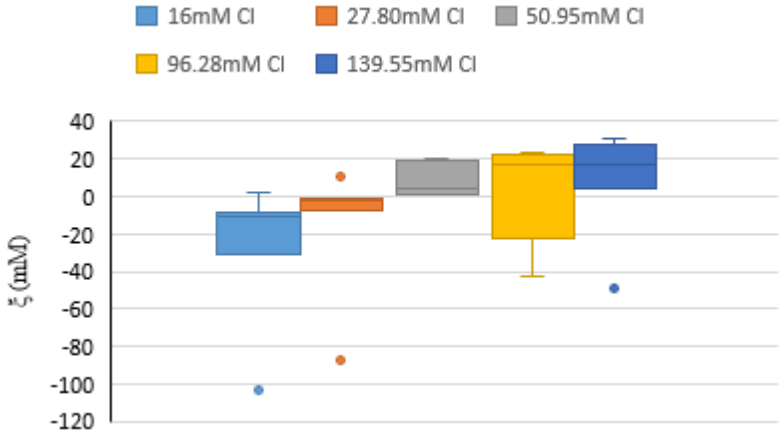

Figure 5.11. Box plots displaying the distribution of accuracy of extrapolated concentration values, ξ, grouped in terms of test Cl^- concentration. Dots denote outliers.

We can see from figure 5.10 that the accuracy of the extrapolated concentrations varies from test to test. The largest ranges are seen in Tests 2 and 7, the tests in which data points were omitted from the offset calculation. This has a particular effect on Test 2, where it causes the large spread of accuracy values shown by the large inter quartile range (IQR) in figure 5.10. However, both the comparison graph in figure 5.9 (a) and the non-asterisked accuracy values shown in Table 5.4 demonstrate that the extrapolated concentrations match up reasonably well to the known values. This, too, is the case for Test 7. Conversely, figure 5.10 shows that tests

6, 8, and 9 all display comparatively narrow spreads roughly centred around ξ = 0 mM. This reinforces the data displayed in figure 5.9 (b, d, e) which shows that the On-Body measurements align very closely to that of the Lab Bench tests. When the accuracy values are collated in terms of the Cl^- test concentration (figure 5.11) the largest spreads are given by the 96.28 mM and 139.55 mM test concentrations used. Test 7's accuracy value of ξ = -42.30 mM for the 96.28 mM test concentration contributes to this despite the measured potential only being slightly greater than that of the Lab Bench 2 linear relation, as shown in Figure 5.9 (c). The remaining test concentrations displayed in figure 5.11 display relatively narrow spreads of accuracy, accounting for outliers.

5.4 Conclusion

This section has exhibited the results of the healthy volunteer study carried out in which the pHEMA Woundsense electrode developed throughout this piece was placed, alongside artificial sweat-saturated foam, on the forearm of volunteers. With the foam's Cl^- concentration incrementally increased, the study was performed to examine the pHEMA electrode's capability to potentiometrically monitor the Cl^- concentration in a real-world setting.

The challenges which on-body testing presents resulted in a number of the tests displaying noisy measurements or no discernible sensitivity. The electrode adapter's lack of insulation, and artefacts caused by the movement of the participant were two possible explanations for these occurrences.

However, a number of the on-body tests did, in fact, display a high degree of sensitivity toward the Cl^- concentration and compared very well to the Lab Bench tests using the same electrode. Collectively, the information given in this section demonstrates that the pHEMA electrodes developed have the capability of being applied to the skin and monitoring, to a good level of accuracy, Cl^- concentrations across a clinically significant range.

These investigations, therefore, provided a vital test in gauging the device's ability to operate in a real-world environment. As such, it would be desirable that any future iterations of the device should be further tested on human subjects. This may involve analysis of biological sweat rather than an artificial substitute; the investigation into alternate device placement sites on the skin; or the effect that environmental factors such as ambient or participant temperature has upon the device's output.

6. Conclusion and Future Work

6.1 Summary of Clinical Motivation

Cystic Fibrosis is a genetic disease which affects around 1 in 2000 people (35). CF sufferers possess a mutation on the gene responsible for the synthesis of the CFTR protein, which acts to regulate Cl^- transport across various epithelial cells throughout the body. As such, CF is systemic and can lead to life-limiting conditions in the liver, pancreas, gastrointestinal organs, and lungs of sufferers. The inability of the CF sweat duct to sufficiently resorb sweat Cl^- before it reaches the skin surface means that CF patients exhibit elevated levels of sweat Cl^- in comparison to healthy individuals. A new generation of CF treatments, known as CFTR modulators, are emerging which are designed to improve CFTR functionality. The efficacy of these treatments can, therefore, be gauged by monitoring patients' sweat Cl^- concentrations over the course of their treatment. Current techniques of sweat Cl^- measurement, like the Sweat Test, are time-consuming or unsuitable for this task. Hence, the development of a wearable device capable of monitoring sweat Cl^- levels in a minimally invasive and time-effective manner, is of great significance within this field.

6.2 Summary and Conclusions of CF Patient Monitor Development

This thesis detailed the work undertaken to develop a CF patient monitor in the form of a wearable Cl^- ion-selective electrode. Woundsense Ag/AgCl electrodes were adapted through the deposition of a HEMA hydrogel mixture onto one of the substrate's two electrode contacts. The HEMA mixture was polymerised using a purpose-built UV LED array and the resultant pHEMA electrodes then immersed in a KCl DI water solution to facilitate the hydrogel's saturation with Cl^- ions. This allowed the pHEMA-covered electrode to be utilised as a quasi-reference electrode (QRE). Alongside the unaltered Ag/AgCl working electrode, the electrode pair formed a compact Cl^- concentration cell configuration where the measured potential is proportional to the Cl^- concentration of the solution with which the electrodes are in contact.

The length of time in which the HEMA mixture is polymerised, the length of time which the pHEMA is conditioned in the KCl solution, as well as the concentration of the conditioning solutions were variables examined during the development of the device. After the conditioning process had been established, lab bench tests demonstrated that the pHEMA Woundsense electrode exhibited good sensitivity toward the Cl^- concentration of test solutions, with the calibration curve possessing a sensitivity of 64.34 mV/dec over a concentration range of 10 - 100 mM. This compares well to the reported sensitivities of 58 mV/dec and 58.5 mV/dec of Cl^- sensitive hydrogel electrodes from the literature (70,75) (Section 1.3.2.3). Tests showed that our pHEMA QRE was able to provide a stable reference potential for 1 hour whilst immersed in a test solution before significant drift was observed. In comparison, the device detailed in (75) displays a relatively constant reference potential for 2 hours. However, if the rate of drift of our pHEMA electrode is corrected for, the period of stable potential can be extended to at least 8 hours. Additionally, the electrodes displayed low sensitivity toward lactate and bicarbonate (1.84 mV/dec and 4.32 mV/dec respectively), the main competing anions found in human sweat.

A HVS was conducted to examine the ability of the pHEMA Woundsense electrode to operate effectively whilst placed on the forearm of participants. These studies highlighted some of the operational challenges of wearable devices such as the type and condition of the skin upon which the electrode is placed. It is believed this may have acted to introduce a source of interference within at least two of the tests carried out (Section 5.2.2.3). Potentials measured from the electrode whilst placed on the body also exhibited a near-constant offset in relation to the potentials measured upon the lab bench, possibly originating from a change in the circuit grounding between the two configurations. The HVS did, however, demonstrate that the pHEMA electrodes were able to monitor the CF-relevant Cl^- concentration of a solution whilst placed on the skin surface. Five of the tests conducted demonstrated a sensitivity to the Cl^- concentration within the foam over a range of 16 – 140 mM. Furthermore, they did so to a

comparable level of sensitivity to that of the lab bench examinations conducted on the same electrodes. After compensating for the offset between the On-Body and Lab Bench potentials, the measured Cl^- concentrations from the On-Body tests compared well with the true Cl^- concentration within the foam. Despite one outlier with a percentage error of 228%, the remaining On-Body concentration measurements had a percentage error within 1–50%, demonstrating that the pHEMA electrode was able to monitor the Cl^- test concentration whilst placed on the skin to a good level of accuracy.

Therefore, the work contained within this thesis charts the development of the technology capable of forming the basis of a wearable sweat Cl^- monitor for CF patients, providing a method to gauge the efficacy of emerging, and potentially life-saving treatments.

6.3 Future Work

It is proposed that future work should include:

- Investigation into how composition of pHEMA gel mixture affects potentiometric. performance of sensor, specifically the onset of potential drift.
- Study into use of different electrode substrates.
- Study into long-term storage of sensors and their potential reusability.
- Investigation into source of voltage offset when sensor is placed on-body.
- Utilising pHEMA sensor to make on-body measurements of real sweat samples.
- Study into skin permeability to Cl^- ions and skin Cl^- concentrations.
- Explore effects of ambient and volunteer temperatures for on-body measurements.
- Conversion of sensor hardware into PCB platform to enable miniaturisation of device.
- Study to directly compare the accuracy of sweat Cl^- measurements made by pHEMA. Woundsense sensor to those made via CF Sweat Test.
- Investigation into feasibility of integration of Cl^- sensor into a wider sensor platform, forming the basis of a hydration and wellbeing monitor.

If this research was to be passed on to someone else, it is the author's opinion that the focus should be on performing more on-body tests, ideally using biological sweat, in order to further study of the device performance on-skin. Additionally, efforts should be made to miniaturise the device. Adapting the device in such a manner may have an effect on its performance, therefore re-examining aspects of the device's potentiometric performance should be accounted for when planning any future work. Appendix: B gives an account of a preliminary study into the miniaturisation of the configuration, utilising the pHEMA Woundsense electrode alongside an op-amp voltage follower circuit, microcontroller and Bluetooth module. The results suggest that with further development, the technology could be further miniaturised to form a compact wearable sweat Cl^- device. Limitations to this scalability may include the finite size of the QRE matrix which has to maintain a volume of Cl^- above the electrode contact in order to function. However, as the pHEMA sample is currently only 4mm in diameter this is not expected to be an issue. More pertinent is the global shortage and manufacturing bottleneck of semiconductor materials, which could impact on the production of PCBs for the device. It is hoped that such delays have alleviated by the time future iterations of the device at the point of being rolled out for manufacture. Such a device would not only be of great benefit in evaluating CF treatments, but could also be applied to sport and lifestyle, forming part of a hydration and wellbeing monitor.

References

1. Cuthbert AW. New horizons in the treatment of cystic fibrosis. Br J Pharmacol. 2011;163(1):173–83.

2. Filbrun AG, Ren CL, Lahiri T. Handbook of Cystic Fibrosis. 2016. 99 p.

3. Bear CE, Li C, Kartner N, Bridges RJ, Jensen TJ, Ramjeesingh M, et al. Purification and functional reconstitution of the cystic fibrosis transmembrane conductance regulator (CFTR). Cell. 1992 Feb 21;68(4):809–18.

4. Riordan JR, Rommens JM, Kerem B, et al. Identification of the cystic fibrosis gene: cloning and characterization of complementary DNA. Science (80-). 1989;245:1066–73.

5. Busch R. On the history of cystic fibrosis. Acta Univ Carol Med (Praha). 1990;36(1–4):13–5.

6. Taylor CJ, Hardcastle J, Southern KW. Physiological Measurements Confirming the Diagnosis of Cystic Fibrosis: The Sweat Test and Measurements of Transepithelial Potential Difference. Vol. 10, Paediatric Respiratory Reviews. 2009. p. 220–6.

7. Gibson LE, Cooke RE. A test for concentration of electrolytes in sweat in cystic fibrosis of the pancreas utilizing pilocarpine by iontophoresis. Pediatrics. 1959;23(3):545–9.

8. Rosenstein BJ, Cutting GR. The diagnosis of cystic fibrosis: A consensus statement. J Pediatr. 1998;132(4):589–95.

9. Wescor. Macroduct Sweat Collection System. 2004;

10. LeGrys VA, Yankaskas JR, Quittell LM, Marshall BC, Mogayzel PJ. Diagnostic Sweat Testing: The Cystic Fibrosis Foundation Guidelines. J Pediatr. 2007;151(1):85–9.

11. Wescor. Macroduct ® /Sweat @BULLET Chek ™ ELITechGroup WESCOR ® M E D I C A L D E V I C E S. 2008;

12. Green A. Guidelines for the Performance of the Sweat Test for the Investigation of Cystic Fibrosis in the UK - Report from the Multi-Disciplinary Working Group. 2003.

13. Taccetti G. Sweat testing in newborns positive to neonatal screening for cystic fibrosis. Arch Dis Child - Fetal Neonatal Ed. 2004;89(5):F463–4.

14. Farrell PM, White TB, Ren CL, Hempstead SE, Accurso F, Derichs N, et al. Diagnosis of Cystic Fibrosis: Consensus Guidelines from the Cystic Fibrosis Foundation. J Pediatr. 2017;181:S4-S15.e1.

15. Castellani C, Cutting G, Sosnay P, Siklosi K, Lewis MH, Penland C, et al. CFTR2: How will it help care? Paediatr Respir Rev. 2013;14(SUPPL.1):2–5.

16. De Boeck K. Cystic fibrosis: terminology and diagnostic algorithms. Thorax. 2006;61(7):627–35.

17. Crossley JR, Smith PA, Edgar BW, Gluckman PD, Elliott RB. Neonatal screening for cystic fibrosis, using immunoreactive trypsin assay in dried blood spots. Clin Chim Acta. 1981 Jun 18;113(2):111–21.

18. Alton EW, Currie D, Logan-Sinclair R, Warner JO, Hodson ME, Geddes DM. Nasal potential difference: a clinical diagnostic test for cystic fibrosis. Eur Respir J Off J Eur Soc Clin Respir Physiol. 1990;3(8):922–6.

19. Sermet-Gaudelus I, Girodon E, Roussel D, Deneuville E, Bui S, Huet F, et al. Measurement of nasal potential difference in young children with an equivocal sweat test following newborn screening for cystic fibrosis. Thorax. 2010;65(6):539–44.

20. Cohen-Cymberknoh M, Shoseyov D, Kerem E. Managing cystic fibrosis: Strategies that increase life expectancy and improve quality of life. Am J Respir Crit Care Med. 2011;183(11):1463–71.

21. Gibson RL, Burns JL, Ramsey BW. Pathophysiology and Management of Pulmonary Infections in Cystic Fibrosis. Am J Respir Crit Care Med. 2003;168(8):918–51.

22. Fajac I, Wainwright CE. New treatments targeting the basic defects in cystic fibrosis. Vol. 46, Presse Medicale. 2017. p. e165–75.

23. Mondejar-Lopez P, Pastor-Vivero MD, Sanchez-Solis M, Escribano A. Cystic fibrosis treatment: targeting the basic defect. Vol. 5, Expert Opinion on Orphan Drugs. 2017. p. 181–92.

24. Lopes-Pacheco M. CFTR Modulators: The Changing Face of Cystic Fibrosis in the Era of Precision Medicine. Front Pharmacol. 2020;10(February):1–29.

25. Mall MA, Galietta LJV. Targeting ion channels in cystic fibrosis. Vol. 14, Journal of Cystic Fibrosis. 2015. p. 561–70.

26. Davies JC, Cunningham S, Harris WT, Lapey A, Regelmann WE, Sawicki GS, et al. Safety, pharmacokinetics, and pharmacodynamics of ivacaftor in patients aged 2-years with cystic fibrosis and a CFTR gating mutation (KIWI): An open-label, single-arm study. Lancet Respir Med. 2016 Feb 1;4(2):107–15.

27. Reihill JA, Douglas LEJ, Martin SL. Modulation of ion transport to restore airway hydration in cystic

fibrosis. Genes (Basel). 2021;12(3).

28. Mayer M. Lumacaftor-ivacaftor (Orkambi) for cystic fibrosis: behind the “breakthrough”. Evid Based Med. 2016;21(3):83–6.

29. Donaldson SH, Pilewski JM, Griese M, Cooke J, Viswanathan L, Tullis E, et al. Tezacaftor/Ivacaftor in Subjects with Cystic Fibrosis and F508del/F508del-CFTR or F508del/G551D-CFTR. AJRCCM Artic Press. 2017 Sep 20;201704–17.

30. Brodlie M, Haq IJ, Roberts K, Elborn JS. Targeted therapies to improve CFTR function in cystic fibrosis. Genome Med. 2015 Sep 24;7(1):101.

31. Goor F Van, Straley KS, Cao D, González J, Hadida S, Joubran J, et al. Rescue of dF508-CFTR trafficking and gating in human cystic fibrosis airway primary cultures by small molecules Fredrick. Am J Physiol. 2006;(848):1–57.

32. Wainwright CE, Elborn JS, Ramsey BW, Marigowda G, Huang X, Cipolli M, et al. Lumacaftor–Ivacaftor in Patients with Cystic Fibrosis Homozygous for Phe508del CFTR. N Engl J Med. 2015;373(3):220–31.

33. NHS-England. NHS England concludes wide-ranging deal for cystic fibrosis drugs [Internet]. [cited 2021 Oct 9]. Available from: https://www.england.nhs.uk/2019/10/nhs-england-concludes-wide-ranging-deal-for-cystic-fibrosis-drugs/

34. MacGregor G. New medicines for CF ARTP. Glasgow; 2019.

35. MacGregor G. Cystic Fibrosis: CFTR Modulator Drugs. Glasgow; 2021.

36. Meoli A, Fainardi V, Deolmi M, Chiopris G, Marinelli F, Caminiti C, et al. State of the art on approved cystic fibrosis transmembrane conductance regulator (Cftr) modulators and triple-combination therapy. Pharmaceuticals. 2021;14(9).

37. Cystic Fibrosis Trust. Kaftrio (Trikafta in the US) – Triple combination therapy [Internet]. [cited 2021 Oct 9]. Available from: https://www.cysticfibrosis.org.uk/the-work-we-do/campaigning-hard/life-saving-drugs/triple-combination-therapy

38. Kerem E, Konstan MW, De Boeck K, Accurso FJ, Sermet-Gaudelus I, Wilschanski M, et al. Ataluren for the treatment of nonsense-mutation cystic fibrosis: A randomised, double-blind, placebo-controlled phase 3 trial. Lancet Respir Med. 2014 Jul 1;2(7):539–47.

39. Alton EWFW, Beekman JM, Boyd AC, Brand J, Carlon MS, Connolly MM, et al. Preparation for a first-

in-man lentivirus trial in patients with cystic fibrosis. Thorax. 2017 Feb 1;72(2):137–47.

40. Cystic Fibrosis Foundation. Gene Editing for Cystic Fibrosis [Internet]. [cited 2021 Oct 11]. Available from: https://www.cff.org/Research/Research-Into-the-Disease/Restore-CFTR-Function/Gene-Editing-for-Cystic-Fibrosis/

41. Cystic Fibrosis News Today. CRISPR/Cas9 Approach for Cystic Fibrosis Treatment [Internet]. [cited 2021 Oct 11]. Available from: https://cysticfibrosisnewstoday.com/crisprcas9-approach-for-cystic-fibrosis/

42. Mengstie MA, Wondimu BZ. Mechanism and applications of crispr/ cas-9-mediated genome editing. Biol Targets Ther. 2021;15:353–61.

43. DeMarco ML, Dietzen DJ, Brown SM. Sweating the small stuff: Adequacy and accuracy in sweat chloride determination. Clin Biochem. 2015;48(6):443–7.

44. Teymourian H, Barfidokht A, Wang J. Electrochemical glucose sensors in diabetes management: An updated review (2010-2020). Chem Soc Rev. 2020;49(21):7671–709.

45. Rathee K, Dhull V, Dhull R, Singh S. Biosensors based on electrochemical lactate detection: A comprehensive review. Biochem Biophys Reports. 2016;5:35–54.

46. Ching TS, Connolly P. Simulataneous transdermal extraction of glucose and lactate from human subjects by reverse iontophoresis. Int J Nanomedicine. 2008;3(2):211–23.

47. Piwek L, Ellis DA, Andrews S, Joinson A. The Rise of Consumer Health Wearables: Promises and Barriers. PLoS Med. 2016;13(2).

48. Niknejad N, Ismail WB, Mardani A, Liao H, Ghani I. A comprehensive overview of smart wearables: The state of the art literature, recent advances, and future challenges. Eng Appl Artif Intell. 2020;90(October 2019):103529.

49. Rhodes H. Accessing and using data from wearable fitness devices. J AHIMA. 2014;85(9):48–50.

50. Baxendale G. Health Wearables. Vol. 58, ITNOW. 2016. p. 42–3.

51. Moonen EJM, Haakma JR, Peri E, Pelssers E, Mischi M, den Toonder JMJ. Wearable sweat sensing for prolonged, semicontinuous, and nonobtrusive health monitoring. View. 2020;1(4):20200077.

52. Baker LB, Model JB, Barnes KA, Anderson ML, Lee SP, Lee KA, et al. Skin-interfaced microfluidic system with personalized sweating rate and sweat chloride analytics for sports science applications. Sci

Adv. 2020;6(50):17–9.

53. Bandodkar AJ, Wang J. Non-invasive wearable electrochemical sensors: A review. Vol. 32, Trends in Biotechnology. 2014. p. 363–71.

54. Vaddiraju S. Technologies for Continuous Glucose Monitoring: Current Problems and Future Promises. J Diabetes Sci Technol. 2010;4(6):1540–62.

55. Medtronic. Guardian RT Continuous Glucose Monitoring System.

56. Fokkert MJ, van Dijk PR, Edens MA, Abbes S, de Jong D, Slingerland RJ, et al. Performance of the FreeStyle Libre Flash glucose monitoring system in patients with type 1 and 2 diabetes mellitus. BMJ Open Diabetes Res Care. 2017;5(1):e000320.

57. Chan M, Estève D, Fourniols J-Y, Escriba C, Campo E. Smart wearable systems: Current status and future challenges. Artif Intell Med. 2012;56(3):137–56.

58. Bard AJ, Faulkner LR. ELECTROCHEMICAL METHODS Fundamentals and Applications. New York: Wiley; 2001. 3–7 p.

59. Bühlmann P, Chen LD. Ion-Selective Electrodes With Ionophore-Doped Sensing Membranes. Supramolecular Chemistry. 2012.

60. Gross EM, Kelly RS, Cannon D.M. J. Analytical Electrochemistry: Potentiometry. J Anal Sci Digit Libr. 2008;10052.

61. Schazmann B, Morris D, Slater C, Beirne S, Fay C, Reuveny R, et al. A wearable electrochemical sensor for the real-time measurement of sweat sodium concentration. Anal Methods. 2010;2(4):342.

62. Hu J, Stein A, Bühlmann P. Rational design of all-solid-state ion-selective electrodes and reference electrodes. Vol. 76, TrAC - Trends in Analytical Chemistry. 2016. p. 102–14.

63. Zuliani C, Matzeu G, Diamond D. A liquid-junction-free reference electrode based on a PEDOT solid-contact and ionogel capping membrane. Talanta. 2014;125:58–64.

64. Gao W, Emaminejad S, Nyein HYY, Challa S, Chen K, Peck A, et al. Fully integrated wearable sensor arrays for multiplexed in situ perspiration analysis. Nature. 2016;529(7587):509–14.

65. Buenger D, Topuz F, Groll J. Hydrogels in sensing applications. Vol. 37, Progress in Polymer Science. 2012. p. 1678–719.

66. Gyurcsányi RE, Rangisetty N, Clifton S, Pendley BD, Lindner E. Microfabricated ISEs: Critical comparison of inherently conducting polymer and hydrogel based inner contacts. Talanta. 2004;63(1):89–99.

67. Bobacka J. Conducting polymer-based solid-state ion-selective electrodes. Electroanalysis. 2006;18(1):7–18.

68. Cranny A, Harris NR, Nie M, Wharton JA, Wood RJK, Stokes KR. Screen-printed potentiometric Ag/AgCl chloride sensors: Lifetime performance and their use in soil salt measurements. In: Sensors and Actuators, A: Physical. 2011. p. 288–94.

69. Bockris JOM, Reddy AKN, Gamboa M. Modern Electrochemistry 2A. Modern Electrochemistry 2A. Kluwer Academic Publishers; 2002.

70. Dam VAT, Zevenbergen MAG, van Schaijk R. Toward wearable patch for sweat analysis. Sensors Actuators, B Chem. 2016;236:834–8.

71. Dam VAT, Goedbloed M, Zevenbergen MAG. Solid-Contact Reference Electrode for Ion-Selective Sensors †. 2017;1–4.

72. Gonzalo-Ruiz J, Mas R, de Haro C, Cabruja E, Camero R, Alonso-Lomillo MA, et al. Early determination of cystic fibrosis by electrochemical chloride quantification in sweat. Biosens Bioelectron. 2009;24(6):1788–91.

73. Dam VAT, Zevenbergen MAG, Van Schaijk R. Flexible Ion Sensors for Bodily Fluids. In: Procedia Engineering. 2016. p. 93–6.

74. Choi D-H, Kim JS, Cutting GR, Searson PC. Wearable Potentiometric Chloride Sweat Sensor: The Critical Role of the Salt Bridge. Anal Chem. 2016;88(24):12241–7.

75. Choi DH, Li Y, Cutting GR, Searson PC. A wearable potentiometric sensor with integrated salt bridge for sweat chloride measurement. Sensors Actuators, B Chem. 2017;250:673–8.

76. Choi DH, Thaxton A, Jeong I cheol, Kim K, Sosnay PR, Cutting GR, et al. Sweat test for cystic fibrosis: Wearable sweat sensor vs. standard laboratory test. Journal of Cystic Fibrosis. 2018;

77. Underwood AL. Photometric Titrations. J Chem Educ. 1954 Aug;31(8):394.

78. Varcoe JS. Clinical Biochemistry: Techniques and Instrumentation. WORLD SCIENTIFIC; 2001.

79. Elitech. Laboratory Procedure for the ChloroChek ® Chlorodometer ® Sweat Chloride Analyzer. 2014.

80. Munns R, Wallace PA, Teakle NL, Colmer TD. Plant Stress Tolerance. In: NIH Public Access. 2010. p. 1–14.

81. Bishop ML. Clinical Chemistry: Principles, Techniques, and Correlations, Enhanced Edition: Principles, Techniques, and Correlations, Enhanced Edition. 8th ed. Jones & Bartlett Learning, 2020; 2020.

82. NCCLS. Sweat Testing : Sample Collection and Quantitative Analysis ; Approved Guideline — Second Edition. Vol. 20. 2008.

83. CLSI. CLSI Announces New Sweat Testing Guideline for the Diagnosis of Cystic Fibrosis. Lab Med. 2010 May 1;41(5):308–9.

84. Licht TS, Stern M, Shwachman H. Measurement of the electrical conductivity of sweat. Clin Chem. 1956;3(1):37–48.

85. Sands D, Ołtarzewski M, Nowakowska A, Zybert K. Bilateral sweat tests with two different methods as a part of cystic fibrosis newborn screening (CF NBS) protocol and additional quality control. Folia Histochem Cytobiol. 2010;48(3):358–65.

86. Lezana JL, Vargas MH, Karam-Bechara J, Aldana RS, Furuya MEY. Sweat conductivity and chloride titration for cystic fibrosis diagnosis in 3834 subjects. J Cyst Fibros. 2003;2(1):1–7.

87. Wescor. SWEAT@BULLETCHEK ™ SWEAT CONDUCTIVITY ANALYZER Model 3120 Instruction/Service Manual. 2005;

88. Boisvert P, Candas V. Validity of the Wescor's sweat conductivity analyzer for the assessment of sweat electrolyte concentrations. Eur J Appl Physiol Occup Physiol. 1994;69(2):176–8.

89. Mastella G, Di Cesare G, Borruso A, Menin L, Zanolla L. Reliability of sweat-testing by the Macroduct® collection method combined with conductivity analysis in comparison with the classic Gibson and Cooke technique. Acta Paediatr Int J Paediatr. 2000;89(8):933–7.

90. Hanna. INSTRUCTION MANUAL HI 96717 Range ISM. 2011.

91. Cirello-Egamino J, Brindle ID. Determination of chloride ions by reaction with mercury thiocyanate in the absence of iron(III) using a UV-photometric, flow injection method. Analyst. 1995;120(1):183.

92. A. Koh, Kang D, Xue Y, Lee S, Pielak RM, Kim J, et al. A soft, wearable microfluidic device for the

capture, storage, and colorimetric sensing of sweat. Biosensors. 2016;8(366).

93. Dehdashtian A, Stringer TP, Warren AJ, Mu EW, Amirlak B, Shahabi L. Anatomy and physiology of the skin. In: Melanoma: A Modern Multidisciplinary Approach. 2018. p. 15–26.

94. Kent M. Van De Graaff, R. Ward Rhees SLP. Schaum`s outline of human anatomy and physiology. 3rd ed. McGraw-Hill USA; 2009.

95. Van Der Maaden K, Jiskoot W, Bouwstra J. Microneedle technologies for (trans)dermal drug and vaccine delivery. J Control Release. 2012;161(2):645–55.

96. Bouwstra JA, Ponec M. The skin barrier in healthy and diseased state. Biochim Biophys Acta - Biomembr. 2006;1758(12):2080–95.

97. Hou L, Hagen J, Wang X, Papautsky I, Naik R, Kelley-Loughnane N, et al. Artificial microfluidic skin for in vitro perspiration simulation and testing. Lab Chip. 2013;13(10):1868–75.

98. Alkilani AZ, McCrudden MT, Donnelly RF. Transdermal drug delivery: Innovative pharmaceutical developments based on disruption of the barrier properties of the stratum corneum. Vol. 7, Pharmaceutics. 2015. p. 438–70.

99. Prausnitz MR, Langer R. Transdermal drug delivery. Nat Biotechnol. 2008;26(11):1261–8.

100. Li LC, Scudds RA. Iontophoresis: An overview of the mechanisms and clinical application. Arthritis Rheum. 1995;8(1):51–61.

101. Brown MB, Martin GP, Jones SA, Akomeah FK. Dermal and transdermal drug delivery systems: Current and future prospects. Drug Deliv J Deliv Target Ther Agents. 2006;13(3):175–87.

102. Bos JD, Meinardi MMHM. The 500 Dalton rule for the skin penetration of chemical compounds and drugs. Exp Dermatol. 2000;9(3):165–9.

103. Yang NJ, Hinner MJ. Getting across the cell membrane: an overview for small molecules, peptides, and proteins. Vol. 1266, Methods in molecular biology (Clifton, N.J.). 2015. p. 29–53.

104. Weaver JC, Smith KC, Esser AT, Son RS, Gowrishankara TR. A brief overview of electroporation pulse strength-duration space: A region where additional intracellular effects are expected. Bioelectrochemistry. 2012;87:236–43.

105. Khan A, Yasir M, Asif M, Chauhan I, Singh AP, Sharma R, et al. Iontophoretic drug delivery: History and

applications. J Appl Pharm Sci. 2011;1(3):11–24.

106. Pikal MJ. The role of electroosmotic flow in transdermal iontophoresis. Adv Drug Deliv Rev. 2001;46(1–3):281–305.

107. Banga AK, Bose S, Ghosh TK. Iontophoresis and electroporation: Comparisons and contrasts. Int J Pharm. 1999;179(1):1–19.

108. Srinivasan V, Higuchi WI, Sims SM, Ghanem AH, Behl CR. Transdermal iontophoretic drug delivery: Mechanistic analysis and application to polypeptide delivery. J Pharm Sci. 1989;78(5):370–5.

109. Tierney MJ, Tamada JA, Potts RO, Jovanovic L, Garg S. Clinical evaluation of the GlucoWatch® biographer: A continual, non-invasive glucose monitor for patients with diabetes. Biosens Bioelectron. 2001;16(9–12):621–9.

110. McCormick C, Heath D, Connolly P. Towards blood free measurement of glucose and potassium in humans using reverse iontophoresis. Sensors Actuators, B Chem. 2012 May 20;166–167:593–600.

111. Sieg A, Guy RH, Delgado-Charro MB. Noninvasive glucose monitoring by reverse iontophoresis in vivo: Application of the internal standard concept. Clin Chem. 2004;50(8):1383–90.

112. Dhote V, Bhatnagar P, Mishra PK, Mahajan SC, Mishra DK. Iontophoresis: A potential emergence of a transdermal drug delivery system. Sci Pharm. 2012;80(1):1–28.

113. Cullander C. What are the pathways of iontophoretic current flow through mammalian skin? Adv Drug Deliv Rev. 1992;9(2–3):119–35.

114. Abramson HA, Gorin MH. Skin reactions. IX - The electrophoretic demonstration of the patent pores of the living human skin; Its relation to the charge of the skin. J Phys Chem. 1940;44(9):1094–102.

115. Baker LB. Physiology of sweat gland function: The roles of sweating and sweat composition in human health. Temperature. 2019;6(3):211–59.

116. Hodge BD, Brodell RT. Anatomy, Skin, Sweat Glands. StatPearls. StatPearls Publishing; 2018.

117. Murphrey MB, Vaidya T. Histology, Apocrine Gland. StatPearls. StatPearls Publishing; 2019.

118. Shelley WB, Hurley HJ. The physiology of the human axillary apocrine sweat gland. J Invest Dermatol. 1953;20(4):285–97.

119. Braun-Falco O, Plewig G, Wolff HH, Winkelmann RK, Braun-Falco O, Plewig G, et al. Diseases of the

Apocrine Sweat Glands. In: Dermatology. Springer Berlin Heidelberg; 1991. p. 744–6.

120. Cui CY, Schlessinger D. Eccrine sweat gland development and sweat secretion. Vol. 24, Experimental Dermatology. 2015. p. 644–50.

121. Sato K., Kang W., Saga K, Sato K. Biology of sweat glands and their disorders I. J Am Acad Dermatol. 1989;20(5):713–26.

122. Lu C, Fuchs E. Sweat gland progenitors in development, homeostasis, and wound repair. Cold Spring Harb Perspect Med. 2014;4(2).

123. Wilke K, Martin A, Terstegen L, Biel SS. A short history of sweat gland biology. International Journal of Cosmetic Science John Wiley & Sons, Ltd; Jun 1, 2007 p. 169–79.

124. Cui CY, Sima J, Yin M, Michel M, Kunisada M, Schlessinger D. Identification of potassium and chloride channels in eccrine sweat glands. Vol. 81, Journal of Dermatological Science. Elsevier Ireland Ltd; 2016. p. 129–31.

125. Sato K, Sato F. Role of calcium in cholinergic and adrenergic mechanisms of eccrine sweat secretion. Am J Physiol - Cell Physiol. 1981;10(2):113–20.

126. Baker LB, Wolfe AS. Physiological mechanisms determining eccrine sweat composition. Vol. 120, European Journal of Applied Physiology. Springer Berlin Heidelberg; 2020. 719–752 p.

127. Toyomoto T, Knutsen D, Soos G, Sato K. Na-K-2Cl cotransporters are present and regulated in simian eccrine clear cells. Am J Physiol - Regul Integr Comp Physiol. 1997;273(1 42-1).

128. Orlov SN, Koltsova S V., Kapilevich L V., Gusakova S V., Dulin NO. NKCC1 and NKCC2: The pathogenetic role of cation-chloride cotransporters in hypertension. Vol. 2, Genes and Diseases. Chongqing Medical University; 2015. p. 186–96.

129. Quinton PM. Cystic Fibrosis: Lessons from the Sweat Gland. Physiology. 2007;22(3):212–25.

130. Reddy MM, Quinton PM. Control of dynamamic CFTR selectivity by glutamate and ATP in epithelial cells. Nature. 2003;423(6941):756–60.

131. Buono MJ, Claros R, DeBoer T, Wong J. Na+ secretion rate increases proportionally more than the Na+ reabsorption rate with increases in sweat rate. J Appl Physiol. 2008;105(4):1044–8.

132. Shibasaki M, Crandall CG. Mechanisms and controllers of eccrine sweating in humans. Front Biosci - Sch.

2010;2 S(2):685–96.

133. Shibasaki M, Kondo N, Crandall CG. Non-thermoregulatory modulation of sweating in humans. Exerc Sport Sci Rev. 2003;31(1):34–9.

134. Tansey EA, Johnson CD, Johnson CD. Staying Current Recent advances in thermoregulation. Adv Physiol Educ. 2015;39:139–48.

135. Schmidt R, Weidner C, Schmelz M. Time course of acetylcholine-induced activation of sympathetic efferents matches axon reflex sweating in humans. J Peripher Nerv Syst. 2011 Mar;16(1):30–6.

136. Magerl W, Westerman RA, Möhner B, Handwerker HO. Properties of transdermal histamine iontophoresis: Differential effects of season, gender, and body region. J Invest Dermatol. 1990;94(3):347–52.

137. Simmers P, Li SK, Kasting G, Heikenfeld J. Prolonged and localized sweat stimulation by iontophoretic delivery of the slowly-metabolized cholinergic agent carbachol. J Dermatol Sci. 2018 Jan 1;89(1):40–51.

138. Boyle MP, De Boeck K. A new era in the treatment of cystic fibrosis: Correction of the underlying CFTR defect. Vol. 1, The Lancet Respiratory Medicine. 2013. p. 158–63.

139. Stutts M, Canessa C, Olsen J, Hamrick M, Cohn J, Rossier B, et al. CFTR as a cAMP-dependent regulator of sodium channels. Science (80-). 1995;269(5225):847–50.

140. Mall M, Bleich M, Greger R, Schreiber R, Kunzelmann K. The amiloride-inhibitable Na+ conductance is reduced by the cystic fibrosis transmembrane conductance regulator in normal but not in cystic fibrosis airways. J Clin Invest. 1998;102(1):15–21.

141. Mall M, Grubb BR, Harkema JR, O'Neal WK, Boucher RC. Increased airway epithelial Na+ absorption produces cystic fibrosis-like lung disease in mice. Nat Med. 2004 May 11;10(5):487–93.

142. Stoltz DA, Meyerholz DK, Welsh MJ. Origins of Cystic Fibrosis Lung Disease. N Engl J Med. 2015;372(4):351–62.

143. Hauser AR, Jain M, Bar-Meir M, McColley SA. Clinical significance of microbial infection and adaptation in cystic fibrosis. Clin Microbiol Rev. 2011;24(1):29–70.

144. Harrison F. Microbial ecology of the cystic fibrosis lung. Microbiology. 2007;153(4):917–23.

145. Cystic Fibrosis Trust. UK Cystic Fibrosis Registry Annual data report 2019. Registry. 2020;(September).

146. Hassett DJ, Sutton MD, Schurr MJ, Herr AB, Caldwell CC, Matu JO. Pseudomonas aeruginosa hypoxic or

anaerobic biofilm infections within cystic fibrosis airways. Vol. 17, Trends in Microbiology. 2009. p. 130–8.

147. Ledder O, Haller W, Couper RTL, Lewindon P, Oliver M. Cystic fibrosis: An update for clinicians. Part 2: Hepatobiliary and pancreatic manifestations. J Gastroenterol Hepatol. 2014;29(12):1954–62.

148. The Pancreas and Its Functions | Columbia University Department of Surgery [Internet]. 2016 [cited 2017 Oct 9]. p. 1. Available from: http://columbiasurgery.org/pancreas/pancreas-and-its-functions

149. Haller W, Ledder O, Lewindon PJ, Couper R, Gaskin KJ, Oliver M. Cystic fibrosis: An update for clinicians. Part 1: Nutrition and gastrointestinal complications. J Gastroenterol Hepatol. 2014;29(7):1344–55.

150. Moran A, Dunitz J, Nathan B, Saeed A, Holme B, Thomas W. Cystic Fibrosis–Related Diabetes: Current Trends in Prevalence, Incidence, and Mortality. Diabetes Care. 2009;32:1626–31.

151. Sato K. The physiology, pharmacology, and biochemistry of the eccrine sweat gland. Rev Physiol Biochem Pharmacol Vol 79 SE - 2. 1977;79:51–131.

152. Quinton PM, Bijman J. Higher bioelectric potentials due to decreased chloride absorption in the sweat glands of patients with cystic fibrosis. N Engl J Med. 1983 May 19;308(20):1185–9.

153. Bockris JOM, Devanathan MA V., Muller K. On the structure of charged interfaces. Proc R Soc. 1963;1(274):55–79.

154. Del Gratta C, Romani GL. MEG: Principles, methods, and applications. Biomed Tech. 1999;44(s2):11–23.

155. Bockris JOM, Reddy AKN, Gamboa M. Modern electrochemistry 2B: Fundamentals of electrodics. Vol. 2B. 2015. 561 p.

156. Zoski CG. Handbook of electrochemistry. Handbook of Electrochemistry. Elsevier; 2007. 892 p.

157. Klotz I., Rosenburg R. Chemical Thermodynamics : Basic Concepts and Methods. 7th ed. John Wiley & Sons, Inc.; 2008.

158. Atkins P, de Paula J. Physical Chemistry for the Life Sciences. Oxford University Press; 2006. 634 p.

159. Inzelt G. Pseudo-reference electrodes. In: Handbook of Reference Electrodes. Springer Berlin Heidelberg; 2013. p. 331–2.

160. Keyes TE, Forster RJ. Spectroelectrochemistry. In: Handbook of Electrochemistry. 2007. p. 591–635.

161. Paul A, Laurila T, Vuorinen V, Divinski S V. Thermodynamics, diffusion and the kirkendall effect in solids. Vol. 9783319074, Thermodynamics, Diffusion and the Kirkendall Effect in Solids. 2014. 1–530 p.

162. Hennink W., van Nostrum C. Novel crosslinking methods to design hydrogels. Adv Drug Deliv. 2001;54:13–36.

163. Milne SD, Seoudi I, Hamad H Al, Talal TK, Anoop AA, Allahverdi N, et al. A wearable wound moisture sensor as an indicator for wound dressing change: An observational study of wound moisture and status. Int Wound J. 2016;13(6):1309–14.

164. Mucci V, Vallo C. Efficiency of 2,2-dimethoxy-2-phenylacetophenone for the photopolymerization of methacrylate monomers in thick sections. J Appl Polym Sci. 2012;123(1):418–25.

165. Glöckner P. Radiation Curing: Coatings and Printing Inks. Hannover: Vincentz Network; 2008. p. 34.

166. Sigma Aldrich. Application: Free Radical Initiators [Internet]. [cited 2020 Jan 20]. p. 5–19. Available from: www.sigma-aldrich.com.

167. Bijman J, Quinton PM. Lactate and bicarbonate uptake in the sweat duct of cystic fibrosis and normal subjects. Pediatr Res. 1987;21(1):79–82.

168. Connolly P, Cotton C, Morin F. Opportunities at the skin interface for continuous patient monitoring: A reverse iontophoresis model tested on lactate and glucose. IEEE Trans Nanobioscience. 2002;1(1):37–41.

169. Patterson MJ, Galloway SDR, Nimmo MA. Variations in regional sweat composition in normal human males. Exp Physiol. 2000;85(6):869–75.

170. Simonis A, Dawgul M, Lüth H, Schöning MJ. Miniaturised reference electrodes for field-effect sensors compatible to silicon chip technology. In: Electrochimica Acta. 2005. p. 930–7.

171. Achilias DS, Siafaka PI. Polymerization kinetics of poly(2-hydroxyethyl methacrylate) hydrogels and nanocomposite materials. Processes. 2017;5(2).

172. Deligkaris K, Tadele TS, Olthuis W, van den Berg A. Hydrogel-based devices for biomedical applications. Sensors Actuators, B Chem. 2010;147(2):765–74.

173. Lee JH, Bucknall DG. Swelling behavior and network structure of hydrogels synthesized using controlled UV-initiated free radical polymerization. J Polym Sci Part B Polym Phys. 2008;46(14):1450–62.

174. Li L, Lee LJ. Photopolymerization of HEMA/DEGDMA hydrogels in solution. Polymer (Guildf).

2005;46(25):11540–7.

175. Kim BK, Sy S, Yu A, Zhang J. Electrochemical Supercapacitors for Energy Storage and Conversion. Handb Clean Energy Syst. 2015;1–25.

176. Brazel CS, Peppas NA. Dimensionless analysis of swelling of hydrophilic glassy polymers with subsequent drug release from relaxing structures. Biomaterials. 1999;20(8):721–32.

177. Brazel CS, Peppas NA. Mechanisms of solute and drug transport in relaxing, swellable, hydrophilic glassy polymers. Polymer (Guildf). 1999;40(12):3383–98.

178. Franson NM, Peppas NA. Influence of copolymer composition on non-fickian water transport through glassy copolymers. J Appl Polym Sci. 1983;28(4):1299–310.

179. Szubzda B, Szmaja A, Ozimek M, Mazurkiewicz S. Polymer membranes as separators for supercapacitors. Appl Phys A Mater Sci Process. 2014;117(4):1801–9.

180. Stepniak I, Ciszewski A. Electrochemical characteristics of a new electric double layer capacitor with acidic polymer hydrogel electrolyte. Electrochim Acta. 2011;56(5):2477–82.

181. Castro-Gutiérrez J, Celzard A, Fierro V. Energy Storage in Supercapacitors: Focus on Tannin-Derived Carbon Electrodes. Front Mater. 2020;7(July):1–25.

182. Kim D, Kannan PK, Chung CH. High-Performance Flexible Supercapacitors Based on Ionogel Electrolyte with an Enhanced Ionic Conductivity. ChemistrySelect. 2018;3(7):2190–5.

183. Kularatna N, Gunawardane K. Capacitors as energy storage devices: Simple basics to current commercial families. Energy Storage Devices Renew Energy-Based Syst. 2021;(0):181–97.

184. Volfkovich YM. Electrochemical Supercapacitors (a Review). Russ J Electrochem. 2021;57(4):311–47.

185. Turner Alfrey J, Gurnee E., Lloyd W. Diffusion in glassy polymers. J Polym Sci. 1966;(12):249–61.

186. Wang TT, Kwei TI, Risch HLE. Diffusion in Glassy Polymers. 111. J Polym Sci. 1969;7:2019–28.

187. Kwei TI, Wang TT, Zupko H. Diffusion in Glassy Polymers . V . Combination of Fickian and Case II Mechanisms. 1972;5(5):645–6.

188. HOPFENBERG HB, FRISCH HL. Transport of Organic Micromolecules in Amorphous Polymers. Am Chem Soc-Div Polym Chem. 1969;10(2 Papers for New York meeting):999–1003.

189. Button VLDSN. Electrodes for Biopotential Recording and Tissue Stimulation. Principles of Measurement

and Transduction of Biomedical Variables. 2015. 25–76 p.

190. Grimnes S, Martinsen ØG. Electrodes. In: Bioimpedance and Bioelectricity Basics. 2015. p. 179–254.

191. Grimnes S, Martinsen ØG. Passive Tissue Electrical Properties. Bioimpedance and Bioelectricity Basics. 2015. 77–118 p.

192. Buxi D, Kim S, Van Helleputte N, Altini M, Wijsman J, Yazicioglu RF, et al. Correlation between electrode-tissue impedance and motion artifact in biopotential recordings. IEEE Sens J. 2012;12(12):3373–83.

193. Keithley. Low Level Measurements Handbook- Precision DC current, voltage and resistance measurements. 6th ed. Book. 2004. 239 p.

194. Assambo C, J. M. Low-Frequency Response and the Skin-Electrode Interface in Dry-Electrode Electrocardiography. Adv Electrocardiograms - Methods Anal. 2012;(January).

195. Martinsen ØG, Pabst O, Tronstad C, Grimnes S. Sources of error in ac measurement of skin conductance. J Electr Bioimpedance. 2015;6(1):49–53.

Appendix: A

This appendix provides the results of comparison studies conducted between the commercial Palmsens potentiostat and the Portable Electrochemical Analyser (PEA) utilised for the healthy volunteer study (Section 5). Each plot shown below was obtained using a single electrode (electrode number provided). The PEA data points represent the electrode's mean potentiometric responses ± SD toward the KCl DI water test solutions as measured by the PEA device over five OCP test procedures (n = 5). The Palmsens data points represent potentiometric responses (n = 1) to test solutions as measured by the Palmsens. They show that despite the two devices recording different magnitudes of potential for each test concentration, the offset was relatively consistent over the full concentration for each electrode. The two devices were therefore consistent in recording the electrode's sensitivity toward the test Cl^- concentration.

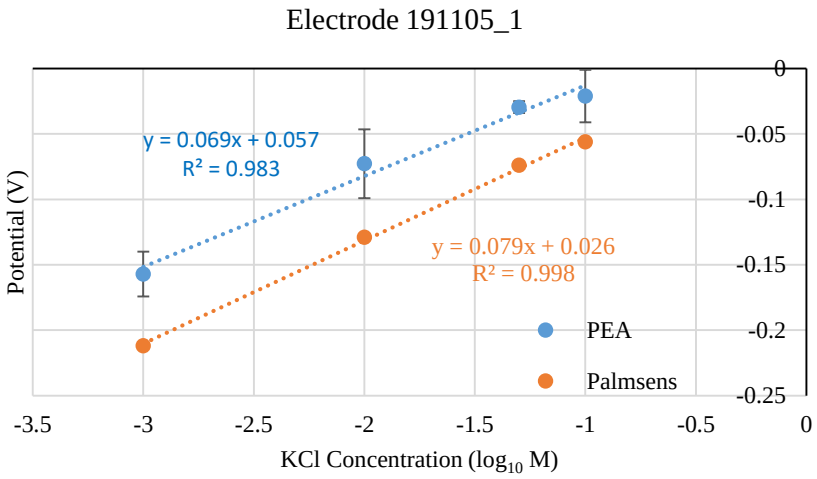

Electrode 191105_3

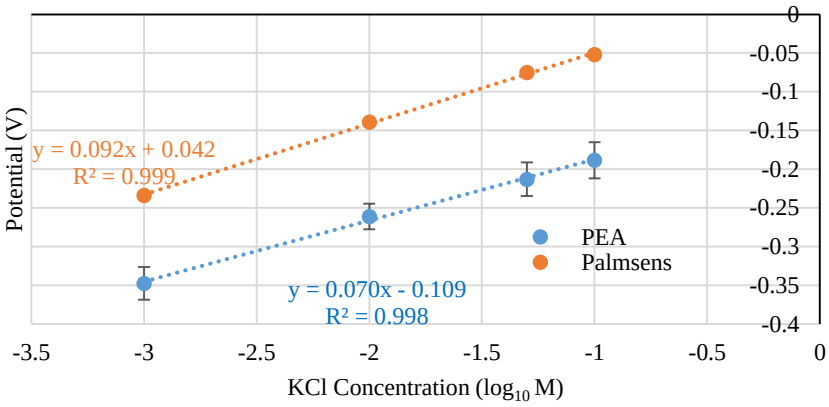

Electrode 191126

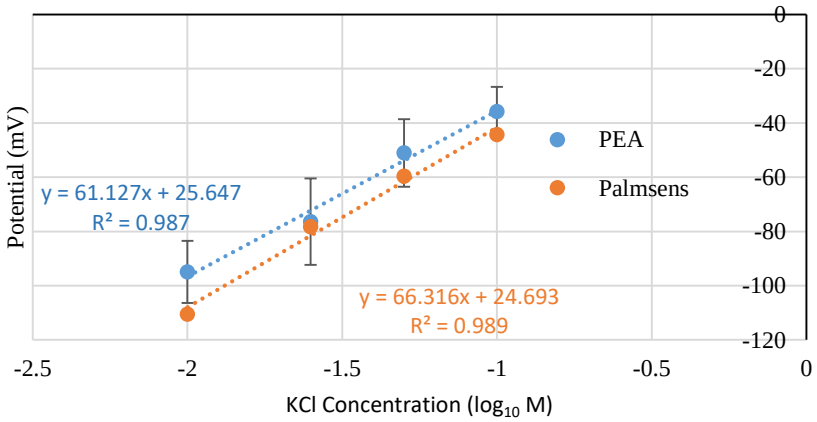

Appendix: B

This appendix presents the results of a preliminary investigation into the miniaturisation of the potentiostat element of the pHEMA Woundsense configuration. As noted throughout the thesis, the potential developed by the pHEMA electrode was monitored using the Palmsens potentiostat for every test barring the HVS. To investigate if the potentiostat element could be miniaturised and form part of a future compact wearable device, a voltage follower circuit was made utilising a ADA4530-1 op-amp (Analogue Devices, Norwood, MA), as shown in figure B.1. This was integrated with an Arduino microcontroller (Arduino, Boston, MA) and HC-06 Bluetooth module (DSD Tech, London, UK), as shown in figure B.2. The configuration was used to record the mean potentiometric responses of pHEMA Woundsense electrodes toward KCl DI water test solutions. This process was repeated with the same electrodes and test solutions, using the Palmsens to record the electrodes' responses. Table B.1 shows this data and figure B.3 displays the mean potential responses measured by the two devices plotted against the test solution concentration. The data shows the two potentiostats return values of similar magnitude with the addition of a near-constant offset of ~10 mV over the full test concentration range. This demonstrates that with further development, the potentiostat element could be miniaturised and conceivably integrated into a compact device alongside the Cl^- ISE component to form a compact wearable device capable of monitoring sweat Cl^- concentration.

(a)

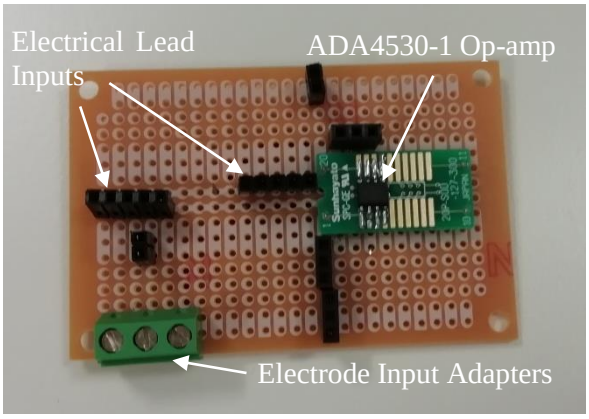

(b)

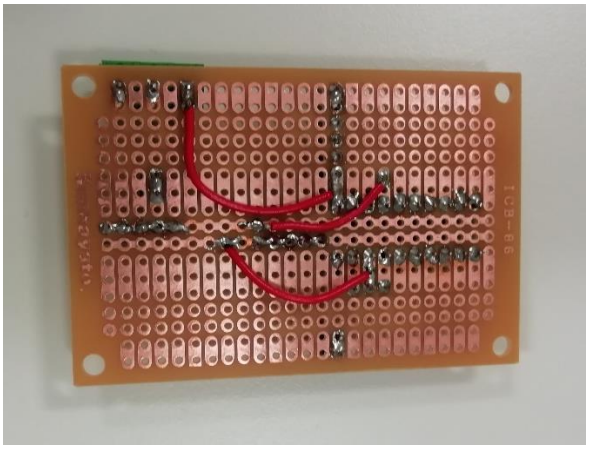

Figure B.1. Test setup for ADA4530-1 op-amp. (a) Top side of veroboard showing the op-amp fixed to its adapter, in addition to the adapters utilised to allow access to electrical leads to power the op-amp and observe its output. (b) Underside of veroboard voltage follower setup.

(a)

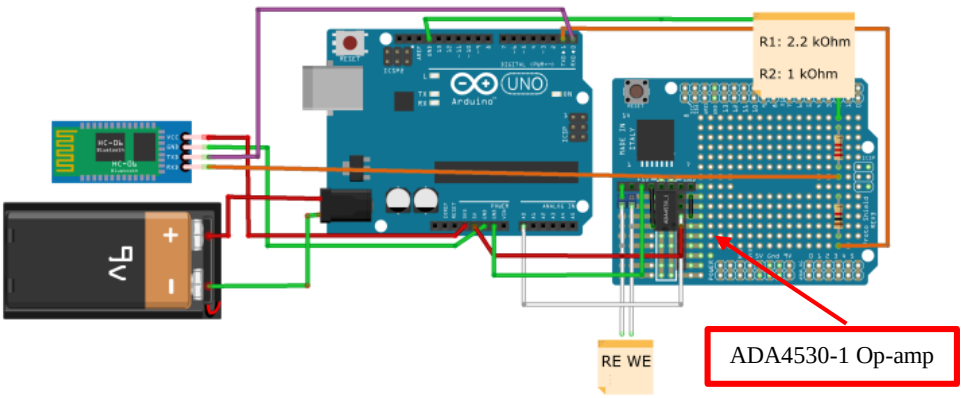

(b)

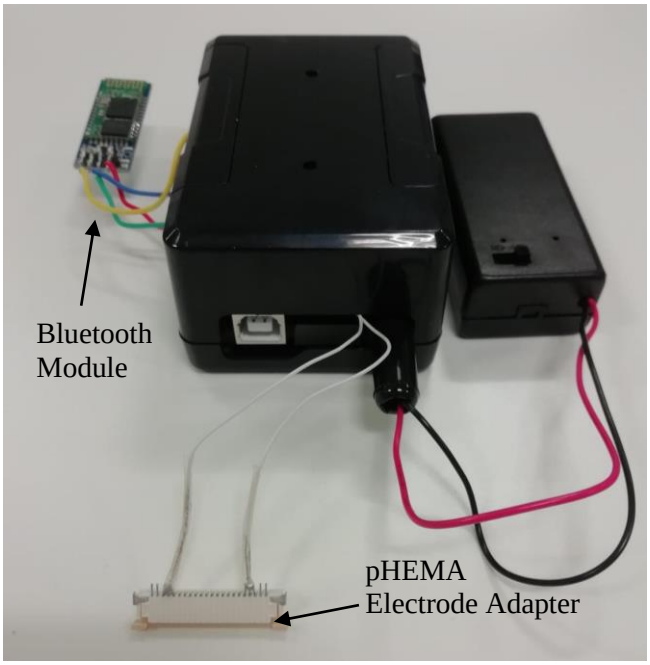

(c)

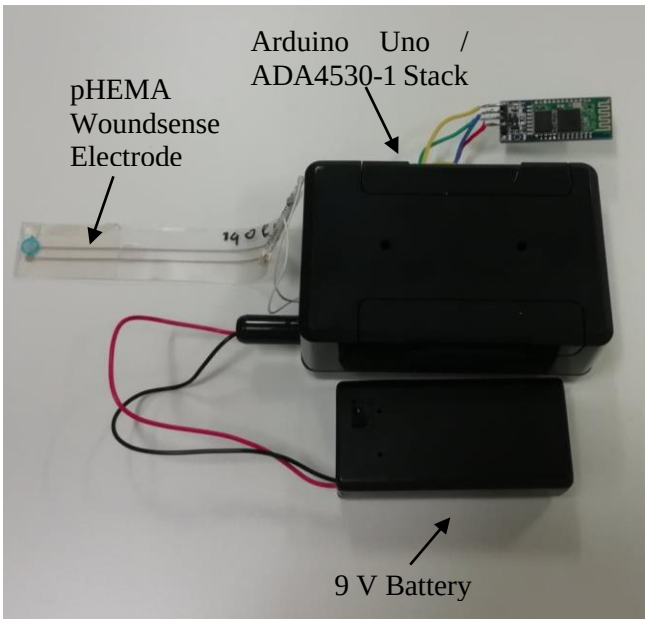

Figure B.2. (a) Schematic of wiring between ADA4530-1, Arduino Uno and HC-06. **(b)-(c)** Experimental configuration of ADA4530-1, Arduino Uno and HC-06.

Table B.1. Average potentiometric responses of pHEMA Woundsense electrodes toward KCl DI water test solutions measured using Palmsens potentiostat and ADA4530-1 voltage follower potentiostat. Number of electrodes used to obtain the average response is indicated.

KCl Concentration (mM)	Average PS-Measured Potential (mV)	SD (± mV)	Average ADA-Measured Potential (mV)	SD (± mV)	Difference [PS - ADA] (mV)	No. of Electrodes Used
10	115.42	4.12	105.62	2.00	9.79	5
25	83.92	4.64	76.29	1.13	7.63	4
50	63.37	3.00	53.88	0.84	9.49	5
75	54.69	2.26	42.81	2.17	11.87	4
100	48.05	1.65	36.88	2.13	11.16	5

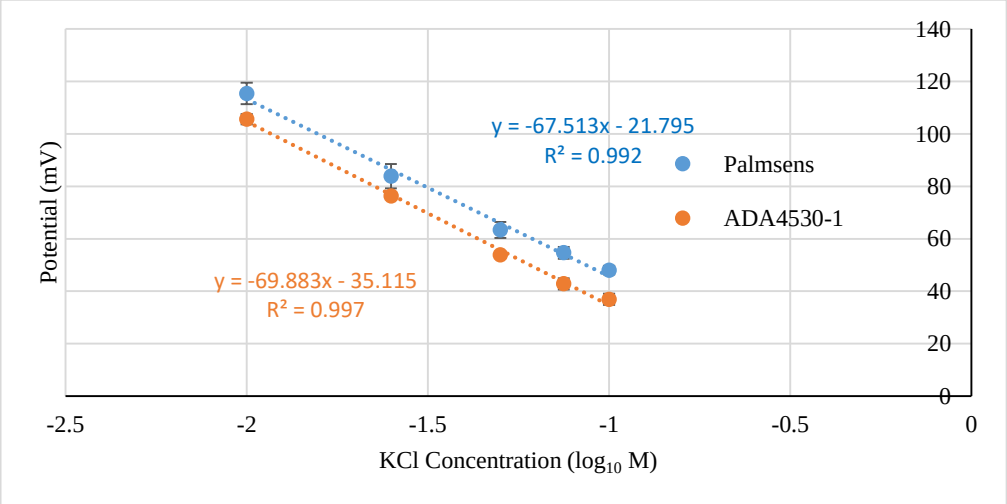

Figure B.3. Potentiometric responses of pHEMA Woundsense electrodes toward KCl DI water test solutions measured using Palmsens and ADA4530-1 potentiostats, plotted against test concentration. Data points represent mean measured potential of electrodes ± SD. Number of electrodes used to calculate each data point is indicated in Table C.1.